Bárbara Martins Paiva da Cunha

Mestre em Biotecnologia

Development of integrated strategies for the downstream processing of human stem cells for clinical application

Dissertação para obtenção do Grau de Doutor em Bioengenharia

Orientador: Doutora Margarida Serra, ITQB-NOVA

Co-orientador: Prof. Doutora Paula M. Alves, ITQB-NOVA
Co-orientador: Doutora Cristina Peixoto, ITQB-NOVA

Júri

Presidente: Prof. Doutor José Paulo Mota
Arguentes: Prof. Doutor Marcel Ottens
Doutor Brian Murphy
Prof. Doutora Cláudia Lobato da Silva

FACULDADE DE CIÊNCIAS E TECNOLOGIA
UNIVERSIDADE NOVA DE LISBOA

Novembro 2016

Development of integrated strategies for the downstream processing of human stem cells for clinical application

Copyright © Bárbara Martins Paiva da Cunha, Faculdade de Ciências e Tecnologia, Universidade Nova de Lisboa.

A Faculdade de Ciências e Tecnologia e a Universidade Nova de Lisboa têm o direito, perpétuo e sem limites geográficos, de arquivar e publicar esta dissertação através de exemplares impressos reproduzidos em papel ou de forma digital, ou por qualquer outro meio conhecido ou que venha a ser inventado, e de a divulgar através de repositórios científicos e de admitir a sua cópia e distribuição com objectivos educacionais ou de investigação, não comerciais, desde que seja dado crédito ao autor e editor.

Em memória da tia Bé beta e da Dri
À minha família

"Failure is a prerequisite for learning.
I have not failed. I've just found 10,000 ways that won't work."

Thomas A. Edison

Acknowledgements

I would like to express my deepest gratitude to all the people that contributed directly or indirectly to this thesis. I will do my very best to put in words what I feel, thus I apologize in advance if in some cases I can't do it properly – some things are just meant to be felt.

First and foremost, I would like to thank to Dr Paula Alves and to Professor Manuel Carrondo. I consider that both you have not just given me the infrastructure and opportunity to work at Animal Cell Technology Unit (ACTU), but you have pushed me in so many different ways that shaped the accomplished and successful person that I consider to be today. I will never forget my first DSP cluster with you – that was the moment when I knew if I could beat that challenge, I could actually do this until the end. To Dr. Paula Alves, my co-supervisor, I deeply thank you for your support, for your guidance, for teaching me what was (truly) to have rigor, how to be a scientist and to think ahead and beyond the basics. For teaching me that the PhD journey is much more than science and that there are lessons that I will bring with me my entire life. To Professor Carrondo, you have taught me so much. You are one of a kind, and I am truly honored to have had the chance to have cross my path with you. I can never thank you enough for your guidance, for sharing your knowledge, for the encouragement in all the right moments, and for making me learn engineering from scratch. Thank you for being demanding and for always pushing me forward. Life is though, and eventually I will get used to it. It was truly a pleasure working and learning from you.

I would like to acknowledge Dr Margarida Serra, my supervisor, for introducing me to the fascinating field of stem cell bioprocessing, for sharing her knowledge and experience with me, and mostly for letting me grow as a scientist and as a person. I learned more lessons than those I could count for.

To Dr Cristina Peixoto, my co-supervisor, for the constant support, for never giving up on me, for believing until the end. Thank you for picking up this area and for pushing me forward. Without you, this work would have not been possible.

To Dr Patrícia Alves, I wouldn't even know where to start. I don't know enough words to express how grateful I am to have met you (serendipity!) and the joy to have shared this journey with you. Thank you for your guidance, your patience, your support, for all the science, for being also my north when I needed one, for pushing me forward, for always, always, no matter what believing in me, even when I didn't. When I think in a role model, I think of you – you're a complete scientist and person. I deeply admire you and all I can wish for is to be 1/10 of who you are. More than a colleague, I take a friend for all life time. Thank you.

To Tiago Aguiar, thank you for giving me the opportunity to teach you and for embracing this challenge with me. There is no other person I would have trusted my work with. Seeing you grow both professionally and personally was a true reward. You also taught me a lot. Without your commitment and hard work, this would not have been possible as it was.

To Dr Ricardo Silva, for being there for me since the very beginning. For all that you taught me, for all the discussions, for teaching engineering to this biochemist. For all the laughs, and advice. Thank you for helping me grow as a person, as a scientist and as an engineer. You were fundamental, and I couldn't have done it without you.

To Dr Catarina Brito, for your confidence, motivation, timely guidance, but most importantly, for your friendship.

To Dr Julia Hupfeld and all the apceth team for such a warm welcoming in your company during the tech transfer. Servus!

To our collaborators, Bixente Martirene and John Daicic for your support and for all the invaluable discussions throughout this thesis.

To all ACTU group. To the stem group. A special thank you to Marta Silva, Carina Silva, and to the DSP team Pier, Ricardo, Sofia, Mafalda, Júnior e Sara. Thank you all for your support, strong team spirit, and essential good mood that pushed us forward one more day.

To Marcos Sousa for all the knowledge and support on the bioprocess field.

To the UniMS team, specially to São, Ricardo and Catarina. Thank you for helping and participating in some parts of this work, and for your always good energy.

To all iBET and ITQB staff, because we are only as good as the structure we have – thank you to Pilot plant team, Bayer team, iBET's accounting team, HR, security and economato!

To my CAT, specially Prof. Paulo Mota and Dr Greg Russotti, for the great discussion in my pre-thesis, and for all the support.

To Fundação para a Ciência e Tecnologia for financial support.

To the MIT-Portugal program and all my professors for the intensive learning experience in the field of bioengineering systems. A special thanks needs mandatorily to be to José Silva Lopes. Also to my long date (half) friends António and Ché – thank you for sharing this journey with me.

Aos meus amigos – Ui Ca Bom! Estes anos sem vocês tinham sido impossíveis. Obrigada pelos almoços cheios de boa disposição, pelas palhaçadas, pelo convívio, enfim, pela vida. Sou uma sortuda por ter encontrado amigos no meu trabalho.

Aos amigos de sempre, à minha M, Miguel, madrinha e UCL – obrigada por compreenderem as minhas ausências e independentemente disso estarem sempre tão perto e

fazerem com que tudo fique na mesma. Todos vocês são uma parte central de quem eu sou. Obrigada!

À minha família: para mim seremos sempre os fantásticos 10, porque embora já não cá estejamos todos, sei que estamos sempre juntos. Sou tão sortuda por ter uma família como vocês. A vossa presença e apoio incondicional fazem de mim uma pessoa melhor todos os dias. Aos meus avós Júlia e Aníbal, os meus segundos pais. À minha mãe e irmão por me acompanharem na minha jornada, pela paciência sem fim, apoio, carinho e por fazerem de mim quem eu sou hoje. Obrigada por não me terem posto o saco do Lidl à porta. Obrigada por sempre terem acreditado em mim, me terem dado tudo, mesmo nas situações mais difíceis, por me mostrarem que é sempre possível dar a volta e que por muito más que as situações sejam, vão sempre melhorar.

Ao Luís, porque se estou onde estou, é graças a ti. Porque quando a vida não ficou mais fácil, tu ensinaste-me a ser mais forte. A verdade é esta: tu é que me dás alento e na verdade tu é que és o forte de nós. Por seres o meu lugar favorito, todos os dias, bons ou maus. Obrigada pela tua dedicação, por não me teres deixado desistir, e por me teres feito sempre acreditar no dia de amanhã. Obrigada acima de tudo por nós, porque no final do dia é isto que dá sentido à vida.

Abstract

During the past decades, human stem cells (hSC) have emerged as a therapeutic alternative for several diseases. However, their clinical transfer still faces major challenges. Amongst them are the production of high cell amounts, the delivery of those high cell numbers at low volumes with minimal presence of residuals, while assuring the desired phenotype and function/potency. Although substantial efforts have been placed on the large-scale production of hSC and/or derivatives, the development of scalable approaches for downstream processing (DSP) of hSC and the establishment of fully integrated platforms for cell manufacturing has been long awaited.

The goal of this PhD project was to establish scalable and integrated DSP strategies for the clarification, volume reduction (concentration) and washing unit operations for human-derived adult and pluripotent SC. Human mesenchymal stem cells (hMSC) and human induced pluripotent stem cells (hiPSC) were used as challenging and complex cell-based products. Combining membrane technology and chromatographic tools, a flexible platform based on cost-effective, robust, scalable, and compatible with current good manufacturing practices (cGMP) processes, compliant with different stem cell types and that can be transferred to clinical/industrial settings was developed.

Initially, it was evaluated the applicability of filtration methodologies, as dead end filtration and tangential flow filtration, for the clarification and concentration of hMSC, respectively. Different process parameters and their impact on hMSC quality were studied. Polypropylene filters with pore sizes higher than 75 µm ensured the efficient removal of microcarriers from the cell suspension bulk, without compromising cells' recovery yields or viability. Furthermore, hMSC could be successfully concentrated up to a factor of 10 while maintaining their identity, differentiation capacity and high cell viability, allowing for the recovery of over 80% of viable cells; an initial cell concentration higher than 2 x 10^5 cell/mL, and polysulfone membranes with pore sizes higher than 0.45 µm were identified to be key conditions to obtain such concentration factors; shear rate and permeate flux were also shown to impact cells' recovery yields, viability and quality.

The applicability of the previously developed TFF methodologies to hiPSC processing, was assessed applying a Design of Experiments (DoE) approach. The impact of the process parameters of the volume reduction unit operation on hiPSC's recovery, viability, expression of pluripotency markers and pluripotency differentiation potential was assessed and compared with results previously attained with hMSC. A mathematical model of the process was designed

and after understanding how the shear rate, permeate flux and cell load factors interacted between them, the condition that maximized cell recovery and viability showed to be similar between both stem cell types. A robustness analysis was performed and the success rate of these operating conditions was assessed (65 - 70%). A parametric study was then conducted, identifying that increasing the shear rate (up to 3370 s^{-1}) allowed to achieve the specified requirements for cell recovery yield (> 80%) and viability (> 90%) in 100% of the cases and no impact in hiPSC's proliferation capacity, expression of pluripotency markers and differentiation potential was observed.

Also, a proof of concept of the integration of up- and down- stream unit operations, i.e. continuous perfusion culture in bioreactors with a TFF system for the volume reduction and washing of hMSC, was performed. Process integration can result in the elimination of hold steps, thus decreasing the footprint and ultimately can create robust closed system operations and is therefore desirable for the bioprocess of hMSC. A continuous alternative for concentrating hMSC was also evaluated. Results showed that expanding cells in a continuous perfusion operation mode provided a higher expansion ratio and led to a shift in cell's metabolism. TFF operated either in continuous or discontinuous allowed to concentrate cells, with high cell recovery (> 80%) and viability (> 95%). Furthermore, continuous TFF permitted to operate longer with higher cell concentrations. Continuous diafiltration led to higher protein clearance (98%) with lower cell death, when comparing to discontinuous diafiltration. Overall, an integrated process allowed for a shorter process time, recovering 70% of viable hMSC (> 95%), 10% more than having separated unit operations, with no changes in cells' critical quality control attributes (QCA) such as morphology, immunophenotype, proliferation capacity and multipotent differentiation potential.

To deliver the required cell numbers and doses to therapy ($10^6 - 10^9$ cells/patient), scaling up production and purification processes at least to the liter scale while maintaining cells' characteristics is compulsory. Therefore, a proof of concept of the scalability of expansion, detachment and volume reduction unit operations for hMSC isolated from different tissues (bone marrow (BM) and adipose tissue (AT)) was performed. The impact of scaling-up these steps on cells' recovery yield and characteristics was studied. To accomplish the volume reduction step, a comparison between hollow fiber cartridges (HF) and flat sheet cassettes (FSC) was conducted. The scale-up of TFF process was performed increasing the area available for filtration, maintaining constant the load (cell/cm^2), shear rate and permeate flux parameters. In both devices, TFF's scale-up was fairly linear, with the need to slightly adjust the permeate flux to maximize cell recovery yield. Nonetheless, FSC allowed to recover 18% more cells after a

volume reduction factor of 50. Differences on the membrane's material and on the flow regimen might explain the observed differences. Overall, at the end of the bioprocess (USP and DSP operations) more than 70% of highly viable hMSC could be recovered without compromising cell's CQA.

To improve the previously established TFF-based washing process, further increasing hMSC purity, the applicability of expanded bed adsorption (EBA) chromatography operated in negative mode was evaluated. For this purpose, a new multimodal prototype matrix based on core-shell bead technology was used. The matrix was first characterized and a stable expanded bed could be obtained using standard equipment adapted from what is used for conventional packed bed chromatography processes. The effect of different expansion rates on cell recovery yield and protein removal capacity was assessed. The best trade-off between cell recovery (89%) and protein clearance (67%) was achieved using an intermediate expansion bed ratio (1.4). Moreover, it was also showed that EBA chromatography can be efficiently integrated on the already established process for the DSP of hMSC, where it improved the washing efficiency more than 10-fold, recovering approximately 70% of cells after total processing. This strategy showed not to impact cell viability (> 95%), neither hMSC's CQA.

To further gain insights on how processing (both up- and downstream) was affecting hSC characteristics (total proteome), a proteomics workflow based on state of the art mass spectrometry (MS) tools was established and applied alongside the standard quality assays for hMSC. Overall, 1359 proteins were significantly differently expressed between BM-MSC after DSP and after expansion in bioreactors (BR). Biological functions associated with cellular assembly and organization (22.3%) and cellular movement (21%) corresponded to functions highly represented in BM-MSC after expansion, which become downregulated after the volume reduction step. Conversely, cellular growth and proliferation (32.5%), and protein degradation (7.8%) were observed the biological function upregulated in BM-MSC after DSP.

Overall, this thesis contributed to generate knowledge regarding the impact that critical process parameters of chromatography and filtration-based methods have on hSC's recovery, viability and characteristics. By combining membrane technology and chromatographic tools, a DSP train comprised by clarification, cell concentration and washing unit operations was established. The processes herein described contributed to achieve a volume reduction factor of 50, guaranteeing high cell recovery yields (more than 80%) with high purity levels (no microcarriers, endotoxin-free, and more than 99% of protein clearance), and without compromising cells' characteristics in terms of viability, identity and potency. Additionally, it is also proposed the application of a proteomics workflow based on state of the art MS tools

alongside standard quality control assays as an additional tool to characterize hSC. The application of such methodology will permit to understand the impact of processing in cells' characteristics, therefore allowing to better design processes for cell therapy applications.

Keywords: Cell therapy, downstream processing, filtration, stem cells, process development, cell characterization

Resumo

Durante as últimas décadas, as células estaminais humanas (hSC) têm emergido como uma alternativa terapêutica para diversas doenças. No entanto, a sua transferência para a clínica ainda encontra bastantes desafios. Entre eles, encontram-se a produção de elevados números de células, a entrega dessas mesmas quantidades em volumes reduzidos com a presença mínima de contaminantes, assegurando o fenótipo e função/potência desejada. Esforços significativos têm-se vindo a focar no desenvolvimento de plataformas de produção em larga escala deste tipo de produtos. Desta forma, o estabelecimento e desenvolvimento de plataformas integradas para a produção e purificação de células estaminais humanas tem sido muito aguardado.

O objectivo desta tese de doutoramento baseia-se no estabelecimento de estratégias escalonáveis e integradas compreendidas por unidades de operação de clarificação, redução de volume (concentração) e purificação para células estaminais humanas adultas e pluripotentes. Para este fim, as células mesenquimais humanas (hMSC) e células pluripotentes induzidas humanas (hiPSC) foram utilizadas como modelos complexos de produtos celulares. A combinação de tecnologia de membranas com cromatografia levou ao desenvolvimento de uma plataforma flexível, economicamente viável, robusta, escalonável e compatível com as práticas correntes de boa manufactura, para a purificação de diferentes tipos de células estaminais humanas e que tem o potencial de ser facilmente transferida para um contexto clínico/industrial.

Inicialmente foi avaliada a aplicabilidade de utilizar filtração, filtração normal e tangencial (TFF), para a clarificação de concentração de hMSC, respectivamente. Foi estudado o impacto que diferentes parâmetros de processo têm na qualidade das hMSC. Filtros de polipropileno com tamanho médio de poro maior que 75 µm garantiu a remoção completa de *microcarriers* da suspensão celular sem comprometer o rendimento de recuperação de células ou a sua viabilidade. Adicionalmente, as hMSC foram concentradas 10 vezes, tendo recuperado mais de 80% de células viáveis, e mantiveram as suas características de identidade, capacidade de diferenciação e viabilidade. Parâmetros de processo tais como concentração celular inicial maior que 2 x 10^5 células/mL e membranas de polissulfona com tamanho médio de poro superior a 0.45 µm revelaram ser condições chave para atingir este factor de concentração. A tensão de corte e o fluxo de permeado também mostraram ter um impacto significativo no rendimento de recuperação de células do processo, bem como na viabilidade e qualidade celular.

A aplicabilidade da TFF para concentrar hiPSC foi também avaliada utilizando o método de desenho de experiências (DoE). Foi avaliado o impacto dos parâmetros de processo da unidade de operação de redução de volume na recuperação das hiPSC, na sua viabilidade, expressão de marcadores de pluripotência e capacidade de diferenciação, e comparado aos resultados obtidos previamente com hMSC. Foi desenvolvido um modelo matemático que descreve o processo de concentração. Após perceber como os parâmetros de processo de tensão de corte, fluxo do permeado e quantidade do produto interagem entre eles, a condição que maximizou a recuperação de células e a viabilidade, mostrou ser semelhante entre os dois tipos de células estaminais. Foi realizada também uma análise de robustez, e foi determinada a taxa de sucesso da operação (65 - 70%). Um ainda efectuado um estudo paramétrico, que identificou que aumentando a tensão de corte (até 3370 s^{-1}) permitiu atingir as especificações em termos de recuperação de células (> 80%) e viabilidade (> 90%) em 100% dos casos, sem influenciar as características das hiPSC em relação a expressão de marcadores de pluripotência, proliferação e capacidade de diferenciação.

Foi também realizada uma prova de conceito sobre a integração de operações unitárias de expansão e purificação, i.e., cultura de perfusão contínua em biorreactores com um sistema de TFF para a redução de volume e purificação de hMSC. A integração de processo pode resultar na eliminação de passos de espera, diminui a pegada industrial e tem ainda o potencial de permitir o desenho de operações fechadas, pelo que é desejável para o processamento de hMSC. Alternativamente, foi ainda avaliada uma operação contínua em TFF para concentrar as hMSC. Os resultados mostraram que cultura de perfusão contínua permitiu atingir rácios de expansão mais elevados e levou também a uma alteração no metabolismo das células. A TFF operada quer continua quer descontinuamente possibilitou a concentração das hMSC com elevados rendimentos de recuperação celular (> 80%) e viabilidade celular (> 95%). De notar que a TFF contínua permitiu operar durante mais tempo com uma maior concentração celular. Comparando a diafiltração descontínua e contínua, a última permitiu remover mais proteínas (98%), tendo assegurado também uma menor morte celular. Globalmente, a integração do processo levou a uma redução no tempo global, e permitiu recuperar 70% de hMSC viáveis (> 95%), 10% mais do que tendo operações unitárias separadas, sem observar alterações nos atributos críticos de qualidade (CQA) das células, tais como morfologia, imunofenótipo, capacidade de proliferação e potencial de diferenciação multipotente.

Para entregar a quantidade necessária de células e doses para terapia (10^6 – 10^9 células/paciente), o *scale-up* da produção e purificação pelo menos à escala de 1 L é essencial. Assim, foi efectuada uma prova de conceito do *scale-up* das operações unitárias de expansão,

dissociação dos *microcarriers*, e redução de volume para hMSC isoladas de diferentes tecidos – medula óssea (BM-MSC) e tecido adiposo (AT-MSC), avaliando o impacto do *scale-up* destes passos no rendimento de recuperação e viabilidade celular. Para realizar a redução de volume, foi comparada a *performance* de módulos de fibras ocas (HF) e cassetes de membrana plana (FSC). O *scale-up* do processo de TFF foi realizado através do aumento da área disponível para realizar a filtração, mantendo a carga (células/cm^2), a tensão de corte e o fluxo de permeado constantes. Em ambos os módulos, o *scale-up* da TFF mostrou-se ser relativamente linear, com a necessidade de ajustar ligeiramente o fluxo de permeado de forma a maximizar o rendimento de recuperação celular. Contudo, as FSC permitiram recuperar mais 18% de células após uma concentração de 50 vezes. As diferenças dos materiais das membranas e no regime de fluídos podem explicar as diferenças observadas. Assim, no fim do bioprocesso (expansão e purificação) mais de 70% de hMSC viáveis foram recuperadas sem comprometer os seus CQA.

De forma a melhorar os processos de purificação com TFF, aumentando assim a pureza das hMSC, foi avaliada a aplicabilidade de utilizar cromatografia em leito expandido (EBA) em modo negativo para este fim. Para tal, foi utilizado um novo protótipo multimodal baseado na tecnologia de *core-shell*. A matriz foi primeiro caracterizada, e posteriormente foi obtido um leito estável e expandido utilizando equipamento comum a processos de cromatografia compacta convencionais. Foi avaliado o efeito de diferentes velocidades de expansão no rendimento de recuperação celular e na capacidade de remoção de proteínas. O melhor compromisso entre rendimento de recuperação celular (89%) e remoção de proteína (67%) foi obtido ao usar uma velocidade de expansão intermédia. Adicionalmente, foi também mostrado que a EBA pode ser eficientemente integrada no fluxo de purificação já estabelecido para as hMSC, tendo melhorado a eficiência de purificação em 10 vezes e recuperado cerca de 70% de células no fim do processo. Esta estratégia mostrou não ter influência na viabilidade celular (> 95%) nem nos CQA das hMSC.

Para melhor perceber o impacto dos processos unitários aqui descritos (expansão e purificação) nas características das hMSC (proteoma total), paralelamente aos ensaios de controlo de qualidade normalmente efectuados, foi estabelecido um protocolo de proteómica com ferramentas de espectrometria de massa. 1359 proteínas foram identificadas como estando diferencialmente expressas entre as BM-MSC após a expansão em biorreactores e após o processo de purificação. A organização e *assembly* (22.3%) e movimento celular (21%) foram as funções biológicas mais representadas nas BM-MSC após expansão em biorreactores, que ficam *downregulated* após o processo de purificação. Contrariamente, as funções de crescimento

e proliferação celular (32.5%), bem como degradação proteica (7.8%) correspondem a funções biológicas *upregulated* nas BM-MSC após os processos de purificação.

Assim, esta tese contribuiu para aumentar o conhecimento científico no que diz respeito ao impacto que os parâmetros críticos de processo das operações de cromatografia e de filtração têm nos rendimentos de recuperação celular e nos CQA das hSC. A combinação de tecnologia de membranas com cromatografia permitiu o estabelecimento de um processo global de purificação composto pelas operações unitárias de clarificação, concentração celular e purificação. Os processos aqui descritos permitiram atingir um factor de concentração de 50, rendimentos elevados de recuperação celular (80%), elevada pureza (sem presença de microcarriers, sem endotoxinas e mais de 99% de remoção proteica), sem influenciar os CQA das hSC. Adicionalmente, é também proposto a aplicação adicional de um protocolo de proteómica paralelamente aos ensaios convencionais de controlo de qualidade para caracterizar as hSC. A aplicação deste tipo de métodos, possibilitam compreender o impacto que os processos de produção e purificação têm nas características das células, e permitem melhor desenhar e desenvolver processos de *manufacturing* para produtos celulares.

Palavras-chave: Terapia celular, purificação, filtração, células estaminais, desenvolvimento de processo, caracterização de produto

Thesis Publications

Cunha B, Silva RJS, Aguiar T, Serra M, Daicic J, Maloisel JL, Clachan J, Åkerblom A, Carrondo MJT, Peixoto C, Alves PM, "Improving washing strategies of human mesenchymal stem cells using negative mode expanded bed chromatography", Journal of Chromatography A, 1429:292-303, 2016. doi:10.1016/j.chroma.2015.12.052 (IF_{2015}: 3.926, Q1)

Cunha B, Aguiar T, Silva MM, Silva R, Sousa MF, Peixoto C, Serra M, Carrondo MJT, Alves PM, "Exploring continuous and integrated strategies for the up- and downstream processing of human mesenchymal stem cells", Journal of Biotechnology, 213:97-108, 2015. doi:10.1016/j.jbiotec.2015.02.023 (IF_{2015}: 2.667, Q1)

Cunha B, Peixoto C, Silva MM, Carrondo MJT, Serra M, Alves PM, "Filtration methodologies for the clarification and concentration of human mesenchymal stem cells", Journal of Membrane Science, 478:117–129, 2015. doi: 10.1016/j.memsci.2014.12.041 (IF_{2015}: 5.557, Q1)

Cunha B, Serra M, Peixoto C, Silva M, Carrondo MJT, Alves PM, "Designing clinical-grade integrated strategies for the downstream processing of human mesenchymal stem cells", BMC Proceedings 2013, 7(Suppl 6):P103. doi:10.1186/1753-6561-7-S6-P103

Cunha B, Aguiar T, Silva MM, Carvalho SB, Gomes RA, Carrondo MJT, Gomes-Alves P, Peixoto C, Serra M, Alves PM, "Bioprocess integration for human mesenchymal stem cells: from up to downstream processing scale-up to cell proteome characterization", Journal of Biotechnology, *accepted*.

Cunha B & Silva RJS, Correia C, Koshkin A, Carrondo MJT, Serra M, Peixoto C, Alves PM, "Finding the design space using design of experiments of a filtration-based operation for the concentration of human pluripotent stem cells", *submitted*.

Cunha B, Aguiar T, Carrondo MJT, Peixoto C, Serra M, Alves PM, "Scalable workflow for volume reduction and washing of human stem cells using tangential flow filtration technology", *in preparation*.

Cunha B, Aguiar T, Silva MM, Carrondo MJT, Peixoto C, Gomes-Alves P, Serra M, Alves PM, "Impact of bioreactor design and continuous perfusion strategies on human mesenchymal stem cells' secretome", *in preparation*.

Additional Publications

Santo VE, Babo P, Amador M, Correia C, **Cunha B**, Coutinho D, Neves N, Mano J, Reis R, Gomes M, "Engineering enriched microenvironments with gradients of platelet lysate in hydrogel fibers", Biomacromolecules, 17(6):1985−1997, 2016. 10.1021/acs.biomac.6b00150 (IF_{2015}: 5.583, Q1)

Table of Contents

ACKNOWLEDGEMENTS ..... **IX**
ABSTRACT ..... **XIII**
RESUMO ..... **XVII**
THESIS PUBLICATIONS ..... **XXI**
ADDITIONAL PUBLICATIONS ..... **XXII**
TABLE OF CONTENTS ..... **XXIII**
LIST OF FIGURES ..... **XXVII**
LIST OF TABLES ..... **XXIX**
LIST OF ABBREVIATIONS ..... **XXXI**

INTRODUCTION **35**

1. THE LANDSCAPE OF CELL-BASED THERAPIES **38**

1.1. The promise of stem cells 38
1.2. Human stem cells in clinical trials 41

2. STEM CELL MANUFACTURING **44**

2.1. General considerations 44
2.2. Product requirements and process development 45
2.3. hMSC expansion for clinical applications 49
2.4. Downstream processing of hMSC 53
2.4.1. Technology landscape 53
2.4.2. Continuous centrifugation 56
2.4.3. Filtration 57

3. AIMS AND SCOPE **59**

REFERENCES **62**

OPTIMIZATION OF FILTRATION METHODOLOGIES FOR THE DOWNSTREAM PROCESSING OF HUMAN MESENCHYMAL STEM CELLS: CLARIFICATION AND CONCENTRATION UNIT OPERATIONS **71**

ABSTRACT **74**

1. INTRODUCTION **75**

2. MATERIALS AND METHODS **77**

2.1 Cell expansion 78
2.2 Downstream processing 79
2.3 Cell viability and characterization assays 83
2.4 Statistical Analysis 86

3. RESULTS **86**

3.1 hMSC clarification (microcarrier removal) using dead end filtration....86
3.2 Cell concentration/volume reduction using tangential flow filtration....88

4. DISCUSSION 96

5. ACKNOWLEDGMENTS 99

REFERENCES 101

FINDING THE DESIGN SPACE OF TANGENTIAL FLOW FILTRATION OPERATION FOR THE CONCENTRATION OF HUMAN PLURIPOTENT STEM CELLS 105

ABSTRACT 108

1. INTRODUCTION 109

2. MATERIALS AND METHODS 110

2.1 Human induced pluripotent stem cell culture 110
2.2 Downstream processing 110
2.3 Cell viability and characterization assays....111
2.4 Statistical Analysis 115

3. RESULTS AND DISCUSSION 116

4. CONCLUSION 124

5. ACKNOWLEDGMENTS 124

REFERENCES 126

SUPPLEMENTARY DATA 128

EXPLORING CONTINUOUS AND INTEGRATED STRATEGIES FOR THE DOWNSTREAM PROCESSING OF HUMAN MESENCHYMAL STEM CELLS: CELL WASHING UNIT OPERATION AND PROCESS INTEGRATION 129

ABSTRACT 132

1. INTRODUCTION 133

2. MATERIALS AND METHODS 133

2.1 Cell culture....134
2.2 Downstream processing 136
2.3 Integration of hMSC cell expansion, concentration and diafiltration processes 140
2.4 Cell viability and characterization assays....140
2.5 Statistical Analysis 144

3. RESULTS 144

3.1 hMSC expansion in continuous perfusion and semi-continuous cultures 144
3.2 Concentration and diafiltration processes using tangential flow filtration 147
3.3 Integration of hMSC cell expansion, concentration and diafiltration processes 150

4. DISCUSSION 155

5. ACKNOWLEDGMENTS 157

6. SUPPLEMENTARY DATA 158

REFERENCES 160

BIOPROCESS INTEGRATION FOR HUMAN MESENCHYMAL STEM CELLS: FROM UP TO DOWNSTREAM PROCESSING SCALE-UP TO CELL PROTEOME CHARACTERIZATION 163

ABSTRACT 166

1. INTRODUCTION 167

2. MATERIALS AND METHODS 168

2.1 hMSC Expansion 168
2.2 Downstream processing 170
2.3 Cell viability and characterization assays 171
2.4 Statistical Analysis 175

3. RESULTS 176

3.1 Scale-up of hMSC's expansion in single-use bioreactors 176
3.2 Scale-up of TFF process for the concentration of hMSC 179

4. DISCUSSION 188

5. CONCLUSION 190

6. ACKNOWLEDGMENTS 191

7. SUPPLEMENTARY DATA 192

REFERENCES 193

IMPROVING WASHING STRATEGIES OF HUMAN MESENCHYMAL STEM CELLS USING NEGATIVE MODE EXPANDED BED CHROMATOGRAPHY 197

ABSTRACT 200

1. INTRODUCTION 201

2. MATERIALS AND METHODS 202

2.1 Cell culture 202

2.2 Downstream processing (DSP) 203
2.3 Cell characterization assays 206
2.4 Statistical Analysis 209

3. RESULTS AND DISCUSSION 209

3.1 Characterization of the core-shell bead prototype matrix 209
3.2 Packed bed and expanded bed chromatography 212
3.3 Integration of EBA chromatography on hMSC's DSP 217

5. CONCLUSIONS 220

6. ACKNOWLEDGMENTS 221

7. SUPPLEMENTARY DATA 222

REFERENCES 223

DISCUSSION AND PERSPECTIVES 227

1. DISCUSSION 230

1.1. Establishing a DSP workflow for hMSC 230
1.2. Biomanufacturing workflow of hMSC 235

2. CONCLUSION AND PERSPECTIVES 236

REFERENCES 238

List of Figures

FIGURE 1.1 38
FIGURE 1.2. 40
FIGURE 1.3. 41
FIGURE 1.4 43
FIGURE 1.5. 44
FIGURE 1.6. 47
FIGURE 1.7. 51
FIGURE 1.8 57
FIGURE 1.9 60
FIGURE 2.1 77
FIGURE 2.2 87
FIGURE 2.3 89
FIGURE 2.4 90
FIGURE 2.5 91
FIGURE 2.6 93
FIGURE 2.7 94
FIGURE 2.8 95
FIGURE 2.9 97
FIGURE 3.1. 117
FIGURE 3.2 119
FIGURE 3.3 120
FIGURE 3.4 123
FIGURE 3.5. 125
FIGURE 4.1 134
FIGURE 4.2 137
FIGURE 4.3 146
FIGURE 4.4 148
FIGURE 4.5 150
FIGURE 4.6 152
FIGURE 4.7 153
FIGURE 4.8 154
SUPPLEMENTARY DATA 4.1. 158
SUPPLEMENTARY DATA 4.2 159
FIGURE 5.1 177
FIGURE 5.2 180
FIGURE 5.3 181
FIGURE 5.4 182
FIGURE 5.5 184
FIGURE 5.6 185
FIGURE 5.7 187
SUPPLEMENTARY DATA 5.1 192
FIGURE 6.1 211
FIGURE 6.2 213
FIGURE 6.3 214
FIGURE 6.4 216
FIGURE 6.5 218
FIGURE 6.6 219

SUPPLEMENTARY DATA 6.1 222
FIGURE 7.1 235

List of Tables

TABLE 1.1 46
TABLE 1.2 50
TABLE 1.3 52
TABLE 1.4. 54
TABLE 1.5 58
TABLE 2.1 80
TABLE 2.2 81
TABLE 2.3 81
TABLE 3.1. 112
TABLE 3.2. 116
TABLE 3.3 121
TABLE 3.4 121
TABLE S3.1 128
TABLE 4.1 145
TABLE 5.1 171
TABLE 5.2 178
TABLE 5.3 183
TABLE 6.1 210
TABLE 6.2 215

List of Abbreviations

2D	Two-dimensional
3D	Three-dimensional
A	Area
AT	Adipose tissue
AT-MSC	Adipose tissue-derived hMSC
ANOVA	Analysis of variance
BCA	Bicinchoninic acid assay
BM	Bone marrow
BM-MSC	Bone marrow-derived hMSC
BR	Bioreactor(s)
BSA	Bovine serum albumin
CFU-F	Colony Forming Unit
cGMP	Current Good Manufacturing Practices
CIP	Cleaning in Place
COGS	Cost of Goods
CPP	Critical Process Parameters
CQA	Critical Quality attributes
d	Diameter
DoE	Design of Experiments
DPBS	Dulbecco's phosphate-buffered saline
DSP	Downstream processing
EBA	Expanded Bed Adsorption
FBC	Fluidized Bed Centrifugation
FBS	Fetal Bovine Serum
FDA	Fluorescein diacetate
FDR	False discovery rate
FSC	Flat sheet cassettes
FSG	Fish skin gelatin
GvHD	Graft versus Host Disease
hESC	Human Embryonic Stem Cell(s)
HF	Hollow fiber cartridge

hFF	Human Foreskin Fibroblast(s)
hiPSC	Human Induced Pluripotent Stem Cell(s)
HLA	Human Leukocyte Antigen
hMSC	Human mesenchymal stem cell(s)
HPMK	High performance media kit
hPSC	Human Pluripotent Stem Cell(s)
hSC	Human Stem Cell(s)
HSC	Human Hematopoietic Stem Cell(s)
IDA	Information-dependent acquisition
ISCT	International Society for Cellular Therapy
J	Inlet Flux
J_p	Permeate Flux
LDH	Lactate dehydrogenase enzyme
LMH	$L.m^{-2}.h^{-1}$
mAb	Monoclonal Antibody
MF	Microfiltration
MS	Mass spectrometry
NFF	Normal Flow Filtration
NMWC	Nominal Molecular Weight Cut-off
PAT	Process Analytical Technology
PCA	Principal components analysis
PD	Population doubling
PDL	Population doubling level
PES	Polyethersulfone
P_f	Inlet/Feed Pressure
PFA	Paraformaldehyde
PGA	Polygalacturonic acid
PI	Propidium iodide
P_r	Retentate pressure
P_p	Permeate pressure
PS	Polysulfone
Q	Flow Rate
QbD	Quality by Design

q_{MET}	Specific metabolic rates
QTPP	Quality Target Product Profile
r	Radius
SU	Single-use
SWATH	Sequential Windowed data independent Acquisition of the Total High-resolution Mass Spectra
TFF	Tangential flow filtration
TGF-β	Transforming Growth Factor-beta
TMP	Transmembrane pressure
u	Cross-flow velocity
USP	Upstream processing
V	Volume
VR	Volume reduction
VRF	Volume reduction factor
XIC	Extracted ion chromatogram
$Y_{LAC/GLC}$	Apparent yields of lactate from glucose
$Y_{NH3/GLN}$	Apparent yields of ammonia from glutamine
$Y_{O2/GLC}$	Apparent yields of oxygen from glucose
γ	Shear rate
τ	Shear stress

Introduction

Table of Contents

1. THE LANDSCAPE OF CELL-BASED THERAPIES 38

1.1. The promise of stem cells 38
1.2. Human stem cells in clinical trials 41

2. STEM CELL MANUFACTURING 44

2.1. General considerations 44
2.2. Product requirements and process development 45
2.3. hMSC expansion for clinical applications 49
2.4. Downstream processing of hMSC 53
2.4.1. Technology landscape 53
2.4.2. Continuous centrifugation 56
2.4.3. Filtration 57

3. AIMS AND SCOPE 59

REFERENCES 62

1. The landscape of cell-based therapies

1.1. The promise of stem cells

Stem cells (SC) have been revolutionizing therapies, offering the hope of cure for innumerous untreated diseases and injuries (Trounson and McDonald, 2015a). Discoveries of the molecular mechanisms that determine and maintain the differentiation fate of pluripotent cells have allowed the generation of cells that can be used for transplantation or for regenerative therapies: restoring, correcting or modifying physiological functions by exerting a pharmacological, immunological or metabolic action while also supporting medical diagnosis (European Medicines Agency, 2004), and potentiating the development of cellular models to understand diseases' biology and drug discovery (Nirmalanandhan and Sittampalam, 2009).

Pluripotent stem cells (PSC) present a long-term self-renewal capacity and have a unique ability to differentiate into all mature cells of the human body. PSC can give rise to new SC and can differentiate into adult stem cells, which have a restricted renewal potential and that ultimately give rise to terminally differentiated cells (Figure 1.1).

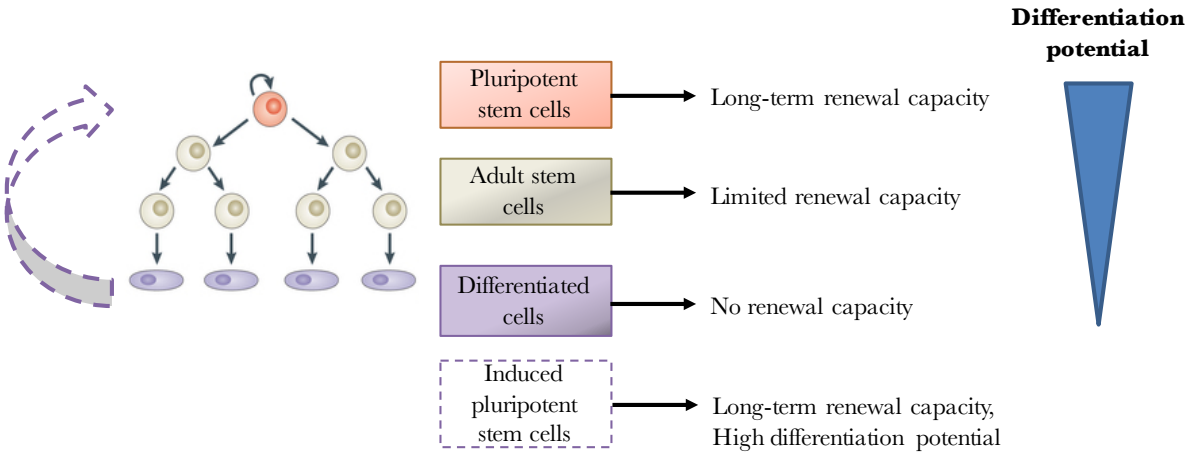

Figure 1.1 – Renewal capacity of pluripotent stem cells, adult stem cells and terminally differentiated cells. Adapted from (Beck and Blanpain, 2013).

Ten years ago, Yamanaka and co-workers discovered the possibility to terminally reverse differentiated cells into a pluripotency state using specific transcription factors known to be required for maintenance of pluripotency and proliferation (Oct3/4, Sox2, c-Myc, and Klf4) (Takahashi and Yamanaka, 2006). The generation of human induced pluripotent stem cells (hiPSC) readily gained popularity amongst the scientific community. Their resemblance with human embryonic stem cells (hESC) in terms of cell morphology, cell-surface marker expression, self-renewal ability, and potential to differentiate *in vitro* and *in vivo* into cells derived from all three germ layers (Takahashi et al., 2007), while overcoming the hESC's ethical

drawback associated with the use of embryos, made them a promise for cell therapy and clinical research. A decade later (Takahashi and Yamanaka, 2016), these cells have also been revolutionizing pre-clinical research, as a tool to generate effective disease models and for drug discovery (Avior et al., 2016).

Another stem cell class that has been emerging over the last decade as attractive candidates for cell therapy applications are human mesenchymal stem cells (hMSC) (Wei et al., 2013; Zaher et al., 2014). These cells were first isolated and characterized by Friedenstein and co-workers in the 1960s-1970s (Friedenstein et al., 1974; 1966), who isolated stromal cells from bone marrow (BM) by their plastic adherence, their colony-forming capacity (CFU-F) and ability to regenerate or support ectopic bone, stroma and hematopoietic tissues. Since then, MSC have also been isolated and characterized from several other adult and fetal tissues, including adipose tissue (AT) (Zuk et al., 2002), synovial membrane (De Bari et al., 2001), umbilical cord blood (Lee et al., 2004), amniotic fluid (Anker et al., 2003), placenta (Anker et al., 2004), amongst others (Murphy et al., 2013).

Due to their ability of being induced into osteogenic, chondrogenic and adipogenic lineages among other mesenchymal phenotypes, they were later named as 'mesenchymal stem cells' (Caplan, 1991). Since then, the defining characteristics of MSC are inconsistent among researchers and institutions (Dominici et al., 2006). Owen and co-workers, based on Friedenstein's work, established that CFU-F could be found in the BM stroma (Owen, 1988); thus, the International Society for Cellular Therapy (ISCT) established that MSC's designation should be 'multipotent mesenchymal stromal cells' (Horwitz et al., 2005). Nonetheless, recent trends in the scientific community suggest that MSC are derived from perivascular cells, pericytes, instead of originating from the marrow stroma (Caplan, 2008; Crisan et al., 2008), therefore it is expected that MSC's accurate terminology continues to evolve.

Since no specific cell surface markers have been identified to univocally classify MSC, the ISCT also established minimal criteria to characterize these cells: i) MSC must be plastic--adherent when expanded in standard culture conditions using tissue culture flasks; iia) more than 95% of the MSC population must express CD105 (endoglin, component of the transforming growth factor-beta (TGF-β) receptor complex (Pierelli et al., 2009)), CD73 (ecto 5' nucleotidase, responsible for the hydrolysis of AMP to adenosine and phosphate (Sträter, 2006)) and CD90 (Thy-1, glycoprotein involved in cellular adhesion and migration (Rege and Hagood, 2006)), as measured by flow cytometry; iib) MSC must lack expression (2-5% positive) of hematopoietic and other markers typical of cells present in MSC culture, such as CD45 (pan-leukocyte's marker), CD34 (primitive hematopoietic progenitors and endothelial cells' marker),

CD14 or CD11b (monocytes and macrophages' markers), CD79a or CD19 (B cells' markers) and HLA class II (activated MSC marker); and finally iii) MSC must have the ability for trilineage mesenchymal differentiation, differentiating into osteoblasts, adipocytes and chondroblasts using standard *in vitro* tissue culture differentiating conditions (Dominici et al., 2006).

Besides their mesenchymal stem differentiation potential, MSC have the capacity to migrate and engraft in sites of inflammation after systematic administration (Wang et al., 2012), secreting large quantities of multiple bioactive molecules (growth factors, cytokines and chemokines) with a regenerative potential (Caplan and Dennis, 2006), as presented in Figure 1.2. Thus, MSC can be considered as the body's natural "drugstore" (Caplan and Correa, 2011).

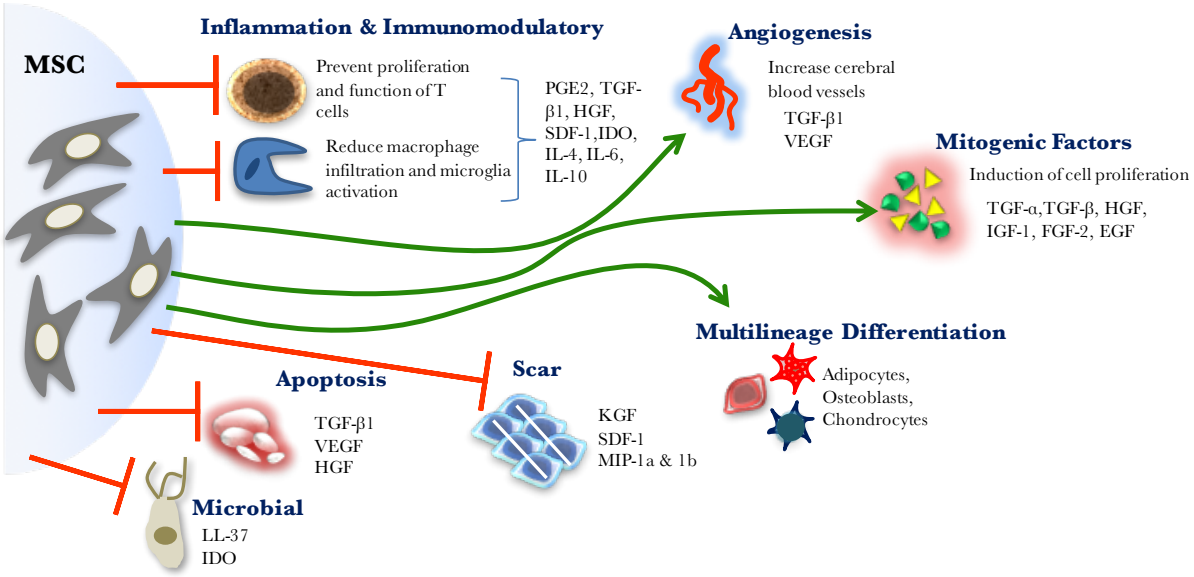

Figure 1.2 – MSC differentiation and secretory potential. Beside MSC's multipotent differentiation capacity, they can respond to the microenvironment by secreting trophic (angiogenic, mitogenic, anti-apoptotic anti-scarring), anti-inflammatory, immunomodulatory or antimicrobial factors. Adapted from (Murphy et al., 2013; Russotti, 2015).

MSC's trophic capacity is primarily correlated with their capacity in secreting growth factors and other chemokines (Figure 1.2), which induce cell proliferation and angiogenesis (Caplan and Dennis, 2006). Furthermore, they also produce mitogenic proteins (Figure 1.2) that can enhance vascular fibroblast, epithelial and endothelial cell division (Caplan and Correa, 2011). MSC's trophism is also correlated with the secretion of bioactive cues involved in the prevention of apoptosis and scar formation (Figure 1.2) (Caplan and Dennis, 2006). Moreover, MSC also have anti-microbial effects and possess the ability to modulate the regenerative environment via anti-inflammatory and immunomodulatory mechanisms (Figure 1.2) (Murphy et al., 2013).

Given MSC's dual functionality, it is important that cells' potency evaluation correlates with the their clinical purpose (Carmen et al., 2011). In fact, some authors have proposed additional phenotypic analysis correlated with MSC's secretome to be used in combination with the existing ISCT criteria, allowing an improved assessment of the potency of MSC before being used in a clinical setting (Samsonraj et al., 2015).

1.2. Human stem cells in clinical trials

The cell therapy field has been presenting a strong progression in the last years (Lipsitz et al., 2016; Mason et al., 2013), where forecasts estimate an annual turnover of $20bn worldwide by 2025 (Coopman and Medcalf, 2008), mainly by the use of stem cells, as the final product, in clinical applications.

Cell-based therapies can be either patient-specific (autologous), or based on healthy universal donors (allogeneic). Depending on the nature of the medical condition to be treated, either autologous or allogeneic therapies can be chosen (Malik, 2012). The choice between the two types of therapy drives the product safety and efficacy model as well as the approaches for manufacturing, transportation and clinical delivery of the product (Figure 1.3) (Hourd et al., 2008).

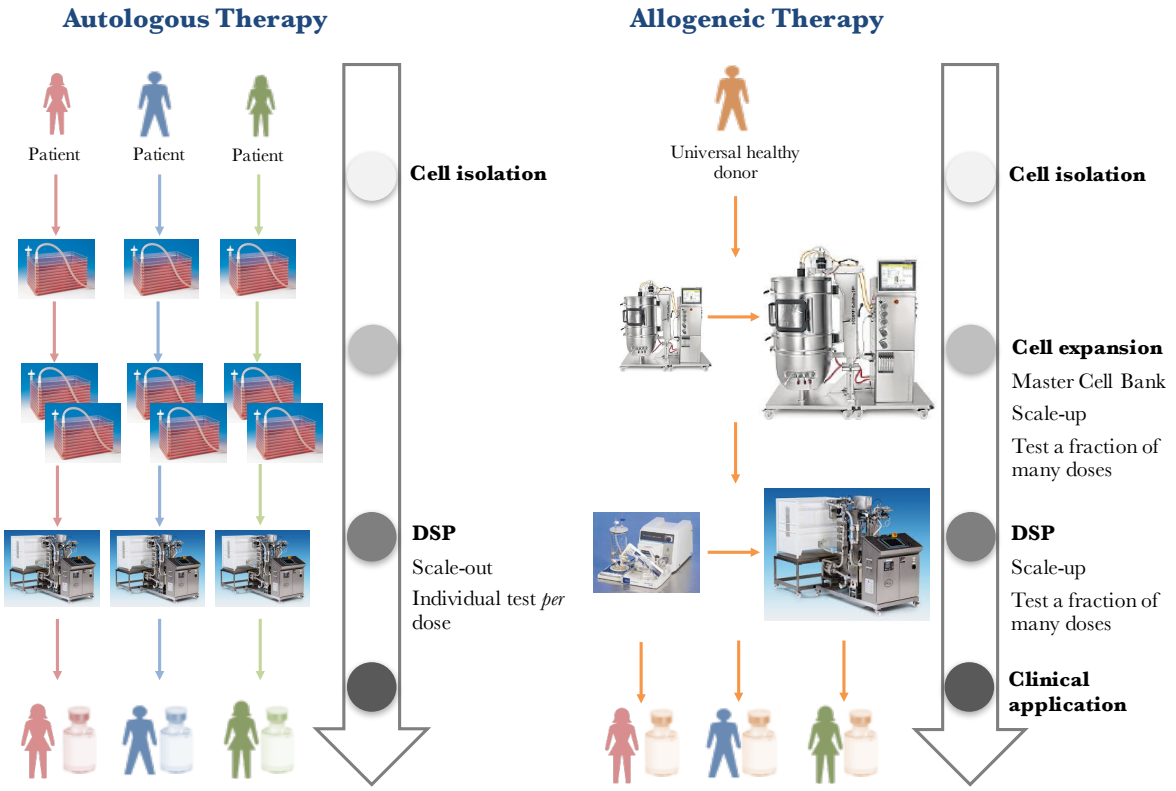

Figure 1.3 – Biomanufacturing workflow for autologous and allogeneic therapies. Autologous therapies are patient-specific, i.e., after cell isolation from the patient production processes are scaled-out, having a large number of small batches, requiring individual testing before clinical application. In allogeneic therapies,

cells are isolated from universal healthy donors, master cell banks are created, and a scale-up of the production is sought, having a small number of large batches, requiring testing of only a fraction of the lots before clinical application.

In autologous therapies, cells are harvested from the patient, sent away to a facility for manufacturing and then returned to the clinic for delivery into the patient. In terms of manufacturing, since the product is individualized, it is required to replicate several times the manufacturing line/unit operation to increase the number of batches (scale-out). Moreover, since each batch is intended for different patients, quality testing is required for each produced batch before clinical application (Eaker et al., 2013). This operation model presents several drawbacks related with the large holding time between the harvesting and infusion of cells, which may be crucial depending on the urgency of treatment (Hourd et al., 2008), and with age-related changes (for older patients) in cells that may compromise both their quality and quantity reducing the efficacy of treatment (Stolzing et al., 2008). In allogeneic cell-based therapies cells are derived from a healthy donor and are sent away to a facility to be expanded and to create a master cell bank; then after manufacturing, cells are shipped to the physician for subsequent delivery into the patient. In this case, the manufacturing output is increased by increasing the volume or number of cells processed for each batch (scale-up). Since there are no individualized batches, quality testing is required only for a small fraction of the production before clinical application (Hourd et al., 2008; Smith, 2012). Thus, in this case it is possible to have an "off-the-shelf" product, bypassing the holding time typical for autologous therapies. Furthermore, by establishing a GMP master cell bank from healthy donors, it is possible to decrease the impact of donor-to-donor variability in terms of treatment efficacy (de Soure et al., 2016).

Figure 1.4 shows the stem cells types currently used in a clinical setting both in autologous and allogeneic therapies. As observed in Figure 1.4A, hPSC use in therapies has already covered heart, eye diseases and diabetes (Lipsitz et al., 2016; Trounson and McDonald, 2015b). However, these comprise less than 3% of the current clinical trials, mainly due to hPSC ability in forming teratomas *in vivo* (Yamanaka, 2012), coupled with uncertainty within the scientific community regarding their characterization and safety. Currently, the vast majority of the clinical trials use hematopoietic stem cells (HSCs) and hMSC (https://clinicaltrials.gov/). Focusing on hMSC, beside their regenerative and secretory properties, these cells express moderate levels of human leukocyte antigen (HLA) major histocompatibility complex class I, lack major histocompatibility complex class II expression, and do not express costimulatory molecules B7 and CD40 ligand (Williams and Hare, 2011); thus, patients present a high

tolerance towards hMSC's transplant (as an allogeneic source). These reasons have contributed to the use of hMSC in therapies in more than 300 clinical trials at different phases (Figure 1.4B) for a variety of therapies (Figure 1.4C), including arthritis, cardiovascular, autoimmune and gastrointestinal diseases as well as in cancer, diabetes, and for the treatment of graft versus host disease (GvHD) (https://clinicaltrials.gov/; Murphy et al., 2013; Wei et al., 2013).

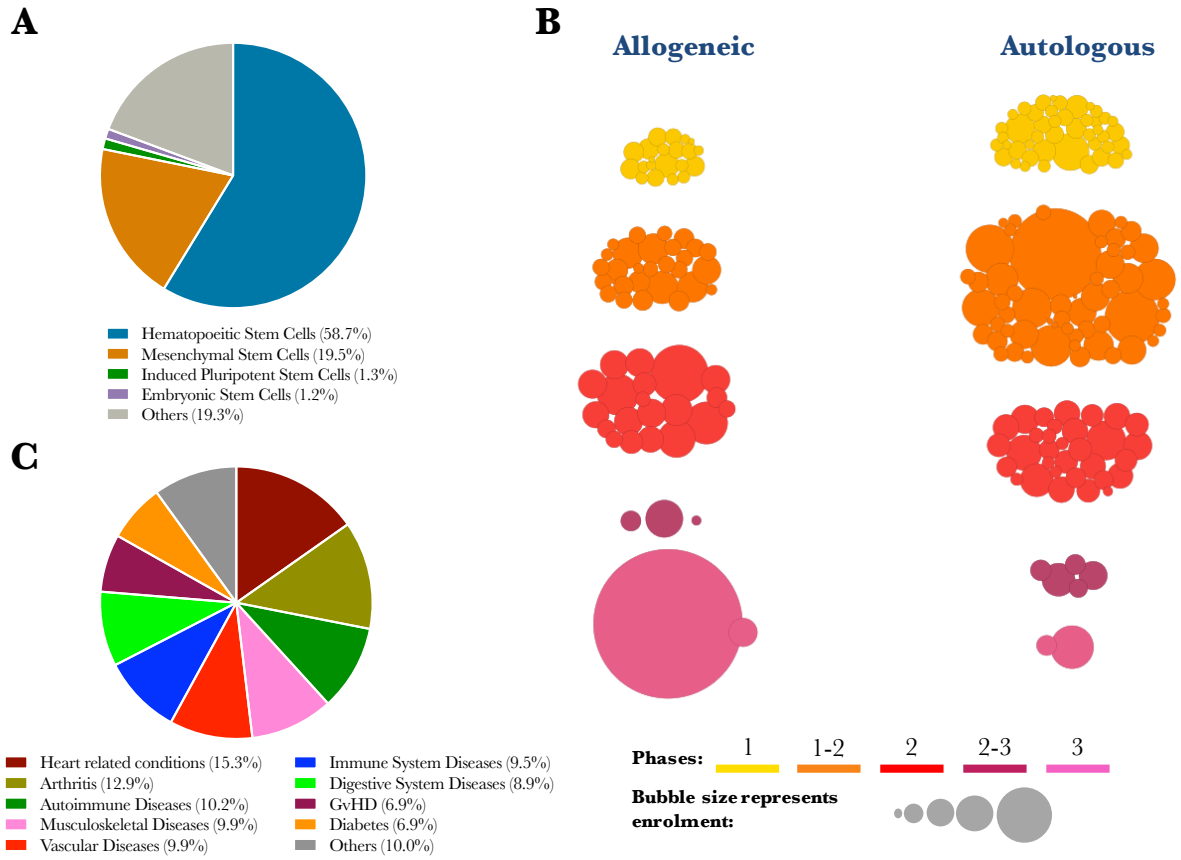

Figure 1.4 – Use of stem cells in cell therapy applications. (A) Types of stem cell used in clinical trials. **(B)** Clinical phases of autologous and allogeneic clinical trials of mesenchymal stem cells. **(C)** Common diseases treated with mesenchymal stem cells in clinical trials. Adapted from (https://clinicaltrials.gov/; https://www.terumobct.com/assets/data-vis/msc-clinical-trials/#).

Clinical trials already in Phase 3, correspond to the use of hMSC in the treatment of chronic heart failure (NCT02032004) and acute GvHD (NCT02336230) (allogeneic therapies) and in the treatment of early stage osteonecrosis (NCT01529008) and cirrhosis (NCT01854125) (autologous therapies) (https://clinicaltrials.gov/). More recently, some hMSC-based products have already received regional approvals for GvHD (Prochymal®, Osiris, Maryland, USA) and osteoarthritis (Cartistem®, Medipost, Co., Ltd., Gyeonggi-do, South Korea).

2. Stem cell manufacturing

2.1. General considerations

The use of cells as the final product in therapies has been bringing new biomanufacturing challenges, since cells possess a unique complexity when comparing to other biotherapeutics as small molecules (e.g. aspirin®), recombinant proteins (e.g. monoclonal antibodies, mAb), other biologicals (e.g. insulin) or vaccines. This complexity relies dually on their considerably high size, which can differ in surface area more than 6000 fold from a mAb, but also in the fact that cells are living and interacting entities that can trigger responses to the physical and chemical environment that surrounds them (Agashi et al., 2009; Al-Rubeai et al., 1995; Kretzmer, 2000). Thus, it is crucial that processes and unit operations previously optimized to process other biotherapeutics are redesigned and optimized to accommodate this new therapeutic product.

Depending on the nature of the cells, different therapies will require different bioprocessing techniques – e.g. cell separation, concentration, purification. However, all cell-based products will likely require a broadly common bioprocess workflow (Lapinskas, 2010), as presented in Figure 1.5.

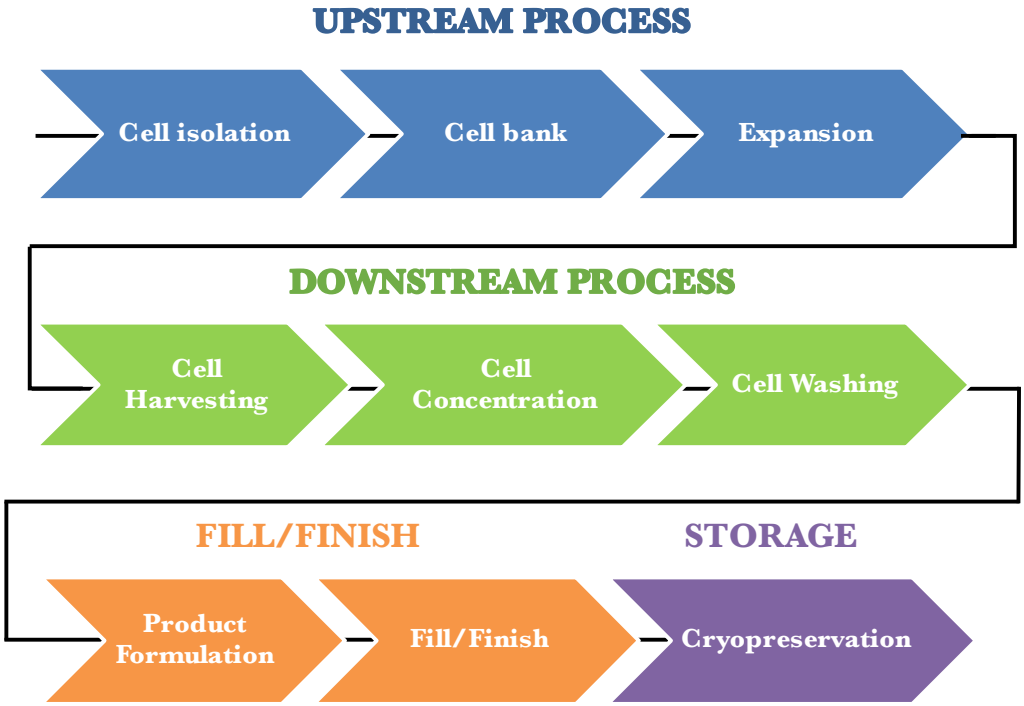

Figure 1.5 – Bioprocess workflow for cell-based therapies. Before being delivered to the clinic, cells need to be expanded in vitro up to numbers relevant for therapy. After harvesting, cells are concentrated, washed from remaining residuals from the expansion process, formulated into a cryopreservation medium, filled into aliquots and cryopreserved.

The establishment of robust and cost-effective manufacturing platforms that can ensure the efficient production, purification and formulation, while maintaining regulatory agencies' requirements in terms of identity, purity, potency, and viability throughout processing is still a challenge. Cellular therapies often require large cell numbers *per* dose (from 10^5 to 10^9 cells *per* patient) to be used in a clinical setting (Murphy et al., 2013; Simaria et al., 2014). Given cells' low abundance *in vivo* (Caplan, 1991), technologies that can successfully expand cells up to numbers relevant for therapies are still maturing (Rowley et al., 2012a), where microcarrier-based stirred culture systems have mostly been adopted to sustain cell expansion of adherent cells (Chen et al., 2013; Serra et al., 2012).

Furthermore, since cells are meant to be implanted, transplanted or infused into a human patient, they should meet specific criteria to be used as therapeutics (Murphy et al., 2013), in order to guarantee their safety and efficacy. To fulfill the purification requirements, after cell detachment from the microcarriers, cell clarification (i.e. cell-microcarrier removal), cell concentration (volume reduction) and cell washing (removal of remaining impurities) will be necessary (Pattasseril et al., 2013). The concentrated and purified cells need afterwards to be formulated with a cryopreservation buffer, where usually the cell concentration is adjusted so that the final filled product dose delivers the specified quantity of cells for the therapeutic action. The formulated bulk cell suspension is then filled into containers, cryopreserved using controlled-rate freezers and stored in the vapor phase of liquid-nitrogen (Pattasseril et al., 2013), ready to be delivered to the clinic.

2.2. Product requirements and process development

Despite the cell therapy strategy (autologous or an "off-the-shelf allogeneic" model), it is necessary to thoroughly characterize the therapeutic cell, defining the properties that confirm acceptable production, and thereby reduce the risk of incorporating variances in cell function, which may compromise safety or efficacy. Common considerations of robustness, reproducibility of manufacturing processes include the use of well-defined raw materials and the application of methods under current good manufacturing practice (cGMP), which are necessary for regulatory approval and batch consistency. Moreover, the control of the cost of goods (COGs) is fundamental, since manufacturing and testing processes beside being complex and labor-intensive, often use expensive raw materials (Campbell et al., 2015).

When establishing biomanufacturing processes for cellular products, it is fundamental to define the quality target product profile (QTPP), as it will directly affect the process development (Lipsitz et al., 2016). The QTPP describes the properties of the desired end

product, such as identity, potency and purity, and is the starting point for all quality-by-design (QbD) approaches (Food and Drug Administration, 2009). As an example, an overview of the QTPP for a hMSC cell therapy product in phase 3 clinical trial (NCT02336230) is provided in Table 1.1.

Table 1.1 – Quality target product profile (QTPP) for a hMSC cell therapy product. The information provided corresponds to MSC-100-IV (Mesoblast Ltd, Melbourne, Australia) for the treatment of acute GvHD (Lipsitz et al., 2016).

Property	Acute GvHD
Therapy type (patient specific or off-the-shelf)	Allogeneic
Identity (cell phenotype, morphology)	ISCT panel (section 1.1)
Viability	High cell viability (typically >70–80%)
Potency (ability of cells to perform desired action)	Secreted factor profile
Dose and administration (quantity of desired cells)	2×10^6 cells/kg Administered twice a week (intravenous) for 4 weeks
Cellular impurity to minimize (cells in final product to minimize)	None
Impurities and microbiology (below threshold)	Endotoxin, mycoplasma, bacteria, viruses, particulates, ancillary materials
Karyotype (as expected)	Normal
Storage and stability (assessed by potency assay)	Frozen product stable >6 months
Reference	(Newman et al., 2009)

After defining the QTPP, the attributes that directly influence the safety and efficacy of the product (critical quality attributes, CQA), and the parameters that influence these same attributes (critical process parameters, CPP) are identified, developing a design space that quantifies how parameter variability affects the quality attributes, usually incorporating the strategies of design of experiments (DoE) and process analytical technology (PAT) (Campbell et al., 2015; Lipsitz et al., 2016). Consequently, a control strategy is developed to maintain process parameters within a range that ensure product quality, and the process is validated at scale. In contrast to traditional control strategies based on discrete set points, QbD identifies acceptable operating intervals, or multivariate design spaces, within which a process will

produce high-quality products. Once implemented, the design and process development and optimization steps have an interactive relationship that is continually refined, as the process knowledge increases (Figure 1.6) (Lipsitz et al., 2016).

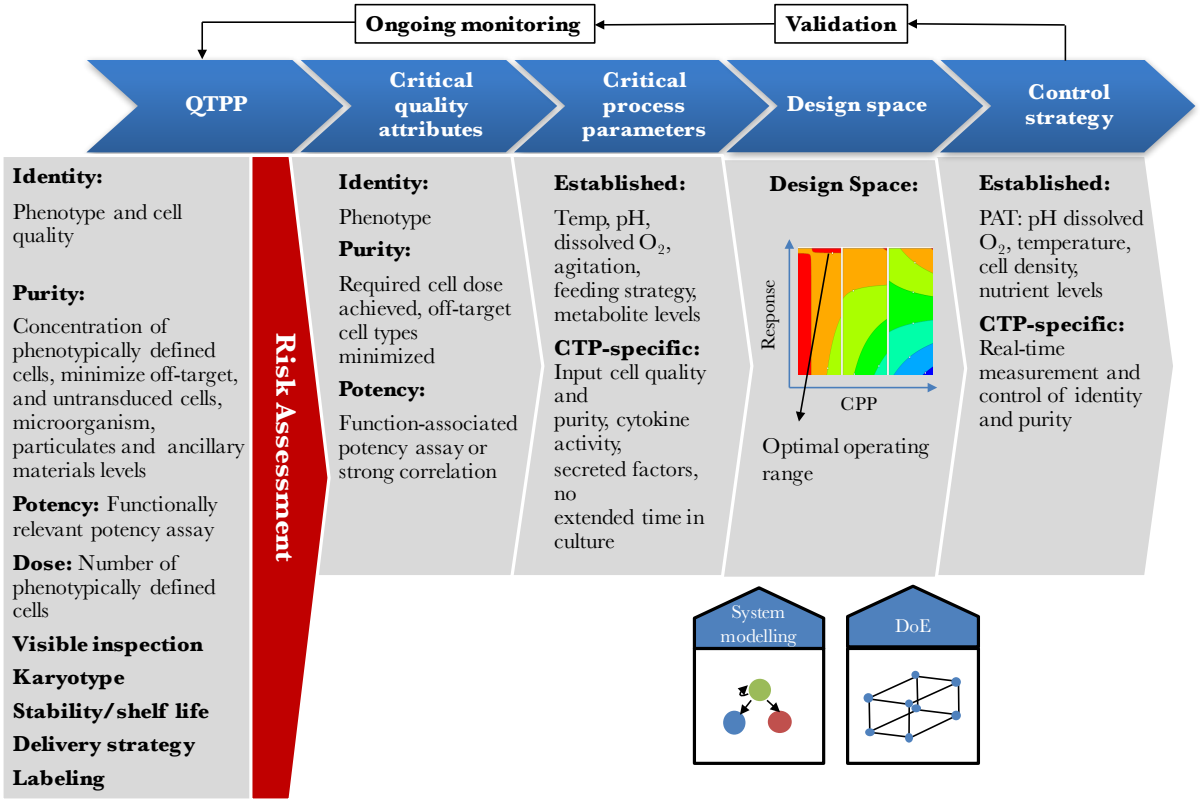

Figure 1.6 – The QbD process. The quality target product profile (QTPP) in terms of quality, safety, and efficacy is first defined. Then, the quality attributes that are critical for meeting the QTPP are determined by a risk assessment. The critical process parameters (CPP) and materials attributes that affect the critical quality attributes (CQA) are identified, and their effects on critical quality attributes are quantified in a design space. Usually, a control strategy can be developed to ensure that CPP remain within the optimal operating range, in which production of quality product is ensured. Finally, the process is validated in the manufacturing facility at the desired scale, and is continually monitored and improved during manufacturing, as the process knowledge increases. Adapted from (Lipsitz et al., 2016) (CTP: Cell therapy product).

It is accepted at the moment that CQA of cell therapy products correspond to their identity, purity and potency (Campbell et al., 2015; Lipsitz et al., 2016; Pattasseril et al., 2013).

Cell identity (immunophenotype) is often complex and not always entirely understood. Identity is usually demonstrated by flow cytometry through the expression of cell surface marker proteins, which are related with functional activity (Lipsitz et al., 2016). However, due to the targeted nature of this approach, frequently other markers whose expression varies during the manufacturing process are ignored. Thus, the establishment and development of more sensitive and robust methodologies (e.g. "omics"), which allow for a better cell characterization, increasing product and process understanding are fundamental (Campbell et

al., 2015; Gomes-Alves et al., 2016; Martin et al., 2016). For the particular case of hMSC, since their clinical focus is now shifting from a multipotent cell-replacement therapy towards immune modulation therapies, and given the multiplicity of source tissues containing hMSC, some authors have proposed the establishment of new identity criteria, complementing ISCT's to specify the therapeutically relevant subpopulations under consideration (Lipsitz et al., 2016; Samsonraj et al., 2015).

Since cell therapy products are meant to be delivered to human patients, it is crucial to ensure that they are pure enough to be safe to administer. Impurities can include undesirable cell types, components from the expansion process, ancillary materials and particulates, and the thresholds for cell purity may vary between therapies (Lipsitz et al., 2016). An important purity concern corresponds to cells' contamination by microorganisms (bacterial, fungal and mycoplasma), endotoxins and cell line cross-contamination, which may hamper their use in therapies (Pattasseril et al., 2013). Unlike other biotherapeutics, cells are too big to be terminally sterilized; thus, functionally closed processing system and the use of disposable materials ensuring sterile production, significantly reduces the risk of exogenous contamination. Non-cell particulates (e.g. plastic fragments from disposables and residual microcarriers) from manufacturing equipment and materials may cause secondary adverse effects when administered, and therefore must be controlled and minimized throughout processing (Clarke et al., 2016). Finally, ancillary materials used for the production of cell therapy product as bioactive chemicals, including cytokines, small molecules, serum and vectors must be removed before the delivery of the final product. Several research groups and companies still expand hMSC using expansion media supplemented using fetal bovine serum (FBS) (Capelli et al., 2015; Rafiq et al., 2013). Given the main drawback associated with the use of FBS (Léo et al., 2008), regulatory agencies stipulate that if serum is used at any stage of the bioprocess workflow, its concentration in the final formulation shall not exceed 1 ppm (Food and Drug Administration, 2014). Thus, to achieve acceptable levels of ancillary materials on the QTPP to ensure product safety (Atouf et al., 2013), additional processing may be necessary, which can affect the final cell recovery yield (Lipsitz et al., 2016).

Alongside the desirable identity and purity of cell therapy products, it is also essential to evaluate their function, as demonstrated by *in vitro*, and if necessary *in vivo*, functional assays. Cells' potency provides a measure of activity for the intended use and is an important tool to evaluate the impact of processing on the cells' CQA (Bravery et al., 2013). Potency corresponds to the effectiveness of the cell therapy product towards a clinical indication and should be considered together with the quantity of viable cells in a dose. Ideally, it is expected that cell

therapy products have a minimum acceptable viability of 70% (ideally >85%) when delivered to the clinic (Pattasseril et al., 2013). From a risk and cost perspective, cell therapy products with high potency at the lowest minimum acceptable viability are preferred (Lipsitz et al., 2016). Moreover, the development of potency assays that allow to evaluate cells' mechanisms of action towards the intended clinical use need to be developed; assays of trilineage differentiation potential as a measure of MSC potency are appropriate if they are intended to be used in regenerative medicine applications (Law and Chaudhuri, 2013). Since many MSC therapies are now exploiting the secretion ability of paracrine factors, testing the bioactivity of secreted cytokines is a more appropriate measure of potency for these cases (Samsonraj et al., 2015).

2.3. hMSC expansion for clinical applications

Cell therapy products demands high numbers of cells, with lot sizes ranging from 10^8 to 10^{12} cells, as exemplified in Table 1.2. Typically, manufacturing platforms achieve one log of expansion, thus manufacturing at this scale can be challenging (Rowley et al., 2012a).

Due to hMSC low frequency *in vivo*, their expansion *in vitro* is compulsory. hMSC are adherent cells, hence traditional strategies for their *in vitro* expansion of these cells typically rely on static planar systems (e.g. multi and mono-layered tissue culture flasks). However, the inherent uncontrollability, heterogeneity and limited productivities typical for this system has been driving the cell therapy industry towards dynamic stirred culture systems using microcarriers (Chen et al., 2013). Figure 1.7 presents a comparison between static planar and dynamic stirred culture systems using microcarrier technology.

Depending on the therapy type, it is estimated that cell doses of from 10^6 to 10^7 cells can be produced using planar technology either by manual or automated manipulation (Simaria et al., 2014). However, when the demand increases further, cell expansion becomes extremely labor intensive, costly, and impractical (Rowley et al., 2012a). Therefore, under these scenarios ($> 10^7$ cells/dose) microcarrier technology and stirred tank bioreactors become the most cost effective approach for cell expansion.

Table 1.2 – Characteristics of cell therapy products' doses currently in clinical trials. Data shown in this table correspond to allogeneic therapies. Adapted from (Simaria et al., 2014).

Indication	Cell types under investigation	Cells/dose
Acute kidney injury	Bone-marrow (BM) derived hMSC	2×10^8
Acute myocardial infarction	BM or other nonembryonic tissue source-derived Multistem	$0.2 - 1 \times 10^8$
Chronic Discogenic Lumbar Back Pain	BM derived adult mesenchymal precursor cells	$0.6 - 1.8 \times 10^7$
Congestive heart failure	BM derived adult mesenchymal precursor cells	1.5×10^8
Critical limb ischemia	Placenta-derived PLX-PAD stromal cells (hMSC-like)	$1.5 - 3 \times 10^8$
Crohn's disease	Adipose tissue (AT) derived expanded stem cells (eASCs); BM derived hMSC	2.4×10^7; $6 - 12 \times 10^8$
Dry eye related macular degeneration	Embryonic stem cell derived retinal pigment epithelial (RPE) cells	$0.5 - 2 \times 10^5$
Graft vs. host disease	Umbilical cord blood derived hMSC; BM derived hMSC; BM or other nonembryonic tissue source-derived Multistem	$1 - 5 \times 10^8$; 1.6×10^9; $0.5 - 1 \times 10^9$
Ischemic stroke	Human foetal brain stem cell-derived hNSC; BM derived hMSC; BM derived hMSC	2×10^7; $0.5 - 1.5 \times 10^8$; 2×10^8
Liver disease	AT derived stromal cells	$0.1 - 1 \times 10^9$
Osteoarthritis	BM derived hMSC; Umbilical cord blood-derived hMSC (hUCB-MSC)	$5 - 15 \times 10^7$; 3.5×10^7
Peripheral vascular diseases	Menstrual blood-derived Endometrial regenerative cells (hMSC-like)	$0.25 - 1 \times 10^8$
Prostate cancer	Prostate tumour derived cancer cell line	$2 - 4 \times 10^7$
Rheumatoid arthritis aggravated	AT derived expanded stem cells (eASC)	$1 - 4 \times 10^8$
Spinal cord injury	hESC-derived oligodendrocyte progenitor cells; Foetal-derived hNSCs; Brain-derived hNSCs	2×10^6; 2×10^7; 1×10^8
Type I diabetes	BM derived hMSC	6×10^8
Type II diabetes	BM derived adult mesenchymal precursor cells	$0.1 - 2 \times 10^8$
Ulcerative colitis	BM derived multipotent adult progenitor cell (MAPC)	1.8×10^8

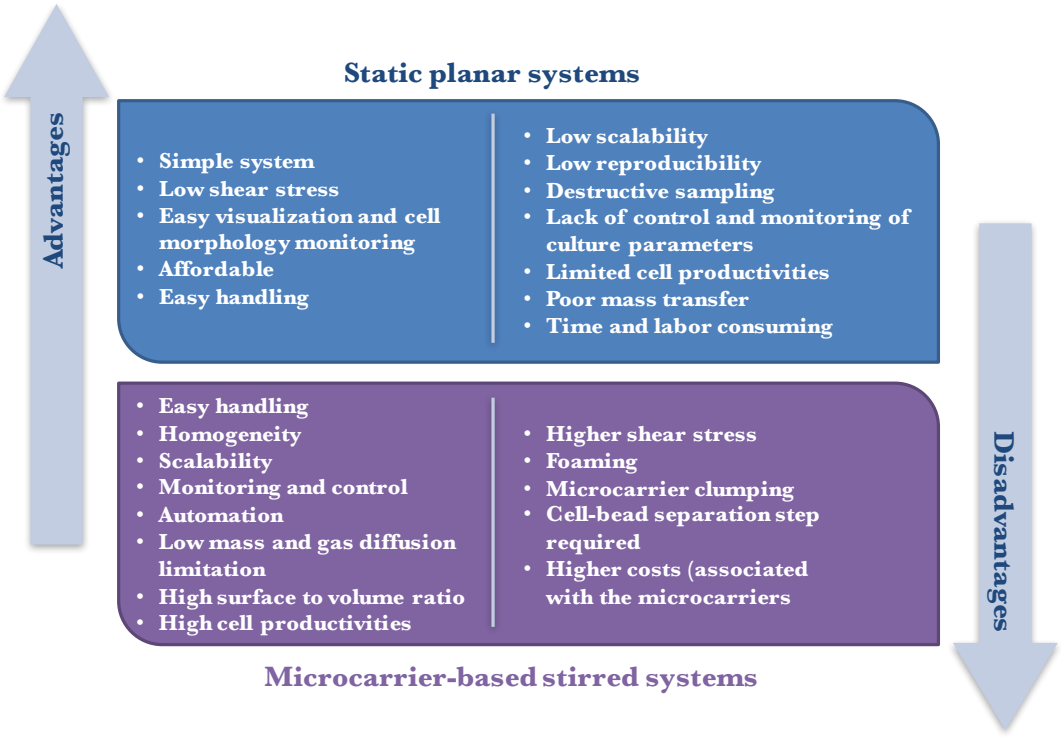

Figure 1.7 – Comparison between static planar and dynamic stirred systems using microcarrier technology. Adapted from (Castilho et al., 2008).

There are many closed systems exploiting the use of disposable materials commercially available for the expansion of stem cells. Examples include stirred tank single-use bioreactors (as Mobius CellReady, Millipore, Massachusetts, USA, or Univessel, Sartorius Stedim Biotech, Göttingen, Germany) (Niss et al., 2013), wave bag bioreactor (Cultibag, Sartorius Stedim Biotech, or WAVE bioreactor, GE Healthcare Bio-Sciences, Björkgatan, Sweden) (Correia et al., 2014), pneumatically mixed bioreactor (PBS 3, PBS Biotech, California USA) (Sousa and Silva et al., 2015) or hollow fiber perfusion culture (Quantum cell expansion system, Terumo BCT, California, USA) (Martin-Manso and Hanley, 2015). Many studies reported in the literature have been supporting the use of these systems using either bovine serum or serum-free, xeno-free expansion media for cell therapy applications (Table 1.3).

hMSC are anchorage-dependent cells, and thus require a support matrix (microcarrier) that allows their expansion in suspension systems. Microcarriers have high surface-to-volume ratios, accommodating higher cell densities than static cultures *per* volume of culture. The surface area available for cell growth can be adjusted by manipulating the amount of microcarriers, which further facilitates the process' scale-up (Castilho et al., 2008).

Table 1.3 - Studies reporting hMSC's expansion in different bioreactor systems, followed by DSP. (MC: microcarriers; DMEM: Dulbecco's modified Eagle's medium; FBS: fetal bovine serum; N/A: Not applicable/not performed; SFM: Serum free media; XF: xeno-free media; ST: stirred tank)

USP process conditions	DSP operating conditions		Results	Reference
System: ST bioreactor (disposable) Volume: 3 L Medium: DMEM+10% FBS+supplements Strategy: BM-MSC in MC	Clarification: Volume reduction: Cell washing:	Not performed Not performed Not performed	**USP:** 12 days max: 2 x 10^5 cell/mL **DSP:** N/A	(Niss et al., 2013)
System: ST bioreactor (disposable) Volume: 2 L (1), 35 L (2) Medium: Lonza Medium + 5% FBS Strategy: AT-MSC in ProNectin® F-Coated MC	Clarification: Volume reduction: Cell washing:	63 µm sieve (3) Not performed Not performed	**USP:** (1) 7 days (max: 2.7 x 10^5 cell/mL) (2) 8 days (max: 3.1 x 10^5 cell/mL) **DSP:** (3) 90% Cell recovery yield	(Schirmaier et al., 2014)
System: ST bioreactor Volume: 1 L Medium: StemPro® MSC SFM XF Strategy: BM-MSC in Plastic MC (1) AT-MSC in Plastic MC (2) BM-MSC in Plastic MC (3) (Perfusion in 0.4 L ST)	Clarification: Volume reduction: Cell washing:	Not performed Not performed Not performed	**USP:** (1) 7 days (max: 1.1 x 10^5 cell/mL) (2) 7 days (max: 4.5 x 10^4 cell/mL) (3) 11 days (max: 5.0 x 10^5 cell/mL) **DSP:** N/A	(dos Santos et al., 2014)
System: ST bioreactor Volume: 2.5 L Medium: DMEM + 10% FBS Strategy: BM-MSC in Plastic MC	Clarification: Volume reduction: Cell washing:	60 µm sieve Not performed Not performed	**USP:** 9 days (max: 1.7 x 10^5 cell/mL) **DSP:** cell recovery yield not reported	(Rafiq et al., 2013)
System: ST bioreactor Volume: 1.5 L Medium: DMEM/F12 + 3% FBS Strategy: BM-MSC in Cytodex-3 MC	Clarification: Volume reduction: Cell washing:	Not performed Not performed Not performed	**USP:** 5 days (max: 2.6 x 10^6 cell/mL) **DSP:** N/A	(Zhou et al., 2013)

Moreover, microcarrier cultures also offer the possibility of increasing the number of population doublings by the addition of empty microcarriers during culture time; hence, hMSC can transfer from bead to bead, colonizing the empty added microcarriers, extending culture periods without needing an enzymatic dissociation step (Hervy et al., 2014; Schop et al., 2010). This has a significant impact in manufacturing, reducing the costs of cell expansion by reducing the amount of media, growth factors and other expensive supplements used in stem cell growth. Nowadays, there is a wide range of microcarrier types commercially available. Microcarriers have different physical properties (as stiffness and nanotopography) and can be either porous or non-porous; they can be manufactured from different materials as polystyrene, gelatin, glass, alginate or dextran (de Soure et al., 2016). Moreover, microcarriers can be functionalized with different coating materials (ECM proteins, small molecules) in order to further improve cell attachment and growth.

2.4. Downstream processing of hMSC

2.4.1. Technology landscape

A comprehensive knowledge of cells' CQA can dictate the requirements of downstream processing technologies (Table 1.4). Effective cell separation methodologies should ensure high purity and yield while maintaining cell function. These can exploit either cells' physicochemical properties - such as size (centrifugation and filtration), density (density gradient centrifugation), light scattering properties (cell sorter), membrane potential, pH, electrical impedance and charge (aqueous two-phase system and free-flow electrophoresis), - or can exploit affinity interactions (using cell-surface molecules) (González-González et al., 2011).Thus, depending on the cell type used for therapies, beside the typical DSP train for purification (microcarrier removal, volume reduction and cell washing), cell separation may also be required. For example, hPSC therapy carry a risk of teratoma formation by residual undifferentiated cells remaining among the differentiated products (Blum and Benvenisty, 2008). Hence, several research groups have been exploring affinity methods to eliminate pluripotent cells (Ben-David et al., 2013; Tang et al., 2011). However, these still pose several limitations to be used at larger scales (Kumar and Srivastava, 2010). In order to overcome these, researchers have been trying to implement chromatography for stem cell separation, exploring monolithic chromatography columns (Kumar and Srivastava, 2010), or immunoaffinity expanded bed adsorption (EBA) (monocyte-human peripheral blood separation) (Ujam et al., 2003).

Table 1.4 – Product and DSP requirements for cell-based therapies. Adapted from (Pattasseril et al., 2013).

Product requirement	Relation to DSP requirement
Cell viability: >80%	Frozen at >85% viability; Controlled freezing profiles; Controlled processing times, <4 h *per* unit operation; Same-day processing (up to 12 h).
Specified number of viable cells: >80% viable cell recovery	Consistent and accurate fill volumes; Minimal volume loss during thaw; Robust formulation step.
Cell concentration: 10 – 100 x 10^6 cell/mL	Achieve high concentration factor during volume reduction step with minimal cell loss or damage; Low system volume (hold-up volume) in the volume reduction step.
Single-cell suspension	No/minimal clumps of cells at fill; No pelleting.
Impurities: < 1 ppm	No other cellular impurities; High efficiency wash step; Cells in suspension during wash step (avoid aggregation); Low system volume.
Maintenance of product quality attributes	No cell damage; Low-shear processing; low processing time.

Only a limited number of DSP technologies can comply with the particular manufacturing specifications for volume reduction and cell washing unit operations of autologous and allogeneic cell therapies. Technology requirements include having methodologies that can be easily scalable, automated and provide a low-shear processing environment (Pattasseril et al., 2013). DSP technologies must be flexible to cope with different scales of production (scale-up and scale-out), and withstand achieving a wide range of cell concentrations (10 – 100 x 10^6 cells/mL) (Table 1.2). Furthermore, it is highly desirable to perform process integration by accomplishing different unit operations (e.g. volume reduction and washing steps) using the same device, thus decreasing footprint. The processing time should be minimized, and cell viability should be ideally higher than 85% (Pattasseril et al., 2013). As mentioned in the previous section, because cells cannot be terminally sterilized, DSP technologies should be closed and use disposable components to reduce the risk of exogenous cross contamination, while ensuring consistency and efficiency during processing (Placzek et al., 2009; Ratcliffe et al., 2011).

Early downstream processing efforts focused on using technologies that applied centrifugation, separation and/or filtration principles adapted from the blood processing

industry to process the harvested volumes of cell therapy. An example corresponded to the use of the COBE 2991 (Terumo BCT), which operates by density gradient centrifugation. This system provided automation, increased control, and could concentrate and wash cells through disposables to prevent possible contamination issues. However, it was soon found that the scale of this system was a limitation, since less than one liter could be processed *per* cycle (Pattasseril et al., 2013). The Carr Centritech Cell II (Pneumatic Scale Angelus, Barry-Wehmiller Company, Missouri, USA) and the Elutra Cell (Terumo BCT) separation systems, operated by continuous flow centrifugation, were also initially used. Nonetheless, either the lack of automation or the inability to easily integrate a washing step within the same device, were important drawbacks that hampered their adoption in cell therapy manufacturing (Hassan et al., 2015; Pattasseril et al., 2013).

To suit these particular demands for the downstream processing of therapeutic cells, mature DSP technologies from well-established applications, based on filtration, size exclusion and centrifugation (Pattasseril et al., 2013), are now being rethought and redesigned to perform cell clarification, cell concentration and washing (Table 1.5). Fluidized bed centrifugation (FBC), as kSEP® (a fluidized bed centrifuge made by kSep Systems Inc., KBI Biopharma, Durham, USA) (Dragani et al., 1990; Ko and Bhatia, 2012), and tangential flow filtration (TFF) (Cheryan, 1998; van Reis et al., 1997) technologies have been considered to have significant potential for DSP large-scale concentration and washing of therapeutic cells, not only due to their mild operation mode, but also for their scalability, use of disposable devices, applicability to both scale-out and scale-up manufacturing approaches, and capability to integrate both volume reduction (VR) and washing steps in the same device (Pattasseril et al., 2013). From an economical point of view, it would be advantageous to perform microcarrier removal and VR and cell washing unit operations using the same technology, minimizing losses between steps (Hassan et al., 2015). Thus, the use of kSEP® and TFF would be desirable to perform this DSP step. However, either engineering challenges or lack of devices with an appropriate pore size, have been delaying the use of TFF membrane technology for this purpose. Alternatively, other technologies for microcarrier separation are being developed based on dead-end filtration using microfiltration membranes (Szczypka et al., 2014); an example corresponds to the Harvestainer® (ThermoFisher™ Scientific, Massachusetts, USA) used to separate viable cells from microcarriers at larger volumes.

Nevertheless, before their application, it is fundamental to understand how the process parameters impact not only cell recovery yields, but also cells' characteristics and quality. The choice between these two technologies should be dependent on the dose planned to be delivered

to patients, and done early on the bioprocess timeline to ensure later-stage success and also to minimize eventual manufacturing bottlenecks, as well as further comparability studies.

2.4.2. Continuous centrifugation

Centrifugation is widely applied both in research as well as in an industry setting for processing biopharmaceuticals. Its low running costs, straightforward process development and operating robustness (Axelsson, 2002), makes it extensively used for concentrating and washing cell therapy products at research scale (Heathman et al., 2015; Veraitch et al., 2008). However, it is heavily operator dependent and prone to contamination. Continuous centrifugation, as opposed to batch centrifugation, emerged as a time-saver technique, allowing to centrifuge large volumes of material at high centrifugal forces without needing to fill or decant centrifuge tubes, or frequently starting and stopping the operation (Roush and Lu, 2008). Continuous centrifugation can be operated either in an orthogonal flow or in a counterflow (or fluidized bed) operation mode.

In orthogonal continuous centrifugation, the fluid flows perpendicular to the centrifugal force, and thus particles may be concentrated by pelleting onto the wall of the rotor bowl or by banding in a gradient (Roush and Lu, 2008). This operation may be performed using a continuous orthogonal flow with single-chamber (e.g. Unifuge, Carr Centritech) or with disc-stack systems (e.g. Culturefuge, Alfa Laval, Lund Sweden) (Pattasseril et al., 2013) (Table 1.5). In these systems, cells are compacted, which decreases the washing efficiency. Separate washing steps could be performed to remove residuals, which is undesirable since it can lead to cell losses of 10–30% (Pattasseril et al., 2013), hampering its use for cell therapy applications.

In counterflow operation (or fluidized bed centrifugation) there is a balance between the application of opposing forces as the fluid flow and centrifugal force, resulting in the formation of a fluidized bed of cells. FBC is a low shear technology, since cells are not packed against the centrifuge wall, but remain in suspension while the supernatant and residuals are cleared instead (Ko and Bhatia, 2012). The Elutra cell separation system and kSEP® are examples of counterflow continuous centrifugation systems (Table 1.5). The kSEP® system enables the recovery of over 80% of cells, while maintaining high cell viability (> 90%) and allows for efficient removal of residuals after washing (Pattasseril et al., 2013). These systems (https://www.ksepsytsems.com) have a wide range of single-use chamber capacities, ranging from 0.4 to 6 L, which can potentially handle hundreds of liters from the expansion process. This system, although having a remarkable potential for cell therapy applications, has a high capital expense to be used for cGMP, and the process development costs can also be high for

processing the large number of cells required for meaningful development runs because scale-down modeling is not achievable (Pattasseril et al., 2013). Nonetheless, for higher cells per lot (dose of 10^8 and higher) achieved in large single-use bioreactors (typical for allogeneic therapies), FBC is the most feasible option for cell concentration and washing (Hassan et al., 2015).

2.4.3. Filtration

Filtration has been widely used in many different areas from the food to the biopharmaceutical industry. This methodology allows to physically separate solid particles from a fluid-solid mixture according to their size differences, by forcing the fluid through a filter-membrane (Doran, 1995), where particles smaller than the pores of the membrane will permeate through, whereas larger components than the pores will be retained. Filtration can be performed either using a normal flow (dead-end filtration) or a cross flow (tangential flow filtration) (Figure 1.8). In both cases, the pressure gradient formed across the membrane (trans-membrane pressure), is the driving force of this process (Cheryan, 1998). Given the cell size (15 - 25 µm), typically microfiltration membranes are used for cell separation processes (Charcosset, 2012).

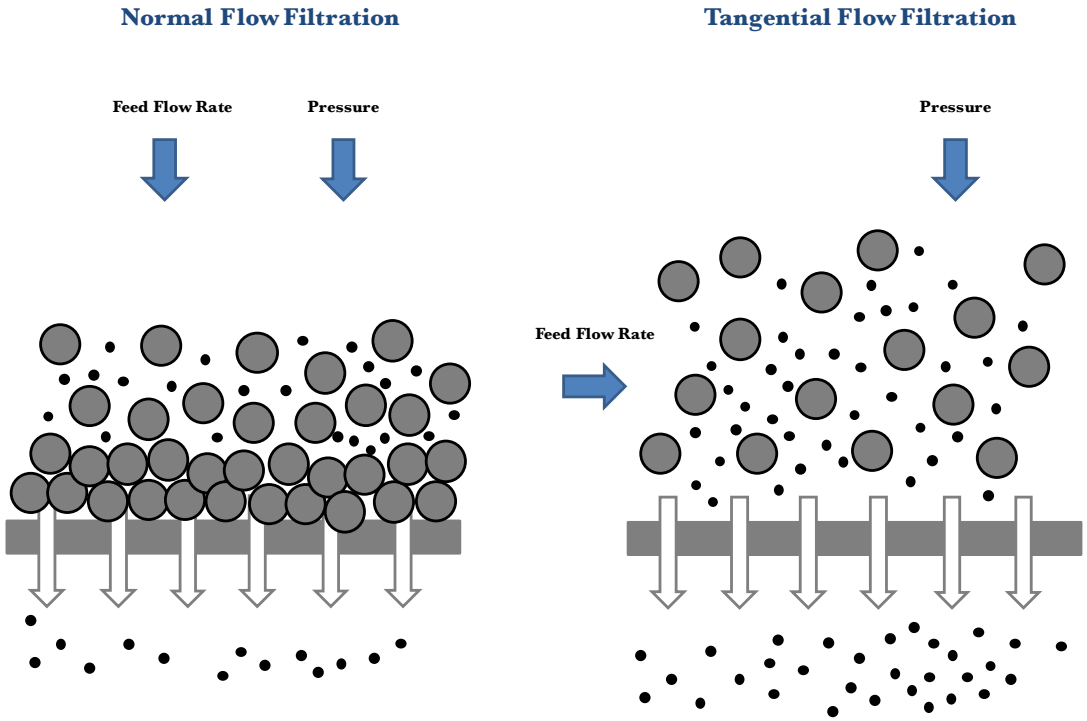

Figure 1.8 – Normal flow and tangential flow filtration processes. In normal flow filtration operation, the fluid flows perpendicular to the filter membrane, whereas in tangential flow filtration the fluid flows parallel to the filter membrane.

Table 1.5 – Scalable technologies for cell therapy downstream processing. Comparison of different available technologies in terms of system attributes, and performance. Adapted from (Pattasseril et al., 2013).

Technology	**Filtration**		**Continuous centrifugation**	
	Cell therapy industry-TFF		**Fluidized Bed**	**Orthogonal**
Product name (manufacturer)	CT-TFF (Lonza)	Uniflux (GE Healthcare)	kSep 400 and 6000S (KBI Biopharma)	Carr Centritech (Pneumatic S. Angelus)
System Attributes				
Autologous/allogeneic	Both	Allogeneic	Allogeneic	Allogeneic
Closed system	Yes	Yes	Yes	Yes
Integrated concentration and washing	Yes	Yes	Yes	No
Degree of automation	Medium	High	High	High
Disposability, ready to use	Yes	Not yet	Yes	Yes
Additional equipment/ utilities required	None	None	Tube welder and sealer	Air
System set-up and risk	Easy/low	Easy/low	Difficult/medium	Easy/medium
Tubing connections (flexibility)	Highly flexible, integrated, quick connections	Flexible	Not flexible, must use welder and sealer	Flexible
Performance Attributes				
Flow rate capacity (L/h)	1 – 750	25 – 1250	1 – 720	6 – 360
Cell number capacity	1 – 100 x 10^7	>100 x 10^7	6 – 30 x 10^7	20 – 100 x 10^7
Scalability	High	High	Medium	Low
Operational labor	Medium	High	Medium	Medium
Process/product monitoring	High	High	Low	Low
In-line metrics	Pressure, flow, viable cell density	Pressure, flow, temperature	Speed, flow	Speed, flow, temperature

In normal- flow filtration (NFF), liquid flows perpendicular to a filter membrane, typically involving disc or cartridge type filters. This type of filtration is primarily used for systems in which the retained components are present at very low concentrations (van Reis and Zydney, 2007). Thus, NFF is typically applicable for sterilization and/or separating submicron molecules and is not ideal for processing large volumes of liquid that contain large- size molecules and whole cells due to cake formation on top of the filter (Cheryan, 1998).

In TFF, the fluid flows parallel to the surface of the membrane, sweeping retained components off the membrane, minimizing fouling of the membrane. TFF can be performed using either hollow fiber devices or flat sheet membrane cassette devices (Cheryan, 1998). Hollow fiber devices generally have a lower hold-up volume, and are commercially available in ready-to-use pre-sterilized formats, unlike flat sheet membrane cassettes in which pre-sterilization is still a challenge for manufacturers (Schnitzler et al., 2016). Besides flexibility, TFF's advantages also include linear scale-up behavior and fairly low shear forces and pressures applied throughout processing (Maiorella et al., 1991). Due to the minimization of fouling throughout the filtration operation, this technology has been widely applied for the DSP of complex biopharmaceuticals, such as recombinant proteins (van Reis et al., 1991), and virus-like particles (Vicente et al., 2014). Given its broad application, there is a large offer of fully automated, disposable and integrated (concentration and washing) TFF systems, with a wide range of processing capabilities, reducing the process development costs, making TFF generally more cost effective for processing lower number of cells/lot (dose of $10^6 - 10^7$) for cell therapy applications (Hassan et al., 2015) (Table 1.5). Nonetheless, in DSP of other biotherapeutics, cells are merely a by-product, where the main goal is to clear them from the system. Thus, there has been an effort to rethink and redesign TFF processes in order to adapt this technique to suit the demands for cell-based therapies, where cells are intended as the final product (Pattasseril et al., 2013). Companies, such as Lonza (Walkersville, USA), have been investing on the optimization the TFF process set-up and operating conditions for both cell concentration and washing of therapeutic cells (PCT Publication number WO2011091248 A1) (Rowley et al., 2012b).

3. Aims and scope

The clinical transfer of human stem cells towards cell therapy applications still faces major challenges. Amongst them are the production of high cell amounts, the delivery of those high cell numbers at low volumes with minimal presence of residuals, while assuring the desired phenotype and function/potency. The goal of this PhD project was to establish a streamlined

DSP train based on scalable and integrated DSP unit operations of clarification, volume reduction and washing for human SC, as schematically represented in Figure 1.8. hMSC and hiPSC were used as challenging and complex cell-based products. Combining membrane technology and chromatographic tools, a flexible platform based on robust, scalable, and cGMP-compatible processes that can be transferred to clinical/industrial settings, was developed.

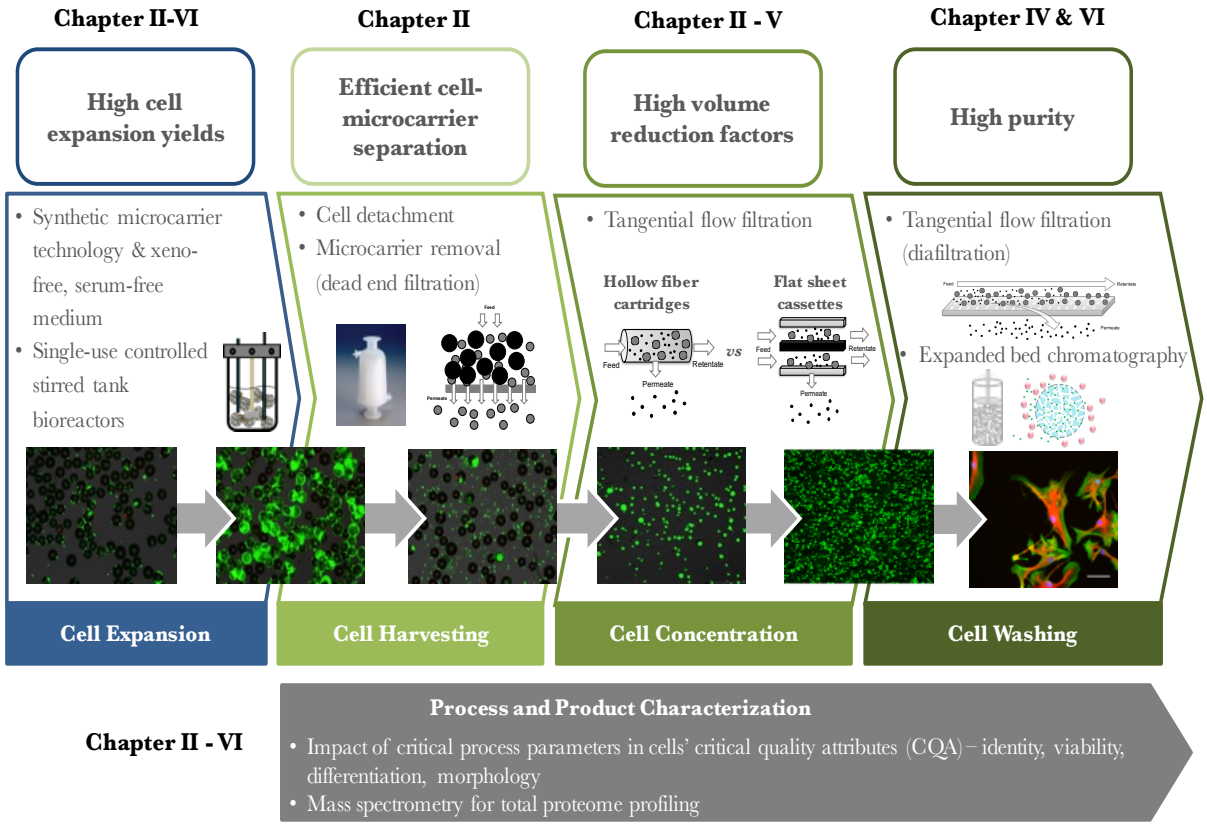

Figure 1.9 – Schematic representation of the major aims of this thesis. The biomanufacturing workflow for cell-based therapies comprising up and downstream unit operations is presented. The major goals and conditions tested are represented.

In **Chapter II** the applicability of filtration methodologies, as dead end filtration and tangential flow filtration, for the clarification and concentration of hMSC, respectively are evaluated. In particular, different materials and pore sizes were studied to accomplish an effective removal of microcarriers without compromising cell recovery yield and viability. The impact of TFF's CPP as initial cell suspension conditions, characteristics of the membrane device, shear rate and permeate flux on cell recovery yield and hMSC's CQA (identity, multilineage differentiation potential and viability) was assessed.

The applicability of the previously developed TFF methodologies for hMSC to hiPSC processing, was evaluated applying a Design of Experiments (DoE) approach (**Chapter III**). The impact of the process parameters of the volume reduction unit operation on hiPSC's

recovery yield and CQA in terms of recovery, viability, identity and pluripotent potential was assessed and compared with results previously attained with hMSC. A mathematical model of the process was designed and after understanding how the shear rate, permeate flux and cell load factors interacted between them, the condition that maximized cell recovery and viability responses was sought. A risk analysis was conducted for the optimized conditions obtained.

Also, a proof of concept of the integration of up- and down- stream unit operations, cell expansion in bioreactors with microcarrier removal and a TFF system for the volume reduction and washing of hMSC, is described in **Chapter IV**. Different operation modes both in up and downstream were compared for the manufacturing of hMSC.

The aim of **Chapter V** consisted on proving scalability of this integrated streamlined cGMP-compatible bioprocess comprised by cell expansion, harvesting and volume reduction unit operations using hMSC isolated from bone marrow (BM-MSC) and adipose tissues (AT-MSC). To accomplish the volume reduction step, a comparison between hollow fiber cartridges (HF) and flat sheet cassettes (FSC) was conducted. The impact of scaling-up these steps on cells' recovery yield and CQA was studied. Alongside the standard quality assays for evaluating hMSC's CQA, a proteomics workflow based on mass spectrometry tools was established to characterize the impact of processing on hMSC' CQA.

In **Chapter VI**, the applicability of expanded bed adsorption (EBA) chromatography operated in negative mode was evaluated to improve the previously established TFF-based washing process, further increasing hMSC purity. For this purpose, a new multimodal prototype matrix based on core-shell bead technology was used. The matrix was characterized, and different modes of chromatography were optimized to conduct this purification step.

Finally, the results obtained in this thesis were discussed in **Chapter VII**, contextualizing the findings with the available literature and state-of-the-art for the field addressed throughout the previous chapters.

References

Agashi, K., Chau, D.Y.S., Shakesheff, K.M., 2009. The effect of delivery via narrow-bore needles on mesenchymal cells. Regen. Med. 4, 49–64.

Al-Rubeai, M., Singh, R.P., Emery, A.N., Zhang, Z., 1995. Cell cycle and cell size dependence of susceptibility to hydrodynamic forces. Biotechnol. Bioeng. 46, 88–92.

Anker, P., Scherjon, S.A., Keur, der, C.K.-V., Noort, W.A., Claas, F.H.J., Willemze, R., Fibbe, W.E., Kanhai, H.H.H., 2003. Amniotic fluid as a novel source of mesenchymal stem cells for therapeutic transplantation. Blood 102, 1548–1549.

Anker, P., Scherjon, S.A., Kleijburg van der Keur, C., de Groot Swings, G.M.J.S., Claas, F.H.J., Fibbe, W.E., Kanhai, H.H.H., 2004. Isolation of Mesenchymal Stem Cells of Fetal or Maternal Origin from Human Placenta. Stem Cells 22, 1338–1345.

Atouf, F., Provost, N.M., Rosenthal, F.M., 2013. Standards for ancillary materials used in cell-and tissue-based therapies. BioProcess Int. 11, 12–21.

Avior, Y., Sagi, I., Benvenisty, N., 2016. Pluripotent stem cells in disease modelling and drug discovery. Nat. Rev. Mol. Cell Biol. 17, 170–182.

Axelsson, H., 2002. Cell Separation, Centrifugation. John Wiley & Sons, Inc., Hoboken, NJ, USA.

Beck, B., Blanpain, C., 2013. Unravelling cancer stem cell potential. Nat. Rev. Cancer 13, 727–738.

Ben-David, U., Nudel, N., Benvenisty, N., 2013. Immunologic and chemical targeting of the tight-junction protein Claudin-6 eliminates tumorigenic human pluripotent stem cells. Nat. Comm. 4, 1992–2000.

Blum, B., Benvenisty, N., 2008. The Tumorigenicity of Human Embryonic Stem Cells, in: Advances in Cancer Research. Elsevier, pp. 133–158.

Bravery, C.A., Carmen, J., Fong, T., Oprea, W., Hoogendoorn, K.H., Woda, J., Burger, S.R., Rowley, J.A., Bonyhadi, M.L., Van't Hof, W., 2013. Potency assay development for cellular therapy products: an ISCT* review of the requirements and experiences in the industry. Cytother. 15, 9–19.e9.

Campbell, A., Brieva, T., Raviv, L., Rowley, J., Niss, K., Brandwein, H., Oh, S., Karnieli, O., 2015. Concise Review: Process Development Considerations for Cell Therapy. Stem Cells Transl. Med. 4, 1155–1163.

Capelli, C., Pedrini, O., Valgardsdottir, R., Da Roit, F., Golay, J., Introna, M., 2015. Clinical grade expansion of MSCs. Immunol.y Lett. 222–227.

Caplan, A.I., 2008. All MSCs Are Pericytes? Stem Cell 3, 229–230.

Caplan, A.I., 1991. Mesenchymal stem cells. J. Orthop. Res. 9, 641–650.

Caplan, A.I., Correa, D., 2011. The MSC: An Injury Drugstore. Stem Cell 9, 11–15.

Caplan, A.I., Dennis, J.E., 2006. Mesenchymal stem cells as trophic mediators. J. Cel. Biochem. 98, 1076–1084.

Carmen, J., Burger, S.R., McCaman, M., Rowley, J.A., 2011. Developing assays to address identity, potency, purity and safety: cell characterization in cell therapy process development. Regen. Med. 7, 85–100.

Castilho, L.R., Moraes, A.M., Augusto, E., Butler, M., 2008. Animal Cell Technology. Taylor and Francis Group, New York.

Charcosset, C., 2012. Principles on membrane and membrane processes, in: Membrane Processes in Biotechnology and Pharmaceutics. Kidlington, Oxford, U.K. : Elsevier, pp. 1–30.

Chen, A.K.-L., Reuveny, S., Oh, S.K.W., 2013. Application of human mesenchymal and pluripotent stem cell microcarrier cultures in cellular therapy: Achievements and future direction. Biotechnol. Adv. 31, 1032–1046.

Cheryan, M., 1998. Ultrafiltration and Microfiltration Handbook, 1st ed. Technomic Publishing AG, Basel.

Clarke, D., Stanton, J., Powers, D., Karnieli, O., Nahum, S., Abraham, E., Parisse, J.-S., Oh, S., 2016. Managing particulates in cell therapy: Guidance for best practice. Cytother. 18, 1063–1076.

Coopman, K., Medcalf, N., 2008. From production to patient: challenges and approaches for delivering cell therapies. StemBook.

Correia, C., Serra, M., Espinha, N., Sousa, M., Brito, C., Burkert, K., Zheng, Y., Hescheler, J., Carrondo, M.J.T., Saric, T., Alves, P.M., 2014. Combining Hypoxia and Bioreactor Hydrodynamics Boosts Induced Pluripotent Stem Cell Differentiation Towards Cardiomyocytes. Stem Cell Rev. Rep. 10, 786–801.

Crisan, M., Yap, S., Casteilla, L., Chen, C.-W., Corselli, M., Park, T.S., Andriolo, G., Sun, B., Zheng, B., Zhang, L., Norotte, C., Teng, P.-N., Traas, J., Schugar, R., Deasy, B.M., Badylak, S., Bűhring, H.-J., Giacobino, J.-P., Lazzari, L., Huard, J., Péault, B., 2008. A Perivascular Origin for Mesenchymal Stem Cells in Multiple Human Organs. Stem Cell 3, 301–313.

De Bari, C., Dell'Accio, F., Tylzanowski, P., Luyten, F.P., 2001. Multipotent mesenchymal stem cells from adult human synovial membrane. Arthritis Rheumatol. 44, 1928–1942.

Dominici, M., Le Blanc, K., Mueller, I., Slaper-Cortenbach, I., Marini, F., Krause, D., Deans, R., Keating, A., Prockop, D., Horwitz, E., 2006. Minimal criteria for defining multipotent mesenchymal stromal cells. The International Society for Cellular Therapy position statement. Cytother. 8, 315–317.

Doran, P.M., 1995. Bioprocess engineering principles. Academic Press Limited, London, U.K.

Dragani, A., Angelini, A., Iacone, A., D'Antonio, D., Torlontano, G., 1990. Comparison of five methods for concentrating progenitor cells in human marrow transplantation. Blut 60, 278–281.

Eaker, S., Armant, M., Brandwein, H., Burger, S., Campbell, A., Carpenito, C., Clarke, D., Fong, T., Karnieli, O., Niss, K., Van't Hof, W., Wagey, R., 2013. Concise review: guidance in developing commercializable autologous/patient-specific cell therapy manufacturing. Stem Cells Transl. Med. 2, 871–883.

European Medicines Agency, 2004. Directive 2001/83/EC, amended by 2004/27/EC.

Food and Drug Administration, 2014. Code of Federal Regulations Title 21. Subchapter F -- Biologics; Part 610 -- General Biological Products Standards; Subpart B -- General Provisions; Sec. 610.15 Constituent Materials.

Food Drug and Administration, 2009. Guidance for Industry: Q8(R2) pharmaceutical development. https://www.fda.govdownloadsDrugs...Guidancesucm.pdf. (accessed 8.6.16).

Friedenstein, A.J., Chailakhyan, R.K., Latsinik, N.V., Panasyuk, A.F., Keiliss-Borok, I.V., 1974. Stromal cells responsible for transferring the microenvironment of the hemopoietic tissues. Cloning in vitro and retransplantation in vivo. Transplantation 17, 331–340.

Friedenstein, A.J., Piatetzky-Shapiro, I.I., Petrakova, K.V., 1966. Osteogenesis in transplants of bone marrow cells. J. Embryol. Exp. Morphol. 16, 381–390.

Gomes-Alves, P., Serra, M., Brito, C., Ricardo, C.P., Cunha, R., Sousa, M.F., Sanchez, B., Bernad, A., Carrondo, M.J.T., Rodriguez-Borlado, L., Alves, P.M., 2016. In vitro expansion of human cardiac progenitor cells: exploring 'omics tools for characterization of cell-based allogeneic products. Transl. Res. 171, 96–110.e3.

González-González, M., Vázquez-Villegas, P., García-Salinas, C., Rito-Palomares, M., 2011. Current strategies and challenges for the purification of stem cells. J. Chem. Technol. Biotechnol. 87, 2–10.

Hassan, S., Simaria, A.S., Varadaraju, H., Gupta, S., Warren, K., Farid, S.S., 2015. Allogeneic cell therapy bioprocess economics and optimization: downstream processing decisions. Regen. Med. 10, 591–609.

Heathman, T.R.J., Glyn, V.A.M., Picken, A., Rafiq, Q.A., Coopman, K., Nienow, A.W., Kara, B., Hewitt, C.J., 2015. Expansion, harvest and cryopreservation of human mesenchymal stem cells in a serum-free microcarrier process. Biotechnol. Bioeng. 112, 1696–1707.

Hervy, M., Weber, J.L., Pecheul, M., Dolley-Sonneville, P., Henry, D., Zhou, Y., Melkoumian, Z., 2014. Long term expansion of bone marrow-derived hMSCs on novel synthetic microcarriers in xeno-free, defined conditions. PLoS ONE 9, e92120.

Horwitz, E.M., Le Blanc, K., Dominici, M., Mueller, I., Slaper-Cortenbach, I., Marini, F.C., Deans, R.J., Krause, D.S., Keating, A., 2005. Clarification of the nomenclature for MSC: The International Society for Cellular Therapy position statement. Cytother. 7, 393–395.

Hourd, P., Chandra, A., Medcalf, N., Williams, D.J., 2008. Regulatory challenges for the manufacture and scale-out of autologous cell therapies. StemBook.

https://clinicaltrials.gov/ (accessed 16.08.16).

https://www.ksepsytsems.com/ (accessed 20.08.16).

https://www.terumobct.com/assets/data-vis/msc-clinical-trials/# (accessed 23.08.16).

Ko, H.-F., Bhatia, R., 2012. Evaluation of Single-Use Fluidized Bed Centrifuge System for Mammalian Cell Harvesting. BioPharm Int. 25, 34–40.

Kretzmer, G., 2000. Influence of stress on adherent cells. Adv. Biochem. Eng. Biotechnol. 67, 123–137.

Kumar, A., Srivastava, A., 2010. Cell separation using cryogel-based affinity chromatography. Nat. Protocols 5, 1737–1747.

Lapinskas, E., 2010. Scaling Up Research to Commercial Manufacturing. Chem. Eng. Prog. 106, 44–49.

Law, S., Chaudhuri, S., 2013. Mesenchymal stem cell and regenerative medicine: regeneration versus immunomodulatory challenges. Am. J. Stem Cells 2, 22–38.

Lee, O.K., Kuo, T.K., Chen, W.-M., Lee, K.-D., Hsieh, S.-L., Chen, T.-H., 2004. Isolation of multipotent mesenchymal stem cells from umbilical cord blood. Blood 103, 1669–1675.

Léo, P., Galesi, A., Suazo, C.A.T., Moraes, A., 2008. Animal cells: basic concepts, in: Animal Cell Technology: From Biopharmaceuticals to Gene Therapy. Taylor & Francis Group., New York, pp. 1–565.

Lipsitz, Y.Y., Timmins, N.E., Zandstra, P.W., 2016. Quality cell therapy manufacturing by design. Nat. Biotechnol. 34, 393–400.

Maiorella, B., Dorin, G., Carion, A., 1991. Crossflow microfiltration of animal cells. Biotechnol. Bioeng. 37, 121–126.

Malik, N., 2012. Allogeneic Versus Autologous Stem-Cell Therapy. BioPharm Int. 25.

Martin, C., Olmos, É., Collignon, M.-L., De Isla, N., Blanchard, F., Chevalot, I., Marc, A., Guedon, E., 2016. Revisiting MSC expansion from critical quality attributes to critical culture process parameters. Process Biochem., *in press.*

Martin-Manso, G., Hanley, P.J., 2015. Using the quantum cell expansion system for the automated expansion of clinical-grade bone marrow-derived human mesenchymal stromal cells. Methods Mol. Biol. 1283, 53–63.

Mason, C., Mason, J., Culme-Seymour, E.J., Bonfiglio, G.A., Reeve, B.C., 2013. Cell therapy companies make strong progress from October 2012 to March 2013 amid mixed stock market sentiment. Stem Cell 12, 644–647.

Murphy, M.B., Moncivais, K., Caplan, A.I., 2013. Mesenchymal stem cells: environmentally responsive therapeutics for regenerative medicine. Exp. Mol. Med. 45, 54–70.

Newman, R., Yoo, D., LeRoux, M., Danilkovitch-Miagkova, A., 2009. Treatment of Inflammatory Diseases with Mesenchymal Stem Cells. Inflammation & Allergy - Drug Targets 8, 110–123.

Nirmalanandhan, V.S., Sittampalam, G.S., 2009. Stem cells in drug discovery, tissue engineering, and regenerative medicine: emerging opportunities and challenges. J. Biomol. Screen 14, 755–768.

Niss, K., Sunil, N., Murrel, J., Punreddy, S., Kehoe, D., Rook, M., Jing, D., Aysola, M., 2013. Growth Kinetics of Human Mesenchymal Stem Cells in a 3L Single-Use, Stirred Tank Bioreactor, BioPharm Int.

Owen, M., 1988. Marrow stromal stem cells. J. Cell Sci. 1988, 63–76.

Pattasseril, J., Varadaraju, H., Lock, L., Rowley, J.A., Rowley, J.A., 2013. Downstream Technology Landscape for Large-Scale Therapeutic Cell Processing. BioProcess Int. 11, 38–47.

Pierelli, L., Bonanno, G., Rutella, S., Marone, M., Scambia, G., Leone, G., 2009. CD105 (Endoglin) Expression on Hematopoietic Stem/Progenitor Cells. Leuk. Lymphoma. 42, 1195-206.

Placzek, M.R., Chung, I.-M., Macedo, H.M., Ismail, S., Mortera Blanco, T., Lim, M., Cha, J.M., Fauzi, I., Kang, Y., Yeo, D.C.L., Ma, C.Y.J., Polak, J.M., Panoskaltsis, N., Mantalaris, A., 2009. Stem cell bioprocessing: fundamentals and principles. J. R. Soc. Interface 6, 209–232.

Sousa, M.F.Q and Silva, M.M., Roldão, A., Alves, P.M., Serra, M., Giroux, D., Hashimura, Y., Wesselschmidt, R., Lee, B., Carrondo, M.J.T., 2015. Production of oncolytic

adenovirus and human mesenchymal stem cells in a single-use, vertical-Wheel bioreactor system: Impact of bioreactor design on performance of microcarrier-based cell culture processes. Biotechnol. Prog. 31,1600-1612.

Rafiq, Q.A., Brosnan, K.M., Coopman, K., Nienow, A.W., Hewitt, C.J., 2013. Culture of human mesenchymal stem cells on microcarriers in a 5 l stirred-tank bioreactor. Biotechnol. Lett. 35, 1233–1245.

Ratcliffe, E., Thomas, R.J., Williams, D.J., 2011. Current understanding and challenges in bioprocessing of stem cell-based therapies for regenerative medicine. Br. Med. Bul. 100, 137–155.

Rege, T.A., Hagood, J.S., 2006. Thy-1 as a regulator of cell-cell and cell-matrix interactions in axon regeneration, apoptosis, adhesion, migration, cancer, and fibrosis. FASEB J. 20, 1045–1054.

Roush, D.J., Lu, Y., 2008. Advances in Primary Recovery: Centrifugation and Membrane Technology. Biotechnol. Prog. 24, 488–495.

Rowley, J., Abraham, E., Campbell, A., Brandwein, H., Oh, S., 2012a. Meeting Lot-Size Challenges of Manufacturing Adherent Cells for Therapy. BioProcess Int. 3, 16–22.

Rowley, J., Pattasseril, J., Mohamed, A., 2012b. High yield method and apparatus for volume reduction and washing of therapeutic cells using tangential flow filtration. WO 2011091248 A1.

Russotti, G., 2015. Cell Therapy Setbacks, Hopes, and Challenges, in: Oral presentation at the 9th International Meeting of the Portuguese Society for Stem Cells Cell Therapy, Oeiras.

Samsonraj, R.M., Rai, B., Sathiyanathan, P., Puan, K.J., Roetzschke, O., Hui, J.H., Raghunath, M., Stanton, L.W., Nurcombe, V., Cool, S.M., 2015. Establishing Criteria for Human Mesenchymal Stem Cell Potency. Stem Cells 33, 1878–1891.

dos Santos, F., Campbell, A., Fernandes-Platzgummer, A., Andrade, P.Z., Gimble, J.M., Wen, Y., Boucher, S., Vemuri, M.C., da Silva, C.L., Cabral, J.M.S., 2014. A xenogeneic-free bioreactor system for the clinical-scale expansion of human mesenchymal stem/stromal cells. Biotechnol. Bioeng. 111, 1116–1127.

Schirmaier, C., Jossen, V., Kaiser, S.C., Jüngerkes, F., Brill, S., Safavi Nab, A., Siehoff, A., Bos, C., Eibl, D., Eibl, R., 2014. Scale-up of adipose tissue-derived mesenchymal stem cell production in stirred single-use bioreactors under low-serum conditions. Eng. Life Sci. 14, 292–303.

Schnitzler, A.C., Verma, A., Kehoe, D.E., Jing, D., Murrell, J.R., Der, K.A., Aysola, M., Rapiejko, P.J., Punreddy, S., Rook, M.S., 2016. Bioprocessing of human mesenchymal

stem/stromal cells for therapeutic use: Current technologies and challenges. Biochem. Eng. J. 108, 3–13.

Schop, D., van Dijkhuizen-Radersma, R., Borgart, E., Janssen, F.W., Rozemuller, H., Prins, H.-J., de Bruijn, J.D., 2010. Expansion of human mesenchymal stromal cells on microcarriers: growth and metabolism. J. Tissue Eng. Regen. Med. 4, 131–140.

Serra, M., Brito, C., Correia, C., Alves, P.M., 2012. Process engineering of human pluripotent stem cells for clinical application. Trends Biotechnol. 30, 350–359.

Simaria, A.S., Hassan, S., Varadaraju, H., Rowley, J., Warren, K., Vanek, P., Farid, S.S., 2014. Allogeneic cell therapy bioprocess economics and optimization: single-use cell expansion technologies. Biotechnol. Bioeng. 111, 69–83.

Smith, D.M., 2012. Assessing commercial opportunities for autologous and allogeneic cell-based products. Regen. Med. 7, 721–732.

de Soure, A.M., Fernandes-Platzgummer, A., da Silva, C.L., Cabral, J.M.S., 2016. Scalable microcarrier-based manufacturing of mesenchymal stem/stromal cells. J. Biotechnol. *in press*.

Stolzing, A., Jones, E., McGonagle, D., Scutt, A., 2008. Age-related changes in human bone marrow-derived mesenchymal stem cells: Consequences for cell therapies. Mech. Ageing Dev. 129, 163–173.

Sträter, N., 2006. Ecto-5'-nucleotidase: Structure function relationships. Purinergic Signalling 2, 343–350.

Szczypka, M., Splan, D., Woolls, H., Brandwein, H., 2014. Single-use bioreactors and microcarriers scalable technology for cell-based therapies. BioPharm Int. 12, 54–64.

Takahashi, K., Tanabe, K., Ohnuki, M., Narita, M., Ichisaka, T., Tomoda, K., Yamanaka, S., 2007. Induction of pluripotent stem cells from adult human fibroblasts by defined factors. Cell 131, 861–872.

Takahashi, K., Yamanaka, S., 2016. A decade of transcription factor-mediated reprogramming to pluripotency. Nat. Rev. Mol. Cell Biol. 17, 183–193.

Takahashi, K., Yamanaka, S., 2006. Induction of pluripotent stem cells from mouse embryonic and adult fibroblast cultures by defined factors. Cell 126, 663–676.

Tang, C., Lee, A.S., Volkmer, J.-P., Sahoo, D., Nag, D., Mosley, A.R., Inlay, M.A., Ardehali, R., Chavez, S.L., Pera, R.R., Behr, B., Wu, J.C., Weissman, I.L., Drukker, M., 2011. An antibody against SSEA-5 glycan on human pluripotent stem cells enables removal of teratoma-forming cells. Nat. Biotechnol. 29, 829–834.

Trounson, A., McDonald, C., 2015a. Stem Cell Therapies in Clinical Trials: Progress

and Challenges. Stem Cell 17, 11–22.

Trounson, A., McDonald, C., 2015b. Stem Cell Therapies in Clinical Trials: Progress and Challenges. Stem Cell 17, 11–22.

Ujam, L.B., Clemmitt, R.H., Clarke, S.A., Brooks, R.A., Rushton, N., Chase, H.A., 2003. Isolation of monocytes from human peripheral blood using immuno-affinity expanded-bed adsorption. Biotechnol. Bioeng. 83, 554–566.

van Reis, R., Gadam, S., Frautschy, L.N., Orlando, S., Goodrich, E.M., Saksena, S., Kuriyel, R., Simpson, C.M., Pearl, S., Zydney, A.L., 1997. High Performance Tangential Flow Filtration. Biotechnol. Bioeng. 56, 71–82.

van Reis, R., Leonard, L.C., Hsu, C.C., Builder, S.E., 1991. Industrial scale harvest of proteins from mammalian cell culture by tangential flow filtration. Biotechnol. Bioeng. 38, 413–422.

van Reis, R., Zydney, A., 2007. Bioprocess membrane technology. J. Membr. Sci. 297, 16–50.

Veraitch, F.S., Scott, R., Wong, J.-W., Lye, G.J., Mason, C., 2008. The impact of manual processing on the expansion and directed differentiation of embryonic stem cells. Biotechnol. Bioeng. 99, 1216–1229.

Vicente, T., Burri, S., Wellnitz, S., Walsh, K., Rothe, S., Liderfelt, J., 2014. Fully aseptic single-use cross flow filtration system for clarification and concentration of cytomegalovirus-like particles. Eng. Life Sci. 14, 318–326.

Wang, S., Qu, X., Zhao, R.C., 2012. Clinical applications of mesenchymal stem cells. J. Hematol. Oncol. 5, 1.

Wei, X., Yang, X., Han, Z.-P., Qu, F.-F., Shao, L., Shi, Y.-F., 2013. Mesenchymal stem cells: a new trend for cell therapy. Acta Pharmacol. Sin. 34, 747–754.

Williams, A.R., Hare, J.M., 2011. Mesenchymal Stem Cells. Circ. Res. 109, 923–940.

Yamanaka, S., 2012. Induced Pluripotent Stem Cells: Past, Present, and Future. Stem Cell 10, 678–684.

Zaher, W., Harkness, L., Jafari, A., Kassem, M., 2014. An update of human mesenchymal stem cell biology and their clinical uses. Arch. Toxicol. 88, 1069–1082.

Zhou, L., Kong, J., Zhuang, Y., Chu, J., Zhang, S., Guo, M., 2013. Ex vivo expansion of bone marrow mesenchymal stem cells using microcarrier beads in a stirred bioreactor. Biotechnol. Bioprocess Eng. 18, 173–184.

Zuk, P.A., Zhu, M., Ashjian, P., De Ugarte, D.A., Huang, J.I., Mizuno, H., Alfonso, Z.C., Fraser, J.K., Benhaim, P., Hedrick, M.H., 2002. Human adipose tissue is a source of

multipotent stem cells. Mol. Biol. Cell 13, 4279–4295.

II

Optimization of filtration methodologies for the downstream processing of human mesenchymal stem cells: clarification and concentration unit operations

This chapter was adapted from:

Cunha B, Peixoto C, Silva MM, Carrondo MJT, Serra M, Alves PM (2015). Filtration methodologies for the clarification and concentration of human mesenchymal stem cells. Journal of Membrane Science 478:117–129.

Cunha B, Serra M, Peixoto C, Silva MM, Carrondo MJT, Alves PM (2013). Designing clinical-grade integrated strategies for the downstream processing of human mesenchymal stem cells. BMC Proceedings 7(Suppl 6):P103.

Table of Contents

ABSTRACT 74

1. INTRODUCTION 75

2. MATERIALS AND METHODS 77

2.1 Cell expansion 78
2.2 Downstream processing 79
2.3 Cell viability and characterization assays 83
2.4 Statistical Analysis 86

3. RESULTS 86

3.1 hMSC clarification (microcarrier removal) using dead end filtration 86
3.2 Cell concentration/volume reduction using tangential flow filtration 88

4. DISCUSSION 96

5. ACKNOWLEDGMENTS 99

REFERENCES 101

Abstract

Currently human mesenchymal stem cells (hMSC) are expanded using microcarrier-based stirred culture systems from one to hundreds of liters of culture volume to guarantee the required cell numbers to be delivered to the clinic. Such culture volumes need to be clarified, ensuring efficient removal of microcarriers, and concentrated without compromising the cells' characteristics. The aim of this work was to evaluate the applicability of filtration methodologies, as dead end filtration and tangential flow filtration, for the clarification and concentration of hMSC, respectively.

Different process variables and their impact on hMSC quality were evaluated, showing that polypropylene filters with pore sizes higher than 75 µm can ensure the removal of microcarriers from the cell suspension bulk, without compromising cells' recovery or viability. Furthermore, hMSC could be successfully concentrated up to a factor of ten while maintaining their identity, potency and high cell viability, allowing for the recovery of over 80% of viable cells; an initial cell concentration higher than 2×10^5 cell/mL, and polysulfone membranes with pore sizes higher than 0.45 µm were identified to be key conditions to obtain such concentration factors; shear rate and permeate flux were also shown to impact the cells' recovery yields, viability and quality.

Keywords: human mesenchymal stem cells; microcarriers; tangential flow filtration; downstream processing; cell concentration.

1. Introduction

Given the particular immunomodulatory characteristics (Iyer and Rojas, 2008) and the capacity to secrete bioactive molecules with anti-inflammatory and regenerative features (Haynesworth et al., 1996), human mesenchymal stem cells (hMSC) have become key candidates for autologous and allogeneic therapies. Currently, over 300 clinical trials are taking place using hMSC for a variety of therapies, including bone/cartilage, cardiovascular, neurodegenerative and gastrointestinal diseases as well as in diabetes, and for the treatment of graft-versus-host disease (Murphy et al., 2013).

However, clinical transfer of hMSC still faces several challenges; high doses (from 10^5 to 10^9 cells *per* patient) (Mason and Dunnill, 2009) coupled with autologous or even allogeneic options, require suitable scales for expansion, where microcarrier-based stirred culture systems have mostly been adopted to sustain cell expansion (Chen et al., 2013). Since hMSC are meant to be implanted, transplanted or infused into human patients, efficient purification processes are essential, as reviewed by Serra et al. (Serra et al., 2012), while compliant with FDA and EMA requirements in terms of identity, purity, potency, and viability throughout processing. To fulfill the purification requirements, cell clarification (including efficient cell-microcarrier separation), cell concentration (volume reduction) and cell washing (Pattasseril et al., 2013; Serra et al., 2012) will be necessary. Due to the non-biodegradable nature of the majority of microcarriers, their removal becomes compulsory. Therefore, several companies and research groups have been already exploring alternatives for microcarrier separation and cell concentration based on filtration methodologies (Kehoe, 2014.; Lilova, 2014.; Nienow et al., 2014).

Tangential flow filtration (TFF) is a well established technology, commonly used for the initial clarification of therapeutic proteins from mammalian, yeast, and bacterial cell cultures (van Reis et al., 1991), as well as for the purification and concentration of virus particles (Vicente et al., 2009). In the majority of biopharmaceutical clarification processes, cells are merely a by-product of the process, where the main goal is to clear them from the system. Conversely, for cell therapy utilizations, TFF processes have to be redesigned to meet the new demands, where cells are intended as the final product. Nonetheless, the impact of the TFF process parameters on the cells' characteristics needs assessment. TFF poses several advantages making it an attractive solution for cell therapy DSP; since this technology is widely used in protein and virus processing, there is a large offer of fully automated, disposable and integrated (concentration and washing) TFF systems, with a wide range of processing capabilities. Besides flexibility, TFF's

advantages also include linear scale-up behavior and fairly low shear forces and pressures (Maiorella et al., 1991; Saha et al., 1994), justifying its growing use in perfusion systems (Clincke et al., 2013).

The main goal of this study was to assess several process parameters of well-established and compatible with current good manufacturing practices (cGMP) filtration techniques, dead end filtration and TFF, on the efficiency in removing microcarriers from hMSC culture bulk, and on the concentration of hMSC (up to a concentration factor of ten), respectively. In particular, for the clarification step, the influence of different filter materials and pore sizes on cell recovery yield and viability were evaluated. For the cell concentration step, the impact of cell concentration, membrane material and pore size, as well as operating conditions of shear rate and permeate flux on cell recovery yields and quality was evaluated.

2. Materials and Methods

The followed workflow is presented in Figure 2.1A.

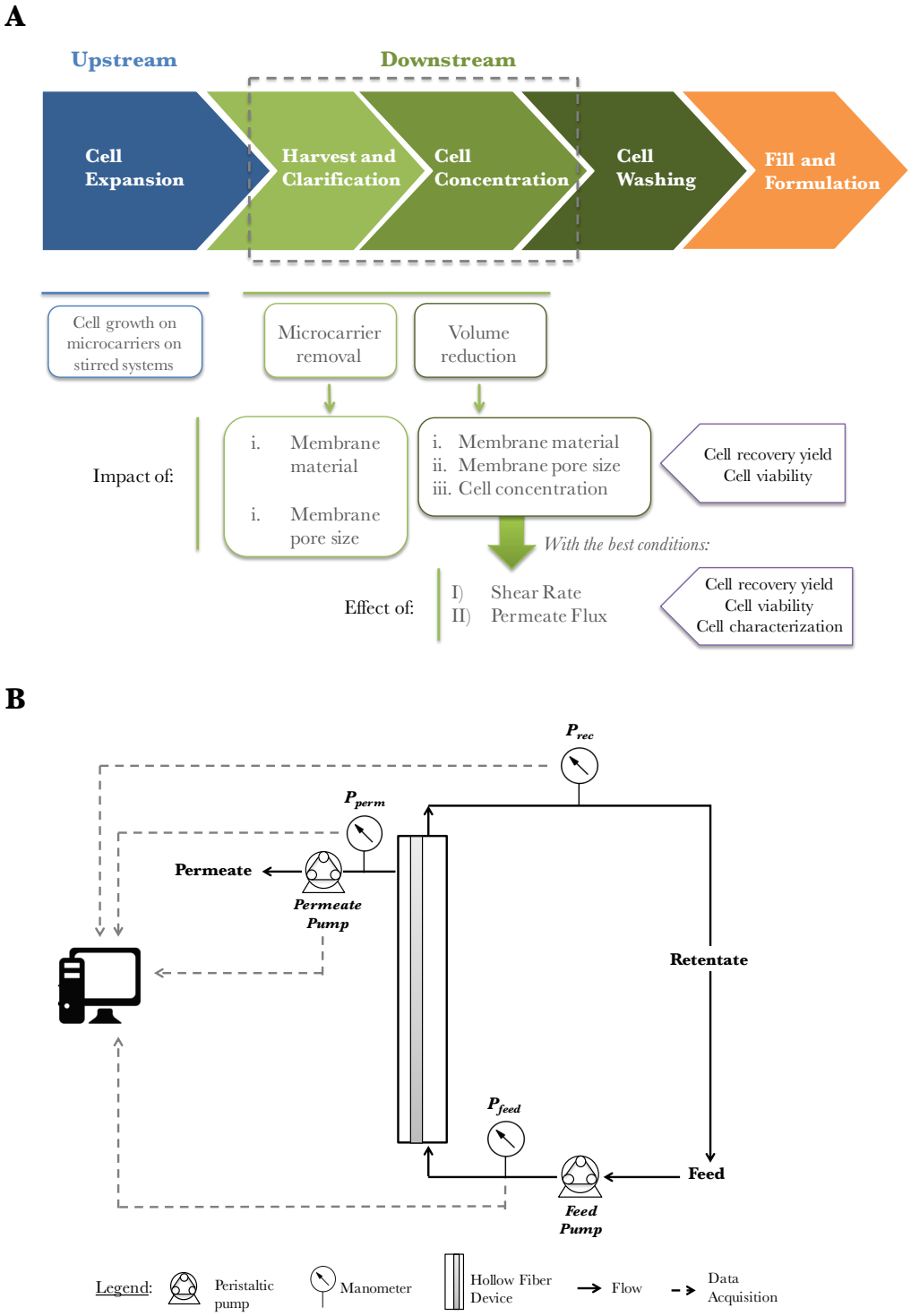

Figure 2.1 – Schematic representations of the (A) experimental workflow (A) and (B) layout of the tangential flow filtration (TFF) concentration step (B). After cell expansion and harvesting, (A) the cell bulk suspension was clarified from microcarriers and hMSC were concentrated. The influence of filter materials, pore sizes, cell concentrations, and operation parameters (shear rate and permeate flux) on cell recovery yield and cell's characteristics have been studied. In (B), the clarified hMSC cell suspension is pumped from the feed vessel into the feed port of the hollow fiber device, across the membrane surface (crossflow), out from the

retentate port and back into the feed vessel. The crossflow ensures that larger molecules than the membrane pores are retained inside the fibers, whereas smaller molecules pass along (permeate). The permeate flux is controlled throughout the process by setting initially either a valve or a pump to a fixed value. When necessary, a valve was positioned at the retentate port to restrict the tubing, increasing the transmembrane pressure (TMP). The pressure on the feed ($\boldsymbol{P_f}$), retentate ($\boldsymbol{P_r}$), and permeate ($\boldsymbol{P_p}$) ports are monitored by SciPres Luer pressure sensors. Weight and pressure data are acquired every 15 seconds.

2.1 Cell expansion

In this work, human bone marrow-derived mesenchymal stem cells (hMSC), obtained from STEMCELL™ Technologies (Grenoble, France), were used. Cells were expanded in static or stirred culture conditions. All reagents used to perform the cell culture were purchased from ThermoFisher™ Scientific (Massachusetts, USA), unless otherwise stated.

2.1.1 Static Culture

hMSC were routinely cultured in MesenCult®-XF Medium (STEMCELL™ Technologies) supplemented with 2 mM L-Glutamine and propagated in tissue culture flasks (Thermo Scientific™ Nunc™), previously coated with MesenCult™-SF Attachment Substrate (STEMCELL™ Technologies), at 37 ºC in a humidified atmosphere of 5% CO_2 in air. At 70 – 80% cell confluency, the medium was removed and cells were washed with Dulbecco's phosphate-buffered saline (DPBS) and incubated with TrypLE Select (1X) dissociation reagent for 5 minutes at 37 ºC. After cell detachment, hMSC were resuspended in MesenCult®-XF medium, and centrifuged at 300x*g* for 5 minutes at room temperature. The cell pellet was resuspended in MesenCult®-XF medium and transferred to new pre-coated culture flasks, at an inoculum cell concentration of 4 x 10^3 cell/cm^2. 50% of the culture medium was exchanged at day 5.

2.1.2 Stirred Cultures

hMSC were inoculated at 2.5 x 10^4 cell/mL in 125 mL spinner vessels (Corning Inc., New York, USA) containing Synthemax II microcarriers (at 16 or 48 g/L; Corning) and half of final the working volume of culture medium (MesenCult®-XF). The spinner vessels were placed inside an incubator (37 ºC, humidified atmosphere of 5% CO_2 in air) under intermittent stirring (On: 30 rpm, 1 min; Off: 0 rpm, 20 min). After 5 hours, fresh MesenCult®-XF Medium was added up to 100% of final working volume to the cultures, and stirring (at 30 rpm) was turned on. Five days after expansion, 50% of the culture medium was exchanged. At 70 – 80% cell confluency (day 7), cells were detached from the microcarriers and the culture bulk was harvested from the spinner vessel: Briefly, after washing with DPBS, TrypLE Select (1X) was

added to the cells and the cultures were incubated at 37 ºC for approximately 15 min under continuous stirring (60 rpm) to promote cell detachment.

hMSC were also cultured in Biostat Qplus stirred tank bioreactors (Sartorius Stedim Biotech, Göttingen, Germany) with 0.25 L working volume. Data acquisition and process control were performed using MFCS/Win (Sartorius Stedim Biotech). Cell culture in the bioreactor was performed using dissolved oxygen of 20% oxygen tension, pH of 7.2 and temperature of 37 ºC.

2.2 Downstream processing

2.2.1 Clarification (microcarriers' removal)

After hMSC detachment and harvesting, microcarriers were removed from the cell bulk suspension using dead end filtration. Nylon and polypropylene net disk filters (both from EMD Millipore, Massachusetts, USA) with different pore sizes (100, 80 and 30 µm) were tested to process up to 0.2 L of cell culture bulk. Briefly, filters were previously sterilized with 70% (v/v) ethanol for at least 3 h, assembled into a Sterifil® Aseptic System and Holder (EMD Millipore) and preconditioned with DPBS, following the manufacturer's instructions. The cell culture bulk was filtered coupling a vacuum system to the Sterifil® Aseptic System.

Sterile OptiCap® XL 1 Capsules (EMD Millipore) with 75 and 100 µm pore size were used to filter up to 2 L of cell bulk suspension. Tandem Model 1082 peristaltic pump from Sartoflow® Slice 200 benchtop crossflow system (Sartorius Stedim Biotech) was used and a flow rate of 0.3 L/min was applied to perform the filtration process.

2.2.2 Cell concentration (volume reduction)

The clarified cell suspension was concentrated using tangential flow filtration (TFF), as represented in Figure 2.1B.

Six different hollow fiber devices (HF) were tested (Table 2.1); HF A and B were kindly provided by Asahi Kasei, Tokyo, Japan; HF C, D, E and F were purchased from GE Healthcare Life Sciences, New Jersey, USA; HF G was purchased from Spectrum® Laboratories, Inc., California, USA. First, the influence of the membrane material on the TFF process was determined using HF devices D and G. With the most suitable material, the impact of the pore size was determined using HF C, D, E and F. Having determined the best membrane material and pore size to perform the concentration step, the impact of the initial cell concentrations on cell recovery yields and cell viability was tested. Thereafter, having optimized the membrane's

material, pore size and cell concentration, the performance of different hollow fiber devices (A, B, C and D) with different characteristics was compared.

Table 2.1 – Specifications of the hollow fiber devices used for the concentration step.

Device	Material	Pore size	Inner fiber diameter (mm)	Number of fibers	Surface area (cm^2)
HF_{PS} A	Polysulfone	0.4 µm	1.4	5	50
HF_{PS} B		0.4 µm	1.4	1	4
HF_{PS} C		0.65 µm	0.75	4	24
HF_{PS} D		0.45 µm	1	2	16
HF_{PS} E		0.2 µm	1	2	16
HF_{PS} F		750 kDa	1	2	16
HF_{PES} G	Polyethersulfone	0.5 µm	1	2	13

To start the TFF process, initially the air from the device was removed by filling the recirculation loop with cell suspension using a peristaltic pump (Tandem Model 1081 peristaltic pumps from Sartoflow® Slice 200 benchtop crossflow system, Sartorius Stedim Biotech) on the feed side set up to a fixed flow rate, in order to obtain fluxes of 175, 375 and 750 $L.m^{-2}.h^{-1}$ (LMH) (Table 2.2); on the permeate stream was either i) a valve restricting the tubing at a fixed value or ii) a recirculation pump (Watson Marlow Model 120 S/DV 200 rpm pump, Watson-Marlow Pumps Group, Massachusetts, USA) set to a fixed flow rate, in order to obtain fluxes of 60, 120 and 250 LMH (Table 2.3). In both cases, the control of the permeate stream is fixed and constant throughout the process.

After achieving the desired concentration factor, the TFF loop is completely drained and the cell suspension is recovered. Pressure was monitored using SciPres luer pressure sensors (SciLog, Wisconsin, USA) on the inlet, outlet and permeate stream. Weight and pressure data were monitored and acquired every 15 seconds using the Sartoflow® Slice 200 benchtop crossflow system. The experiments were performed inside of a laminar flow hood chamber in order to ensure a sterile environment.

Table 2.2 – Impact of the shear rate (γ) (modulated by the inlet flux, J) on the hMSC viability (results presented on Figure 2.6)[1]

γ (s^{-1})	J (LMH)	Cell Viability (%), VRF = 4
3000	750	95
1500	375	92
700	175	85

Table 2.3 – Impact of the permeate flux (J_p) on the hMSC viability and on the process time (results presented on Figure 2.8)[2]

J_P (LMH)	Process time (min), VRF = 10	Cell Viability (%), VRF = 10
60	92	92
120	44	98
250	22	99
485	11	97

A water flux test was performed before and after each experiment to determine the membrane's permeability. To ensure sterility, HF were sanitized with 0.5 M NaOH (Sigma-Aldrich, Steinheim, Germany) at 50 ºC for 45 min. The membranes were preconditioned with five membrane volumes of sterile DPBS before the concentration step.

The transmembrane pressure (TMP) in TFF is defined as the difference between the pressure on the feed and on the permeate side; it was maintained below 0.1 bar during all the procedures (unless otherwise stated). For a cross-flow device, the pressure on the feed side is evaluated as the mean of the pressures at the inlet and outlet of the device (Charcosset, 2012) and thus, the TMP can be estimated by the following Equation (1):

$$TMP = \frac{(P_f + P_r)}{2} - P_p \quad (1)$$

where, P_f and P_r are the pressure of the feed solution at the inlet and outlet of the device, respectively, and P_p, is the pressure on the permeate side.

[1] The permeate flux was equally controlled for all experiments at 60 $L.m^{-2}.h^{-1}$

[2] The inlet flux was equally controlled for all experiments at 750 $L.m^{-2}.h^{-1}$

The volumetric permeate flux through the membrane, J_p (expressed in L.m^{-2}.h^{-1} or LMH), is described by Equation 2 (Charcosset, 2012):

$$J_P = \frac{Q_p}{A} \quad (2)$$

where Q_p is the volumetric flow rate of the permeate fluid (L/h), and A the membrane surface area (m^2). In this work, Q_p was measured by the permeated mass over time. Likewise, the inlet flux, J (expressed in L.m^{-2}.h^{-1} or LMH), can be described by Equation 3:

$$J = \frac{Q_{inlet}}{A} \quad (3)$$

where Q_{inlet} is the inlet's volumetric flow rate (L/h).

The filtration throughput (Load, L/m^2), here described as the volume of cell suspension able to be processed *per* membrane area, was calculated by Equation 4:

$$Load = \frac{V_p}{A} \quad (4)$$

where V_p is the permeated volume (L), and A the membrane surface area (m^2).

For Newtonian fluids, the shear rate (γ, expressed in s^{-1}) can be estimated through the use of the Hagen-Poiseuille relation. Therefore, the shear rate at the membrane surface of a tube with a specific diameter (d) is given in terms of the bulk average velocity, i.e. cross-flow velocity (u), (Equation 5) (Cheryan, 1998):

$$\gamma = \frac{8\,u}{d} \quad (5)$$

where the cross-flow velocity (m.s^{-1}) can be expressed by the flow rate that passes through the cross sectional area (Equation 6):

$$u = \frac{Q}{A} \quad (6)$$

Rearranging equations 5 and 6, the shear rate can then be described by Equation 7 (Son, 2007) :

$$\gamma = \frac{4\,Q}{\pi\,r^3} \quad (7)$$

where Q is the flow rate that passes through one hollow fiber with a inner radius r of each device.

The shear stress τ in a fluid is related to the shear rate (γ) as follows (Cheryan, 1998):

$$\tau = \mu \times \gamma \quad (8)$$

where μ represents the fluid's dynamic viscosity.

The turbulence of the system was evaluated by the analysis of the Reynolds Number (Re) (Cheryan, 1998):

$$Re = \frac{d\,u\,\rho}{\mu} \quad (9)$$

where ρ represents the fluid's density. All experiments were performed under laminar flow conditions ($Re < 1800$).

2.3 Cell viability and characterization assays

All reagents used to perform cell characterization assays were purchased from Sigma Aldrich, unless stated otherwise.

2.3.1 Cell concentration and viability

Cell viability and cell membrane integrity were assessed using three different methods:

2.3.1.1 Trypan Blue exclusion method

Cell concentration was estimated through counting cells using a Fuchs–Rosenthal haemocytometer (Brand, Wertheim, Germany). Viable cells were determined by using the trypan blue dye exclusion method. The cell recovery yield is always referred as a percentage, and was estimated taking into account the number of viable cells before (100%) and after processing.

2.3.1.2 Fluorescein diacetate-propidium iodide staining

The qualitative assessment of the cell plasma membrane integrity was also performed using the enzyme substrate fluorescein diacetate (FDA), and the DNA-dye propidium iodide (PI), as described in the literature (Jones and Senft, 1985). Briefly, cell suspensions were incubated with 20 µg/mL FDA and 10 µg/mL PI in DPBS for 5 min and observed using fluorescence microscopy (DMI 600 B, Leica Microsystems GmbH). Representative images were taken using a Leica DFC 360 FX digital camera.

2.3.1.3 Lactate Dehydrogenase (LDH) Assay

The release of intracellular lactate dehydrogenase enzyme (LDH) into the supernatant can be correlated with the extent of cell lysis (Fotakis and Timbrell, 2006). Hence, LDH activity from the supernatant of centrifuged samples (300x*g*, 5 min) was determined by monitoring at 340 nm the oxidation rate of NADH (Sigma-Aldrich®) to NAD+ coupled with the reduction of pyruvate to lactate, as previously described in the literature (Vassault, 1983).

2.3.2 hMSC size

hMSC size was measured using CASY®1 Cell Counter and Analyzer System, (TTC model, Schärfe System GmbH, Reutlingen, Germany). Cell size was also estimated using a phase contrast inverted microscope (DMI 600 B, Leica Microsystems GmbH, Wetzlar, Germany) using the software Leica Application Suite LAS AF by measuring the diameter of each cell, from a minimum of 30 cells, from different cell suspensions.

2.3.3 Apoptosis and metabolic activity assay

For assessing the impact of the DSP on cells' characteristics, the percentage of apoptotic and metabolic active cells was evaluated using Apoptosis Assay Kit NucView™ 488 and MitoView™ 633 (Biotium, Inc., California, USA), following the manufacturer's instructions. This kit contains the green fluorescent NucView 488 caspase-3 substrate and the far-red fluorescent MitoView 633 mitochondrial dye for profiling caspase-3 activity and changes in mitochondrial membrane potential, respectively, in intact cells. After incubation with both reagents, cells were analysed by flow cytometry (CyFlow® space, Partec GmbH, Münster, Germany). At least ten thousand events were registered *per* sample.

2.3.4 hMSC adhesion and proliferation capacity

hMSC were inoculated in static culture conditions, in 6 wells in 24 and 6-well-plates previously coated with MesenCult™-SF Attachment Substrate. A cell inoculum of 5 x 10^3 cell/cm^2 was used and cells were cultured in MesenCult®-XF Medium in a humidified atmosphere of 5% CO_2 in air, as described in a previous section (Cell Culture, Static Culture).

For evaluation of the cell adhesion capacity, the number of adherent cells was monitored 30 minutes after inoculation. The supernatant was gently removed and cells still in suspension were counted (Section Cell concentration and viability, Trypan Blue exclusion method). Adherent cells were washed, detached and counted, as explained in a previous section (Cell Culture, Static Culture and Cell concentration and viability, Trypan Blue exclusion method).

The proliferation capacity of hMSC was assessed by measuring DNA synthesis using Click-iT® EdU Flow Cytometry Assay Kit (Life Technologies™), following the manufacturer's instructions. Three days after inoculation, the percentage of cells in S-phase was determined by the incorporation of the nucleoside analogue to thymidine EdU (5-ethynyl-2′- deoxyuridine) into DNA during active DNA synthesis. The analysis was performed in a CyFlow® space (Partec GmbH) instrument. At least ten thousand events were registered *per* sample.

2.3.5 Flow cytometry

hMSC were washed once with DPBS and a total of 2 x 10^5 cells were incubated with each one of the antibodies (CD44-PE, CD73-PE, CD90-PE, CD105-PE, CD166-PE, CD34-PE, CD45-PE, HLA-DR-PE and isotype controls IgG_1,κ-PE, IgG_{2a},κ-PE and IgG_{2b},κ-PE, all from BD Biosciences) for 1 h at 4 °C. Cells were washed twice in DPBS, and analyzed in a CyFlow® space instrument. At least ten thousand events were registered *per* sample.

2.3.6 Morphology

hMSC were collected before and after TFF, and plated in pre-coated plates. After 3 h, cells were washed with DPBS and fixed in 4% (w/v) paraformaldehyde (PFA) and 4% (w/v) Sucrose in DPBS solution for 15 minutes. Afterwards, cells were permeabilized for 15 minutes in 0.1% (w/v) Triton X-100 and 0.125% (v/v) FSG solution in DPBS and subsequently incubated with Alexa Fluor® 488 dye for 1 h at 4 °C, to detect F-actin (stress fibers). After three washing steps with DPBS, cell nuclei were counterstained with Hoechst 33342 nucleic acid dye. Cells were visualized using inverted (Leica Microsystems GmbH) fluorescence microscopy. Representative images were taken using a digital camera (Leica DFC 360 FX). Moreover, cells' morphology was also monitored through culture time under a phase contrast inverted microscope (Leica Microsystems GmbH).

2.3.7 *In vitro* multipotency assays

At the end of DSP, hMSC potency was evaluated by their capacity in differentiating into three different lineages: adipogenic, osteogenic and chondrogenic.

Adipogenic differentiation: 6 x 10^4 cells were inoculated *per* well (5 wells) in a 24-well-plate. After reaching confluency, differentiation media (StemMACS™ AdipoDiff Media, Miltenyi Biotec, Germany) was added to three wells in each plate, and MEM Alpha (Life Technologies™) supplemented with 10% (v/v) FBS (Life Technologies™) was added to two wells (monitoring spontaneous differentiation). Media was exchanged every two days. After two weeks, cells were washed with DPBS, fixed with 10% (v/v) neutral buffered Formalin and stained with Red-Oil solution (1.8 g/L).

Osteogenic differentiation: 6 x 10^4 cells were inoculated *per* well (5 wells) in a 24-well-plate. After reaching confluency, differentiation media (StemMACS™ OsteoDiff Media, Miltenyi Biotec) was added to three wells in each plate, and MEM Alpha supplemented with 10% (v/v) FBS was added to two wells (monitoring spontaneous differentiation). Media was

exchanged every two days. After three weeks, cells were washed with DPBS, fixed with 10% (v/v) neutral buffered Formalin and stained with Alizarin-staining solution (20 g/L).

Chondrogenesis differentiation: 2.5 x 10^5 cells were inoculated *per* well (4 wells) in a 24-well-plate in three 5 µL droplets. After reaching confluency, differentiation medium (StemPro® Chondrogenesis Differentiation Kit, supplemented with Gentamicin (10 mg/mL)) was added to three wells in each plate, and MEM Alpha supplemented with 10% (v/v) FBS was added to one well (monitoring spontaneous differentiation). The media were exchanged every two days. After three weeks, cells were washed with DPBS fixed with 4% (v/v) PFA and stained with 1% (w/v) Alcian Blue solution.

After staining, cells were visualized using inverted phase contrast microscopy (Leica DMIRB, Leica Microsystems GmbH). Representative pictures were obtained using Leica DFC 295 digital camera.

2.4 Statistical Analysis

All statistical analyses were performed using GraphPad Prism version 5 (GraphPad Software Inc., California, USA). Values are represented as mean ± standard deviation (at least n = 3 replicates were considered) of independent measurements or assays. The statistical significance was evaluated using either Student's T test or one-way ANOVA analysis (repeated measures ANOVA, Tukey analysis). *p* values of less than 0.05 were considered as statistically significant.

3. Results

3.1 hMSC clarification (microcarrier removal) using dead end filtration

Cells were expanded in stirred systems using cationic polystyrene charged microcarriers and harvested as described in Materials and Methods section. Different filter materials, namely nylon and polypropylene, were evaluated for microcarrier removal from the cell bulk suspension using dead end filtration techniques (Figure 2.1A). Due to size differences between cells (15 - 20 µm) and microcarriers (125 - 212 µm) (Figure 2.2A, left panel), several pore sizes were also tested (30, 80 and 100 µm). Their impact on the cell's recovery yield and viability was evaluated (Figure 2.2).

From the initial screenings using disk filters, both materials – nylon and polypropylene – showed to be suitable for the clarification step, since there were no significant differences

concerning cell recovery yields (Figure 2.2B). Moreover, higher cell recovery yields (92%, Figure 2.2B) were obtained when higher pore sizes (80, 100 µm) were used. Although efficient microcarrier removal was achieved in all evaluated strategies (no beads were detected in the filtrate stream by microscopic and visual inspection, Figure 2.2A right panel), lower pore sizes (30 µm) revealed to be unsuitable for the clarification step, since less than 70% of viable cells were recovered (Figure 2.2B). Nonetheless, cells maintained their viability throughout the dead end filtration process (> 96%).

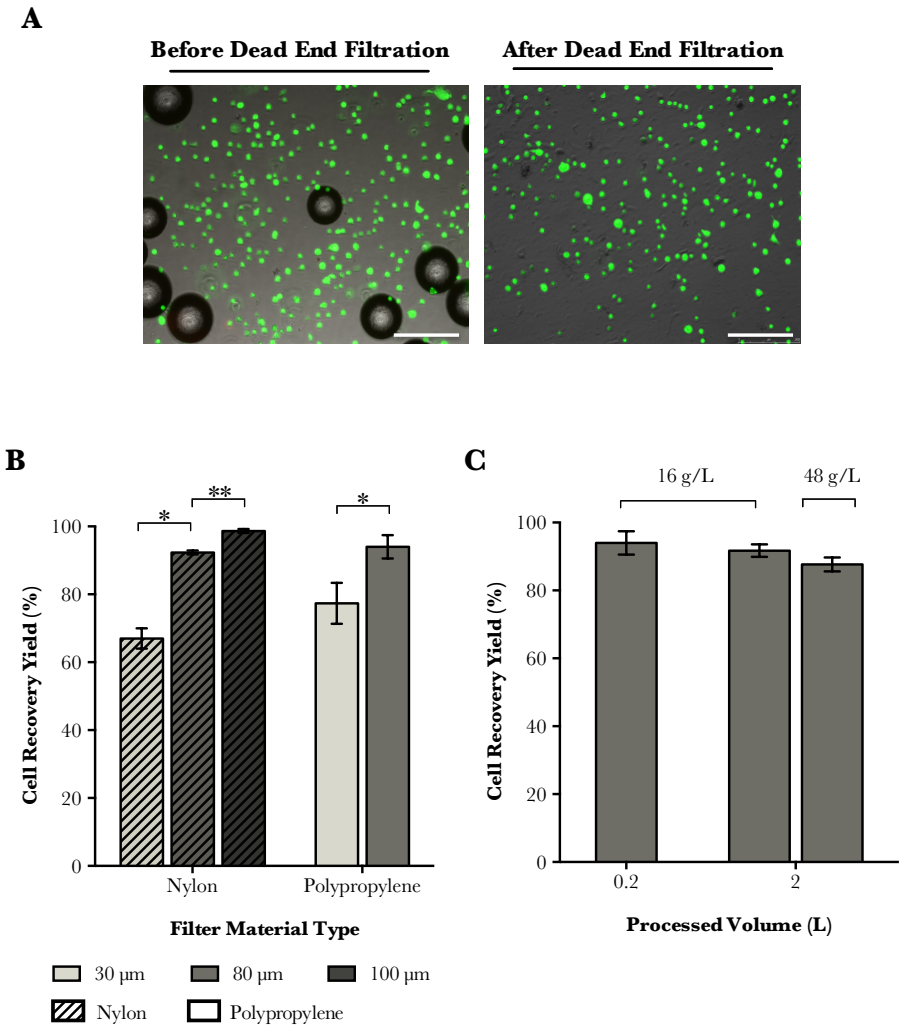

Figure 2.2 – Clarification of microcarriers from the cell bulk. Impact of filter material, filter pore size and working scale on cell recovery yield after dead end filtration step. Phase contrast and fluorescence images (A) of cells before (left panel) and after (right panel) dead end filtration using 75 µm polypropylene filters. Cell viability analysis of hMSC stained with fluoresceine diacetate (FDA - live cells, green) and propidium iodide (PI - dead cells, red). Scale bar: 250 µm. Effect of (B) pore size (30, 80 and 100 µm), material (nylon and polypropylene), (C) processed volume and two microcarrier concentrations (16 and 48 g/L, using 75 µm polypropylene filters) on the cell recovery yield. Statistically significant differences ($P < 0.05$) are * marked, whereas those which do not are marked as **.

From the initial screening in 0.2 L scale, our results indicate that polypropylene filters with pore sizes higher than 30 µm are able to successfully remove at least 92 mg

microcarriers/$cm^2_{membrane}$. Larger scale polypropylene filter capsules (Opticap™-XL) were then used for the scale-up of the clarification step. Nearly the same cell recovery yields were assured when processing up to 2 L of hMSC suspension with either 16 g/L or 48 g/L (Figure 2.2C) of microcarriers. Additionally, no differences in cell recovery yields (97%) and viability (higher than 95%) were observed when using polypropylene filter capsules with even higher pore sizes (100 µm). At the end of the filtration process, no microcarriers were observed in the filtrate stream, as confirmed by microscopic and visual inspection (data not shown).

3.2 Cell concentration/volume reduction using tangential flow filtration

The optimization of the hMSC concentration process using TFF was divided in two phases. Initially, the impact of the membrane material and pore size, as well as the initial cell concentration, on cell recovery yields and cell viability (up to a concentration factor of four) were studied. Thereafter, using the most suitable hollow fiber device and initial cell concentration, our goal was to increase the concentration factor of hMSC up to ten fold. Thus, we have studied the impact that TFF process parameters of shear rate and permeate flux have on the final cell recovery yield and on the hMSC's quality attributes.

3.2.1 Selection of the hollow fiber's characteristics and optimization of initial cell concentrations

Microfiltration membrane materials of polysulfone (PS) and modified polyethersulfone (PES) were tested (Figure 2.3A). PS allowed to recover higher cell numbers (96%) for a two and four fold volume reduction factor than PES material (94%, Figure 2.3A). The modified PES material has also lead to irreversible membrane fouling (observed by the decrease of the permeate flux over time), hampering the concentration process further than a four-fold volume concentration factor (Figure 2.3B).

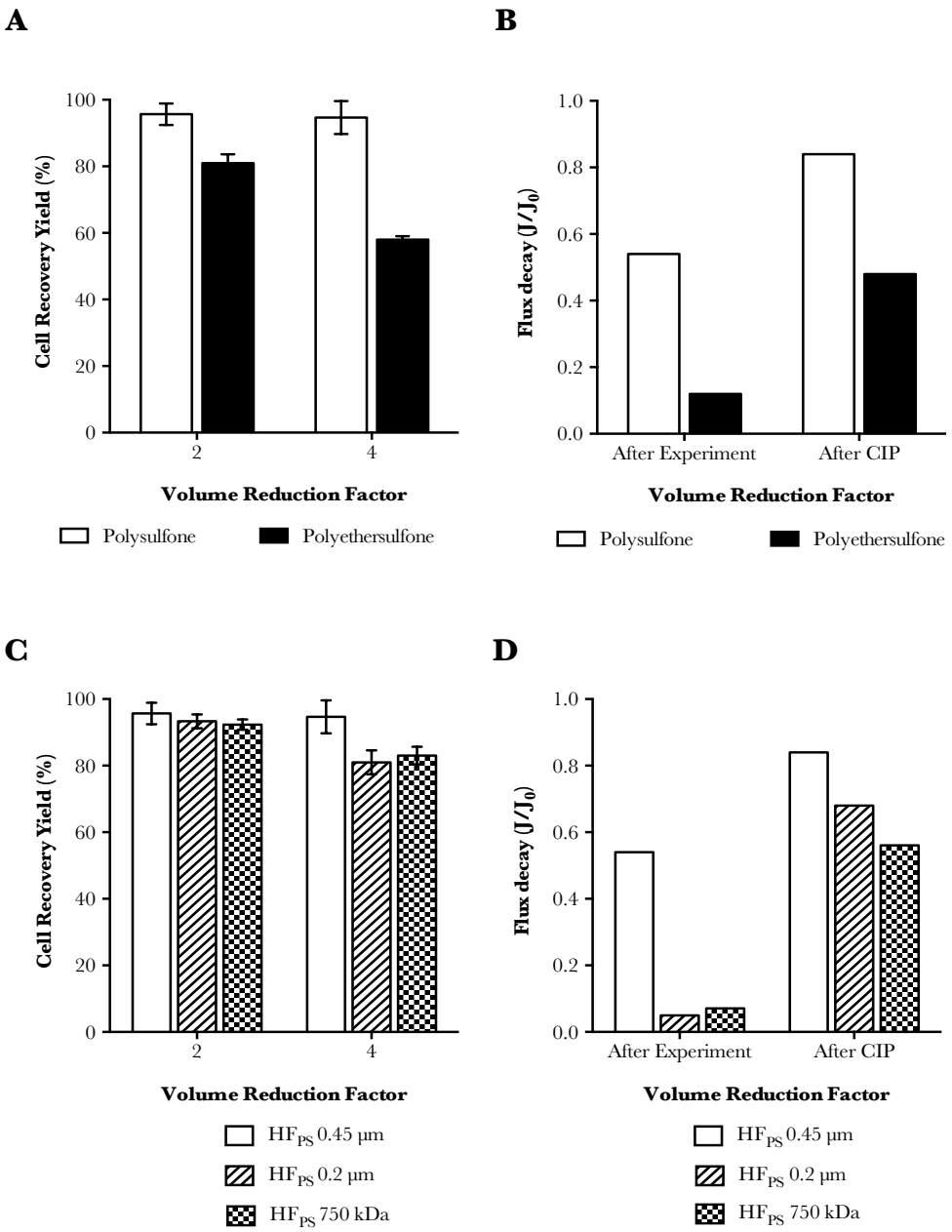

Figure 2.3 – Impact of hollow fiber device's characteristics on the cell recovery of the volume reduction step. Shear rate (3000 s^{-1}), permeate flux (60 LMH) and capacity (80 $L.m^{-2}$) were kept constant for all experiments. The experiments were designed to obtain a volume reduction factor of two and four, using the HF listed on Table 2.1. Different membrane materials were evaluated (A) and permeate flux decay profiles were achieved (B) using polysulfone (HFPS D) and modified polyethersulfone (HFPES G). The impact of the pore size (C) was also studied and permeate flux decay profiles were obtained (D) using 0.45 µm (HFPS D), 0.2 µm (HFPS E) and 750 kDa (HFPS F).

Figure 2.3C depicts the effect of the membrane's pore size on the concentration process. Higher pore sizes (>0.45 µm) allowed to recover over 15% more viable cells for a four fold concentration factor (Figure 2.3C), than lower pore sizes (0.2 µm and 750 kDa). Moreover, lower pore sizes (0.2 µm and 750 kDa) were prone to fouling, leading to a complete clogging of the membrane after a volume reduction factor (VRF) of four (Figure 2.3D).

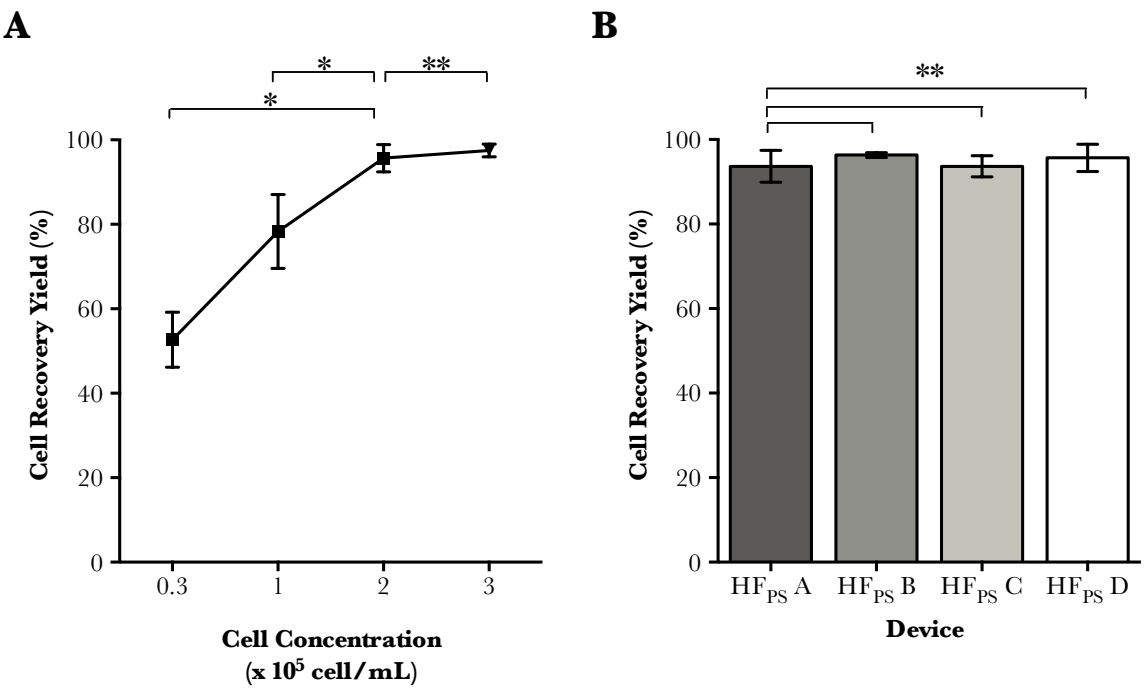

Figure 2.4 – Impact of initial cell concentration on the cell recovery of the volume reduction step. Shear rate (3000 s^{-1}), permeate flux (60 LMH) and capacity (80 $L.m^{-2}$) were kept constant for all experiments. The experiments were designed to obtain a VRF of two, using the hollow fiber devices listed on Table 2.1. (A) Impact of initial cell concentration. (B) Behavior of HF A to D on the concentration step. Statistically significant differences ($P < 0.05$) are marked as *, whereas those which do not are represented as **.

A range of initial cell concentrations was selected in order to study the impact of this parameter (maintaining the filtration throughput constant) on the concentration process for a VRF of two (Figure 2.4A). The rationale behind the selection of these values was based on the range of cell concentrations typically achieved after cell expansion and harvesting (Santos et al., 2011). For lower cell concentrations (0.3 x 10^5 cell/mL, Figure 2.4A) no more than 53% of the cells can be recovered. As the cell concentration increases, cell loss becomes lower, dropping below 5% (Figure 2.4A) at cell concentrations higher than 2 x 10^5 cell/mL (at least 1.8 x 10^6 cells/cm^2). Furthermore, when even high cell concentrations were used (3 x 10^5 cell/mL), no significant differences were observed (Figure 2.4A). For all conducted experiments, cell viability was always higher than 95% and no cell lysis was detected (monitored by the release of LDH to the culture supernatant).

Having optimized the membrane's material, pore size and cell concentration, the performance of different HF with different characteristics was compared (Table 2.1). As shown in Figure 2.4B, no significant differences were observed, all devices (HF_{PS} A – HF_{PS} D, Table 2.1) having enabled to retrieve more than 90% of cells, for a VRF of 2. Therefore, from this point onwards all experiments were conducted with HF with polysulfone membrane with high pore size (0.65 µm) and with the most cost-effective surface area (24 cm^2, HF_{PS} C, Table 2.1) to

perform the process in our working scale (up to 0.25 L), starting with at least a cell concentration of 2 x 10^5 cell/mL, corresponding to 1.8 x 10^6 cells/cm^2.

3.2.2 Impact of process parameters on the concentration step

3.2.2.1 Shear Rate

According to Equation 7 (Materials and Methods), the shear rate is dependent on the inner radius of the hollow fiber and on the inlet flux. In our work, this parameter was modulated through the variation of the inlet flux, by keeping constant the inner radius of the hollow fibers. Due to their resemblance with hMSC, human foreskin fibroblasts (hFF) (Alt et al., 2011) were first used to screen the most appropriate shear rates (3000, 6000, 10,000 and 16,000 s^{-1}, Figure 2.5).

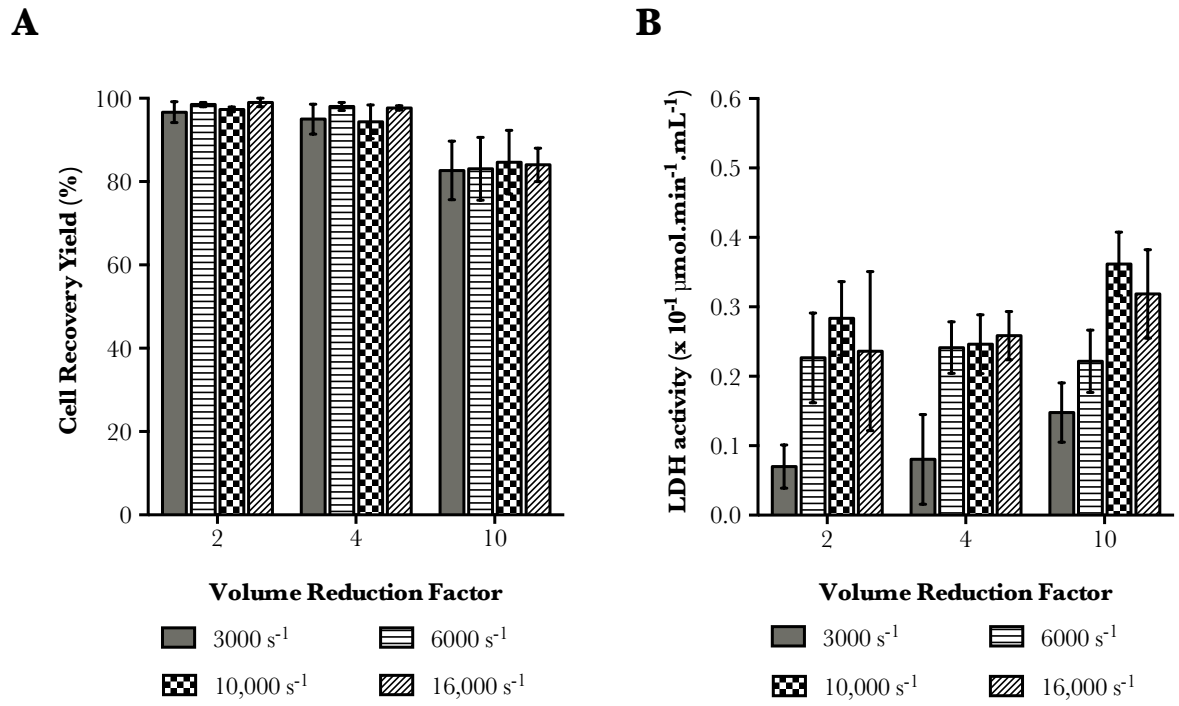

Figure 2.5 – Impact of the shear rate on hFF's cell recovery yield of the concentration process. The shear rate was varied through the inlet flux. Different shear rates were applied aiming at a VRF of two, four and ten (sequentially), using HF_{PS} C. (A) Effect of four shear rates: 3000 s^{-1} (J = 750 LMH), 6000 s^{-1} (J = 1500 LMH), 10,000 s^{-1} (J = 2500 LMH) and 16,000 s^{-1} (J = 4000 LMH) on cell recovery yield. (B) Intracellular LDH release profile over the concentration step.

A shear rate of 3000 s^{-1} was shown to be the most suitable condition, yielding the best compromise between cell recovery (higher than 80%, Figure 2.5A) and cell lysis (Figure 2.5B). Given the already well reported implications of shear stress on cells (Dong et al., 2009; Kretzmer, 2000; Yourek et al., 2010), the impact of even lower shear rates (700, 1500 and 3000 s^{-1}) along the hMSC concentration process was evaluated. In order to achieve the values of shear

rates mentioned above, fluxes of 175, 375 and 750 LMH were applied, respectively (Table 2.2, Figure 2.6).

Up to a volume reduction factor of four (Figure 2.6A), the highest shear rate condition (3000 s^{-1}) allowed to recover higher number of viable cells (88%, Figure 2.6A), with higher viability (95%, Table 2.2), while ensuring lower cell death (Figure 2.6C). Moreover, for the lowest tested shear rate (700 s^{-1}) the permeate flux declined over time (Figure 2.6B), leading to an irreversible fouling of the membrane (Figure 2.6D). It is important to note that cells are not exposed to even higher shear stresses throughout the concentration process (shear stress was kept constant, Equation 8), since the measured viscosity of the processed sample did not increase.

The quality attributes of hMSC before and after TFF (using a shear rate of 3000 s^{-1}) were monitored and compared. Although a high shear rate was applied, this condition has showed not to impact cell size, which remained unaltered (15 – 20 μm), nor cell morphology, since after plating they could successfully re-acquire their typical spindle-like morphology with organized actin fibers (Figure 2.7A). Moreover, cells have maintained their ability to adhere to treated plastic surfaces (no significant differences observed towards hMSC before TFF, Figure 2.9A). The expression of the main characteristic hMSC's surface receptors, as described in the literature (Dominici et al., 2006), remained unaltered after the concentration process (Figure 2.7B). More specifically, hMSC were negative for hematopoietic CD34 and CD45 markers, as well as for HLA-DR and displayed high levels of CD44, CD73, CD105 and CD166 mesenchymal stem markers. Furthermore, hMSC maintained their multipotent differentiation potential, since they could successfully differentiate into adipocytes, osteocytes and chondrocytes (Figure 2.7C). No spontaneous differentiation was observed (data not shown).

3.2.2.2 Permeate Flux

There are several studies that describe constant flux experimental designs either by restricting the permeate flow with a valve or by using a pump to accurately control the permeate flux and to maintain a low transmembrane pressure (Zydney and Kuriyel, 2000). In this work, the control of the permeate flux by means of a pump instead of a permeate valve was studied and showed to maintain constant the permeate flux throughout the process, maximizing the cell recovery yield of the concentration process (Figure 2.8A).

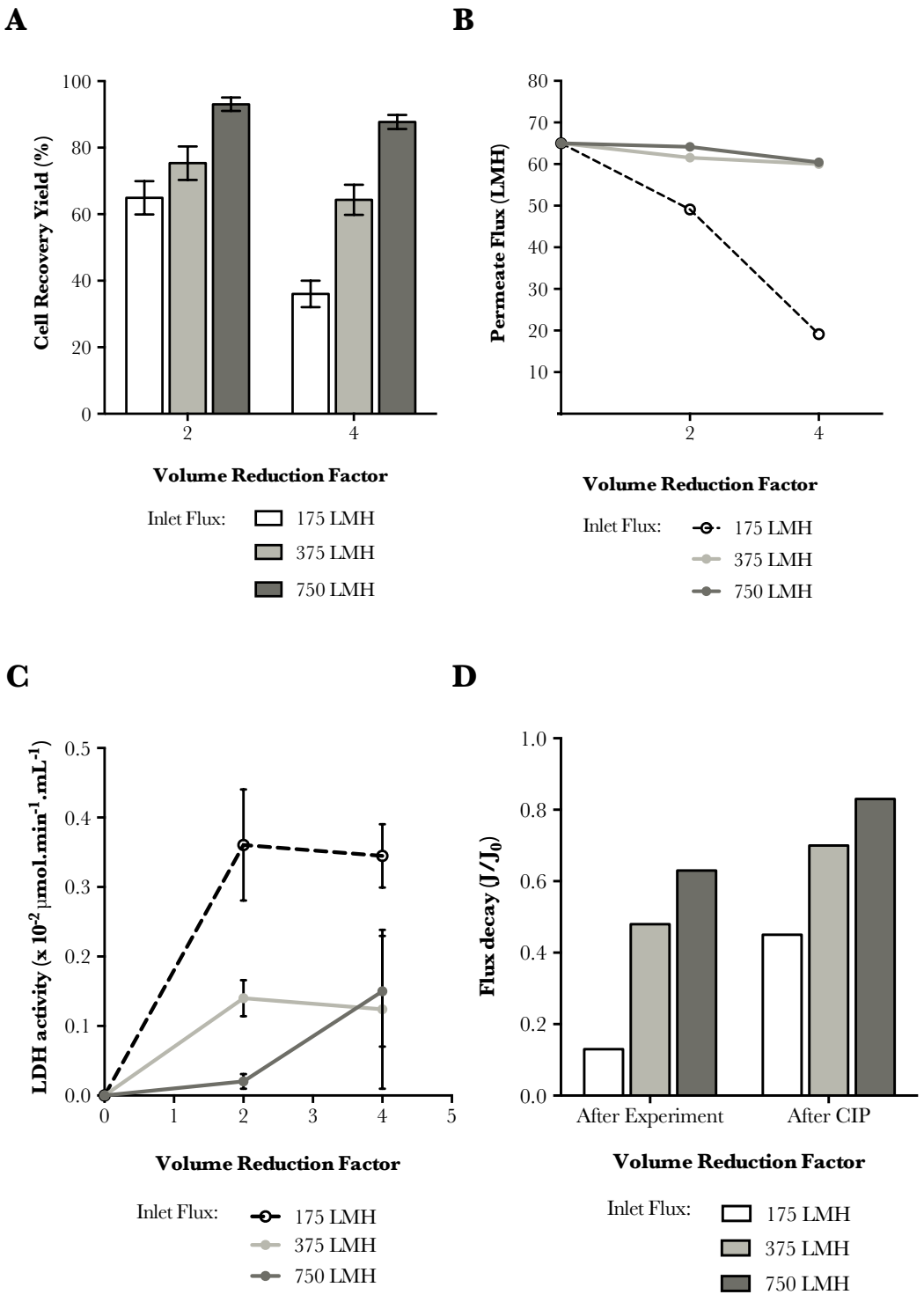

Figure 2.6 – Impact of the shear rate on hMSC's cell recovery yield of the concentration process. The shear rate was varied through the inlet flux (Table 2.2). Different shear rates were applied aiming at a VRF of two and four (sequentially), using HFPS C. (A) Effect of three shear rates: 700 s^{-1} (J = 175 LMH), 1500 s^{-1} (J = 375 LMH) and 3000 s^{-1} (J = 750 LMH) on cell recovery yield. (B) Variation of the permeate flux throughout the concentration process, for the tested shear rates. (C) Intracellular LDH release profile over the concentration step. (D) Permeate flux decay profiles after performing the concentration step and the cleaning in place (CIP).

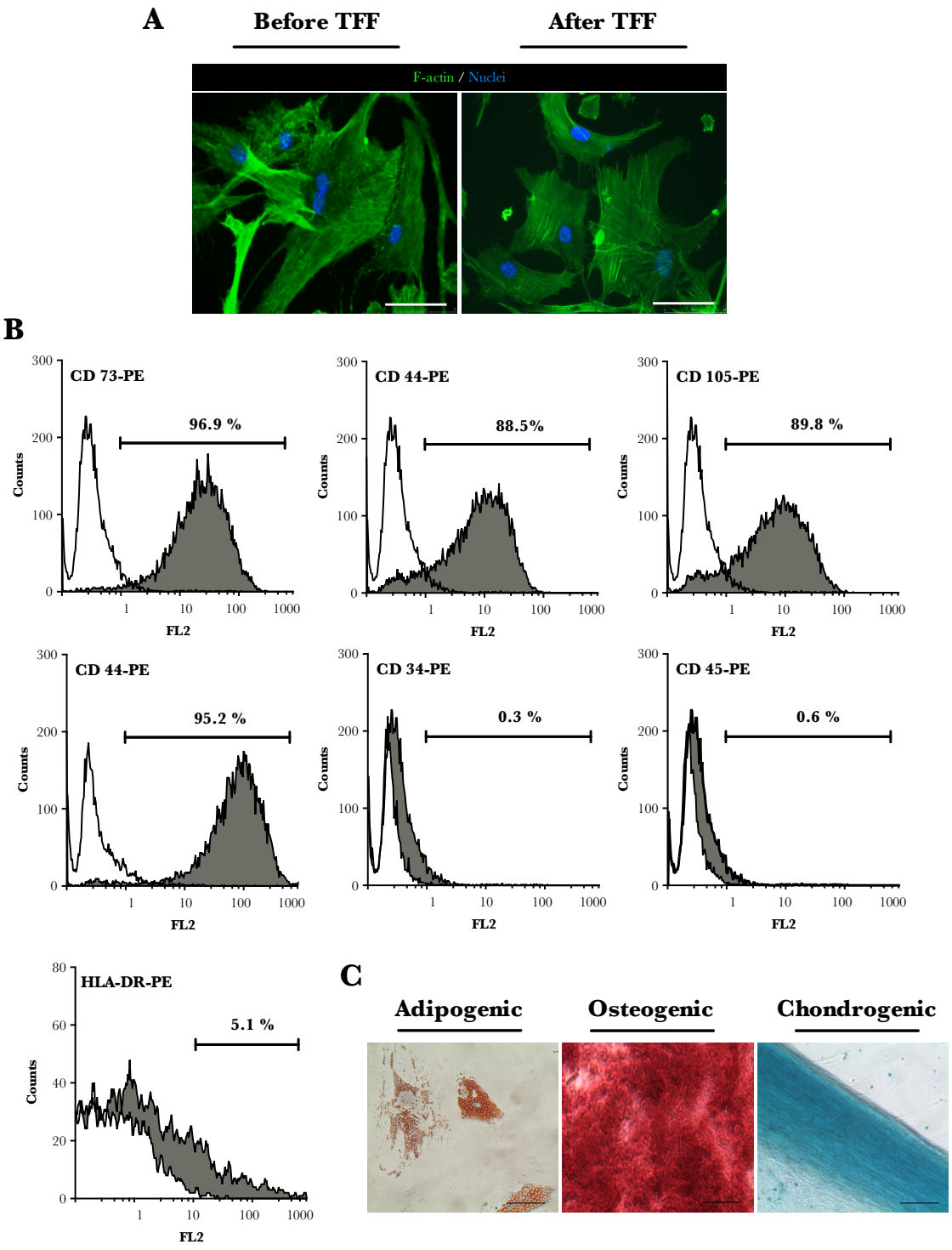

Figure 2.7 – Effect of the concentration step (using a shear rate of 3000 s^{-1}) on hMSC's characteristics. (A) Immunofluorescence staining of actin stress fibers of hMSC collected before (left panel) and after TFF (right panel). Scale bars: 75 µm. (B) Expression of specific cell-surface antigens (CD166, CD105, CD73, CD44, CD45, CD34, HLA-DR) typical for hMSC. (C) Multipotent differentiation potential of concentrated hMSC. Red-oil solution stained lipid droplets (adipocytes, left panel), alizarin red stained calcium deposits (osteoblasts, central panel), and alcian blue stained extracellular matrix proteins (chondrocytes, right panel). Scale bars: 100 µm.

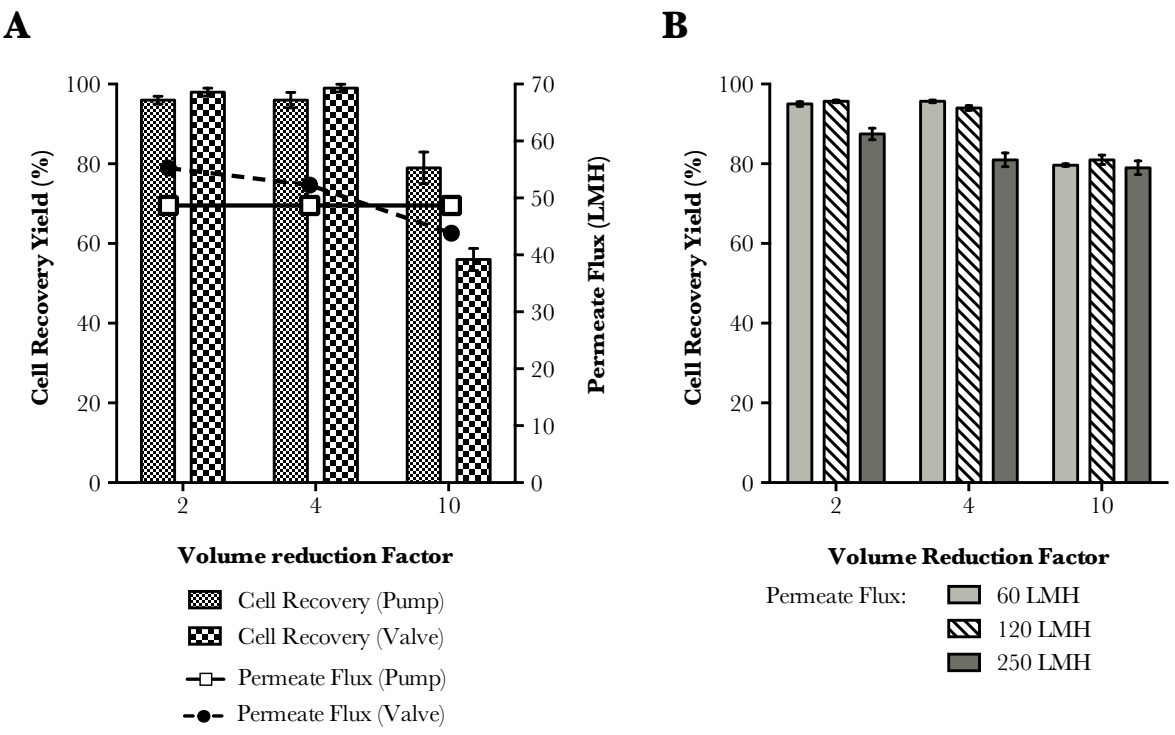

Figure 2.8 – Impact of the permeate flux on hMSC's cell recovery yield of the concentration process. A volume reduction factor of ten was performed using permeate fluxes of 60, 120 and 250 LMH (Table 2.3). (A) Effect of the permeate flux control through a pump (full line) or valve (dashed line) on the cell recovery yield. (B) Cell recovery yield achieved using the tested permeate fluxes (controlled with a pump).

The operation using a permeate valve lead to a decrease of the permeate flux over time, since there is no control of the fouling process, leading to a decrease in cell recovery yield (Figure 2.8A). Similarly to previous studies (Cheryan, 1998; Miller et al., 2013), our data suggests that the control of the permeate flux using a pump is fundamental for the success of the concentration process, since unrestricted permeate flow presents differences in cell recovery yield of 23% (Figure 2.8A).

To decrease the process time, three different permeate fluxes - 60, 120 and 250 LMH (Table 2.3) were evaluated. As observed in Figure 2.8B, the permeate flux does not impact the cell concentration process, since no differences can be observed regarding the cell recovery yield; 80% of viable cells could be recovered after a VRF of 10. The observed 20% cell loss (Figure 2.8B) can be attributed to the entrapment of those cells into the HF modules, since no significant cell death was observed, nor were cells found on the permeate stream (data not shown). Additionally, our data suggests that this phenomenon was not due to a cell concentration effect (high cell concentrations could lead to cell losses through precipitation, aggregation, etc.); when concentrating two fold a cell suspension with an initial cell concentration of 8×10^5 cell/mL (typical cell concentration achieved at VRF of 4), no significant differences were observed regarding cell recovery yield (data not shown).

Although no differences were observed regarding cell recovery yields, a higher permeate flux permitted a four-time faster process (Table 2.3), concomitantly with recovering hMSC with higher quality. Slower process time (when using a permeate flux of 60 LMH) led to a significant decrease in the cells' proliferation capability (Figure 2.9A), as well as a significant increase in apoptosis (Figure 2.9A), when compared to cells before TFF. The combination of these results may explain the differences observed on the cell adhesion kinetics (Figure 2.9A), where using a permeate flux of 60 LMH lead to a decrease in cell adhesion 30 min after plating, while no differences could be observed at a higher permeate flux (250 LMH) (Figure 2.9A). Nonetheless, both permeate fluxes allowed to concentrate hMSC, maintaining their metabolic activity (Figure 2.9A), morphology (Figure 2.9B), identity (Figure 2.9C), potency (Figure 2.9D), and viability (higher than 92%, Table 2.3).

Furthermore, even higher permeate fluxes (Table 2.3) were attempted in order to further decrease the process time. 70% of cells could be recovered after a VRF of 10; the condition led to an irreversible fouling of the membrane, hampering the concentration process.

4. Discussion

Efficient and cGMP compatible downstream processes are needed in order to promote the transition of hMSC to clinical applications. The aim of this work was to develop a scalable downstream process for the clarification (i.e. microcarrier removal) and concentration of hMSC (i.e volume reduction), based on the optimization of well-established filtration techniques (dead end filtration and TFF). Results show that microcarriers can be efficiently removed from the cell suspension using polypropylene filters with pore sizes higher than 75 µm, and that hMSC can be successfully concentrated ten fold using TFF (with over than 80% cell recovery yield) maintaining their viability, identity and potency.

Polypropylene filters were successfully implemented up to a 2 L scale to clarify the cell bulk suspension, with complete microcarriers removal and high hMSC recovery (> 94%) and viability (> 95%). Pore size is critical for the efficiency of the clarification step. High pore size filters (> 75 µm) permitted higher cell recoveries, while lower pore size filters (30 µm) are subjected to microcarrier cake formation, entrapping part of the cell suspension, as previously observed by Nienow's group (Nienow et al., 2014).

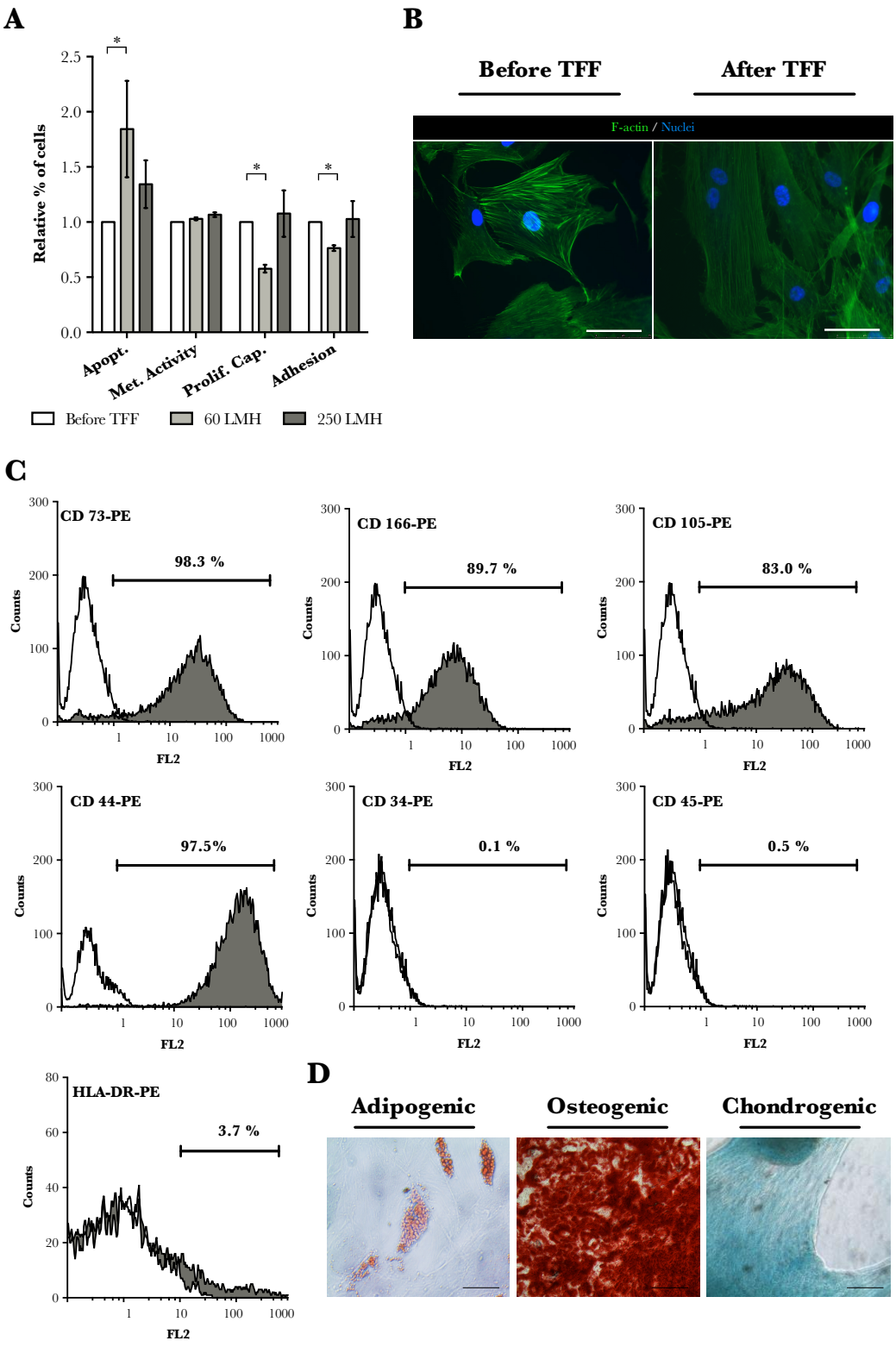

Figure 2.9 – Effect of the permeate flux on hMSC's characteristics, after the concentration step. (A) Cell characterization (apoptosis, metabolic activity, proliferative capability, and cell adhesion) after the concentration process using a permeate flux of 60 and 250 LMH. Each bar represents the fold-increase/decrease, relative to cells before TFF (white). Statistically significant differences ($P < 0.05$) towards hMSC before TFF cells are marked as *. (B) Immunofluorescence staining of actin stress fibers of hMSC collected before (left panel) and after TFF (right panel), using a permeate flux of 250 LMH. Scale bars: 75 µm. (C) Expression of specific cell-surface antigens (CD166, CD105, CD73, CD44, CD45, CD34, HLA-DR) typical for hMSC. (D) Multipotent differentiation potential of concentrated hMSC. Red-oil solution stained lipid droplets (adipocytes, left panel),

alizarin red stained calcium deposits (osteoblasts, central panel), and alcian blue stained extracellular matrix proteins (chondrocytes, right panel). Scale bars: 100 µm.

Cell therapies will need high cell numbers delivered at low volumes (1 - 8 x 10^6 cell/mL, in 40 - 50 mL *per* kg of patient body weight) (Murphy et al., 2013; Patel and Genovese, 2011), e.g. Prochymal®. For the cell concentration step, several process parameters, such as shear rate, and the permeate flux, as well as the initial cell concentration, showed to impact the TFF process performance. Data showed that there was always adsorption of cells to the membrane's surface. Nonetheless, if a minimum cell concentration of 2 x 10^5 cell/mL (corresponding to 1.8 x 10^6 cells/cm^2) is not assured, that adsorption can reach 22 - 50% of the overall cell quantity. Therefore, depending on the therapeutic use, upstream processing has to aim not only to high cell numbers, but also to sufficient volumetric cell productivities (during cell expansion and/or harvesting) to undergo DSP.

Although TFF aims towards the prevention of cake formation, membrane fouling is an inevitable outcome of filtration (van Reis and Zydney, 2007). Results show that the membrane's material and pore size contributed significantly to this phenomenon. As previously reported, higher pore sizes have shown a trend to be less prone to fouling (Castilho and Medronho, 2002). Moreover, the hydrophobicity of PS and PES may lead to an increase of their interaction with a variety of solutes, in comparison to more hydrophilic polymers such as cellulose and regenerated cellulose (Cheryan, 1998). Within this context, lower process times are preferable, decreasing the probability of interaction between hMSC and the membrane's surface, preserving the cells' characteristics.

To avoid cell damage by pushing cells into the membrane pores (Zydney and Kuriyel, 2000), gentler processes, translated by lower permeate fluxes (30 - 50 LMH), are usually preferred for the concentration of biopharmaceuticals (Walter et al., 2011). However, data showed that a permeate flux of 250 LMH was adequate to prevent such damage, allowing to achieve a four-time faster process, for a VRF of 10, recovering 80% of highly viable cells maintaining their potency and identity. In fact, results showed that longer process times, promoted an increase in apoptosis and a decrease in cell's proliferative capacity.

Companies in the cell therapy field are currently considering low-shear processes to perform the volume reduction and washing steps of cell-based products (Pattasseril et al., 2013). The impact of shear rate and shear stress on hMSC viability and differentiation potential have already been reported (Dong et al., 2009; Yourek et al., 2010). High shear rates are known to decrease fouling during microfiltration processes (Wakeman and Williams, 2002). Thus, a trade-off between fouling effects and cell damage shall be reached in order to successfully accomplish

hMSC's concentration. This study indicated that a shear rate of 3000 s^{-1}, already reported for processing other mammalian cells using TFF (Vickroy et al., 2007), was more suitable to perform the concentration process than reduced shear rates (700 s^{-1}), as it led to higher cell recovery yields, correlated with smaller decline on the permeate flux over time. Additionally, a shear rate of 700 s^{-1} led to an increase in cell death and a decreased cell viability, increasing the membrane's fouling. This can be correlated to the increased cells' residence time inside the TFF device (lower inlet flux), increasing the probability of their interaction with the membrane matrix. Since no significant cell numbers could be retrieved from the HF after incubation with TrypLE Select dissociation reagent, it is possible to assume that the cells remain strongly attached and/or entrapped in the matrix. When using a 3000 s^{-1} shear rate, cell viability was higher than 92%, no differences were observed regarding cell size, and hMSC maintained their ability to adhere to plastic surfaces. Cells successfully re-acquired their typical spindle-like morphology with organized actin fibers (Alt et al., 2011; Sonowal et al., 2013). Moreover, after the concentration process, hMSC maintained their immunophenotype, proliferation capacity and multipotent differentiation potential.

In conclusion, the work herein described is the first demonstration of the impact that several parameters of filtration techniques have on hMSC's recovery yield and quality. Due to the characteristics of the applied methodologies, the described DSP train will have applicability for both autologous and allogeneic therapies, fulfilling the particular needs for both scale-up and scale-out. Moreover, by knowing the effects of each of the parameters on the process, more rational approaches can be developed to incorporate an efficient washing step (Chapter 4) and to even increase the concentration factor up to 20 – 50 (Chapter 5). Preliminary data using hFF showed also that a VRF of 20 can be achieved, recovering over 80% of viable cells. This strategy should be applicable to other stem cell types relevant for the cell therapy industry (Chapter 3).

5. Acknowledgments

I would like to acknowledge M.Sc. Duarte Martins and Eng. Marcos Sousa for their technical support and to Dr. Ricardo Silva for fruitful discussions and manuscript revision.

I would like to acknowledge Asahi Kasei (Japan) for the provided materials, and also for the fruitful discussions throughout this work; and Corning Inc. for providing the microcarriers used in this study.

This work was funded by Fundação para a Ciência e Tecnologia (FCT, Portugal) (project EXPL/BBB-EBI/1003/2012 and PhD grant SFRH/BD/51940/2012, MIT-Portugal

Program) and by NanoGene project (EuroNanoMed ERA-Net initiative - ENMED/0001/2010).

References

Alt, E., Yan, Y., Gehmert, S., Song, Y.-H., Altman, A., Gehmert, S., Vykoukal, D., Bai, X., 2011. Fibroblasts share mesenchymal phenotypes with stem cells, but lack their differentiation and colony-forming potential. Biol. Cell 103, 197–208.

Castilho, L.R., Medronho, R.A., 2002. Cell retention devices for suspended-cell perfusion cultures. Adv. Biochem. Eng. Biotechnol. 74, 129–169.

Charcosset, C., 2012. Principles on membrane and membrane processes, in: Membrane Processes in Biotechnology and Pharmaceutics. Kidlington, Oxford, U.K. : Elsevier, pp. 1–30.

Chen, A.K.-L., Reuveny, S., Oh, S.K.W., 2013. Application of human mesenchymal and pluripotent stem cell microcarrier cultures in cellular therapy: Achievements and future direction. Biotechnol. Adv. 31, 1032–1046.

Cheryan, M., 1998. Ultrafiltration and Microfiltration Handbook, 1st ed. Technomic Publishing AG, Basel.

Clincke, M.-F., Mölleryd, C., Zhang, Y., Lindskog, E., Walsh, K., Chotteau, V., 2013. Very high density of CHO cells in perfusion by ATF or TFF in WAVE bioreactor™. Part I. Effect of the cell density on the process. Biotechnol. Prog. 29, 754–767.

Dominici, M., Le Blanc, K., Mueller, I., Slaper-Cortenbach, I., Marini, F., Krause, D., Deans, R., Keating, A., Prockop, D., Horwitz, E., 2006. Minimal criteria for defining multipotent mesenchymal stromal cells. The International Society for Cellular Therapy position statement. Cytotherapy. 8, 315–317.

Dong, J.-D., Gu, Y.-Q., Li, C.-M., Wang, C.-R., Feng, Z.-G., Qiu, R.-X., Chen, B., Li, J.-X., Zhang, S.-W., Wang, Z.-G., Zhang, J., 2009. Response of mesenchymal stem cells to shear stress in tissue-engineered vascular grafts. Acta Pharmacol. Sin. 30, 530–536.

Fotakis, G., Timbrell, J.A., 2006. In vitro cytotoxicity assays: comparison of LDH, neutral red, MTT and protein assay in hepatoma cell lines following exposure to cadmium chloride. Toxicol. Lett. 160, 171–177.

Haynesworth, S.E., Baber, M.A., Caplan, A.I., 1996. Cytokine expression by human marrow-derived mesenchymal progenitor cells in vitro: effects of dexamethasone and IL-1 alpha. J. Cell. Physiol. 166, 585–592.

Iyer, S.S., Rojas, M., 2008. Anti-inflammatory effects of mesenchymal stem cells: novel concept for future therapies. Expert Opin. Biol. Ther. 8, 569–581.

Jones, K.H., Senft, J.A., 1985. An improved method to determine cell viability by simultaneous

staining with fluorescein diacetate-propidium iodide. J. Histochem. Cytochem. 33, 77–79.

Kehoe, D., 2014. Scalable expansion and harvest solutions for allogeneic stem cells, in: Oral presentation at Scale-up and Manufacturing of Cell-Based Therapies III, San Diego, USA.

Kretzmer, G., 2000. Influence of stress on adherent cells. Adv. Biochem. Eng. Biotechnol. 67, 123–137.

Lilova, K., 2014. Process development and scale-up of an allogeneic cell therapy product, in: Oral presentation at Scale-up and Manufacturing of Cell-Based Therapies III, San Diego, USA.

Maiorella, B., Dorin, G., Carion, A., 1991. Crossflow microfiltration of animal cells. Biotechnol. Bioeng. 37, 121–126.

Mason, C., Dunnill, P., 2009. Quantities of cells used for regenerative medicine and some implications for clinicians and bioprocessors. Regen. Med. 4, 153–157.

Miller, D.J., Paul, D.R., Freeman, B.D., 2013. A crossflow filtration system for constant permeate flux membrane fouling characterization. Rev. Sci. Instrum. 84, 035003.

Murphy, M.B., Moncivais, K., Caplan, A.I., 2013. Mesenchymal stem cells: environmentally responsive therapeutics for regenerative medicine. Exp. Mol. Med. 45, 54–70.

Nienow, A.W., Rafiq, Q.A., Coopman, K., Hewitt, C.J., 2014. A potentially scalable method for the harvesting of hMSCs from microcarriers. Biochem. Eng. J. 85, 79–88.

Patel, A.N., Genovese, J., 2011. Potential clinical applications of adult human mesenchymal stem cell (Prochymal R) therapy. Stem Cells Cloning: Adv. Appl. 4, 61–72.

Pattasseril, J., Varadaraju, H., Lock, L., Rowley, J.A., Rowley, J.A., 2013. Downstream Technology Landscape for Large-Scale Therapeutic Cell Processing. BioProcess Int. 11, 38–47.

Saha, K., Lin, Y.C., Wong, P.K., 1994. A simple method for obtaining highly viable virus from culture supernatant. J. Virol. Methods 46, 349–352.

Santos, F.D., Andrade, P.Z., Abecasis, M.M., Gimble, J.M., Chase, L.G., Campbell, A.M., Boucher, S., Vemuri, M.C., Silva, Cabral, J.M.S., 2011. Toward a Clinical-Grade Expansion of Mesenchymal Stem Cells from Human Sources: A Microcarrier-Based Culture System Under Xeno-Free Conditions. Tissue Eng. Part C. 17, 1201–1210.

Serra, M., Brito, C., Correia, C., Alves, P.M., 2012. Process engineering of human pluripotent stem cells for clinical application. Trends Biotechnol. 30, 350–359.

Son, Y., 2007. Determination of shear viscosity and shear rate from pressure drop and flow rate relationship in a rectangular channel. Polymer 48, 632–637.

Sonowal, H., Kumar, A., Bhattacharyya, J., Gogoi, P.K., Jaganathan, B.G., 2013. Inhibition

of actin polymerization decreases osteogeneic differentiation of mesenchymal stem cells through p38 MAPK pathway. J. Biomed. Sci. 20, 71–81.

van Reis, R., Leonard, L.C., Hsu, C.C., Builder, S.E., 1991. Industrial scale harvest of proteins from mammalian cell culture by tangential flow filtration. Biotechnol. Bioeng. 38, 413–422.

van Reis, R., Zydney, A., 2007. Bioprocess membrane technology. J. Membr. Sci. 297, 16–50.

Vassault, A., 1983. Lactate dehydrogenase: UV-method with pyruvate and NADH, in: Bergmeyer, H.U., Grassl, M. (Eds.), Methods of Enzymatic Analysis. John Wiley & Sons, New York, pp. 118–126.

Vicente, T., Peixoto, C., Carrondo, M.J.T., Alves, P.M., 2009. Purification of recombinant baculoviruses for gene therapy using membrane processes. Gene Ther. 16, 766–775.

Vickroy, B., Lorenz, K., Kelly, W., 2007. Modeling Shear Damage to Suspended CHO Cells during Cross-Flow Filtration. Biotechnol. Prog. 23, 194–199.

Wakeman, R.J., Williams, C.J., 2002. Additional techniques to improve microfiltration. Sep. Purif. Technol. 26, 3–18.

Walter, J.K., Jin, Z., Jornitz, M.W., Gottschalk, U., 2011. Membrane separations, in: Janson, J.-C. (Ed.), Protein Purification: Principles, High Resolution Methods, and Applications. John Wiley & Sons, Inc., pp. 279–317.

Yourek, G., McCormick, S.M., Mao, J.J., Reilly, G.C., 2010. Shear stress induces osteogenic differentiation of human mesenchymal stem cells. Regen. Med. 5, 713–724.

Zydney, A.L., Kuriyel, R., 2000. High-Performance Tangential Flow Filtration for Protein Separations, in: Desai, M.A. (Ed.), Downstream Processing of Proteins: Methods and Protocols. Humana Press, Totowa, NJ, pp. 35–46.

III

Finding the design space of tangential flow filtration operation for the concentration of human pluripotent stem cells

This chapter was adapted from:

Cunha B & Silva RJS, Correia C, Koshkin A, Carrondo MJT, Serra M, Peixoto C, Alves PM (2016). Finding the design space of a filtration-based operation for the concentration of human pluripotent stem cells, Biotechnology and Bioengineering, *submitted*.

Table of Contents

ABSTRACT 108

1. INTRODUCTION 109

2. MATERIALS AND METHODS 110

2.1 Human induced pluripotent stem cell culture 110
2.2 Downstream processing 110
2.3 Cell viability and characterization assays 111
2.4 Statistical Analysis 115

3. RESULTS AND DISCUSSION 116

4. CONCLUSION 124

5. ACKNOWLEDGMENTS 124

REFERENCES 126

SUPPLEMENTARY DATA 128

Abstract

Process knowledge for designing robust and reproducible unit operations is essential, especially for complex biological systems. This work describes a shortcut approach for the design of tangential flow filtration for the concentration of human induced pluripotent stem cells (hiPSC), supported by design of experiments. Critical process parameters (CPP) of shear rate, permeate flux and cell load were considered, and their impact on hiPSC recovery yield and viability was studied. A full factorial design confirmed significant interaction effects between all CPP, affecting both responses. The developed statistical model predicted that high shear rate (3000 s^{-1}), permeate flux (250 LMH) and medium cell load (2 x 10^6 cell/cm^2) would maximize both cell recovery yield and viability, where over 80% of hiPSC were recovered after a volume reduction factor of 20 with high viability (over 93%). Such conditions were validated experimentally, and by performing a robustness analysis, the success rate of these operating conditions was assessed (65-70%). A parametric study was then conducted, identifying that increasing the shear rate (up to 3370 s^{-1}) allowed to achieve the specified requirements for cell recovery yield (>80%) and viability (>90%) in 100% of the cases and no impact in hiPSC's identity, proliferation capacity and pluripotency was observed.

Keywords: design of experiments, quality by design, human induced pluripotent stem cells, downstream processing, tangential flow filtration

1. Introduction

From the initial promise of human pluripotent stem cells (hPSC) for clinical application, their use in therapies has already covered heart, eye diseases and diabetes (Lipsitz et al., 2016; Trounson and McDonald, 2015); in particular, human induced pluripotent stem cells (hiPSC) have been revolutionizing pre-clinical research as a tool for disease modelling and drug discovery (Takahashi and Yamanaka, 2016).

Cell therapy manufacturing is usually composed of isolation of the desired cell type, its expansion, harvest, concentration, purification, formulation and fill and finish. This workflow is very challenging since the product correspond to living and interacting entities, which are also very difficult to characterize fully (Lipsitz et al., 2016). Quality-by-design (QbD), a risk-based framework based on relating process parameters and product quality, can cope with such complexity in process design (Rathore and Winkle, 2009). First, critical quality attributes (CQA), corresponding to the characteristics that ensure the final product quality, and critical process parameters (CPP), which directly affect cells' CQA, are identified. Thereafter, a design space is developed, studying how a range of variability in CPP allows to achieve CQA (Food and Drug Administration, 2009). Since all steps in manufacturing have CPP with inherent uncertainty (related with equipment, calibration, materials manufacturing), robustness analysis is a valuable tool to gain confidence in process development, as already demonstrated for process design of other biotherapeutics (Nestola et al., 2015). Tools as design of experiments (DoE) allow to maximize the information obtained *per* experiment (Franceschini and Macchietto, 2008), estimating the main effects and the interactions between variables with minimal number of experiments. Thus, its application to develop a design space for cell therapy manufacturing has been previously pursued (Hunt et al., 2013; Marinho et al., 2015).

Previous work on this thesis focused on optimizing tangential flow filtration (TFF) for the volume reduction of human mesenchymal stem cells (hMSC) (Chapter II); shear rate, permeate flux, and cell load were identified as the CPP affecting cells' CQA. Thereby, in this work a DoE approach testing the impact of such CPP on hiPSC's recovery yield and viability was applied. After understanding how the factors interacted between them, the most suitable operating conditions for TFF to concentrate hiPSC was identified and the impact of CPP on hiPSC's CQA in terms of pluripotency phenotype, proliferation capacity and pluripotency was evaluated. Then, a robustness analysis of the process under uncertainty was carried out and a parametric study further improved the process' success rate.

2. Materials and Methods

All reagents used for hiPSC culture were purchased from ThermoFisher™ Scientific (Massachusetts, USA), unless otherwise stated.

2.1 Human induced pluripotent stem cell culture

Human induced pluripotent stem cell (hiPSC) (reprogrammed from foreskin fibroblasts, DF19-9-11T.H from WiCell, Madison, WI, USA) were routinely propagated in static conditions in 6-well plates (BD Biosciences, Bedford, MS, USA) at 37 ºC in a humidified atmosphere of 5% CO_2 in air. hiPSC were cultured on Matrigel™-coated (Corning, New York, USA) plates using mTESR1 (STEMCELL™ Technologies, Vancouver, Canada) medium until 80 – 90% cell confluency. One hour before cell harvesting, cells were incubated with 5 µM Rho-kinase inhibitor Y-27632 (ROCKi) (Merck, Massachusetts, USA). The medium was removed and cells were incubated with Versene for 7-9 min at 37 ºC in a humidified atmosphere of 5% CO_2 in air. Versene was removed and cells were detached using mTESR1 supplemented with 5 µM ROCKi.

To conduct the volume reduction step within the downstream processing (DSP) workflow (section 2.2.1), cells were resuspended in DMEM supplemented with 10% (v/v) of fetal bovine serum (FBS), as in Chapter II, and 5 µM ROCKi.

2.2 Downstream processing

2.2.1 Cell concentration (volume reduction)

The cell suspension was concentrated by tangential flow filtration (TFF), as described in Chapter II and IV. Optimized conditions of shear rate (3000 s^{-1}), permeate flux (250 LMH), initial cell concentration (2 x 10^5 cell/mL), load (1.8 x 10^6 cell/cm^2), and pore size (> 0.45 µm) were used (Chapter II). Hollow fiber cartridges (HF) with 24 cm^2 (GE Healthcare Life Sciences, New Jersey, USA) were operated until the feed volume was close to the system's hold-up volume (volume reduction factor, VRF, of 20). All experiments were performed at a constant inlet flow rate and no decline on the permeate flux was observed.

Watson Marlow Model 120 S/DV 200 rpm pump (Watson-Marlow Pumps Group, Massachusetts, USA) and Tandem Model 1081 peristaltic pump from Sartoflow® Slice 200 benchtop crossflow system (Sartorius Stedim Biotech) were used as permeate and inlet pumps, respectively. Pressure was monitored using SciPres luer pressure sensors (SciLog, Wisconsin,

USA) on the inlet, outlet and permeate stream. Weight and pressure data were monitored and acquired every 15 seconds.

A water flux test was performed before and after each experiment to determine the membrane's permeability. To ensure sterility, the devices were sanitized with 0.5 M NaOH (Merck) at room temperature (20 - 25 ºC) for 45 min. Membranes were preconditioned with five membrane volumes of sterile DPBS before the concentration step.

2.2.2 Experimental design – Design of Experiments (DoE)

Design generation, data analysis, and model construction were performed with MODDE software version 10.1 (Data Analytics Solutions, Umeå, Sweden). A full factorial (FF) design with three factors (shear rate, permeate flux and load), two levels (high, low), two responses (cell recovery yield and cell viability) and one center point for screening purposes was generated. The limits and factors were chosen based on previous results attained with human mesenchymal stem cells (Chapter II). Data fit used a Multiple Linear Regression (MLR) method, assuming that the responses are independent, as validated by a correlation matrix (Table 3.1).

2.3 Cell viability and characterization assays

All described assays were performed with hiPSC before and after the cell concentration step.

2.3.1 Cell number and viability

Cell viability and cell membrane integrity were assessed using three different methods:

2.3.1.1 Trypan Blue exclusion method

Cell concentration was estimated through cell counting using a Fuchs–Rosenthal counting chamber (Marienfeld Superior, Lauda-Königshofen, Germany). The number of viable cells was determined by the trypan blue dye exclusion method. The cell recovery yield (in percentage) was estimated taking into account the number of viable cells before (considered 100%) and after processing.

Table 3.1 – Correlation matrix over model terms and responses obtained for the volume reduction step of hiPSC.

	Permeate Flux (Jp)	**Shear Rate (γ)**	**Load (L)**	**Jp* γ**	**Jp*L**	**L* γ**	**Cell Recovery Yield (%)**	**Cell Viability (%)**
Permeate Flux (Jp)	1	0.347	-0.029	0.420	-0.070	0.014	0.255	0.561
Shear Rate (γ)	0.347	1	-0.0567	-0.007	0.016	-0.057	0.674	0.143
Load (L)	-0.029	-0.057	1	0.041	0.121	0.227	-0.473	0.490
Jp* γ	0.420	-0.007	0.041	1	-0.094	-0.014	0.326	0.726
Jp*L	-0.070	0.016	0.121	-0.094	1	0.292	0.165	-0.362
L* γ	0.014	-0.057	0.227	-0.014	0.292	1	0.249	0.166
Cell Recovery Yield (%)	0.255	0.674	-0.473	0.326	0.165	0.249	1	0.060[3]
Cell Viability (%)	0.561	0.143	0.490	0.726	-0.362	0.166	0.060	1

[3] Cell recovery yield and cell viability responses are independent and not correlated

2.3.1.2 Fluorescein diacetate-propidium iodide staining

Quantitative assessment of the cell plasma membrane integrity was also performed using fluorescein diacetate (FDA, Sigma-Aldrich®, Merck, Massachusetts, USA), and the DNA-dye propidium iodide (PI, Sigma-Aldrich®), as described in the literature (Jones and Senft, 1985). Briefly, cell suspensions were incubated with 20 µg/mL FDA and 10 µg/mL PI in DPBS for 5 min and analyzed by flow cytometry in a CyFlow® instrument (CyFlow® space, Partec GmbH, Münster, Germany). At least ten thousand events were registered *per* sample.

2.3.1.3 Lactate Dehydrogenase (LDH) Assay

The release of intracellular lactate dehydrogenase enzyme (LDH) into the supernatant can be correlated with the extent of cell lysis (Fotakis and Timbrell, 2006). Hence, LDH activity from the supernatant of centrifuged (300 x *g*, 5 min) samples was determined by monitoring at 340 nm the oxidation rate of NADH (Sigma-Aldrich®) to NAD^+ coupled with the reduction of pyruvate (Sigma-Aldrich®) to lactate, as previously described in the literature (Vassault, 1983).

2.3.2 Cell apoptosis

Apoptotic cells and the mitochondrial membrane potential was evaluated using Apoptosis Assay Kit NucView™ 488 and MitoView™ 633 (Biotium, Inc., California, USA), following the manufacturer's instructions. After incubation with both reagents, cells were analyzed by flow cytometry (CyFlow® space). At least ten thousand events were registered *per* sample.

2.3.3 Metabolic activity

The percentage of metabolically active cells was evaluated using PrestoBlue, according to the manufacturer's recommendations. Metabolic activity was estimated based on fluorescence units normalized by the cell number.

2.3.4 hiPSC growth profile

hiPSC were inoculated and cultured in static culture conditions as described in section 2.1. Cell growth profile was monitored for 7 days. Cell concentration and viability were determined as described in section 2.2.1.1.

2.3.5 Flow cytometry

hiPSC were washed once with Dulbecco's phosphate-buffered saline (DPBS) and a total of 2 x 10^5 cells were incubated with each one of the antibodies – anti-Tra-1-60, anti-SSEA-1, anti-Oct3/4, anti-SSEA-4, anti-nanog and isotype controls IgG-PE, IgG_{2b},κ-PE, IgM,κ-FITC and IgG3-PE (all from Santa Cruz Biotechnology, Texas, USA except anti-nanog which was purchased to BD Biosciences, California, USA) - for 1 h at 4 °C. Unconjugated antibodies were conjugated with secondary antibodies for 30 min at 4 ºC. To detect intracellular components, BD Cytofix/Cytoperm™ (BD Biosciences) was used following the manufacturer's instructions. Cells were washed twice in DPBS, and analyzed in a CyFlow® instrument. At least ten thousand events were registered *per* sample.

2.3.6 Immunocytochemistry

hiPSC were inoculated in static culture conditions, in 24-well-plates, as described in section 2.1. After 24 h, cells' morphology was analyzed as previously described (Serra et al., 2011). Cells were visualized using inverted fluorescence microscopy (DMI 6000, Leica Microsystems GmbH, Wetzlar, Germany). Representative images were taken using a digital camera (Leica DFC 360 FX).

The primary antibodies used were anti-Tra-1-60 and anti-Oct3/4. Anti-Tra-1-60 was conjugated with secondary antibody Alexa Fluor® 488 Goat Anti-Mouse Antibody, whereas anti-SSEA-4 and anti-Oct3/4 were conjugated with Alexa Fluor® 594 Goat Anti-Mouse Antibody. Nuclei were counterstained with DAPI (4',6-Diamidino-2-Phenylindole, Dihydrochloride).

2.3.7 hiPSC *in vitro* pluripotency assay - embryoid body formation and spontaneous differentiation

hiPSC were inoculated in non-adherent ultra-low attachment 24-well plates (Corning) using an inoculum cell concentration of 0.5 x 10^6 cells/mL (1 mL) in KnockOut medium: KnockOut™–DMEM medium supplemented with 20% (v/v) KnockOut™-Serum Replacement, 1% (v/v) MEM non-essential amino acids, 0.1 mM 2-mercaptoethanol, 2 mM GlutaMAX™, and 5 µM ROCKi. Cells were cultured at 37 ºC in a humidified atmosphere of 5% CO_2 in air, and the medium was exchanged once every 7 days.

After this period, aggregates were harvested, re-plated into 24-well plates previously coated with 0.1 % (w/v) gelatin and cultured in KnockOut medium. Medium was exchanged three times per week.

After 2 weeks, cells were washed with DPBS, fixed, permeabilized and analyzed as explained in section 2.3.5. The primary antibodies used were anti-FoxA2 (Santa Cruz Biotechnology), anti-β-III-tubulin (Merck) and anti-smooth muscle actin (Agilent Technologies, California, USA). The antibodies were conjugated with Alexa Fluor® 488 Chicken Anti-Goat Antibody, and with Alexa Fluor® 594 Goat Anti-Mouse Antibody.

2.3.8 hiPSC differentiation potential - targeted differentiation into cardiomyocytes

Cardiac differentiation into cardiomyocytes (CM) was induced as described by Lian et al (Lian et al., 2012) and as previously described (Correia et al., 2016). After CM differentiation, monolayer cultures were dissociated into single cells by incubation with TrypLE™ Select dissociation agent for 5 min at 37 ºC to assess the number of CMs obtained per iPSC inoculated. Furthermore, to determine the purity of the final CM population, cells were analyzed by flow cytometry, as described in section 2.3.4, using the following antibodies: Anti-CD172α/β-PE (SIRPα/β), anti-CD106 (VCAM) (both from BD Biosciences) and anti–cardiac troponin T (cTnT).

2.4 Statistical Analysis

Statistical analysis of the DoE model was performed using MODDE software version 10.1. Differences in fold change between samples before and after processing were analyzed by Mann-Whitney test using GraphPad Prism version 7 (GraphPad Software Inc., California, USA). Values are represented as mean ± standard deviation (at least n = 3 replicates were considered) of independent measurements or assays. P values of less than 0.05 were considered as statistically significant.

In total, n=10 experiments were performed to generate the DoE matrix, and the optimized condition was further validated (n=2). A robustness analysis for the optimal condition (10,000 simulations) was validated experimentally.

3. Results and Discussion

The aim of this work was to find the design space of a TFF operation to accomplish the concentration of hiPSC.

The full factorial design applied considers all possible combinations between the factors, determining the effect of each factor (CPP) on the evaluated responses (cell recovery yield and viability), as well as to identify potential interactions between factors, which are not detected using a stepwise approach. The obtained model (Table S3.1) showed to fit the data with high significance (R^2 = 0.991 and 0.987) and to have a high predictability (Q_2 = 0.922 and 0.611) in terms of cell recovery yield and cell viability, respectively. The most suitable operating conditions for hMSC (Chapter II) were considered as well in the DoE matrix (Table 3.2).

Table 3.2 – DOE matrix representing the design points, factors, levels and responses used for the volume reduction step of hiPSC.

Design points							
A	B	C	**σ (s^{-1})**	**Jp ($L.m^{-2}.h^{-1}$)**	**Load (10^6 cell/cm^2)**	**% Cell Recovery, VRF = 20**	**% Cell Viability, VRF = 20**
-1	-1	-1	50	1000	1.4	80	85
1	-1	-1	200[4]	1200[1]	1.2	65	84
-1	1	-1	50	3000	1.2	78	73
1	1	-1	250	3000	1.0	79	92
-1	-1	1	50	1000	2.7	48	92
1	-1	1	200[1]	1200[1]	2.7	39	87
-1	1	1	50	3000	2.6	69	88
1	1	1	250	3000	2.9	79	95
0	0	0	150	2000	1.8	69	86
1	1	0	250	3000	1.9	84	92

Analysis of the process response variables identified a number of statistically significant ($P < 0.05$) model terms, main and interacting parameter factor effects (Figure 3.1).

[4] To create a TMP (to allow the filtration process), the inlet flux was slightly increased, whereas the permeate flux was decreased from the theoretical points (the flow rates are equal).

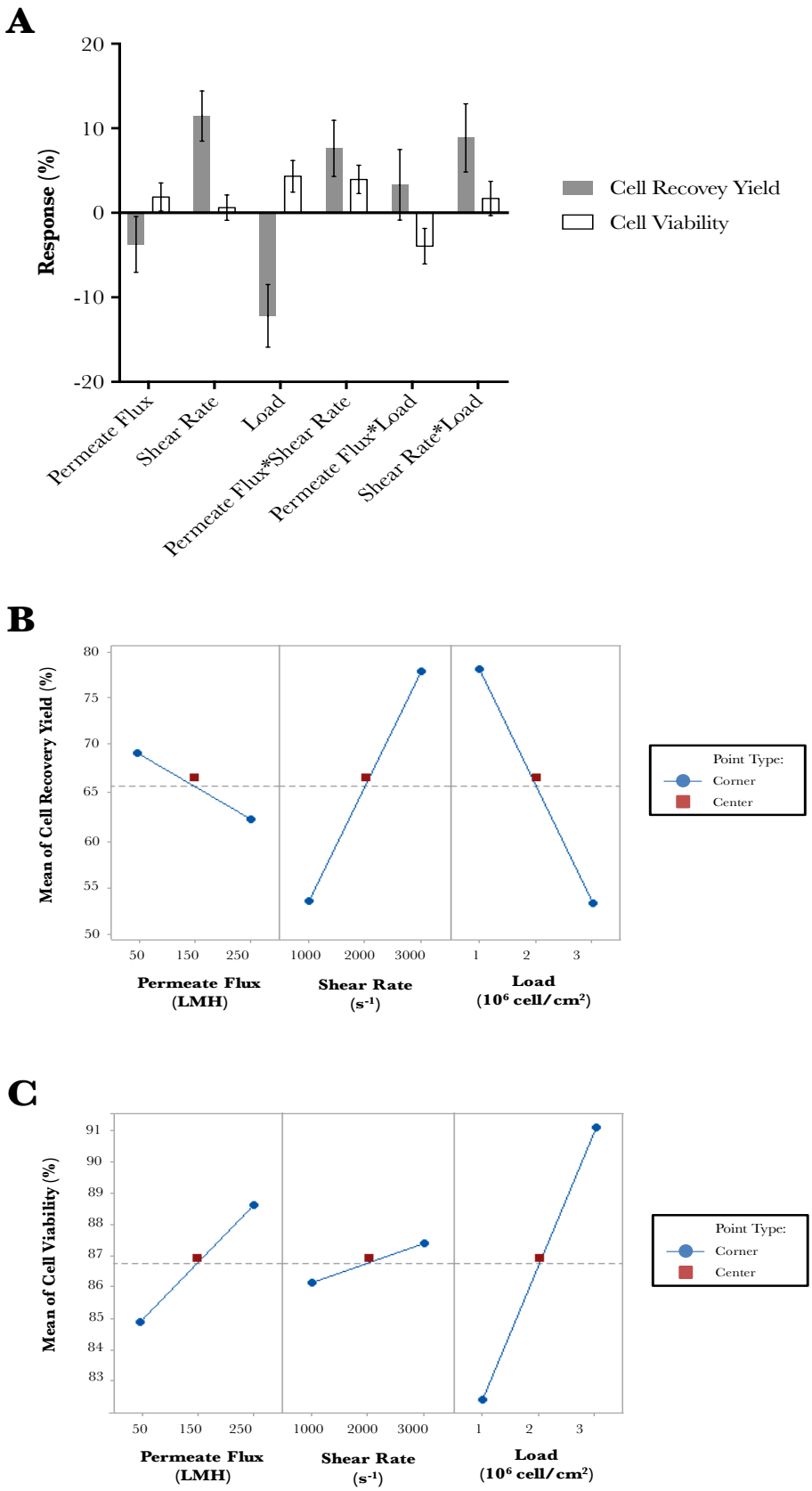

Figure 3.1 – Effect of critical process parameters (CPP) on cell recovery yield and viability. (A) Coefficients scaled and centered for each factor individually and their interactions. Significant effects are characterized by being different from 0. (B, C) Main effect plot of permeate flux (left panel), shear rate (central

panel) and load (right panel) on cell recovery yield (B) and cell viability (C) responses. CPP are represented with corner (-1, +1) and center points (0).

A main effect occurs if a CPP statistically significantly influences a process response regardless of the other CPP levels. CPP of shear rate and load were significant model terms for cell recovery yield response (Figure 3.1A). Moreover, the load showed also to be a significant model term increasing the cell viability response (Figure 3.1A). Thus, hiPSC recovery yield is maximized using high shear rates (3000 s^{-1}) and low load volumes (1 x 10^6 cell/cm^2) (Figure 3.1B), whereas cell viability is maximized when high loads are used (3 x 10^6 cell/cm^2) (Figure 3.1C).

An interacting factor effect exists if the combined effect of two CPP is different from the sum of their individual effects. As observed in Figure 3.1A, all CPP interact with each other; the combination between permeate flux and shear rate significantly increases both responses. The interaction of the permeate flux with load and shear rate with load showed to decrease cell viability and increase cell recovery yield, respectively. These results were also corroborated analyzing the interaction plots, where non parallel lines were observed for all CPP (Figure 3.2). These results suggest that the optimization of a TFF process for hiPSC concentration should not be performed in a stepwise manner, since all considered CPP do not follow consistent trends and their interaction affect differently cell recovery yield and cell viability responses. A similar trend was also observed in other studies conducted to optimize hiPSC production (Hunt et al., 2013), corroborating the use of this type of methodology to further understand and study complex biological systems as hiPSC.

To find the optimal operating conditions, the behavior of both responses was evaluated at different load conditions as a function of shear rate and permeate flux (Figure 3.3).
The contour plots shown that in terms of hiPSC recovery yield (Figure 3.3A), when a low load is used (1 x 10^6 cell/cm^2) the response is maximized using low permeate fluxes (< 100 LMH) combined with any shear rate value, or using high shear rates (3000 s^{-1}) combined with high permeate fluxes (> 140 LMH). When the load is increased to 2 and 3 x 10^6 cell/cm^2, the cell recovery yield is maximized by using only high shear rates (> 2900 s^{-1}) combined with high permeate fluxes (> 220 LMH). On the other hand, cell viability (Figure 3.3B) is maximized using high shear rates (> 2600 s^{-1}) combined with high permeate fluxes (> 240 LMH) despite the cell load. These results are accordant with previous results obtained with hMSC (Chapter II): lower shear rates, characterized by lower inlet flow rates, lead to lower cell recovery yields and cell viabilities; in these cases, cells have higher residence time inside the fibers, and therefore have an increased probability of interaction with the membrane, leading to lower cell recovery

yields due to fouling events. In the same study (Chapter II), it was also observed that although the permeate flux did not affect hMSC's cell recovery yield, lower permeate fluxes affected hMSC's CQA due to longer processing times. In this hiPSC case, similar phenomena may be occurring, explaining the observed results.

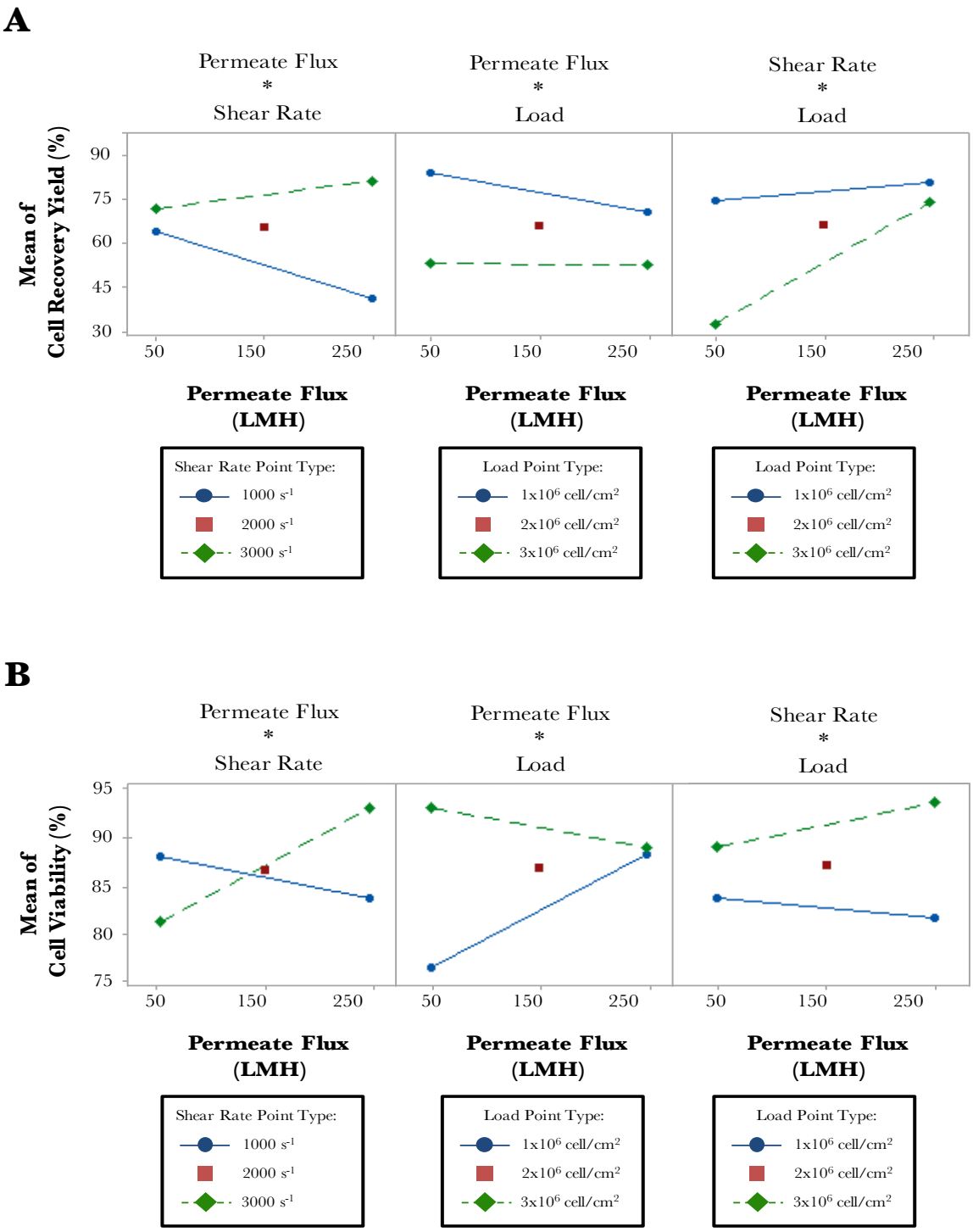

Figure 3.2 – Interaction plots of each CPP for the volume reduction step of hiPSC. The impact of the interaction of the permeate flux, shear rate, and load on cell recovery yield (A) and cell viability (B) responses are depicted.

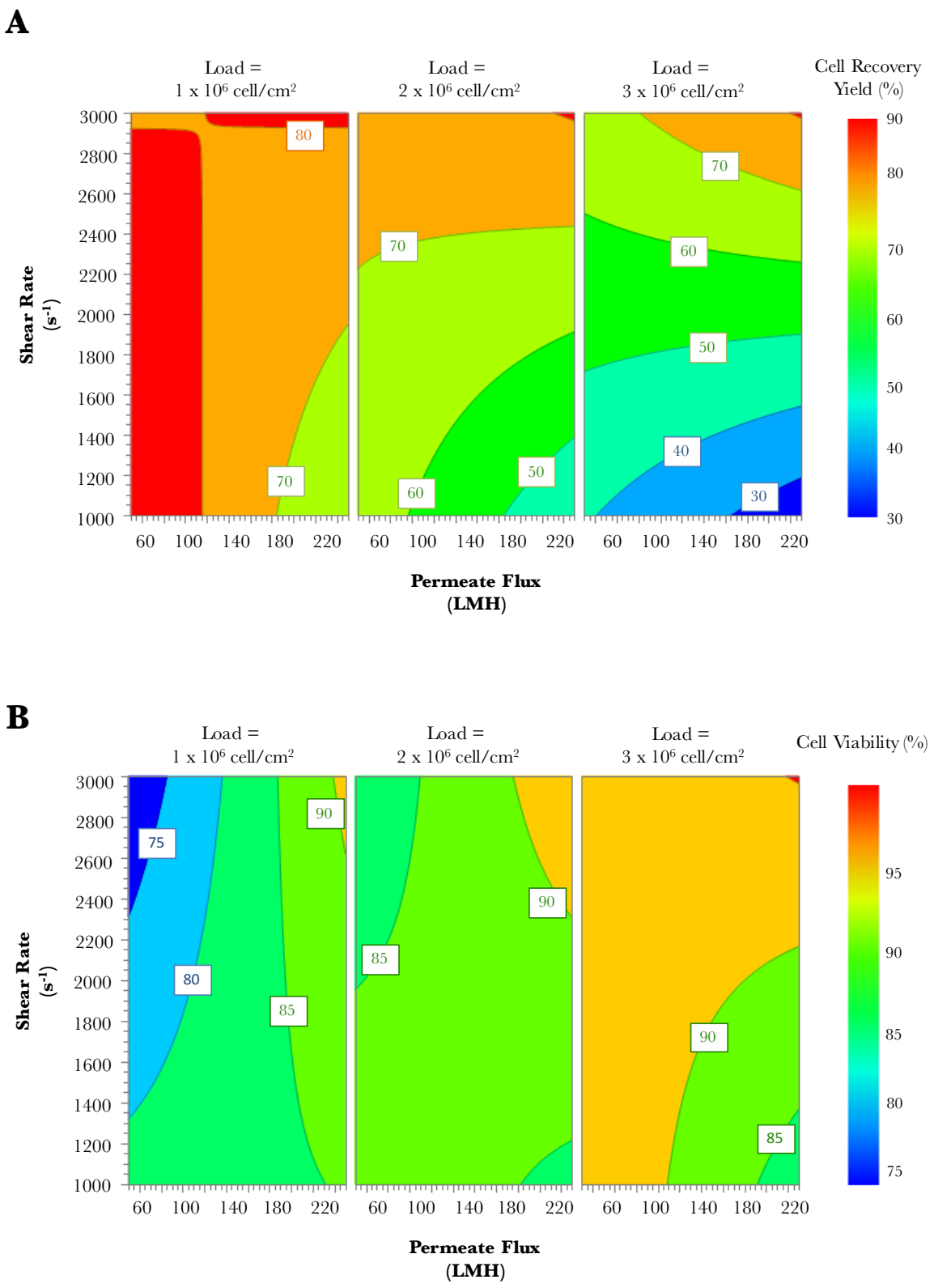

Figure 3.3 – Surface response plots. Variation of the output responses regarding shear rate and permeate flux at different load conditions, in terms of cell recovery yield (A) and cell viability (B). Higher percentages of response are marked as red and orange, whereas lower values are represented in green and blue.

From these results, the optimal operating conditions to maximize the cell recovery yield and viability responses were evaluated (Table 3.3).

Table 3.3 – hiPSC recovery yield and viability response optimization.

Response	Criteria	Min	Target	Expected Value	Experimental Value
Cell Recovery Yield (%)	Maximize	80	93	81	87
Cell Viability (%)	Maximize	90	93	93	93

To challenge the model, 80% and 90% were considered as the minimum acceptable values for cell recovery yield and viability to optimize the TFF step (Table 3.4). The statistical model identified high shear rate (3000 s^{-1}), permeate flux (250 LMH) and medium cell load (2 x 10^6 cell/cm^2) to maximize both responses (Table 3.4), predicting that over 80% of hiPSC could be recovered with high viability (93%) after a VRF of 20.

Table 3.4 – CPP optimization to provide maximized responses of hiPSC recovery yield and viability.

Factor	Value	Factor Contribution (%)
Permeate Flux	250 $L.m^{-2}.h^{-1}$	34
Shear Rate	3000 s^{-1}	57
Load	1.9 x 10^6 cell/cm^2	9

In this case, CPP of shear rate and permeate flux would have the highest impact on the evaluated outcome (57 and 34%, respectively). This condition was validated experimentally and the impact of DSP in hiPSC's CQA in terms of the expression of pluripotent stem cell markers, proliferation capacity and pluripotency was evaluated (Figure 3.4). Results (Table 3.3) confirmed the predictiveness of the model, since 87% of cells could be recovered after a volume reduction of 20-fold, with a viability of 93%.

Permeability data (Figure 3.4A) suggest that the loss of cells may be correlated with fouling during the operation, which may also increase cell lysis (6%, validated by LDH assay). Importantly, it is possible to observe that the conditions found to be optimal to concentrate hiPSC are similar to those used to concentrate hMSC (Chapter II), confirming the robustness of TFF to be applied in different cell-based products. No differences were observed in the number of statistically significant model terms, main and interacting parameter factor effects, when the best condition was validated and inserted into the model.

Overall, the volume reduction unit operation also did not affect hiPSC's CQA: no significant differences ($P > 0.05$) could be observed in hiPSC's viability, metabolic activity, proliferation capacity, and apoptosis (although a decrease was observed, no significant

differences were observed) (Figure 3.4B) when compared to cells before this step. The expression of pluripotency markers remained unaltered after processing (Figure 3.4C): hiPSC expressed high levels of pluripotency markers TRA-1-60, SSEA-4, and lacked the expression of SSEA-1, a marker of early differentiated hPSC (Figure 3.4C and 3.4D). hiPSC showed to maintain their differentiation potential, by differentiating into cardiomyocytes (CM, with beating frequency after day 8) (Figure 3.4E), expressing high levels of cardiac specific markers, as validated by flow cytometry (Figure 3.4E) after day 15 of differentiation. Similar ratio of CM obtained *per* hiPSC inoculated could be achieved for hiPSC after static expansion (2) and after DSP (3). Moreover, hiPSC's pluripotency was further characterized *in vitro* by their ability to form embryoid bodies in static culture and spontaneously differentiate into cells constituting all three somatic germ layers (Figure 3.4F).

Robustness of a process depends on its ability to cope with variations and uncertainties inherent to process parameters; uncertainty in pump operation and calibration, cell counting and in materials manufacturing are foreseeable. A robustness analysis of the optimal operating conditions (Table 3.4 and Figure 3.5) was performed, to determine the process' success rate (cell recovery yield > 80% and cell viability > 90%).

Cell viability response was always kept above specification, despite the uncertainty applied in all CPP (data not shown). Shear rate and cell load significantly affected cell recovery response (Figure 3.1), thus, the major process uncertainty was considered to be related with variability on the pump operation (flow rate) (5%), influencing the permeate flux and shear rate ($\gamma = \frac{4\,Q}{\pi\,r^3}$), the main effect on cell recovery yield response, where Q [mL.min^{-1}] is the inlet flow rate that passes through the fibers with an inner radius r [mm]. The materials' manufacturing has a negligible uncertainty; thus, the inner diameter of the fibers was assumed to be constant. As for the load, a 20% uncertainty related with cell counting, $X = \bar{X} \pm X',\ X' \in [-\partial X, +\partial X]$ was estimated, where $\bar{X}$ corresponds to the average variable (inlet and permeate flow rates and cell load values). X' is a deviation from the nominal value, assumed at first as normally and then uniformly distributed.

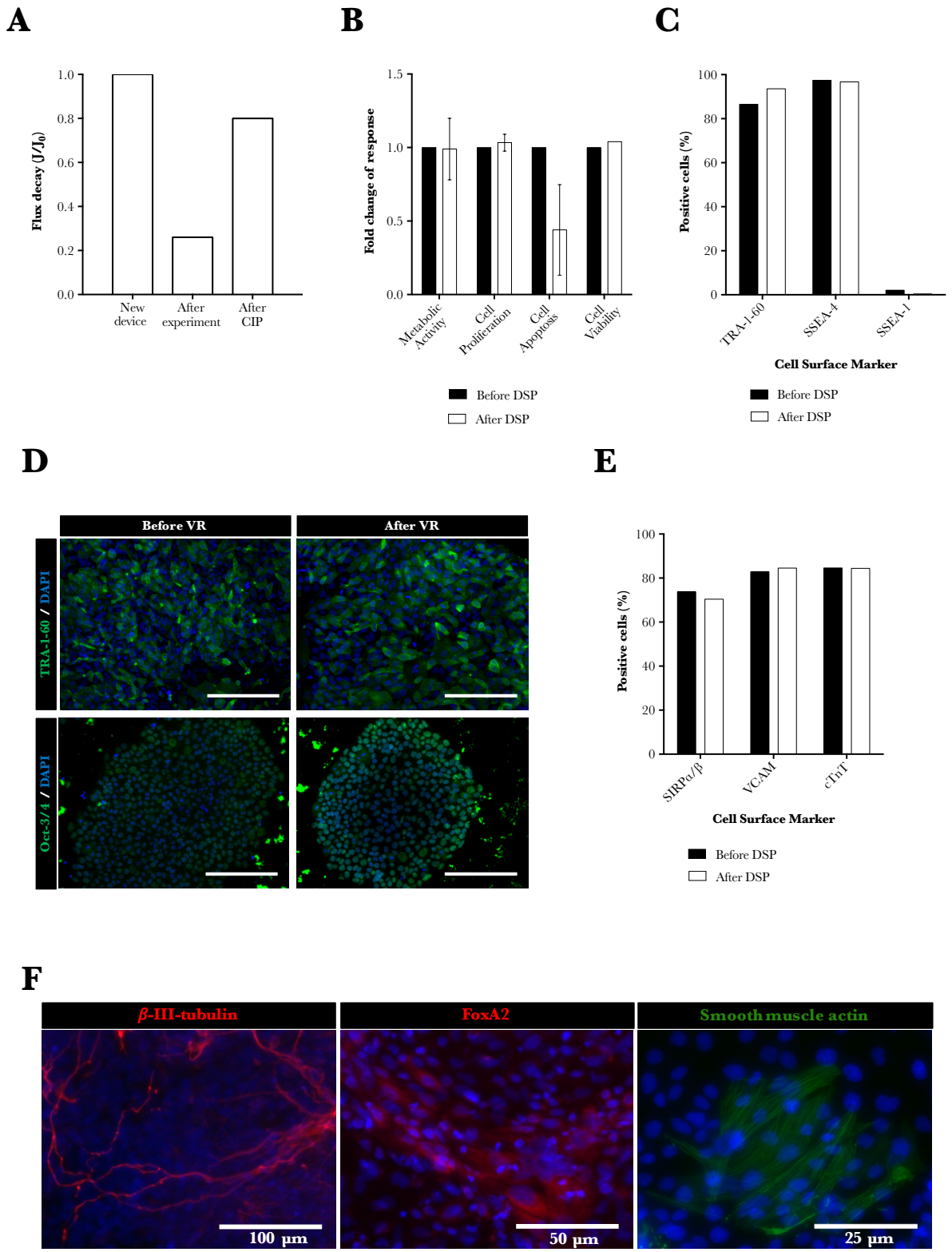

Figure 3.4 – hiPSC characterization upon harvesting and after the volume reduction (VR) step. (A) Permeate flux decay after DSP and after cleaning in place (CIP). Flux decay was estimated regarding the initial value of permeability. (B) Cell characterization in terms of metabolic activity, cell proliferation, cell apoptosis and cell viability. Each bar represents the fold-increase/decrease, relative to cells after expansion (before DSP). No significant differences were observed ($P > 0.05$). (C) Expression of cell-surface antigens (TRA-1-60, SSEA-1, SSEA-4) in hiPSC before and after the VR step. (D) hiPSC morphology before and after VR - immunofluorescence staining of TRA-1-60 (green), Oct-3/4 (green) and cell nuclei (blue). Scale bars: 100 µm. (E-F) Evaluation of hiPSC pluripotency in vitro by (E) targeted differentiation into cardiomyocytes (CM) - expression of CM markers: cell-

surface antigens (SIRPα/β, VCAM) and intracellular marker (cardiac troponin T) – and (F) embryoid body formation and spontaneous differentiation - immunofluorescence staining of β-III-tubulin (ectoderm) (scale bar: 100 μm), FoxA2 (endoderm) (scale bar: 50 μm) and smooth muscle actin (mesoderm) (scale bar: 25 μm).

Analyzing the optimal conditions found to operate TFF (Figure 3.5A-3.5D), is possible to observe that there is a 65%-70% success rate. Then, it was identified which shear rate value would allow to satisfy both cell recovery yield and viability requirements (Figure 3.5E, 3.5F). Results show that flow rates higher than 33.5 mL/min (3370 s^{-1}) reach the specified requirements for cell recovery yield (80%) and viability (90%) in 100% of the cases if data is normally distributed (Figure 3.5E), while 31.5 mL/min (3169 s^{-1}) already allows to meet the specifications in 100% of the cases if the data presents a uniform distribution (Figure 3.5F). This scenario was validated experimentally: hiPSC were successfully concentrated 20-fold, achieving more than 80% cell recovery yield (88%) at high cell viability (> 90%, 98%).

4. Conclusion

This work represents the first study into the identification and quantification of interacting effects between TFF's critical process parameters (CPP) as shear rate, permeate flux and cell load, and hiPSC recovery yield, viability and critical quality attributes (CQA).

The design space (boundaries) during TFF unit operation, in which hiPSC maintained their CQA was defined. A robustness analysis permitted the identification of the operating conditions that ensured cell recovery yield and viability were always met.

TFF emerged as a robust and "universal" platform for cell therapy manufacturing able to concentrate different types of stem cells, pluripotent and adult SC, relevant for pre-clinical research and cell therapy applications. The development of mathematical models by representing the biological system supports process design and optimization.

5. Acknowledgments

I would like to acknowledge Erik Johansson (Data Analytics Solutions) for fruitful scientific discussions and to Tiago Aguiar and Patrícia Duarte for technical support. This work was funded by Fundação para a Ciência e Tecnologia though (FCT)-funded projects CARDIOSTEM (MITP-TB/ECE/0013/2013) and ERAdicatPH (E-Rare3/0002/2015), FCT grant SFRH/BD/51940/2012 (MIT-Portugal), and by iNOVA4Health Research Unit (LISBOA-01-0145-FEDER-007344).

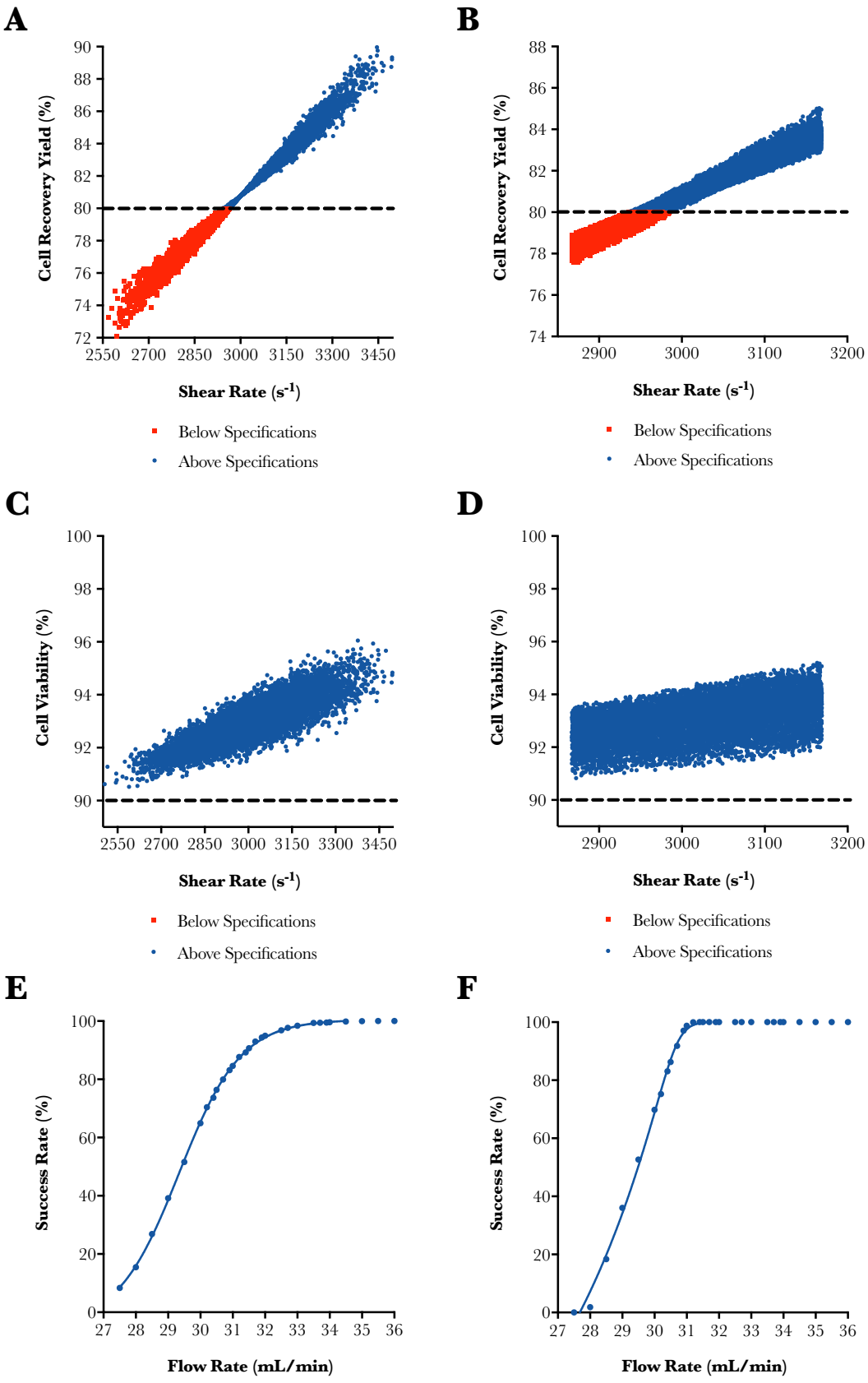

Figure 3.5 – Parametric and robustness analysis of the optimal operation point of TFF. Cell recovery yield (A, B) and viability (C, D) simulating 10,000 runs operated with the optimal conditions of the volume reduction step. Symbols above the horizontal dashed lines satisfy both recovery and viability constraints. (E, F)

Robustness analysis of the optimal point, depicting the success rate in function of the inlet flow rate (direct influence on shear rate). Data was considered to be either normal (A, C, E) or uniformly (B, D, F) distributed.

References

Correia, C., Koshkin, A., Carido, M., Espinha, N., Saric, T., Lima, P.A., Serra, M., Alves, P.M., 2016. Effective Hypothermic Storage of Human Pluripotent Stem Cell-Derived Cardiomyocytes Compatible With Global Distribution of Cells for Clinical Applications and Toxicology Testing. Stem Cells Transl. Med. 5, 658–669.

Food and Drug Administration, Guidance for Industry: Q8(R2) pharmaceutical development. http://www.Fda.govdownloadsDrugs...Guidancesucm.Pdf, 2009 (accessed 16.07.2016).

Fotakis, G., Timbrell, J.A., 2006. *In vitro* cytotoxicity assays: Comparison of LDH, neutral red, MTT and protein assay in hepatoma cell lines following exposure to cadmium chloride. Toxicol. Lett. 160, 171–177.

Franceschini, G., Macchietto, S., 2008. Model-based design of experiments for parameter precision: State of the art. Chem. Eng. Sci. 63, 4846–4872.

M.M. Hunt, G. Meng, D.E. Rancourt, I.D. Gates, M.S. Kallos, 2013. Factorial Experimental Design for the Culture of Human Embryonic Stem Cells as Aggregates in Stirred Suspension Bioreactors Reveals the Potential for Interaction Effects Between Bioprocess Parameters, Tissue Eng. Part C: Methods. 20, 76–89.

Jones, K.H., Senft, J.A., 1985. An improved method to determine cell viability by simultaneous staining with fluorescein diacetate-propidium iodide. J. Histochem. Cytochem. 33, 77–79.

Lian, X., Zhang, J., Azarin, S.M., Zhu, K., Hazeltine, L.B., Bao, X., Hsiao, C., Kamp, T.J., Palecek, S.P., 2012. Directed cardiomyocyte differentiation from human pluripotent stem cells by modulating Wnt/β-catenin signaling under fully defined conditions. Nat. Protoc. 8, 162–175.

Lipsitz, Y.Y., Timmins, N.E., Zandstra, P.W., 2016. Quality cell therapy manufacturing by design. Nat. Biotechnol. 34, 393–400.

Marinho, P.A., Chailangkarn, T., Muotri, A.R., 2015. Systematic optimization of human pluripotent stem cells media using Design of Experiments. Sci. Rep. 5, 9834.

Nestola, P., Silva, R.J.S., Peixoto, C., Alves, P.M., Carrondo, M.J.T., Mota, J.P.B., 2015. Robust design of adenovirus purification by two-column, simulated moving-bed, size-exclusion chromatography. J. Biotechnol. 213, 109–119.

Rathore, A.S., Winkle, H., 2009. Quality by design for biopharmaceuticals. Nat. Biotechnol. 27, 26–34.

Serra, M., Correia, C., Malpique, R., Brito, C., Jensen, J., Bjorquist, P., Carrondo, M.J.T., Alves, P.M., 2011. Microencapsulation technology: a powerful tool for integrating expansion and cryopreservation of human embryonic stem cells. PLoS ONE 6, e23212.

Takahashi, K., Yamanaka, S., 2016. A decade of transcription factor-mediated reprogramming to pluripotency. Nat. Rev. Mol. Cell Biol. 17, 183–193.

Trounson, A., McDonald, C., 2015. Stem Cell Therapies in Clinical Trials: Progress and Challenges. Stem Cell 17, 11–22.

Vassault, A., 1983. Lactate dehydrogenase: UV-method with pyruvate and NADH, in: Bergmeyer, H.U., Grassl, M. (Eds.), Methods of Enzymatic Analysis. John Wiley & Sons, New York, pp. 118–126.

Supplementary Data

Table S3.1 – Model terms coefficients describing the cell recovery yield and viability responses for the volume reduction step of hiPSC.

	Model Term	Coefficient
Cell recovery yield (%)	$Constant\ (K)$	$1.41\text{x}10^{2}$
	$Permeate\ flux\ (J_P)$	$-2.56\text{x}10^{-1}$
	$Load\ (L)$	$-3.49\ \text{x}10^{1}$
	$Shear\ rate\ (\gamma)$	$-1.77\ \text{x}10^{-2}$
	$Permeate\ flux \times Load\ (J_P \times L)$	$3.32\text{x}10^{-2}$
	$Permeate\ flux \times Shear\ rate\ (J_P \times \gamma)$	$7.62\text{x}10^{-5}$
	$Load \times Shear\ rate\ (L \times \gamma)$	$8.87\text{x}10^{-3}$
$Cell\ Rec\ (\%) =$	$1.41\text{x}10^{2} - 2.56\text{x}10^{-1}J_P - 3.49\ \text{x}10^{1}L - 1.77\text{x}10^{-2}\gamma + 3.32\text{x}10^{-2}J_P L + 7.62\text{x}10^{-5}J_P\gamma + 8.87\text{x}10^{-3}L\gamma$	
Cell Viability (%)	$Constant\ (K)$	$8.08\text{x}10^{1}$
	$Permeate\ flux\ (J_P)$	$1.86\text{x}10^{-2}$
	$Load\ (L)$	$6.85\text{x}10^{0}$
	$Shear\ rate\ (\gamma)$	$-8.70\text{x}10^{-3}$
	$Permeate\ flux \times Load\ (J_P \times L)$	$-3.95\text{x}10^{-2}$
	$Perеate\ flux \times Shear\ rate\ (J_P \times \gamma)$	$3.95\text{x}10^{-5}$
	$Load \times Shear\ rate\ (L \times \gamma)$	$1.69\text{x}10^{-3}$
$Cell\ Viab\ (\%) =$	$8.08\text{x}10^{1} + 1.86\text{x}10^{-2}J_P + 6.85\ \text{x}10^{0}L - 8.7\text{x}10^{-3}\gamma - 3.95\text{x}10^{-2}J_P L + 3.95\text{x}10^{-5}J_P\gamma + 1.69\text{x}10^{-3}L\gamma$	

IV

Exploring continuous and integrated strategies for the downstream processing of human mesenchymal stem cells: cell washing unit operation and process integration

This chapter was adapted from:

Cunha B, Aguiar T, Silva MM, Silva RJS, Sousa MFQ, Pineda E, Peixoto C, Carrondo MJT, Serra M, Alves PM (2015). Exploring continuous and integrated strategies for the up- and downstream processing of human mesenchymal stem cells, Journal of Biotechnology, 13:97-108.

Table of Contents

ABSTRACT 132

1. INTRODUCTION 133

2. MATERIALS AND METHODS 133

2.1 Cell culture 134
2.2 Downstream processing 136
2.3 Integration of hMSC cell expansion, concentration and diafiltration processes 140
2.4 Cell viability and characterization assays 140
2.5 Statistical Analysis 144

3. RESULTS 144

3.1 hMSC expansion in continuous perfusion and semi-continuous cultures 144
3.2 Concentration and diafiltration processes using tangential flow filtration 147
3.3 Integration of hMSC cell expansion, concentration and diafiltration processes 150

4. DISCUSSION 155

5. ACKNOWLEDGMENTS 157

6. SUPPLEMENTARY DATA 158

REFERENCES 160

Abstract

The integration of up- and down- stream unit operations can result in the elimination of hold steps, thus decreasing the footprint, and ultimately can create robust closed system operations. This type of design is desirable for the bioprocess of human mesenchymal stem cells (hMSC), where high numbers of pure cells, at low volumes, need to be delivered for therapy applications. This study reports a proof of concept of the integration of a continuous perfusion culture in bioreactors with a tangential flow filtration (TFF) system for the concentration and washing of hMSC. Moreover, we have also explored a continuous alternative for concentrating hMSC.

Results show that expanding cells in a continuous perfusion operation mode yielded higher expansion ratios, and led to a shift in cell's metabolism. TFF operated either in continuous or discontinuous allowed to concentrate cells with high cell recovery (> 80%) and viability (> 95%); furthermore, continuous TFF permitted to operate longer with higher cell concentrations. Continuous diafiltration led to higher protein clearance (98%) with lower cell death, when comparing to discontinuous diafiltration. Overall, an integrated process allowed for a shorter process time, recovering 70% of viable hMSC (> 95%), with no changes in terms of morphology, immunophenotype, proliferation capacity and multipotent differentiation potential.

Keywords: mesenchymal stem cells, cell therapy, perfusion, tangential flow filtration, continuous processing, integration

1. Introduction

Human adult mesenchymal stem cells (hMSC) have been shown over the past years to be effective in the treatment of several diseases in a clinical setting, including immune diseases as well as in wound care, orthopedics, amongst others (Wei et al., 2013). Since therapies require high doses (from 10^5 to 10^9 cells *per* patient) (Mason and Dunnill, 2009; Murphy et al., 2013), and given that these cells have a low abundance *in vivo*, methods that can successfully expand hMSC are compulsory (Hervy et al., 2014). To achieve such demands, extensive efforts have been focused on the development of cost-effective, scalable and robust upstream technologies. The use of microcarrier-based stirred culture systems combined with bioreactor technology (Chen et al., 2013) can significantly increase cost-effectively the therapeutic cell culture productivity (Simaria et al., 2014), while assuming a culture homogeneity and controlling culture parameters. Ultimately, the increase in the cell numbers will also raise the harvest volumes depending on the therapy type (autologous or allogeneic). Large culture volumes will need to be concentrated and washed, in order to ensure efficient removal of impurities (e.g. protein and DNA) (Pattasseril et al., 2013), without compromising the cells' characteristics in terms of identity, potency and viability. Due to its ability for scale-up, and employment of disposables, tangential flow filtration (TFF) appears as an attractive solution for cell therapy downstream processing (DSP) (Pattasseril et al., 2013; Vicente et al., 2014).

The integration of up- and downstream unit operations can result in the elimination of hold steps, shortening residence and cycle times, thus decreasing the footprint, and ultimately creating robust closed system operations for processing biopharmaceuticals (Jungbauer, 2013; Schaber et al., 2011; Warikoo et al., 2012). This approach remains to be explored for cell therapy applications, although preliminary studies already reported the potential of continuous perfusion to expand hMSC (dos Santos et al., 2014).

This work aimed to develop a potentially scalable integrated process for the expansion, volume reduction and washing of hMSC. Our strategy consisted on the evaluation of different operation modes (continuous and discontinuous) for cell expansion and DSP, as well as their impact on cells' recovery yield and quality attributes in terms of morphology, identity, purity, potency, and viability throughout processing.

2. Materials and Methods

The followed workflow is presented in Figure 4.1.

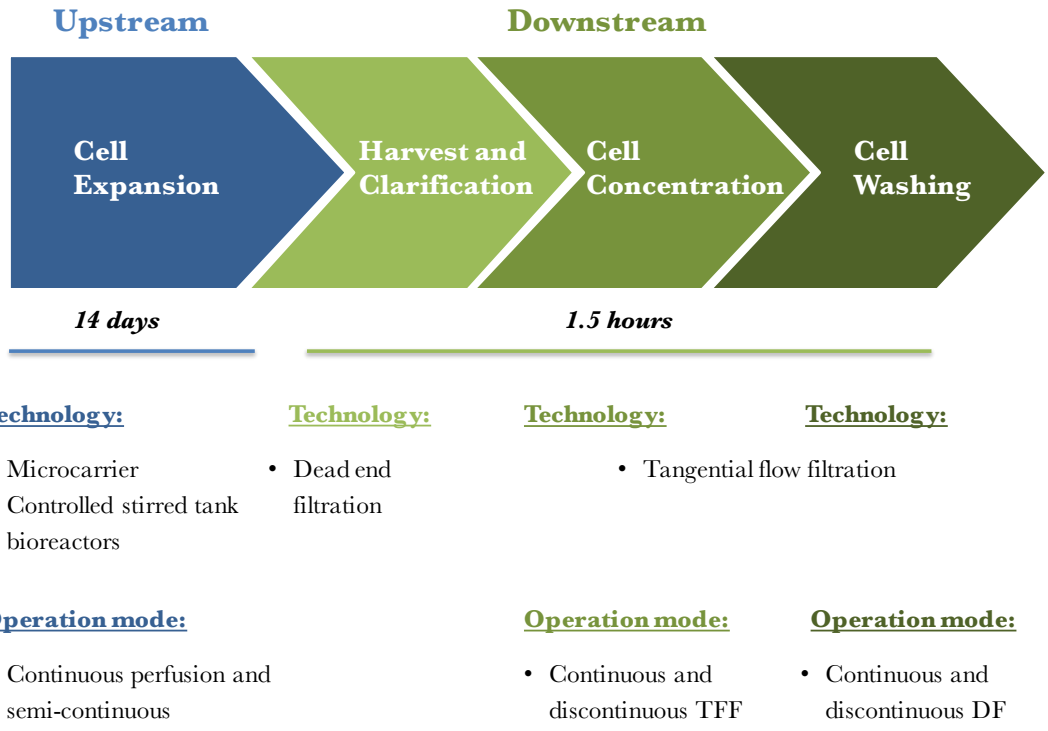

Figure 4.1 – Schematic representation of the experimental workflow. In this work, the impact of different operation modes (continuous and discontinuous) on hMSC's expansion, DSP, and quality attributes in terms of morphology, identity, purity, potency, and viability throughout processing was evaluated. With the most suitable conditions, an integrated process was designed where after hMSC expansion using microcarrier technology in controlled stirred tank bioreactors, cells were concentrated and washed from the system's impurities into a formulation media. At the end of the bioprocess, an expansion factor of 14.6 was obtained, and 70% of hMSC were recovered, presenting proliferating capacity, multipotent differentiation potential, and with unaffected morphology and immunophenotype.

2.1 Cell culture

In this work, human bone marrow-derived mesenchymal stem cells (STEMCELL™ Technologies, Grenoble, France), and human foreskin fibroblasts (hFF, ATCC collection, Cat nr CRL-2429) were used. All reagents used to perform the cell culture were purchased from ThermoFisher™ Scientific (Massachusetts, USA), unless otherwise stated.

2.1.1 Static Culture

hMSC were cultured in MesenCult®-XF Medium (STEMCELL™ Technologies) supplemented with 2 mM L-Glutamine and propagated in tissue culture flasks (Thermo Scientific™ Nunc™), previously coated with MesenCult™-SF Attachment Substrate (STEMCELL™ Technologies), according to the manufacturer's instructions. hFF were expanded using IMDM medium, supplemented with 4 mM GlutaMAX™-I, 10% (v/v) Fetal Bovine Serum (FBS) and with 1% (v/v) PenStrep, in tissue culture flasks (Thermo Scientific™

Nunc™). When cell confluency reached approx. 70 – 80%, hFF were subcultured using a split ratio of 1:6 and 0.25% (v/v) Trypsin-EDTA for cell detachment. Cells were expanded at 37 ºC in a humidified atmosphere of 5% CO_2 in air.

2.1.2 Stirred-tank Bioreactors Culture

hMSC were cultivated in computer-controlled Biostat Qplus stirred tank bioreactors (Sartorius Stedim Biotech, Göttingen, Germany), equipped with low shear stress marine 3-blade impellers, under defined conditions (working volume: 400 mL; pH: 7.2; temperature: 37 ºC; pO_2: 20% air saturation; surface aeration rate: 0.1 vvm). Data acquisition and process control were performed using Multiple Fermenter Control System for Windows Supervisory Control and Data Acquisition software (Sartorius Stedim, Germany). hMSC were inoculated at 0.25 x 10^5 cell/mL onto the bioreactors, containing 200 mL of xeno-free, serum-free Mesencult™-XF culture media (STEMCELL™ Technologies) and Synthemax® II microcarriers (Corning, New York, USA) at a final concentration of 16 g/L. Cells were expanded under intermittent stirring (On: 60 rpm for 1 min; Off: 0 rpm for 20 min) during the first 6 h. After this period, the remaining 200 mL of culture media were added and agitation was set to continuous at 40 – 60 rpm. At day 6 of culture, empty microcarriers were added (32 g/L), increasing the microcarrier concentration up to 48 g/L. To facilitate cell migration from bead to bead, an intermittent stirring rate profile was set (On: 15 rpm for 5 min; Off: 0 rpm for 55 min) from day 6 to day 9. Cells were expanded for 14 days.

Semi-continuous cultures: conducted by replacing 50% of the culture media every 2.5 days, from day 5 to day 14 of culture. This was performed by stopping the agitation, withdrawing culture medium and refeeding fresh medium immediately after microcarrier sedimentation.

Continuous perfusion cultures: performed using a cell retention prototype ATF™ (Repligen Corporation, Massachusetts, USA) or with dip-tube adapted to the bioreactor cap. The ATF™ System is based upon the technology of Alternating Tangential Flow, created by the action of a diaphragm moving upwards and then downwards within a pump head, connected to a filter housing and attached to a standard bioreactor (http://www.refinetech.com/). Perfusion cultures were controlled using an automated gravimetric control system, as earlier described by our group (Serra et al., 2011; Tostões et al., 2011), at a dilution rate of 0.2 day^{-1} from day 5 to day 14 of culture.

2.2 Downstream processing

2.2.1 Cell concentration (volume reduction)

The clarified cell suspension was concentrated using tangential flow filtration (TFF). TFF was operated in two different modes – continuous or discontinuous – as represented in Figure 3.4A. To compare both modes, the retentate pump in the continuous operation was set to deliver the same volumetric concentration factor at the same time, as in the discontinuous operation. Mass balances for both continuous and discontinuous TFF were determined using MATLAB software (MathWorks, Massachusetts, USA).

The cell concentration on the retentate (C_R) and on the permeate (C_P) are related to the membrane's rejection coefficient (R) (Cheryan, 1998):

$$R = 1 - \frac{C_P}{C_R} \quad (1)$$

Moreover, the sieving coefficient (S_0) of a membrane is correlated with its rejection coefficient (Cheng et al., 1998):

$$S_0 = 1 - R \quad (2)$$

The concentration of a solute at any stage of membrane processing is a function of both volume reduction and the value of (R), as described by (3) (Cheryan, 1998):

$$C_R = C_0 \times (VCR)^R \quad (3)$$

where the volume concentration ratio (VCR) is given by (4):

$$VCR = \frac{Initial\ Feed\ Volume\ (V_0)}{Retentate\ Volume\ (V_R)} \quad (4)$$

In TFF, the volumetric permeate flux through the membrane, J_p (expressed in L.m^{-2}.h^{-1} or LMH), is described by (5):

$$J_P = \frac{Q_P}{A} \quad (5)$$

where Q_P is the permeate's flow rate, expressed in L/h and A is the membrane's surface area, expressed in m^2.

Particularly in discontinuous operations (Figure 3.3A), the volume variation dependence on time can be expressed in terms of the permeate flux (6):

$$\frac{dV}{dt} = -A\,J_P \quad (6)$$

Since the process was controlled with a permeate pump and no flux decrease was observed, J_P was assumed to be constant throughout the TFF process.

Moreover, a full rejection of cells (cell number is constant throughout the process) was assumed, i.e., $R = 1$, and that there was no interaction between cells and the membrane. Hence, the concentration process was only dependent on the volume reduction (VR) and on the initial

cell concentration (3). Therefore, cells' concentration throughout time is given by (7) (Cheryan, 1998):

$$\frac{d\,(C_B\,V)}{dt} = 0 \quad (7)$$

After integrating, cell's concentration can be expressed by (8):

$$C_B = \frac{C_{B0} \times V_0}{V_0 - A \times J_P \times t} \quad (8)$$

where V (expressed in L) is the volume inside the feed tank and C_B is the bulk cell concentration. Equation (7) was integrated with the initial conditions of $V\ (t = 0) = V_0$ and $C_B\ (t = 0) = C_{B0}$. Also, the initial cell concentration inside the TFF system (C_{B0}) in discontinuous TFF (Figure 4.4B) was considered to be 1, since the system was first filled with the cell suspension before starting the concentration process.

In the case of continuous TFF process, the premises of the discontinuous process were maintained (R = 1 and no interaction between the cells and the membrane).

An additional diagram (Figure 4.2A and 4.2B) is proposed to describe the implemented piping and instrumentation diagram, since the piping volume of the system needs to be taken into account, evidencing its mixture, using an intermediate stirred tank.

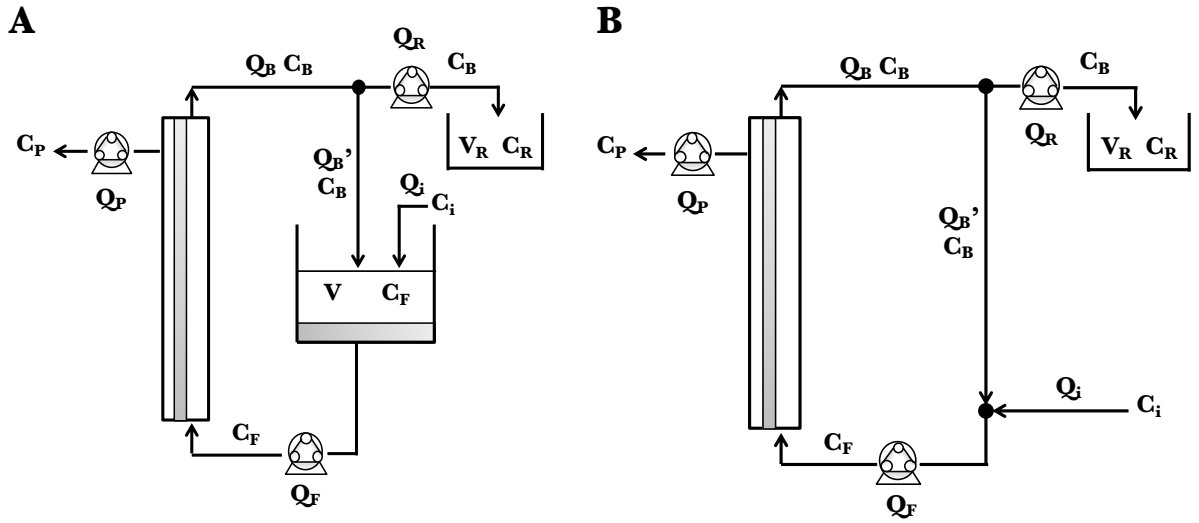

Figure 4.2 – Schematic representation of the continuous TFF concentration process. Briefly, the cell suspension is pumped from the feed vessel into the feed port of the hollow fiber device (HF), across the membrane surface and out from the retentate port. From this point, part of the cell suspension is recirculated back into the feed vessel, and part is removed from the system to the retentate's tank. C_i, C_P, C_B and C_F (expressed in cell/mL) represent the cell concentration on the feed, permeate, and recirculation loop before and after the mixing node, respectively. Likewise, Q_i, Q_P, Q'_B and Q_F (expressed in L/h) represent the flow rates on the feed, permeate, and recirculation loop before and after the mixing node recirculation loop respectively, which are pump controlled and maintained constant. Piping and instrumentation diagrams of the (A) analogy with an intermediate stirred tank representing the mixing node with the feed, and (B) the performed continuous concentration process, are represented.

Thus, the cell concentration inside the tank can be described by (9):

$$\frac{d\,(C_F V)}{dt} = C_B\ Q'_B + C_i\ Q_i - C_F\ Q_F \quad (9)$$

where V is the volume inside the tank and C_i , C_B and C_F (expressed in cell/mL) represent the cell concentration on the feed and recirculation loop before and after the tank, respectively. Likewise, Q_i , Q'_B and Q_F (expressed in L/h) represent the flow rates of the feed and recirculation loop before and after the tank, respectively, which are pump controlled and maintained constant.

Since the volume inside the tank is constant, Equation (9) can be rewritten (10):

$$V\ \frac{d\,(C_F)}{dt} = C_B\ Q'_B + C_i\ Q_i - C_F\ Q_F \quad (10)$$

Also, the addition and removal at the hollow fiber device is mass balance controlled, i.e.:

$$Q'_B = Q_F - Q_i \quad (11)$$

$$Q_F = Q_B + Q_P \quad (12)$$

$$Q_B = Q'_B + Q_R \quad (13)$$

where Q_P , Q_R and Q_B are the flow rates (L/h) of the permeate, retentate and after the device, respectively.

The volume that is continuously accumulated at the retentate tank (V_R) can be described by (14):

$$\frac{d\,V_R}{dt} = Q_R \quad (14)$$

Finally, the number of recovered cells (Figure 3.3B) throughout time can be expressed through the retentate's cell concentration and its flow rate (15):

$$\frac{d\,(C_R\ V_R)}{dt} = Q_R\,C_B \quad (15)$$

Equations (10) and (15) are firstly integrated using initial conditions of $V_R\ (t = 0) = V_{R0}$ and $C_B\ (t = 0) = C_{B0}$. Unlike discontinuous TFF, the initial cell concentration inside the TFF system is 0, since the system was first filled with DPBS before starting the concentration process, and the retentate's tank was initially empty ($V_R = 0$).

In Figure 3.2B is represented the ratio of $\frac{C_R}{C_i}$ throughout time, as determined by equations (8) and (15) for the discontinuous and continuous concentration, respectively.

Hollow fiber (HF) devices with 50 cm^2 kindly provided by Asahi Kasei (Tokyo, Japan), were used to conduct the comparison experiments of continuous and discontinuous TFF. A HF device with 24 cm^2 from GE Healthcare Life Sciences (New Jersey, USA) was used on the integrated process, based on results from Chapter II.

Either Watson Marlow Model 120 S/DV 200 rpm pump (Watson-Marlow Pumps Group, Massachusetts, USA) or Tandem Model 1081 peristaltic pumps from Sartoflow® Slice 200 benchtop crossflow system (Sartorius Stedim Biotech) were used. Pressure was monitored using SciPres luer pressure sensors (SciLog, Wisconsin, USA) on the inlet, outlet and permeate stream. Weight and pressure data were monitored and acquired every 15 sec using the Sartoflow® Slice 200 benchtop crossflow system. In all experiments, HF were operated at constant inlet flux, and by controlling the permeate flux with a peristaltic pump (Watson Marlow Model 120 S/DV 200 rpm).

A water flux test was performed before and after each experiment to determine the membrane's permeability. To ensure sterility, all HF devices were sanitized with 0.5 M NaOH (Sigma-Aldrich, Steinheim, Germany) at 50 ºC for 45 min. The membranes were preconditioned with five membrane volumes of sterile Dulbecco's Phosphate-Buffered Saline (DPBS) before the concentration step.

2.2.1.1 Continuous concentration

To start the continuous TFF (Figure 3.3A), the air from the device was initially removed by filling the recirculation loop with DPBS using a peristaltic pump (Watson Marlow Model 120 S/DV 200 rpm) on the feed side, set up to a flow rate of 200 mL/min, and with the recirculation pump (Tandem Model 1081) set to a flow rate of 30 mL/min. The cell suspension was then pumped into the TFF loop - the feed's peristaltic pump was placed on the retentate stream and set to 30 LMH, whereas the recirculation and permeate pumps were set to 2880 LMH (to ensure a shear rate of 3000 s^{-1}) and to 250 LMH, respectively. Concentrated cells were continuously recovered on the retentate's tank. After all the cell suspension had passed through the feed port, the permeate, recirculation and retentate pumps were stopped, and the cell suspension was completely drained from the TFF loop.

2.2.1.2 Discontinuous concentration

In discontinuous TFF (Figure 3.3A), the recirculation loop was initially filled with cell suspension. The recirculation pump (Tandem Model 1081) was set to 2880 LMH, and the permeate pump set to 250 LMH.

2.2.2 Cell washing (diafiltration)

The diafiltration (DF) step was performed using the same HF device previously used to conduct the concentration process. DPBS and formulation solution (FM) with 2.5% human

serum albumin (HSA; Baxter Healthcare, Berkshire, United Kingdom) were used to validate the DF process. To initiate the DF step, the circulation loop was filled with concentrated cell suspension using a Tandem Model 1081 peristaltic pump set to 750 LMH, clearing all the air from the loop and cartridge. The permeate pump was set to 250 LMH.

In discontinuous DF, the retentate was diluted (1:1) with DF media, and the permeable solutes were cleared on the permeate stream until the initial retentate's volume was reached; this process was repeated until necessary. Whereas in continuous DF, the DF media was continuously added to the feed tank at the same rate as the permeate flux.

2.3 Integration of hMSC cell expansion, concentration and diafiltration processes

A representation of the integrated process is shown in Fig 4.6A.

hMSC were expanded using microcarriers and stirred-tank bioreactors operating in continuous perfusion (section 2.1.2). After 14 days, cells were detached from the microcarriers and harvested as previously described in Chapter II. The microcarriers were then removed from the cell bulk suspension using sterile OptiCap® XL 1 Capsules (Merck Millipore, Massachusetts, USA) with 75 µm pore size, using Tandem Model 1082 peristaltic pump from Sartoflow® Slice 200 benchtop crossflow system (Sartorius Stedim Biotech) operated at a flow rate of 300 $mL.min^{-1}$ (Chapter II). Clarified cells were transferred to an intermediate vessel, and discontinuous TFF (section 2.2.1.2) allowed to concentrate cells up to a concentration factor of 10. At the end, a continuous DF process (using 5 DVs) was accomplished using a formulation solution (section 2.2.2).

2.4 Cell viability and characterization assays

All reagents used to perform cell characterization assays were purchased from Sigma Aldrich, unless stated otherwise.

2.4.1 Cell number and viability

Cell viability and cell membrane integrity were assessed using three different methods:

2.4.1.1 Trypan Blue exclusion method

Cell concentration was estimated through counting cells using a Fuchs–Rosenthal haemocytometer (Brand, Wertheim, Germany). Viable cells were determined by using the trypan blue dye exclusion method. The cell recovery yield is always referred as a percentage,

and was estimated taking into account the number of viable cells before (100%) and after processing.

2.4.1.2 Fluorescein diacetate-propidium iodide staining

The qualitative assessment of the cell plasma membrane integrity was also performed using the enzyme substrate fluorescein diacetate (FDA), and the DNA-dye propidium iodide (PI), as described in the literature (Fotakis and Timbrell, 2006; Jones and Senft, 1985). Briefly, cell suspensions were incubated with 20 µg/mL FDA and 10 µg/mL PI in DPBS for 5 min and observed using fluorescence microscopy (DMI 600 B, Leica Microsystems GmbH). Representative images were taken using a Leica DFC 360 FX digital camera.

2.4.1.3 Lactate Dehydrogenase (LDH) Assay

The release of intracellular lactate dehydrogenase enzyme (LDH) into the supernatant can be correlated with the extent of cell lysis (Fotakis and Timbrell, 2006). Hence, LDH activity from the supernatant of centrifuged samples was determined by monitoring the rate of oxidation of NADH to NAD^+, coupled with the reduction of pyruvate to lactate at 340 nm, as previously described in the literature (Vassault, 1983).

2.4.2 Apoptosis and metabolic activity assay

The percentage of apoptotic and metabolic active cells was evaluated using Apoptosis Assay Kit NucView™ 488 and MitoView™ 633 (Biotium, Inc., California, USA), following the manufacturer's instructions. This kit contains the green fluorescent NucView 488 caspase-3 substrate (detects intracellular caspase-3) and the far-red fluorescent MitoView 633 mitochondrial dye (detects changes in mitochondrial membrane potential). After incubation with both reagents, cells were analyzed by flow cytometry (CyFlow® space, Partec GmbH, Münster, Germany). At least ten thousand events were registered *per* sample.

2.4.3 hMSC's adhesion, growth profile and telomerase activity

hMSC were inoculated in static culture conditions, in 24-well-plates, previously coated with MesenCult™-SF Attachment Substrate. A cell inoculum of 5 x 10^3 cell/cm^2 was used and cells were cultured as described in section 2.1.1 (Cell Culture, Static Culture). For evaluation of the cell adhesion capacity, the number of adherent cells was monitored 60 minutes after inoculation, as previously performed in Chapter II.

Cells' growth profile was monitored for 13 days. Cell concentration and viability were determined as previously described in section 2.3.1.1 (Section Cell number and viability, Trypan Blue exclusion method).

2.4.4 Metabolite analysis

Glucose (GLC) and lactate (LAC) concentrations in the culture were analyzed using YSI 7100MBS (YSI Incorporated, Ohio, USA). Ammonia was quantified enzymatically, using a commercially available UV test (Roche, Basel, Switzerland). The specific metabolic rates (qMet, expressed in $\mu mol.h^{-1}.10^6\ cell^{-1}$), as well as the apparent yields of lactate from glucose ($Y_{LAC/GLC}$), oxygen from glucose ($Y_{O2/GLC}$) and ammonia from glutamine ($Y_{NH3/GLN}$) were determined as described in the literature (Serra et al., 2010; Tostões et al., 2011).

2.4.5 Flow cytometry

hMSC were washed once with DPBS and a total of 2 x 10^5 cells were incubated with each of the antibodies (CD166-PE, CD105-PE, CD90-PE, CD73-PE, CD44-PE, CD45-PE, CD34-PE, CD19-PE, CD14-PE, CD11b-PE, HLA-DR-PE and isotype controls IgG_1,κ-PE, IgG_{2a},κ-PE and IgG_{2b},κ-PE, all from BD Biosciences) for 1 h at 4 °C. Cells were washed twice in DPBS, and analyzed either in a CyFlow® space or in a CyAn™ ADP Analyzer (Beckman Coulter, California, USA) instruments. At least ten thousand events were registered *per* sample.

2.4.6 Morphology

hMSC were inoculated in static culture conditions, in 24-well-plates previously coated with MesenCult™-SF Attachment Substrate, as described in section 2.1.1 (Cell Culture, Static Culture). After 2 days, cells' morphology was analyzed as previously performed in Chapter II. Cells were incubated with each one of the primary antibodies for 2 h at room temperature. After two washing steps with DPBS, cells were incubated with the secondary antibodies for 1 h at room temperature. hMSC were then washed two times with DPBS and cell nuclei were counterstained with 4,6-diamidino-2-phenylindole (DAPI, Life Technologies). Cells were visualized using inverted (Leica Microsystems GmbH) fluorescence microscopy. Representative images were taken using a digital camera (Leica DFC 360 FX).

The primary antibodies used were Alexa Fluor® 488 Phalloidin (Life Technologies), Anti-Vimentin, and Anti-α-Tubulin. Anti-Vimentin and Anti-α-Tubulin were conjugated with secondary antibody Alexa Fluor® 594 Goat Anti-Mouse IgG (H+L) Antibody (Life Technologies).

2.4.7 *In vitro* multipotency assays

hMSC potency was evaluated through their capacity in differentiating into three different lineages (adipogenic, osteogenic and chondrogenic), following the manufacturer's guidelines and as described in Chapter II.

2.4.8 Quantitative real-time-polymerase chain reaction analysis

For real-time polymerase chain reaction (RT-PCR), a two-step PCR run was performed in a LightCycler480 (Roche) using a SYBR Green PCR master mix (Roche), as described elsewhere (dos Santos et al., 2011). Cell's RNA was extracted using High Pure RNA Isolation kit (Roche) and cDNA synthesis was performed using Transcriptor High Fidelity cDNA Synthesis Kit (Roche), following the manufacturer's instructions.

This two-step process consisted on an initial denaturation step at 95 °C, followed by 45 rounds of amplification between 10 s at 95 °C, 10 s at the respective annealing temperature and 10 s at 72 °C. The following primers were used: ALPL (mid osteocyte cell marker, 166 bp) (Fw) 5'-CCA CGT CTT CAC ATT TGG TG-3', (Re) 5'-AGA CTG CGC CTG GTA GTT GT-3'; FABP4 (early adipocyte cell marker, 215bp) (Fw) 5'-TAC TGG GCC AGG AAT TTG AC-3', (Re) 5'-GTG GAA GTG ACG CCT TTC AT-3' and SPP-1 (early chondrocyte cell marker, 229 bp) (Fw) 5'-TGA AAC GAG TCA GCT GGA TG-3', (Re) 5'-TGA AAT TCA TGG CTG TGG AA-3'.

All data was analyzed using the $2^{-\Delta\Delta Ct}$ method for relative gene expression analysis (Livak and Schmittgen, 2001). The changes in gene expression were normalized towards the metabolic housekeeping gene glyceraldehyde-3-phosphate dehydrogenase (GAPDH) as internal control. Data is represented as the relative expression of the gene regarding day 0 of differentiation. Control assays containing no templates were also performed. Three replicates *per* sample were considered.

2.4.9 Protein and DNA quantification

Process samples were centrifuged at 300x*g* for 5 minutes at room temperature, and the supernatant was kept at 4 ºC for further analysis.

Total protein concentration from the process samples was determined using either bicinchoninic acid protein assay (Pierce Biotechnology, Rockford IL, USA), according to the manufacturer's instructions, or using direct detect (Merck Millipore) infrared (IR)-based assay.

Protein samples were analyzed (using standard running conditions) by SDS-PAGE electrophoresis (XCell SureLock mini-cell system; Life Technologies), by loading the same protein amount into NuPAGE™ Novex™ 4–12% (w/v) bis-tris precast polyacrylamide gels (Life Technologies). Proteins were visualized by Instant Blue staining (Expedeon, Harston, UK). Protein clearance (expressed in terms of percentage) was considered as the total amount of protein from the expansion media that is removed from the cell suspension after each DF step.

Total double strand DNA content on the process samples was determined in 96-well plates using PicoGreen™ dsDNA Assay kit (Life Technologies), according to the manufacturer's instructions.

2.5 Statistical Analysis

All statistical analyses were performed using GraphPad Prism version 5 (GraphPad Software Inc., California, USA). All values are represented as mean ± standard deviation (n = 2 replicates were considered) of independent measurements or assays. The statistical significance was evaluated using either Student's T test or one-way ANOVA analysis (repeated measures ANOVA, Tukey analysis). *p* values of less than 0.05 were considered as statistically significant.

3. Results

3.1 hMSC expansion in continuous perfusion and semi-continuous cultures

hMSC were cultured on microcarriers in controlled stirred-tank bioreactors under xeno-free conditions (Stirred-tank Bioreactors Culture, section 2.1.2). The impact of culture operation mode on cell growth, volumetric productivities and metabolism was assessed. Two different culture operation modes were evaluated from day 4 onwards: i) 50% medium renewal every 2.5 days (designated as semi-continuous culture) and ii) continuous perfusion cultures at a dilution rate of 0.2 day^{-1}, which was selected to simulate the media renewal established in semi-continuous culture strategy.

Our results showed that hMSC achieved higher cell concentrations (3.7 x 10^5 cell/mL), expansion ratios (14.6) and maximum growth rate (0.016 h^{-1}) in continuous perfusion culture when compared to the semi-continuous strategy (2.9 x 10^5 cell/mL, 11.5 and 0.011 h^{-1}, respectively) (Figure 4.3A). In both culture strategies, hMSC were able to migrate to empty microcarriers and further proliferate using the bead-to-bead transfer strategy (Hervy et al., 2014). However, the percentage of colonized microcarriers was higher from day 7 onwards in

continuous perfusion cultures (Figure 4.3B). The culture operation mode showed not to impact cells' morphology, since hMSC attached to the microcarriers displayed organized intracellular f-actin during culture (Figure 4.3C).

Measurements of glucose and glutamine confirmed that there was no depletion of these nutrients during culture time (Supplementary data 4.1). Moreover, the accumulation of lactate and ammonia was always below the growth-inhibitory concentrations (<6 mM and <1 mM, respectively) (Schop et al., 2010) (Supplementary data 4.1). From day 4 onwards, lower specific rates of glucose consumption and lactate production were obtained in the continuous perfusion than in semi-continuous culture, although comparable specific rates of oxygen consumption could be observed in both strategies (Table 4.1).

Table 4.1 – Specific rates of glucose and oxygen consumption and lactate production of hMSC cultured on microcarriers using stirred-tank bioreactors operated in continuous perfusion and semi-continuous culture modes.

Culture time (day)	**q_{GLC} (µmol/10^6cell.h)**		**q_{LAC} (µmol/10^6cell.h)**		**q_{O2} (µmol/10^6cell.h)**	
	Cont. Perfusion	**SC**	**Cont. Perfusion**	**SC**	**Cont. Perfusion**	**SC**
0 – 4	0.180 (± 0.053)		0.433 (± 0.204)		0.321 (± 0.079)	
4 – 6	0.055 ± 0.006	0.131 ± 0.009	0.085 ± 0.088	0.297 ± 0.021	0.081 ± 0.015	0.163 ± 0.067
6 – 10	0.060 ± 0.001	0.128 ± 0.009	0.025 ± 0.004	0.256 ± 0.037	0.072 ± 0.005	0.053 ± 0.037
10 – 14	0.054 ± 0.013	0.135 ± 0.010	0.020 ± 0.012	0.225 ± 0.047	0.056 ± 0.003	0.036 ± 0.03

Furthermore, lower $Y_{LAC/GLC}$ (0.40 ± 0.02 *vs* 1.74 ± 0.17, Figure 4.3D) and higher $Y_{O2/GLC}$ (1.11 ± 0.12 *vs* 0.34 ± 0.11, Figure 4.3E) were obtained in continuous perfusion than in semi-continuous culture, suggesting that the continuous perfusion strategy induced a shift on hMSC metabolism towards energy production, whereas semi-continuous favored a more glycolytic metabolic phenotype. Similar profiles of specific rates of glutamine consumption and ammonia production, as well as $Y_{NH3/GLN}$ were observed in both culture strategies (data not shown).

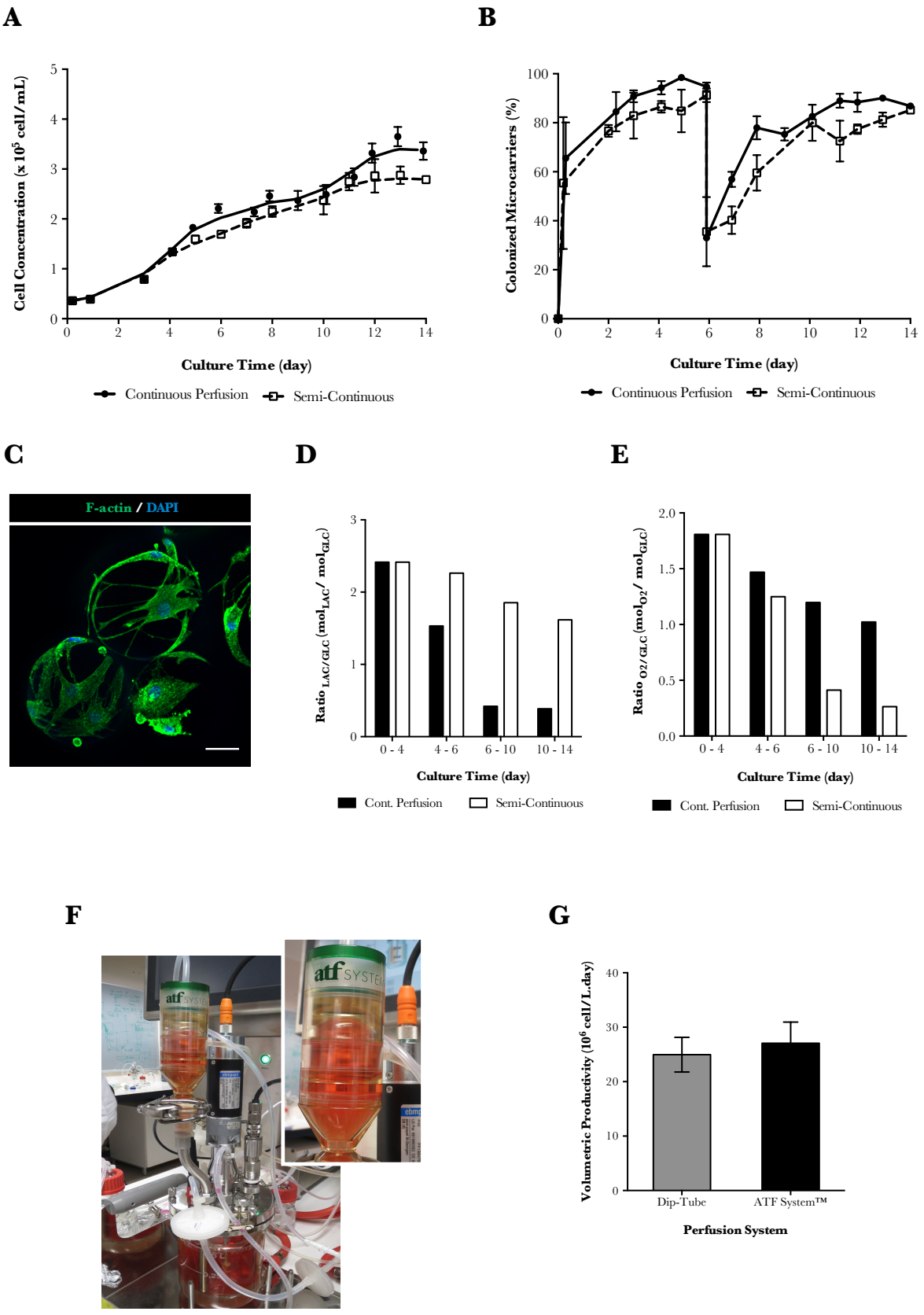

Figure 4.3 – Continuous perfusion and semi-continuous hMSC expansion in controlled stirred tank bioreactors. Growth curves expressing the increasing cell number per volume of medium (A) and percentage of colonized microcarriers (B) throughout the culture time. (C) hMSC adherent to microcarriers morphology during cell expansion - immunofluorescence staining of f-actin (green), and cell nuclei (blue). Scale bars: 100 µm. Metabolic characterization of the cultures - (D) Lactate - glucose and (E) oxygen - glucose ratios. (F)

ATF™ prototype. (G) Volumetric productivities, expressed in million cells per culture volume per day, of both the continuous perfusion (ATF™ and with dip-tube) and semi-continuous cultures.
Values are represented as the average and error bars of 3 measurements.

A prototype ATF™ system was evaluated as an alternative device for continuous perfusion operation mode (Figure 4.3F). In both perfusion cultures, hMSC displayed similar cell growth rates (0.016 day^{-1}), metabolic profiles (data not shown), and volumetric productivities (Figure 4.3G). Furthermore, hMSC showed high viability (> 95%) throughout culture time, as confirmed by trypan blue exclusion method and measurement of LDH release into culture supernatant (data not shown).

3.2 Concentration and diafiltration processes using tangential flow filtration

Due to their resemblance with hMSC (Alt et al., 2011), hFF were used as a proof of concept to evaluate the impact of different operation modes of TFF – continuous and discontinuous – on cell recovery yields and viability during concentration and diafiltration processes. The most suitable operation modes and conditions were then selected for the implementation of an integrated process for hMSC.

3.1.1 Continuous and discontinuous cell concentration

Continuous and discontinuous TFF operations were applied to concentrate cells, according to the schematic diagrams presented in Figure 4.4A.

Both processes (Figure 4.4A) were performed using shear rate and permeate flow conditions in agreement with the operating conditions and methodology previously reported in Chapter II. Cell concentration was performed up to a volume reduction factor of 6 in both TFF processes (Figure 4B). Results showed that cell recovery yield was not affected by the operation mode; continuous and discontinuous modes allowed to recover more than 80% of viable cells (cell viability ≥ 95%) after 9 minutes of operation. The observed cell loss (less than 20%) might be attributed to cell death throughout processing, since an increase in the percentage of apoptotic cells, as well as in DNA and LDH release were observed after both TFF processes (Figure 4.4C). Although the final cell recovery yield was similar on both process modes, the concentration profile was distinct. In continuous TFF, higher concentration factors were achieved sooner than in the discontinuous operation (Figure 4.4B), in agreement with the literature (Ho and Sirkar, 1992). Additionally, the use of a peristaltic pump controlling the feed instead of the permeate flux lead to a decrease of 20% in viable cell recovery yields (data not shown).

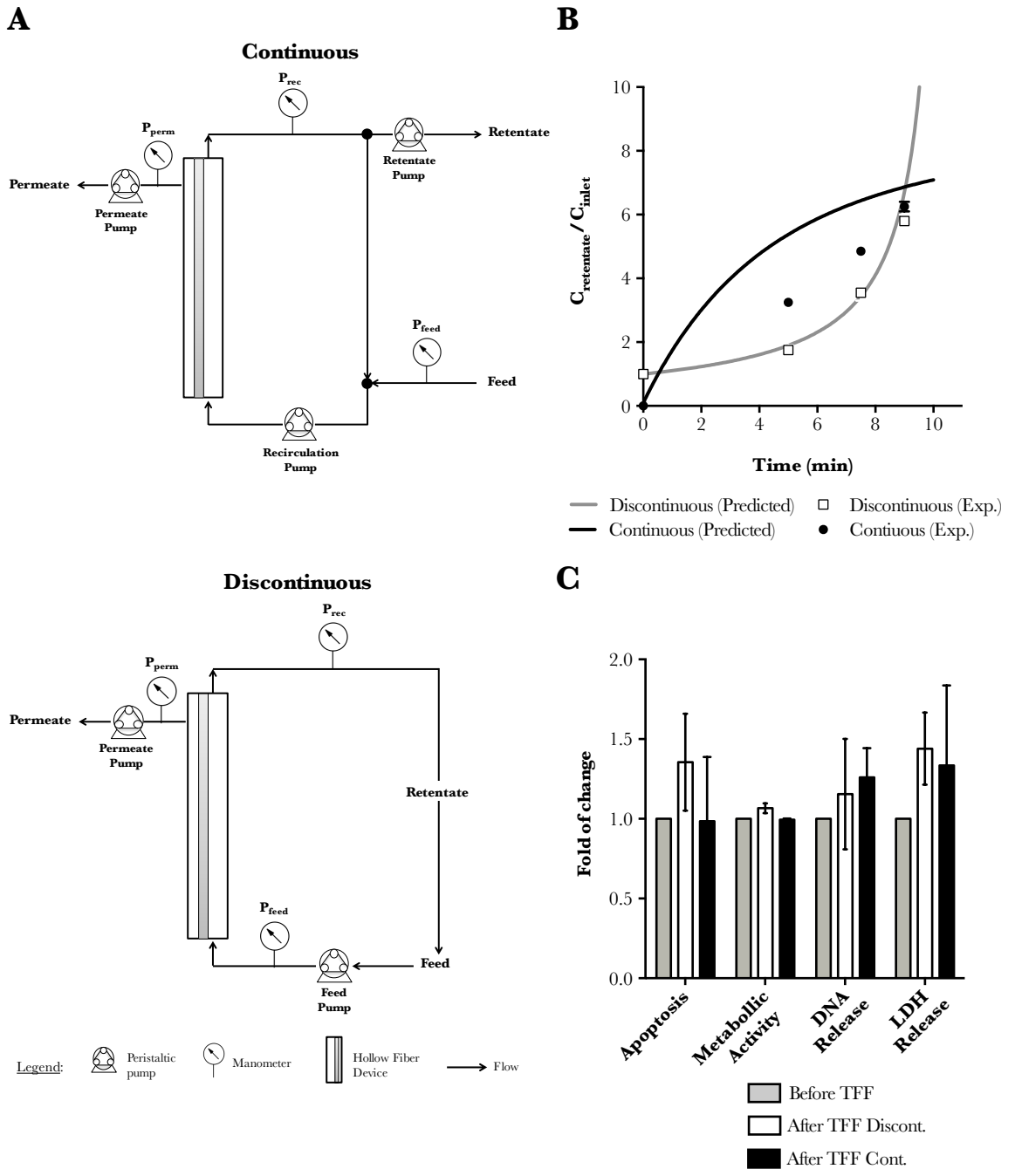

Figure 4.4 – **Continuous and discontinuous cell concentration.** (A) Schematic representation of two TFF operation modes – continuous and discontinuous. (B) Predicted (lines) and experimental (symbols) mass balances throughout the concentration processes. (C) Cell characterization in terms of apoptosis, metabolic activity, LDH and DNA release profile after the concentration processes. Results are presented as fold changes regarding cells before TFF. These proof-of-concept experiments were conducted with hFF. Error bars denote SD of 3 independent experiments. No significant differences were observed ($P > 0.05$).

3.2.2 Continuous and discontinuous cell washing (diafiltration)

Continuous and discontinuous DF were studied and compared to perform cell washing from protein impurities.

The impact of the medium composition on the DF process was evaluated using two different culture media; to compare both operation modes, DMEM supplemented with 10% (v/v) FBS (Nienow et al., 2014) was initially used. Thereafter, with the most suitable conditions, the process was validated with the xeno-free, serum-free Mesencult-XF™ (Swamynathan et al., 2014). Firstly, DPBS was used to characterize the impurities' removal profile. Having determined the most suitable diafiltration volumes (DVs), in a second stage, DF was performed using a formulation solution (with HSA).

In both DF operation modes, results showed that protein clearance increases throughout processing with the increasing number of DVs (Figure 4.5A). Particularly, in continuous DF, the highest protein clearance was obtained from 5 DVs (97.9% *vs.* 93.3%) onwards. Such could also be corroborated by SDS-PAGE, showing a decrease in the total concentration of proteins present, as well as the major impurity (bovine albumin), with increasing number of DVs (Figure 4.5B). Also, results show that throughout the DF process there is a decrease in the cell recovery yield for both processes (Figure 4.5C). However, discontinuous DF has led to higher cell death (assessed by LDH release concentration) after 5 DVs, which also translates in higher DNA concentration on the final cell suspension (Figure 4.5D), than in continuous DF in which cell recovery yields were higher (Figure 4.5C). At this point, five DVs were selected to perform further DF studies, due to the best trade-off between protein clearance (97.9%) and number of recovered cells (80%).

The DF operation was also validated with serum-free culture medium (Figure 4.5A). Although the serum-free culture medium had an initial total protein concentration higher than the serum-based medium (10 *vs* 4 mg/mL), the DF operation showed to be able to clear up to the same protein levels (0.03 *vs* 0.08 mg/mL, corresponding to 99.7 and 97.9%) after 5 DVs. Further increasing the number of DVs up to ten leads to a protein clearance up to 0.01 mg/mL (99.9%) (data not shown), while the major medium component (HSA) being mainly washed out from DV 7 onwards (corroborated by SDS-PAGE, data not shown). Nonetheless, such increase in DVs leads to a cell recovery yield of 60% and also to an increase in cell death (data not shown).

Given the previous results, a continuous operation with 5 DVs (Figure 4.5C) was applied to exchange the cell's media into a formulation media, recovering over than 80% of cells, with cell viabilities higher than 95%; no flux decay was ever observed throughout the process.

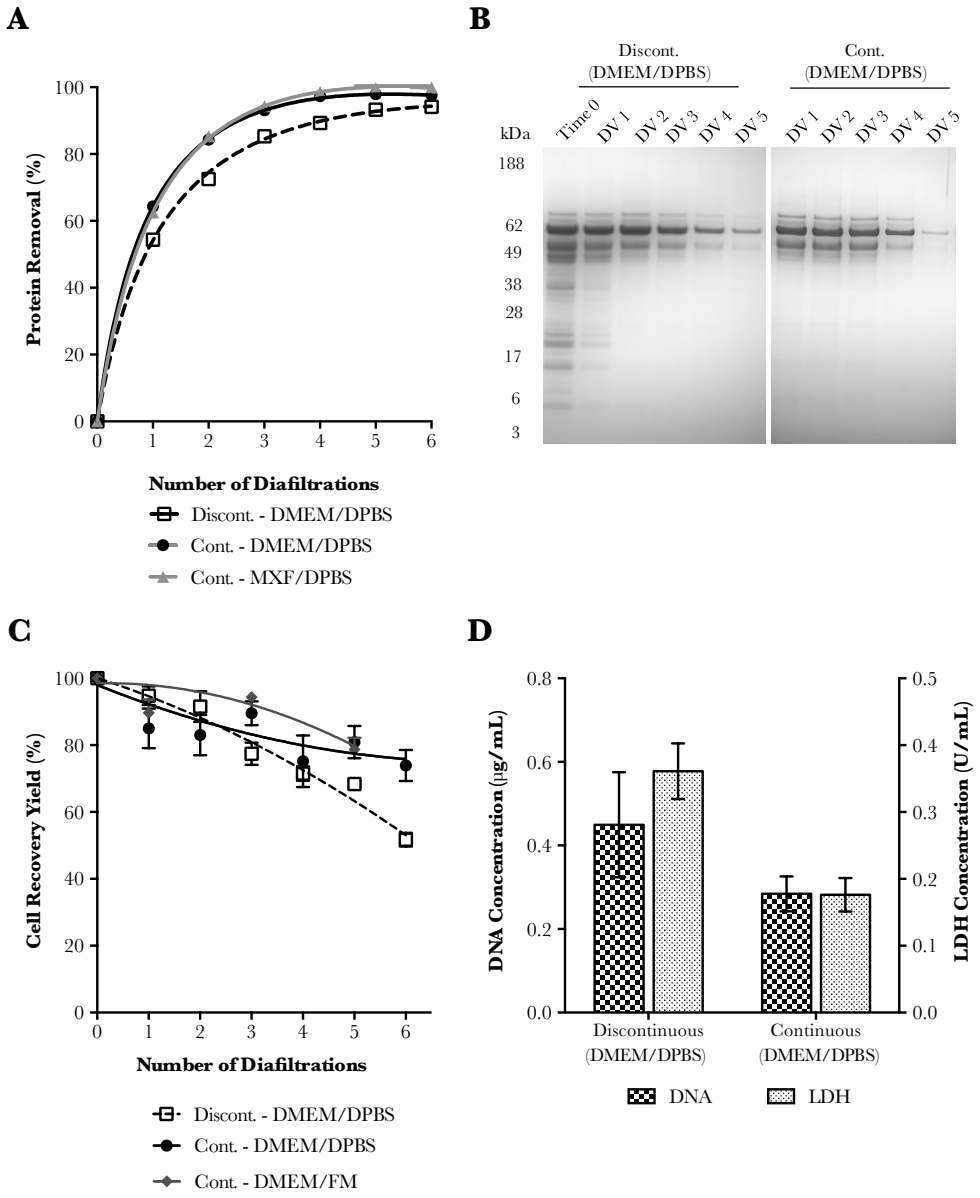

Figure 4.5 – Continuous and discontinuous cell washing. (A) Protein clearance (in percentage) with the increasing number of diafiltration volumes (DVs) on both types of processing with DPBS and using DMEM supplemented with 10% FBS (DMEM/DPBS) and Mesencult™-XF (MXF/DPBS). (B) SDS-PAGE analysis of protein samples from 1 up to 5 DVs for discontinuous and continuous DF (DMEM + 10% FBS with DPBS). Five micrograms (total protein) were loaded in each lane of the gel. (C) Impact of the number DVs of on the cell recovery yield (using DMEM + 10% FBS) during discontinuous and continuous DF using DPBS and formulation media with 2.5% HSA. (D) LDH and DNA release after 5 DVs in continuous and discontinuous DF using DPBS. Error bars denote SD of 3 independent experiments. No significant differences were observed ($P > 0.05$).

3.3 Integration of hMSC cell expansion, concentration and diafiltration processes

Combining the results from the previous result sections, we have designed an integrated process of expansion, concentration and washing for hMSC (Figure 4.1, 4.6A). A workflow of the integrated process after cell expansion is also presented in Figure 4.6B.

After hMSC expansion using microcarriers and stirred-tank bioreactors operating in continuous perfusion, cells were clarified from the microcarriers using the operating conditions present in Chapter II. Cells were then concentrated (up to a concentration factor of 10) and washed (5 DVs) into a formulation media, using the same hollow fiber device and process parameters of shear rate (3000 s^{-1}) and pump controlled permeate flux (250 $L.m^{-2}.h^{-1}$), as described in Chapter II. To integrate both processes in the same HF device, a discontinuous concentration was selected, followed by a continuous diafiltration process (Figure 4.6A and 4.6B). The integrated process allowed for a faster processing after cell expansion (1.5 hours, rather than typical 2 – 3 hours of separated processes), having been able to recover over than 70% (10% more than having separated processes) of highly viable hMSC (> 95%) (Figure 4.6C). The integrated process showed not to impact cell morphology, since after plating hMSC (after up- and downstream processing) could successfully re-acquire their typical spindle-like morphology, presenting organized intracellular f-actin, expressing α-tubulin and the mesenchymal marker vimentin (Figure 4.7A). The expression of the main characteristic hMSC's surface receptors, as described in the literature (Dominici et al., 2006), remained unaltered after processing (Figure 4.7B, Supplementary data 2).

More specifically, hMSC lacked the expression of CD45, CD34, CD14, CD11b and CD19, while displaying high levels of CD44, CD73, CD105 and CD166 mesenchymal stem markers. To be noted that hMSC before and after DSP presented HLA-DR expression higher than 5% (9% and 6%, respectively); previous studies in the literature (Sotiropoulou et al., 2006) have reported that several culture parameters can affect the expression of HLA. Since hMSC after expansion and DSP presented similar HLA-DR expression, the contribution to the presence of $HLA\text{-}DR^+$ cells should be due to the culture parameters used to expand hMSC.

After DSP, hMSC maintained their ability in adhering to plastic surfaces (no significant differences observed towards hMSC before TFF, Figure 4.7C), having more than 88% of adherent cells after 1 h. hMSC also remained metabolically active (no significant differences observed towards hMSC before TFF, Figure 4.7C), having reached a population doubling level (PDL) of approximately 3 after plating (Figure 4.7D).

Furthermore, hMSC after processing have maintained their multipotent differentiation capacity, as observed by the staining of adipocytes, osteocytes and chondroblasts (Figure 4.7E) and by RT-PCR analyses (Figure 4.8A to 4.8C). No spontaneous differentiation was ever observed (data not shown).

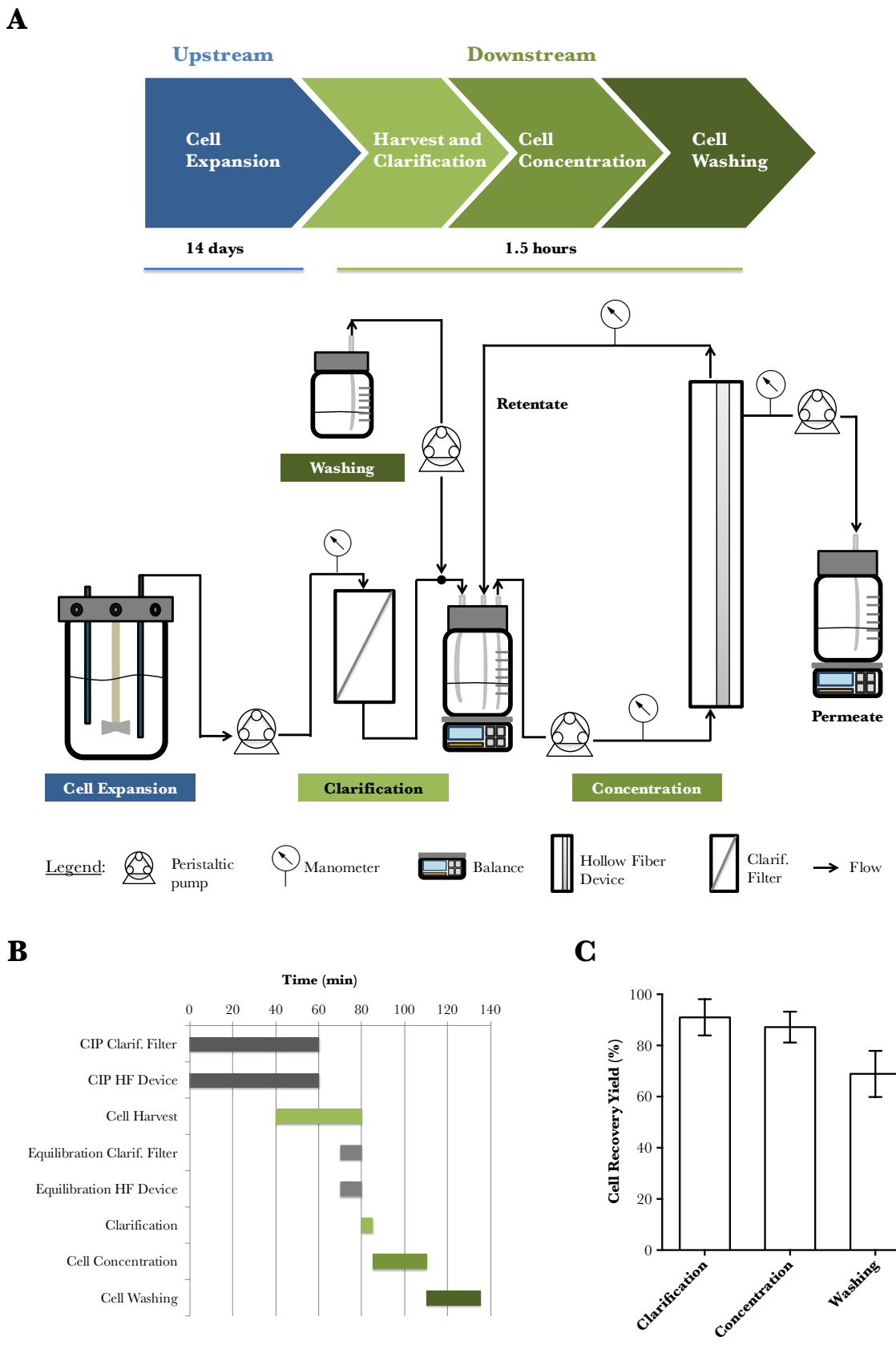

Figure 4.6 – Integrated bioprocess of hMSC. (A) Schematic representation of the experimental layout of the integrated bioprocess. (B) Workflow diagram of the process, clarifying timing and overlaps of the unit operations after cell expansion. (C) Cell recovery yield after clarification, concentration and diafiltration steps. Error bars denote SD of 3 measurements.

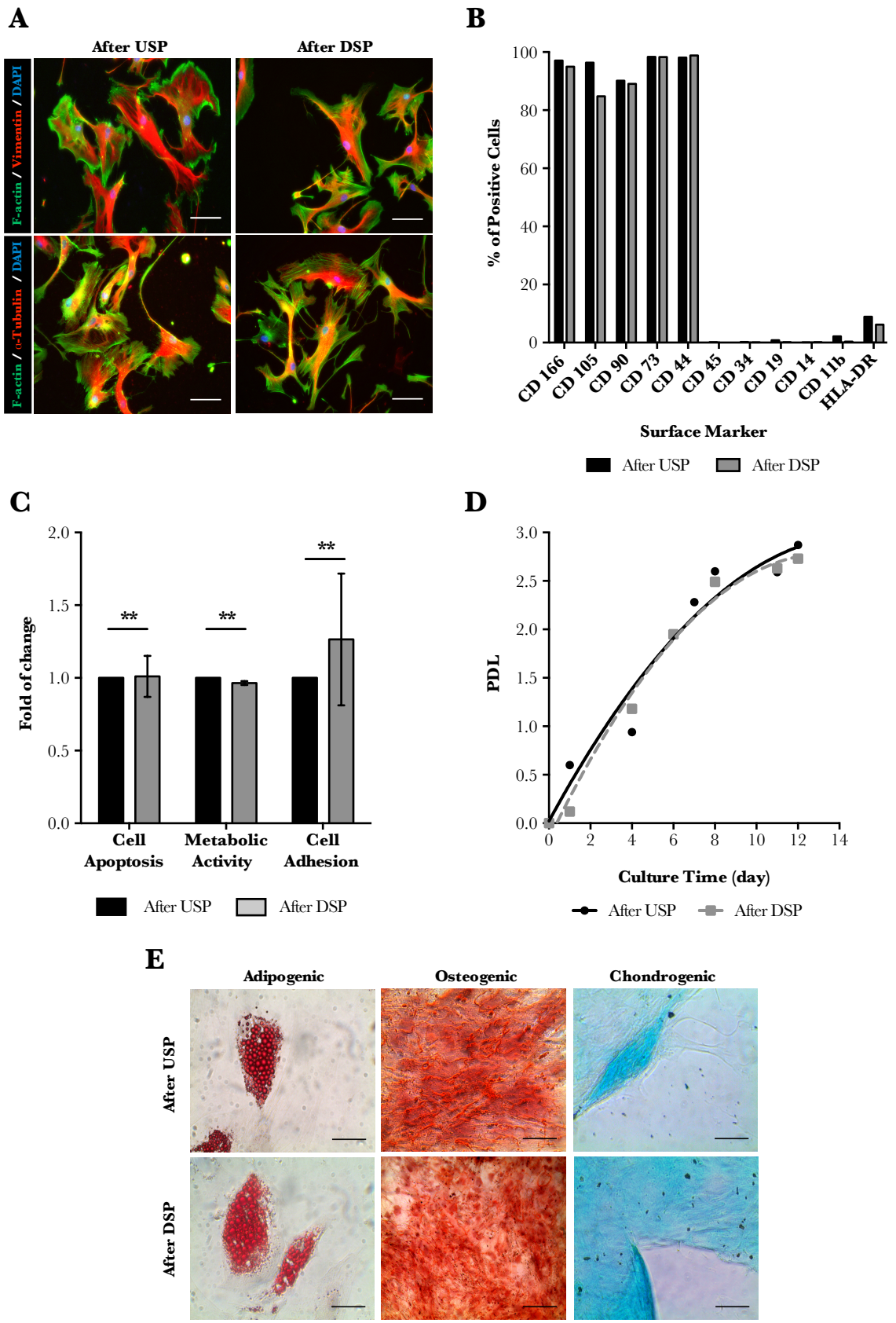

Figure 4.7 – hMSC characterization after the integrated bioprocess. (A) hMSC morphology after up- and downstream processing - immunofluorescence staining of f-actin (green), α-tubulin (red), vimentin (red), and cell nuclei (blue). Scale bars: 100 µm. (B) Expression of specific cell-surface antigens (CD166, CD105, CD73, CD 90, CD44, CD45, CD34, CD19, CD14, CD11b, HLA-DR) typical for hMSC, after up- and downstream processing. (C) Cell characterization (apoptosis, metabolic activity and cell adhesion). Each bar

represents the fold-increase/decrease, relative to cells after USP (black). No statistically significant differences (P > 0.05, marked as **) were found. (D) Growth curves expressing the population doubling level throughout the culture time of re-plated hMSC after up- and downstream processing. Values represent the average of 3 measurements. (E) Multipotent differentiation potential of hMSC. Red-oil solution stained lipid droplets (adipocytes, left panel), alizarin red stained calcium deposits (osteoblasts, central panel), and alcian blue stained extracellular matrix proteins (chondrocytes, right panel). Scale bars: 100 μm.

Quantitative RT-PCR analyses showed an up-regulation of three differentiation genes for the three differentiation lineages – adipogenesis (FABP4, Figure 4.8A), osteogenesis (ALPL, Figure 4.8B) and chondrogenesis (SPP-1, Figure 4.8C) – when comparing with cells before the differentiation processes. hMSC's telomerase activity was also assessed (data not shown). Since no statistically significant differences were found in hMSC after expansion and after DSP (P > 0.05), it is possible to assume that the DSP processes do not contribute to the hMSC's senescence.

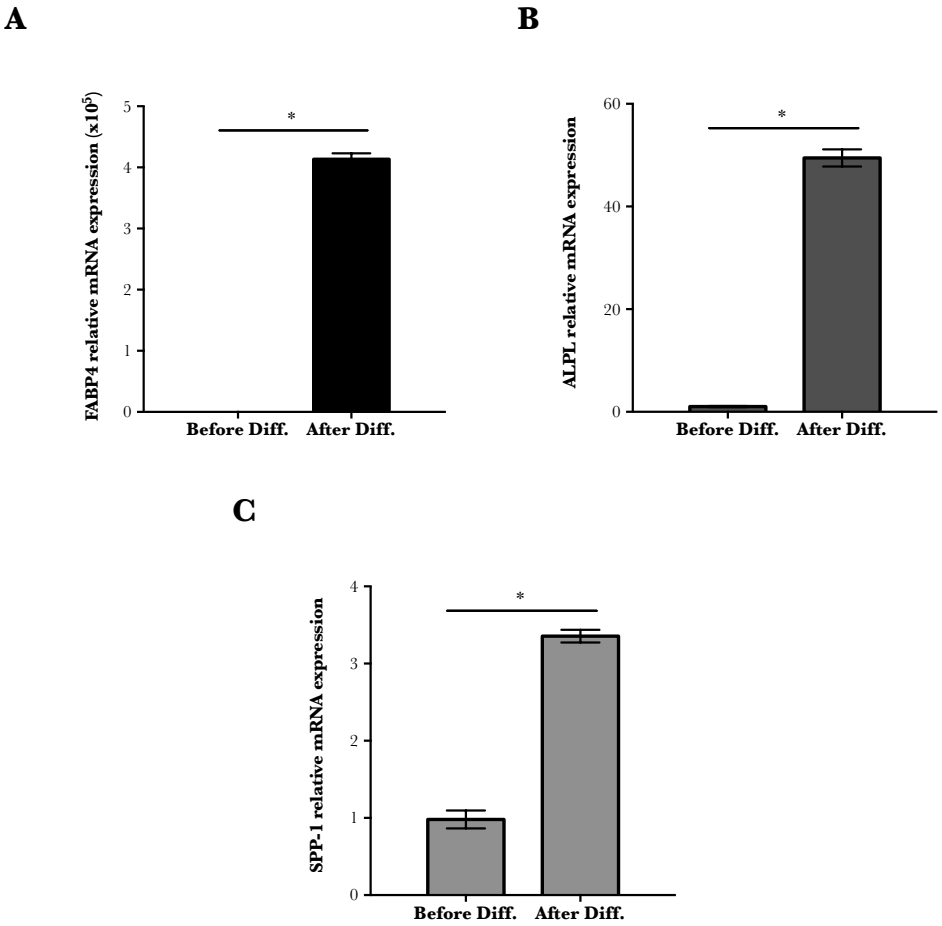

Figure 4.8 – hMSC characterization after the integrated bioprocess. Quantitative RT-PCR analyses of the differentiation processes. Expression of (A) FABP4 (adipogenesis), (B) ALPL (osteogenesis), and (C) SPP-1 (chondrogenesis) genes were analyzed, before and after the differentiation processes. Data is represented as the relative expression of the gene towards the day 0 of differentiation. Statistically significant differences (P < 0.05) towards cells before differentiation are marked as *.

4. Discussion

The biopharmaceutical industry is upgrading into integrated, continuous and single-use bioprocessing strategies. The aim of this work was to explore and develop an integrated bioprocess for the expansion, concentration and washing of hMSC; continuous and discontinuous operation modes for each one of the steps were compared, and with the most suitable conditions an integrated process was designed. Particular focus was given on the effect that continuous and discontinuous operation modes have on hMSC's characteristics. Results show that continuous processes (continuous perfusion, concentration and diafiltration) had higher productivities, *i.e.*, number of expanded/recovered cells *per* unit of time, when compared with discontinuous operations.

hMSC expansion in bioreactors operating in perfusion mode has been preliminarily described (F. dos Santos et al., 2014); however, deep characterization of the effect of different operation modes on cells' growth, metabolism and characteristics was absent. In our study, we have observed that expanding hMSC in a continuous perfusion operation mode provided a higher expansion ratio, and led to changes in the cells' metabolism, particularly after day 4 of culture; $Y_{LAC/GLC}$ ratios decreased and $Y_{O2/GLC}$ ratios remained high, when compared to the semi-continuous culture. The continuous perfusion system appears to be leading to a metabolic shift from a mostly glycolytic metabolism towards a metabolism based on the TCA cycle, which is a more energy-efficient pathway, thus contributing to improved cell growth. The maximum cell concentration achieved in our study (4×10^5 cell/mL) was lower than the one reported by Santos *et al.* (5×10^5 cell/mL) (F. dos Santos et al., 2014). The difference in cell growth profile may reflect the distinct cell origins (hMSC were isolated from the bone marrow of different donors), and the different culture conditions used in both studies, such as the microcarriers' type and the culture medium formulation. In this work, we also showed the feasibility of using a prototype ATF™ system as an alternative device for continuous perfusion of hMSC cultured in microcarrier-based stirred systems. Both perfusion systems assured an efficient and automated operation management, overcoming the major drawbacks of the semi-continuous strategy, which requires repeated manipulation. To be noted that adult stem cells have a limited life span, and their characteristics change along the population doublings. Therefore, for cell therapy products, the advantages of a continuous, integrated process should be evaluated against current strategies where cell expansion is improved through medium renewal.

In optimal continuous operations, the required time to reach steady state is usually negligible when compared to overall process time, leading to higher productivities than in

discontinuous operations (Jungbauer, 2013). Moreover, the residence time of particles within the system is longer in discontinuous processing (Cheryan, 1998). We have observed that continuous and discontinuous TFF operations can be successfully applied to concentrate cells, recovering in both more than 80% of highly viable cells (> 95%). The operation mode provides however different advantages; higher cell concentrations were achieved sooner when operating TFF in a continuous mode, as validated experimentally, leading to a higher productivity (number of concentrated cells *per* unit of membrane area and time). Therefore, if we tailor the system to achieve a determined cell concentration, cells at the intended concentration will be available sooner than when operating in discontinuous mode. Conversely, discontinuous TFF allows to couple a diafiltration step within the same HF device, decreasing not only the equipment's footprint necessary for processing, but also hold up volumes and overall process time. Since both operation modes achieve similar recovery yields, cell concentration factors and viabilities, the choice should depend on the occupational workflow advantages each of them pose. Although conceptually the membrane fully rejects the cells based on its pore size, previous results (Chapter II) showed that the membrane's polysulfone material is prone to interact with the cellular suspension (Koehler et al., 1997); such could explain the observed differences between the experimental data and the predictive mass balance on the continuous TFF concentration process.

Effective removal of host cell contaminants is required by regulatory agencies to ensure product safety (European Medicines Agency, 2008), since trace amounts of host-cell DNA and proteins if injected into patients may potentially cause allergic reactions or even cause transfection of cells, resulting in tumour formation (Wolter and Richter, 2005). Within this context, we have performed cell washing by diafiltration after the concentration process, so that the volume of cell suspension washed minimizes the process time, as well as the volume of wash buffer used. As previously reported (Watler and Rozembersky, 2011), continuous diafiltration showed to be more efficient and gentle than discontinuous DF (Schwartz, 2003), where lower cell recoveries and increased cell death were observed in discontinuous DF. One possible explanation is that the process of concentrating and diluting a solution can affect molecular interactions, causing possible product loss, which may damage cells. Furthermore, the continuous circulation of the diafiltration buffer was shown to improve protein clearance, which increased from 93% (discontinuous DF) to over 98% (continuous DF). Overall, continuous DF cleared up to 3 logs of total protein from the cell suspension.

Overall and for the particular case of hMSC, by evidencing the feasibility and comparing the advantages of continuous and discontinuous operations, it was possible to design a process

that integrates up and downstream operations, by applying a more efficient process workflow. Higher productivities were achieved without compromising cells' characteristics. Moreover, the use of mathematical models for mass balancing throughout time of TFF processes allows prediction and fine tuning of desirable cell concentrations. The work herein described is, to the best of our knowledge, the first demonstration of the impact that continuous and/or integrated processing have on hMSC biomanufacturing, in terms of productivity and cell quality attributes. Furthermore, the described process can comply with future scale-up demand of both autologous and allogeneic therapies, since each of the unitary operations makes use of devices that not only offer surface area and/or volume capacity scalability, but are also cGMP compliant.

5. Acknowledgments

I would like to acknowledge Asahi Kasei (Japan), for the HF devices they provided, Corning Inc. for providing the microcarriers and to Repligen Corporation for providing the ATF™ prototype used in this study.

This work was funded by Fundação para a Ciência e Tecnologia (FCT, Portugal) (project EXPL/BBB-EBI/1003/2012 and PhD grant SFRH/BD/51940/2012, MIT-Portugal Program) and by NanoGene project (EuroNanoMed ERA-Net initiative - ENMED/0001/2010).

6. Supplementary data

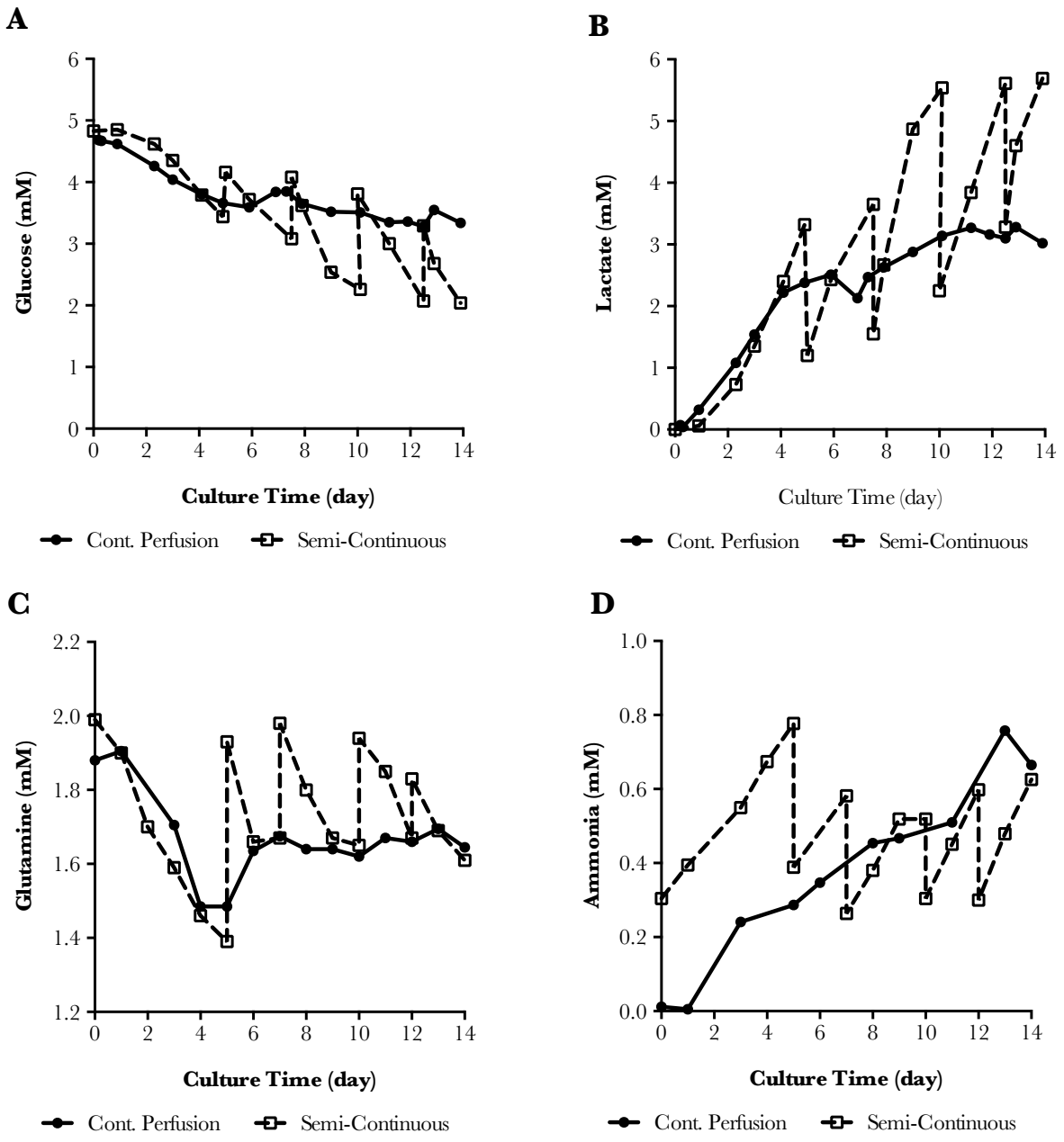

Supplementary data 4.1 – Profiles of Glucose (A), lactate (B), glutamine (C), and ammonia (D) concentration (expressed in mM) through the culture time in both continuous perfusion and semi-continuous cultures.

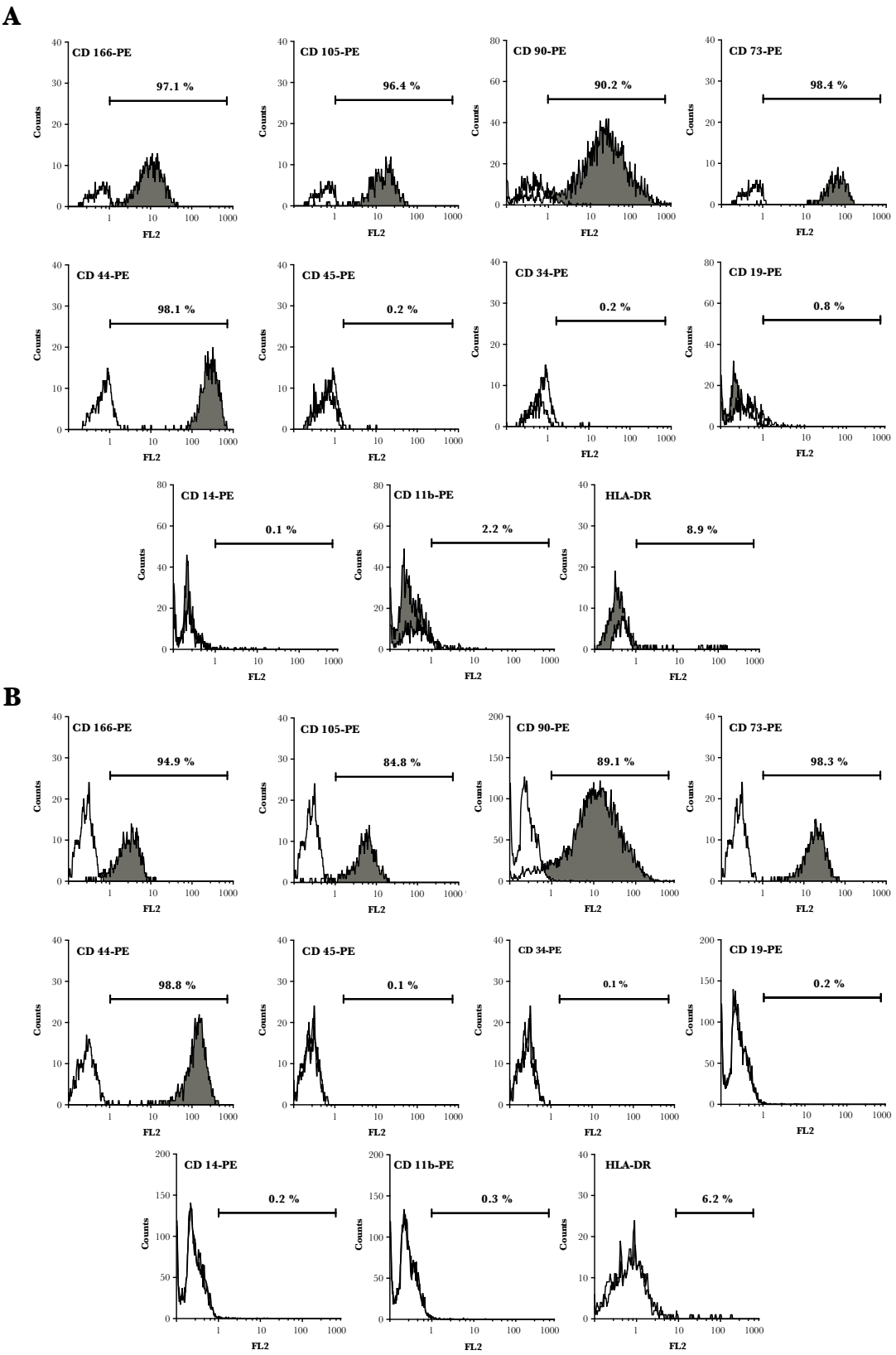

Supplementary data 4.2 – Expression of specific cell-surface antigens (CD166, CD105, CD73, CD90, CD44, CD45, CD34, CD19, CD14, CD11b, HLA-DR) typical for hMSC. Flow cytometry analysis is presented for hMSC after up- (A) and downstream processing (B).

References

Alt, E., Yan, Y., Gehmert, S., Song, Y.-H., Altman, A., Gehmert, S., Vykoukal, D., Bai, X., 2011. Fibroblasts share mesenchymal phenotypes with stem cells, but lack their differentiation and colony-forming potential. Biol. Cell 103, 197–208.

Chen, A.K.-L., Reuveny, S., Oh, S.K.W., 2013. Application of human mesenchymal and pluripotent stem cell microcarrier cultures in cellular therapy: Achievements and future direction. Biotechnology Advances 31, 1032–1046.

Cheng, L.P., Lin, H.Y., Chen, L.W., Young, T.H., 1998. Solute rejection of dextran by EVAL membranes with asymmetric and particulate morphologies. Polymer 39, 2135–2142.

Cheryan, M., 1998. Ultrafiltration and Microfiltration Handbook, 1st ed. Technomic Publishing AG, Basel.

Dominici, M., Le Blanc, K., Mueller, I., Slaper-Cortenbach, I., Marini, F., Krause, D., Deans, R., Keating, A., Prockop, D., Horwitz, E., 2006. Minimal criteria for defining multipotent mesenchymal stromal cells. The International Society for Cellular Therapy position statement. Cytotherapy 8, 315–317.

European Medicines Agency, 2008. EMEA/CHMP Guideline on human cell-based medicinal products (EMEA/CHMP/410869/2006).

Fotakis, G., Timbrell, J.A., 2006. In vitro cytotoxicity assays: comparison of LDH, neutral red, MTT and protein assay in hepatoma cell lines following exposure to cadmium chloride. Toxicol. Lett. 160, 171–177.

Hervy, M., Weber, J.L., Pecheul, M., Dolley-Sonneville, P., Henry, D., Zhou, Y., Melkoumian, Z., 2014. Long term expansion of bone marrow-derived hMSCs on novel synthetic microcarriers in xeno-free, defined conditions. PLoS ONE 9, e92120.

Ho, W., Sirkar, K.K., 1992. Membrane handbook. Springer Science + Business Media, LLC, New York.

Jones, K.H., Senft, J.A., 1985. An improved method to determine cell viability by simultaneous staining with fluorescein diacetate-propidium iodide. J. Histochem. Cytochem. 33, 77–79.

Jungbauer, A., 2013. Continuous downstream processing of biopharmaceuticals. Trends in Biotechnology 31, 479–492.

Koehler, J.A., Ulbricht, M., Belfort, G., 1997. Intermolecular Forces between Proteins and Polymer Films with Relevance to Filtration. Langmuir 13, 4162–4171.

Livak, K.J., Schmittgen, T.D., 2001. Analysis of relative gene expression data using real-time quantitative PCR and the 2(-Delta Delta C(T)) Method. Methods 25, 402–408.

Mason, C., Dunnill, P., 2009. Quantities of cells used for regenerative medicine and some implications for clinicians and bioprocessors. Regen Med 4, 153–157.

Murphy, M.B., Moncivais, K., Caplan, A.I., 2013. Mesenchymal stem cells: environmentally responsive therapeutics for regenerative medicine. Experimental & molecular medicine 45, 54–70.

Nienow, A.W., Rafiq, Q.A., Coopman, K., Hewitt, C.J., 2014. A potentially scalable method for the harvesting of hMSCs from microcarriers. Biochemical Engineering Journal 85, 79–88.

Pattasseril, J., Varadaraju, H., Lock, L., Rowley, J.A., Rowley, J.A., 2013. Downstream Technology Landscape for Large-Scale Therapeutic Cell Processing. BioProcess International 11, 38–47.

Santos, dos, F., Campbell, A., Fernandes-Platzgummer, A., Andrade, P.Z., Gimble, J.M., Wen, Y., Boucher, S., Vemuri, M.C., da Silva, C.L., Cabral, J.M.S., 2014. A xenogeneic-free bioreactor system for the clinical-scale expansion of human mesenchymal stem/stromal cells. Biotechnology and Bioengineering 111, 1116–1127.

Santos, F.D., Andrade, P.Z., Abecasis, M.M., Gimble, J.M., Chase, L.G., Campbell, A.M., Boucher, S., Vemuri, M.C., Silva, Cabral, J.M.S., 2011. Toward a Clinical-Grade Expansion of Mesenchymal Stem Cells from Human Sources: A Microcarrier-Based Culture System Under Xeno-Free Conditions. Tissue Engineering Part C: Methods 17, 1201–1210.

Schaber, S.D., Gerogiorgis, D.I., Ramachandran, R., Evans, J.M.B., Barton, P.I., Trout, B.L., 2011. Economic Analysis of Integrated Continuous and Batch Pharmaceutical Manufacturing: A Case Study. Ind. Eng. Chem. Res. 50, 10083–10092.

Schop, D., van Dijkhuizen-Radersma, R., Borgart, E., Janssen, F.W., Rozemuller, H., Prins, H.-J., de Bruijn, J.D., 2010. Expansion of human mesenchymal stromal cells on microcarriers: growth and metabolism. J Tissue Eng Regen Med 4, 131–140.

Schwartz, L.M., 2003. Diafiltration for desalting or Buffer exchange. BioProcess International 43–49.

Serra, M., Brito, C., Sousa, M.F.Q., Jensen, J., Tostões, R., Clemente, J., Strehl, R., Hyllner, J., Carrondo, M.J.T., Alves, P.M., 2010. Improving expansion of pluripotent human embryonic stem cells in perfused bioreactors through oxygen control. Journal of Biotechnology 148, 208–215.

Simaria, A.S., Hassan, S., Varadaraju, H., Rowley, J., Warren, K., Vanek, P., Farid, S.S., 2014. Allogeneic cell therapy bioprocess economics and optimization: single-use cell expansion technologies. Biotechnology and Bioengineering 111, 69–83.

Sotiropoulou, P.A., Perez, S.A., Salagianni, M., Baxevanis, C.N., Papamichail, M., 2006. Characterization of the optimal culture conditions for clinical scale production of human mesenchymal stem cells. Stem Cells 24, 462–471.

Swamynathan, P., Venugopal, P., Kannan, S., Thej, C., Kolkundar, U., Bhagwat, S., Ta, M., Majumdar, A.S., Balasubramanian, S., 2014. Are serum-free and xeno-free culture conditions ideal for large scale clinical grade expansion of Wharton's jelly derived mesenchymal stem cells? A comparative study. Stem Cell Res Ther 5, 88.

Tostões, R.M., Leite, S.B., Miranda, J.P., Sousa, M., Wang, D.I.C., Carrondo, M.J.T., Alves, P.M., 2011. Perfusion of 3D encapsulated hepatocytes--a synergistic effect enhancing long-term functionality in bioreactors. Biotechnology and Bioengineering 108, 41–49.

Vassault, A., 1983. Lactate dehydrogenase: UV-method with pyruvate and NADH, in: Bergmeyer, H.U., Grassl, M. (Eds.), Methods of Enzymatic Analysis. John Wiley & Sons, New York, pp. 118–126.

Vicente, T., Burri, S., Wellnitz, S., Walsh, K., Rothe, S., Liderfelt, J., 2014. Fully aseptic single-use cross flow filtration system for clarification and concentration of cytomegalovirus-like particles. Engineering in Life Sciences 14, 318–326.

Warikoo, V., Godawat, R., Brower, K., Jain, S., Cummings, D., Simons, E., Johnson, T., Walther, J., Yu, M., Wright, B., McLarty, J., Karey, K.P., Hwang, C., Zhou, W., Riske, F., Konstantinov, K., 2012. Integrated continuous production of recombinant therapeutic proteins. Biotechnology and Bioengineering 109, 3018–3029.

Watler, P.K., Rozembersky, J., 2011. Application of QbD Principles to Tangential Flow Filtration Operations, in: Rathore, A.S., Mhatre, R. (Eds.), Quality by Design for Biopharmaceuticals: Principles and Case Studies. John Wiley & Sons, Inc., New Jersey, pp. 111–126.

Wei, X., Yang, X., Han, Z.-P., Qu, F.-F., Shao, L., Shi, Y.-F., 2013. Mesenchymal stem cells: a new trend for cell therapy. Acta Pharmacol. Sin. 34, 747–754.

Wolter, T., Richter, A., 2005. Assays for controlling host-cell impurities in biopharmaceuticals. BioProcess International.

V

Bioprocess integration for human mesenchymal stem cells: from up to downstream processing scale-up to cell proteome characterization

This chapter was adapted from:

Cunha B, Aguiar T, Carvalho SB, Silva MM, Gomes RA, Carrondo MJT, Gomes-Alves P, Peixoto C, Serra M, Alves PM (2016). Bioprocess integration for human mesenchymal stem cells: from up to downstream processing scale-up to cell proteome characterization, Biotechnology and Bioengineering, *submitted*.

Table of Contents

ABSTRACT 166

1. INTRODUCTION 167

2. MATERIALS AND METHODS 168

2.1 hMSC Expansion 168
2.2 Downstream processing 170
2.3 Cell viability and characterization assays 171
2.4 Statistical Analysis 175

3. RESULTS 176

3.1 Scale-up of hMSC's expansion in single-use bioreactors 176
3.2 Scale-up of TFF process for the concentration of hMSC 179

4. DISCUSSION 188

5. CONCLUSION 190

6. ACKNOWLEDGMENTS 191

7. SUPPLEMENTARY DATA 192

REFERENCES 193

Abstract

To deliver the required cell numbers and doses to therapy, scaling up production and purification processes (at least to the liter-scale) while maintaining cells' characteristics is compulsory. Therefore, the aim of this work was to prove scalability of an integrated streamlined bioprocess compatible with current good manufacturing practices (cGMP) comprised by cell expansion, harvesting and volume reduction unit operations using human mesenchymal stem cells (hMSC) isolated from bone marrow (BM-MSC) and adipose tissues (AT-MSC).

BM-MSC and AT-MSC expansion and harvesting steps were scaled-up from spinner flasks to 2 L scale stirred tank single-use bioreactor using synthetic microcarriers and xeno-free medium, ensuring high cellular volumetric productivities (50 x 10^6 cell.L^{-1}.day^{-1}), expansion factors (14-16 fold) and cell recovery yields (80%). For the concentration step, flat sheet cassettes (FSC) and hollow fiber cartridges (HF) were compared showing a fairly linear scale-up, with a need to slightly decrease the permeate flux (30-50 LMH, respectively) to maximize cell recovery yield. Nonetheless, FSC allowed to recover 18% more cells after a volume reduction factor of 50. Overall, at the end of the entire bioprocess more than 65% of viable (> 95%) hMSC could be recovered without compromising cell's critical quality attributes (CQA) of viability, identity and differentiation potential.

Alongside the standard quality assays for evaluating hMSC's CQA, a proteomics workflow based on mass spectrometry tools was established to characterize the impact of processing on hMSC' CQA; These analytical tools constitute a powerful tool to be used in process design and development.

Keywords: cell therapy, product characterization, process development, mass spectrometry, human mesenchymal stem cells, scale-up

1. Introduction

Human mesenchymal stem cells (hMSC) are relevant for autologous and allogeneic therapies. Their differentiation potential, anti-inflammatory, immunomodulatory and trophic properties (Murphy et al., 2013), justify their use in over 300 clinical trials for the treatment of several diseases as Crohn's disease, graft versus host disease, amongst others (http://clinicaltrials.gov).

For clinical purposes efficient production and purification of hMSC are essential, yielding high cell numbers (10^6 to 10^9 cells are needed *per* patient) (Mason and Dunnill, 2009) with high purity and viability (Pattasseril et al., 2013), maintaining cells' critical quality attributes (CQA) and functionality. "Omic" tools in combination with standard analytical assays allow for a better cell characterization, increasing product and process understanding (Campbell et al., 2015) and are thus fundamental for process development. Regarding hMSC expansion, classic static culture systems such as T-flasks or multi-layer flasks lack scalability (Rowley et al., 2012); therefore, technologies such as stirred tank bioreactors and microcarriers, enabling control and monitoring of culture parameters, maximize cell expansion (Chapter IV) (Chen et al., 2013), becoming cost-effective solutions to scale-up the expansion of hMSC adherent cultures (Simaria et al., 2014).

Increasing the cell numbers will also imply an increase of the harvest volumes, thus downstream processes (DSP) steps, from cell detachment to concentration and washing, need to be properly addressed when handling higher volumes. In microcarrier cultures, detaching cells ensuring high cell recoveries is still a bottleneck. Recently, new detaching methods and protocols (Nienow et al., 2016) have been purposed. Then, to achieve high volume reduction factors (VRF), tangential flow filtration (TFF) using hollow fiber cartridges (HF) or flat sheet cassettes (FSC) can be evaluated to process volumes relevant for therapies (Cheryan, 1998; Hassan et al., 2015). Both devices are compact, closed, scalable and can be manufactured for single-use (Hassan et al., 2015). Previously in Chapter II and IV the key operation parameters of TFF using HF cartridges were identified, allowing to concentrate hMSC while maximizing cell recovery yield. Turbulence promoters used in the feed channel of FSC decrease fouling (Lutz, 2015) and may further increase cell recoveries at this volume reduction unit operation.

Thereby we present herein a proof of concept of the scalability of expansion, harvesting and concentration unit operations compatible with current good manufacturing practices (cGMP); hMSC isolated from bone marrow (BM-MSC) and adipose tissue (AT-MSC) were expanded using single-use (SU) bioreactors (BR, up to 2 L), synthetic microcarriers and xeno-

free culture medium. Afterwards, a short period of intense agitation in the presence of the detaching agent as previously described (Nienow et al., 2016; 2014) was scaled-up, promoting cell detachment from the microcarriers. Finally, the concentration unit operation was scaled-up using two types of TFF devices — HF and FSC. Besides using standard analytical assays for cells' CQA evaluation (viability, identity and multilineage differentiation potential), a proteomics workflow was developed, characterizing the whole cell proteome and gaining better insights into the impact of manufacturing at different stages of processing.

2. Materials and Methods

2.1 hMSC Expansion

Human BM-MSC (donor 00055; RoosterBio, Maryland, USA), and human AT-MSC (donor 060, RoosterBio) were used. All reagents used were purchased from ThermoFisher™ Scientific (Massachusetts, USA), unless otherwise stated.

2.1.1 Static Culture

BM-MSC and AT-MSC were routinely cultured (from population doubling level (PDL) 9 to 20) in High Performance Media Kit (HPMK, RoosterBio) and propagated in tissue culture flasks at 37 ºC in a humidified atmosphere of 5% CO_2 in air, according to the manufacturer's instructions. At 70 – 80% cell confluency, the medium was removed, cells were washed with Dulbecco's phosphate-buffered saline (DPBS) and incubated with TrypLE™ Select (1X) detachment reagent for 12 min (BM-MSC) or 6 min (AT-MSC) at 37 ºC, according to previous experience in our laboratory. After detachment, cells were resuspended in HPMK and centrifuged at 300 x *g* for 5 min at room temperature (RT, 20 - 25 ºC). The cell pellet was resuspended in HPMK and inoculated into culture flasks, at a cell concentration of 3.5 x 10^3 cell.cm^{-2}.

2.1.2 Spinner Flask Culture

hMSC were cultured in spinner flasks (Corning, New York, USA) equipped with flat blade impellers and using 0.12 L working volume. Cells were inoculated at 0.25 x 10^5 cell/mL (corresponding to 4300 cell/cm^2) in the spinner flasks containing 50% (v/v) of the working volume of Mesencult™-XF culture medium (STEMCELL™ Technologies, Vancouver, Canada) and Synthemax® II microcarriers (Corning, New York, USA) for a final culture concentration of 16 g/L. During the first 5 h hMSC were cultured under intermittent stirring

(On: 45 rpm for 1 min; Off: 0 rpm for 20 min) in a magnetic stirrer plate (2mag AG, München, Germany). After this period, working volume was increased up to 0.12 L, and agitation set to continuous at 45 rpm. At day 5, 50% (v/v) of the culture medium was exchanged. Cells were expanded at 37 ºC in a humidified atmosphere of 5% CO_2 in air.

Cell detachment from the microcarriers: Stirring was stopped for 20 min letting the microcarriers settle. Medium was aspirated, and 100% (v/v) of the culture volume of DPBS was used to wash cells attached to the microcarriers. A similar strategy to that reported by Nienow et al (Nienow et al., 2016; 2014) was then used for cell detachment: after DPBS removal, hMSC were incubated with 50% (v/v) of culture volume of TrypLE™ Select (1X) at 150 rpm (corresponding to 13 W/m^3) for 12 (BM-MSC) or 6 min (AT-MSC) (similar to static culture conditions), followed by a final pulse of 200 rpm (corresponding to 32 W/m^3) during 5 sec. Cell detachment was monitored by FDA-PI staining. After reaching 90 - 95% cell detachment, the remaining 50% (v/v) of fresh medium was added to the cell suspension.

2.1.3 2 L Disposable Stirred-tank Bioreactors Culture

hMSC were cultured in 2 L UniVessel® SU bioreactor (Sartorius Stedim Biotech, Göttingen, Germany), under defined conditions (working volume: 2 L; pH: 7.2; temperature: 37 ºC; pO2: 20% air saturation (corresponding to 4% dissolved oxygen); surface aeration rate: 0.1 vvm) using Sartorius Stedim Biotech Data Acquisition software. hMSC were inoculated at 0.25x105 cell/mL on the biroeactor containing 1 L of Mesencult™-XF culture media and Synthemax® II microcarriers for a final culture concentration of 16 g/L. During the first 5 h hMSC were cultured under intermittent stirring (On: 100 rpm for 1 min; Off: 0 rpm for 20 min) (Chapter IV). After this period, working volume was increased up to 2 L and agitation set to continuous at 100 rpm. At day 5, 50% (v/v) of the culture medium was exchanged. The stirring rate used in UniVessel® SU bioreactor (100 rpm) was selected from previous data obtained by Schirmaier and co-workers (Schirmaier et al., 2014), having as scale-up criteria the minimum agitation required for full suspension of the microcarriers (NS1).

Parallel to the bioreactor culture, static expansion was performed as previously performed in Chapter IV, using an inoculum cell concentration of 4300 cell/cm^2. Culture was performed in tissue culture flasks, previously coated with MesenCult™-SF Attachment Substrate (STEMCELL™ Technologies). Cells were expanded at 37 ºC in a humidified atmosphere of 5% CO_2 in air.

Cell detachment from the microcarriers: In all bioreactor cultures, cells were harvested at day 7. Cell detachment was performed as explained in section 2.1.2. By maintaining the transferred energy from the impeller to the liquid, the stirring rates used in the bioreactor were estimated according to Equation 1 (Kadic and Heindel, 2014):

$$P_1 = P_2 \Leftrightarrow \left(\frac{N_p \rho N^3 D_i^5}{V}\right)_1 = \left(\frac{N_p \rho N^3 D_i^5}{V}\right)_2 \Leftrightarrow N_2 = \sqrt[3]{\left(\frac{N_p \rho N^3 D_i^5}{V}\right)_1 \left(\frac{V}{N_p \rho D_i^5}\right)_2} \quad \text{(Eq. 1)}$$

where P corresponds to the power transferred by the impeller *per* volume [W/m^3] (13 and 32 W/m^3, as indicated in section 2.1.2), N_p to the impeller's power number (1 and 1.2, for the spinner and bioreactor, respectively), ρ to the liquid's volumetric mass density [kg/m^3], N to the agitation rate [s^{-1}], D_i to the impeller's diameter [m] (0.04 and 0.054 m, for the spinner and bioreactor, respectively), and V to the volume of liquid [m^3].

Cells were incubated with TrypLE™ Select (1X) at 174 rpm for 12 min (BM-MSC) or 6 min (AT-MSC), followed by a final pulse of 231 rpm during 5 sec. The protocol was repeated twice to ensure efficient AT-MSC cell detachment.

After harvesting, microcarriers were removed from the cell bulk suspension using sterile OptiCap® XL 1 Capsules (Merck, Massachusetts, USA) with 75 µm pore size at 0.3 L.min^{-1}, as previously performed in Chapter II.

2.2 Downstream processing

2.2.1 Volume Reduction

The clarified cell suspension was concentrated by TFF using process parameters and methodologies optimized in Chapters II and IV: shear rate (3000 s^{-1}), permeate flux (250 L.m^{-2}.h^{-1}, LMH), initial cell concentration (2 x 10^5 cell.mL^{-1}), load (1.8 x 10^6 cell.cm^{-2}), and pore size (> 0.45 µm). To conduct the small scale experiments, HF with 24 cm^2 (GE Healthcare Life Sciences, New Jersey, USA) and FSC with 50 cm^2 (Merck) were used. For the scale-up experiments, HF with 120 cm^2 (GE Healthcare Life Sciences) and Sartocon® Slice 200 cassette with 200 cm^2 (Sartorius Stedim Biotech) were used. Characteristics of each device are present on Table 5.1.

All experiments were performed at a constant inlet flux. For HF (24 and 120 cm^2) experiments, an inlet and permeate fluxes of 750 LMH and 250 LMH, respectively, were used (Chapter II). The permeate flux was adjusted to 200 LMH during the HF (120 cm^2) experiment. For FSC (50 cm^2) experiment, an inlet flux of 480 LMH was used based on the manufacturer's instructions; regarding the permeate flux, a TMP excursion was performed and 110 LMH was

found to be the maximal flux without observing a TMP increase. In FSC (200 cm^2) experiments, a similar inlet flux was used (480 LMH). Similarly to the HF experiment, the permeate flux was either maintained at 110 LMH (BM-MSC) or decreased to 84 LMH (AT-MSC) to minimize fouling and maximize the cell recovery yield.

Table 5.1 – Specifications of the hollow fiber (HF) and flat sheet cassette (FSC) devices used for the volume reduction unit operation.

Device	Surface area (cm^2)	Pore size (µm)	Membrane material
HF_{24}	24	0.65	Polysulfone
HF_{120}	120	0.65	
FSC_{50}	50	0.65	PVDF
FSC_{200}	200	0.45	Hydrosart®

2.3 Cell viability and characterization assays

2.3.1 Cell viability and characterization assays

All reagents used to perform cell characterization assays were purchased from Sigma-Aldrich® (Merck) unless stated otherwise.

2.3.1 Cell number and viability

Cell viability and cell membrane integrity were assessed using three different methods:

2.3.1.1 Trypan Blue exclusion method

Cell concentration was estimated through cell counting using a Fuchs–Rosenthal counting chamber (Marienfeld Superior, Lauda-Königshofen, Germany). The number of viable cells was determined by the trypan blue dye exclusion method (Strober, 2015).

The cell recovery yield (in percentage) was estimated taking into account the number of viable cells before (considered 100%) and after processing.

The volumetric productivity was estimated following Equation 2:

$$Volumetric\ Productivity = \frac{(Xf - Xi)}{V\ t} \text{ (Eq. 2)}$$

where Xf and Xi correspond to the number of final and initial cells [10^6 cells], respectively, V to the total culture volume [L] and t to the culture time [day].

The efficiency index was estimated following Equation 3:

$$Efficiency\ index = \frac{(Xf - Xi)}{V_S} \text{ (Eq. 3)}$$

where Xf and Xi correspond to the number of final and initial cells [10^6 cells], respectively, and V_S to the spent culture media *per* experiment [L].

2.3.1.2 Fluorescein diacetate-propidium iodide (FDA-PI) staining

Quantitative assessment of the cell plasma membrane integrity was also performed using fluorescein diacetate (FDA), and the DNA-dye propidium iodide (PI), as described in the literature (Jones and Senft, 1985). Briefly, cell suspensions were incubated with 20 µg/mL FDA and 10 µg/mL PI in DPBS for 5 min and analyzed by flow cytometry in a CyFlow® instrument (CyFlow® space, Partec GmbH, Münster, Germany). At least ten thousand events were registered *per* sample.

2.3.1.3 Lactate Dehydrogenase (LDH) Assay

The release of intracellular lactate dehydrogenase enzyme (LDH) into the supernatant can be correlated with the extent of cell lysis (Fotakis and Timbrell, 2006). Hence, LDH activity in cells' supernatant was determined by monitoring at 340 nm the oxidation rate of NADH to NAD^+ coupled with the reduction of pyruvate to lactate, as previously described in the literature (Vassault, 1983). Cell lysis was quantified by performing a calibration curve with known cell amounts.

2.3.2 Apoptosis and metabolic activity assay

Apoptotic cells and the mitochondrial membrane potential was evaluated using Apoptosis Assay Kit NucView™ 488 and MitoView™ 633 (Biotium, Inc., California, USA), following the manufacturer's instructions. After incubation with both reagents, cells were analyzed by flow cytometry (CyFlow® space). At least ten thousand events were registered *per* sample.

The percentage of metabolically active cells was also evaluated using PrestoBlue (ThermoFisher Scientific™), according to the manufacturer's recommendations in an infinite® 200 PRO series instrument (Tecan Group Ltd., Männedorf, Switzerland). Metabolic activity was estimated based on fluorescence units normalized by the cell number.

2.3.3 hMSC adhesion and growth profile

hMSC were inoculated and expanded in static culture conditions, in 24-well plates as described in section 2.1 (Section Cell Culture). Cells' growth profile was monitored for 7-12

days. Cell concentration and viability were determined as previously described in section 2.2.1.1 (Section Cell number and viability, Trypan Blue exclusion method). To evaluate cells' adhesion properties, the number of adherent cells was monitored 60 min after inoculation.

2.3.4 Metabolite analysis

Glucose (GLC) lactate (LAC) and glutamine (GLN) concentrations in the culture medium were analyzed using YSI 7100MBS instrument (YSI Incorporated, Ohio, USA). Ammonia was quantified by an enzymatic assay using a commercially available kit (NZYTech, Lisboa, Portugal). Specific metabolic rates (q_{MET}, expressed in $\mu mol.h^{-1}.10^6\ cell^{-1}$), as well as the apparent yields of lactate from glucose ($Y_{LAC/GLC}$) and oxygen from glucose ($Y_{O2/GLC}$) were determined as described in the literature (Serra et al., 2010; Tostões et al., 2011).

2.3.5 Expression of cell surface markers

hMSC were washed once with DPBS and a total of 2 x 10^5 cells were incubated with each of the antibodies - CD166-PE, CD105-PE, CD90-PE, CD73-PE, CD44-PE, CD45-PE, CD34-PE, CD19-PE, CD14-PE, CD11b-PE, HLA-DR-PE and isotype controls IgG_1,κ-PE, IgG_{2a},κ-PE and IgG_{2b},κ-PE (all from BD Biosciences, California, USA except CD14-PE which was purchased to Beckman Coulter, California, USA) - for 1 h at 4 °C. Cells were washed twice in DPBS, and analyzed in a CyFlow® instrument. At least ten thousand events were registered *per* sample.

2.3.6 Cell morphology

hMSC were inoculated in static culture conditions, in 24-well-plates, as described in section 2.1 (Cell Culture). After 24 h, cells' morphology was analyzed as previously performed in Chapter IV. Cells were visualized using inverted (Leica Microsystems GmbH, Wetzlar, Germany) fluorescence microscopy. Representative images were taken using a digital camera (Leica DFC 360 FX).

The primary antibodies used were Phalloidin Alexa Fluor® 488 (ThermoFisher™ Scientific) and Anti-α-Tubulin. Anti-α-Tubulin was conjugated with secondary antibody Alexa Fluor® 594 Goat Anti-Mouse Antibody (ThermoFisher™ Scientific).

2.3.7 *In vitro* multipotency assays

hMSC multilineage differentiation assays were performed using StemMACS™ AdipoDiff (Miltenyi Biotec, Germany), StemMACS™ OsteoDiff (Miltenyi Biotec, Germany) and

StemPro® Chondrogenesis (ThermoFisher™ Scientific) differentiation kits, as previously performed in Chapter II.

2.3.8 Proteome analysis: SWATH-MS

Mass spectrometry (MS) data was obtained by UniMS – Mass Spectrometry Unit, ITQB-NOVA/iBET, Oeiras, Portugal.

2.3.8.1 Sample preparation

After upstream processing (USP) and DSP, BM-MSC and AT-MSC ($1x10^6$) were washed twice with DPBS and centrifuged. Supernatants were discarded and cell pellets instantly frozen in N_2 and kept at -80 ºC until further analysis. After thawing, proteins were extracted by resuspending the pellets in 100 µL of lysis buffer [50 mM Tris (pH 7.4); 5 mM EDTA; 150 mM NaCl; 1% (v/v) Triton X-100] supplemented with protease's inhibitors, and incubated at 4 ºC for 30 min. Cells were then passed 30 times through a 301/2 gauge needle at 4 ºC. Samples were centrifuged at 15000x*g* for 15 min at 4 ºC. The supernatant was collected and quantified by Microplate BCA Protein Assay Kit (ThermoFisher™ Scientific). Protein samples were reduced and alkylated with 10 mM of DTT (40 min at 56 ºC) and with 20 mM iodoacetamide (IAA, 30 min at 20 ºC in the dark), respectively, and digested with trypsin overnight at 37 ºC (trypsin:sample = 1:50). A second digestion step was also performed, adding trypsin 80% (v/v) in acetonitrile (trypsin:sample = 1:100) for 3 h at 37 ºC.

2.3.8.2 Generation of the spectral reference library

Three µg of each sample were used for information-dependent acquisition (IDA) analysis by NanoLC-MS using TripleTOF 6600 (ABSciex, Framingham, MA, USA). A reversed phase nanoLC with a trap and elution configuration, using a Nano cHiPLC Trap column (200 µm × 0.5 mm ChromXP C18-CL 3 µm 120 Å) and nano column (75 µm × 15 cm ChromXP C18-CL 3 µm 120 Å) was performed. Water with 0.1% (v/v) formic acid (solvent A) and acetonitrile with 0.1% (v/v) formic acid (solvent B) were used. Sample was loaded in the trap column at a flow rate of 2 µL.min^{-1} for 10 min using 100% (v/v) solvent A. Peptide separation was performed in the nano column at a flow rate of 300 µL.min^{-1} applying a 90 min linear gradient of 5% to 30% (v/v) of solvent B.

Protein samples were subjected to two IDA runs. The mass spectrometer was set for IDA scanning full spectra (400–2000 m/z) for 250 ms. The top 40 ions were selected for subsequent

MS/MS scans (150−1800 m/z for 50 ms each) using a total cycle time of 2.3 s. The selection criteria for parent ions included a charge state between +2 and +5, and counts above a minimum threshold of 125 counts *per* second. Ions were excluded from further MS/MS analysis for 12 s. Fragmentation was performed using rolling collision energy with a collision energy spread of 5.

The spectral library was created by combining all IDA raw files (12 runs in total) using ProteinPilot™ software (v5.0 ABSciex) with the Paragon algorithm and with the following search parameters: search against *Homo sapiens* from Uniprot/SwissProt database (release 2015_05); trypsin digestion; iodoacetamide cysteine alkylation; through identification efforts. After a false discovery rate (FDR) analysis, only FDR<1% were considered (3693 proteins). The output of these searches, in the form of a group file, was used as the reference spectral library.

2.3.8.3 SWATH-MS analysis and targeted data extraction

For quantitative analysis, 3 µg of each sample were subjected to four SWATH - Sequential Windowed data independent Acquisitions of the Total High-resolution Mass Spectra. Similar chromatographic conditions to the previously described IDA run were used. The mass spectrometer was operated in a cyclic product ion data independent acquisition (DIA). A variable windows calculator (AB SCIEX) and SWATH acquisition method editor (AB SCIEX) were used to setup the SWATH acquisition. A set of 32 overlapping windows (containing 1 m/z for the window overlap) was constructed, covering the precursor mass range of 400 − 1200 m/z. A 50 ms survey scan was acquired at the beginning of each cycle, and SWATH MS/MS spectra were collected for 96 ms resulting in a cycle time of 3.172 s. Rolling collision energy with a collision energy spread of 15 was used.

The spectral alignment and targeted data extraction of DIA samples were performed using PeakView v.2.1 (AB SCIEX; Framingham, US) with the reference spectral library. For data extraction the following parameters were used: five peptides/protein, five transitions/peptide, peptide confidence level of >95%, FDR threshold of 1%, excluded shared peptides, and extracted ion chromatogram (XIC) window of 6 min and width set at 20 ppm. A total of 3417 proteins were quantified under these conditions.

2.4 Statistical Analysis

Statistical analyses were performed using GraphPad Prism version 7 (GraphPad Software Inc., California, USA): two biological replicates (n=2) from expansion and DSP of BM-MSC and a validation experiment with AT-MSC (n=1) are represented as mean ± standard deviation

of independent technical measurements or assays. $P<0.05$ were considered as statistically significant and are marked as *.

To analyze expansion (section 3.1) and DSP (section 3.2.1) data, Mann Whitney test was performed using 3 different measurements. Differences in fold increase between samples before and after processing (n=3) were also analyzed by Mann-Whitney test. For MS data analysis (section 3.2.1), principal components analysis (PCA) was performed (using PeakView v.2.1) to study the data's structure. To identify differently expressed proteins between BM-MSC after expansion and after DSP, a t-test analysis was conducted; all proteins with a fold change higher than 1.5 in relative abundance and a $P<0.05$ were considered to be differentially expressed (data not shown). For each sample, at least 3 technical replicates were considered.

3. Results

3.1 Scale-up of hMSC's expansion in single-use bioreactors

In this work, we developed an integrated bioprocess to produce BM-MSC and AT-MSC in single-use bioreactors (2 L) aiming at scaling-up hMSC's expansion under cGMP compatible conditions, using synthetic microcarriers and xeno-free culture medium, ensuring the manufacturing of enough cells to scale-up of the volume reduction step (section 3.2). Stirring speed was chosen as the minimal value to fully suspend the microcarrier culture in the 2 L SU bioreactor (NS1, 100 rpm), as previously reported by Schirmaier et al (Schirmaier et al., 2014).

In all bioreactor cultures, high cell attachment efficiencies and microcarrier colonization (> 85%) after 5 h of inoculation were attained for BM and AT-MSC. Higher cell concentrations ($3.4x10^5$ cell/mL and $4.1x10^5$ cell/mL), expansion ratios (14 and 16) and maximum growth rates (0.016 and 0.018 h^{-1}) were obtained when hMSC (BM-MSC and AT-MSC, respectively) were expanded in bioreactor (*vs* static and spinner cultures, Table 5.2, Figure 5.1A); a 3-fold improvement on volumetric productivity, reaching 50 x 10^6 cells.L^{-1}.day^{-1}, was observed comparing to spinner flasks or static culture (*vs* 18 x 10^6 cells.L^{-1}.day^{-1}, Figure 5.1B).

Furthermore, stirred cultures (spinner and bioreactor) achieved higher cell numbers *per* spent media (Table 5.2) than static cultures, the highest efficiency index for BM-MSC and AT-MSC being observed with the bioreactor system (211 and 253 x 10^6 cell.L^{-1}, respectively).

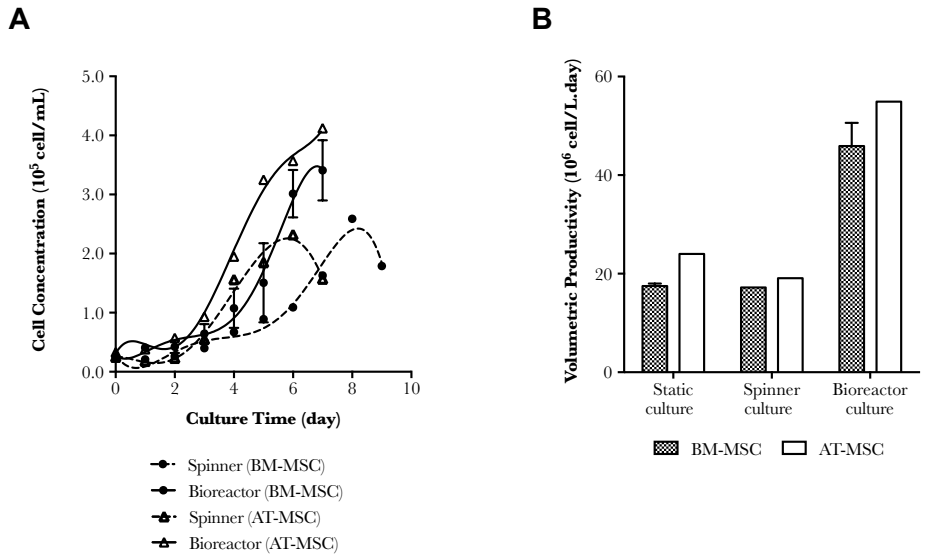

C

	q_{GLC} (µmol/10^6 cell h)	q_{LAC} (µmol/10^6 cell h)	q_{O2} (µmol/10^6 cell h)	$Y_{LAC/GLC}$ (mol_{LAC}/mol_{GLC})	$Y_{O2/GLC}$ (mol_{O2}/mol_{GLC})
BM-MSC#1	0.22 ± 0.10	0.40 ± 0.18	0.27 ± 0.08	1.82 ± 0.67	1.24 ± 0.56
BM-MSC#2	0.28 ± 0.14	0.48 ± 0.22	0.12 ± 0.03	1.75 ± 0.69	0.43 ± 0.57
AT-MSC	0.20 ± 0.16	0.28 ± 0.20	0.48 ± 0.09	1.39 ± 1.06	2.40 ± 0.81

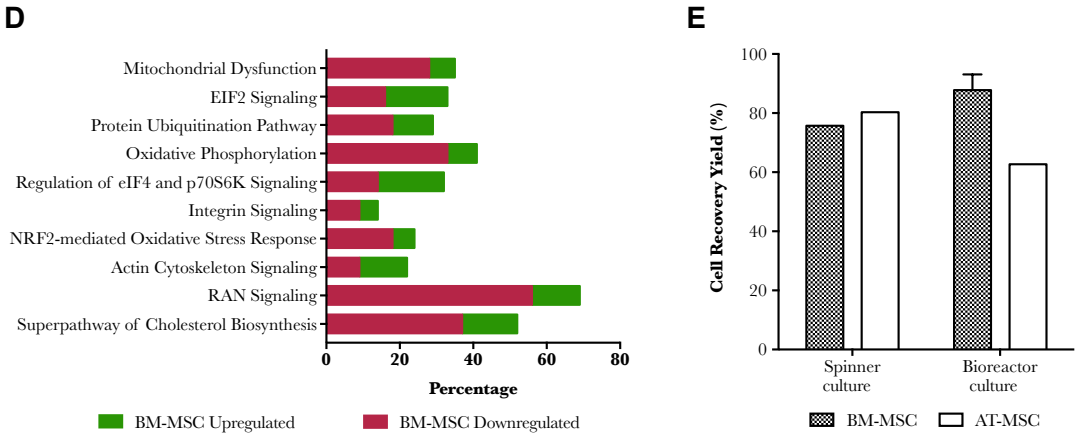

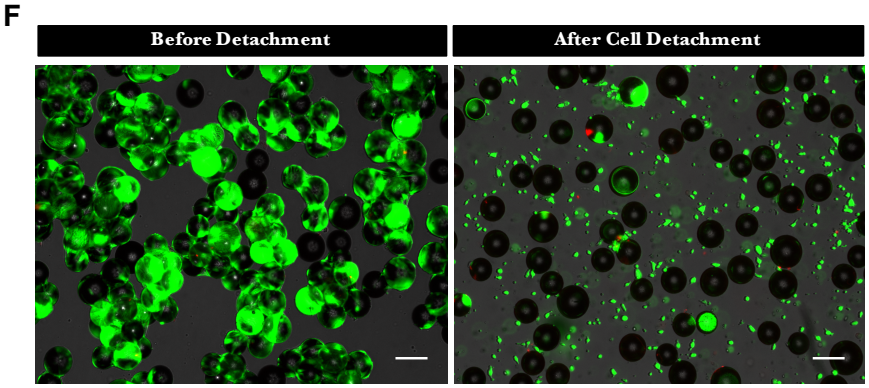

Figure 5.1 – BM-MSC and AT-MSC expansion on synthetic microcarriers using single-use stirred-tank bioreactors (BR) in xeno-free culture medium. (A) BM-MSC and AT-MSC cell concentration profile in spinner (0.12 L, dotted lines) and in bioreactor (2 L, full lines) cultures. (B) Volumetric productivity, i.e., million of BM- or AT-MSC produced per liter per day of culture on static and stirred (spinner

flasks or bioreactors) cultures. (C) $Y_{LAC/GLC}$, $Y_{O2/GLC}$ and specific rates of glucose and oxygen consumption and lactate production of BM and AT-MSC expanded in bioreactor cultures. Data shown for the exponential phase of cell growth (cultures days 2 – 7). (D) Top ten canonical pathways, ordered by ascending negative log of P-values, of upregulated (green) and downregulated (red) proteins of BM-MSC (comparing to AT-MSC) after expansion in bioreactor. Proteins with $P < 0.05$ and fold change > 1.5 were considered to be differently expressed. (E) Cell recovery yield of the cell detachment protocol performed in spinner flasks and in bioreactors. (F) Representative images of FDA (live, green) – PI (dead, red) stained cells (BM-MSC), before (left panel) and after (right panel) the detachment process performed in bioreactor. Scale bars: 200 μm.
Error bars represent the standard deviation of the average of 3 independent technical replicates between the analyzed biological replicates.

Measurements of glucose and glutamine confirmed that there was no depletion of these nutrients during the culture time (Supplementary Figure 5.1A, 5.1B) and the accumulation of lactate and ammonia was kept below growth-inhibitory concentrations (Schop et al., 2010) (Supplementary Figure 5.1C, 5.1D). BM-MSC and AT-MSC had similar specific consumption rate of glucose (Figure 5.1C), and production rate of lactate (Figure 5.1C). Nonetheless, AT-MSC culture demonstrated higher specific oxygen consumption during the exponential phase (e.g. 0.27 ± 0.08 *vs* 0.48 ± 0.09 μmol.10^6 cell^{-1}.h^{-1}, Figure 5.1C), leading to an increased oxygen-glucose ratio (Figure 5.1C), suggesting that AT-MSC diverted their metabolism towards oxidative phosphorylation. To support this, BM-MSC and AT-MSC's total proteome after expansion was analyzed (Figure 5.1D). Results suggested a downregulation of oxidative phosphorylation in BM-MSC compared to AT-MSC, which may corroborate the observed differences.

Table 5.2 – Growth, kinetic and productivity parameters calculated for BM-MSC and AT-MSC cultures on static and on stirred (spinner flask and bioreactor) systems.

Culture system	Expansion ratio (X_{max}/X_0)		Specific growth rate (μ, h^{-1})		Efficiency index (10^6 cell/L)	
	BM-MSC	AT-MSC	BM-MSC	AT-MSC	BM-MSC	AT-MSC
Static	5.9 ± 0.0	7.8	-	-	91 ± 0	125
Spinner	10.4	9.3	0.016	0.016	156	138
Bioreactor	13.6 ± 0.5	12.7	0.015 ± 0.002	0.018	211 ± 23	253

To promote cell detachment, a short period of intense agitation in the presence of a detaching reagent was applied. The scale-up of the harvesting step from the spinner flask to the bioreactor kept constant the transferred energy from the impeller to the liquid. Similar cell recovery yields could be achieved (>78%) for BM-MSC (Figure 5.1E), maintaining high cell viability (>90%, Figure 1F) in spinner flasks and in bioreactor. However, for AT-MSC, even after repeating the detachment cycle twice, only 63% of cells could be recovered (Figure 5.1E).

After harvesting the cell bulk from the bioreactor, microcarriers were removed by dead-end filtration (Chapter II). More than 95% of viable BM and AT-MSC were recovered after the clarification step and no microcarriers were observed after filtration.

Overall, scaling-up the expansion and harvesting steps did not affect hMSC's CQA (Figure 5.2): no differences could be observed compared to static expansion in hMSC's viability (> 95%), plastic adhesion ability, metabolic activity, proliferation, and apoptosis (Figure 5.2A, 5.2B). The expression of the characteristic hMSC's surface receptors (Dominici et al., 2006), remained essentially unaltered after processing (Figure 5.2C, 5.2D). More specifically, BM-MSC lacked the expression of CD45, CD34, CD14, CD19 and CD11b, while more than 95% of hMSC population expressed CD44, CD73, CD90 and CD166. However, under all evaluated conditions (including static expansion), less than 95% of hMSC expressed CD105 (88 and 92% for BM and AT-MSC, respectively). USP did not impact cell morphology: after plating, hMSC presented their typical spindle-like morphology (Figure 5.3), with organized intracellular f-actin and expressing α-tubulin and vimentin. hMSC also maintained their multipotent differentiation capacity, differentiating into adipocytes, osteocytes and chondrocytes (Figure 5.2E). No spontaneous differentiation was ever observed (data not shown).

3.2 Scale-up of TFF process for the concentration of hMSC

3.2.1 Comparison of hollow fiber (HF) and flat sheet cassette (FSC) devices

Scalability studies regarding the volume reduction step were performed aiming to maximize product recovery without compromising cells' CQA. Given their different geometries and characteristics (Table 5.1), two types of TFF devices (HF and FSC) were compared; BM-MSC were used first identifying the most suitable device at two different scales (Figure 5.4), then AT-MSC were used for the validation of the process scale-up (Figure 5.5). The lower scale experiments were carried out maintaining parameters previously optimized in this thesis of initial cell concentration, load (cell/cm^2) and permeate flux (Chapter II). The recirculation flow rate (and therefore shear rate) was based on the membrane manufacturer's recommendations (FSC) or in results from Chapter II (HF) to maximize product recovery and quality. The scale-up was conducted by increasing the filtration area, maintaining the load, inlet and permeate fluxes constant.

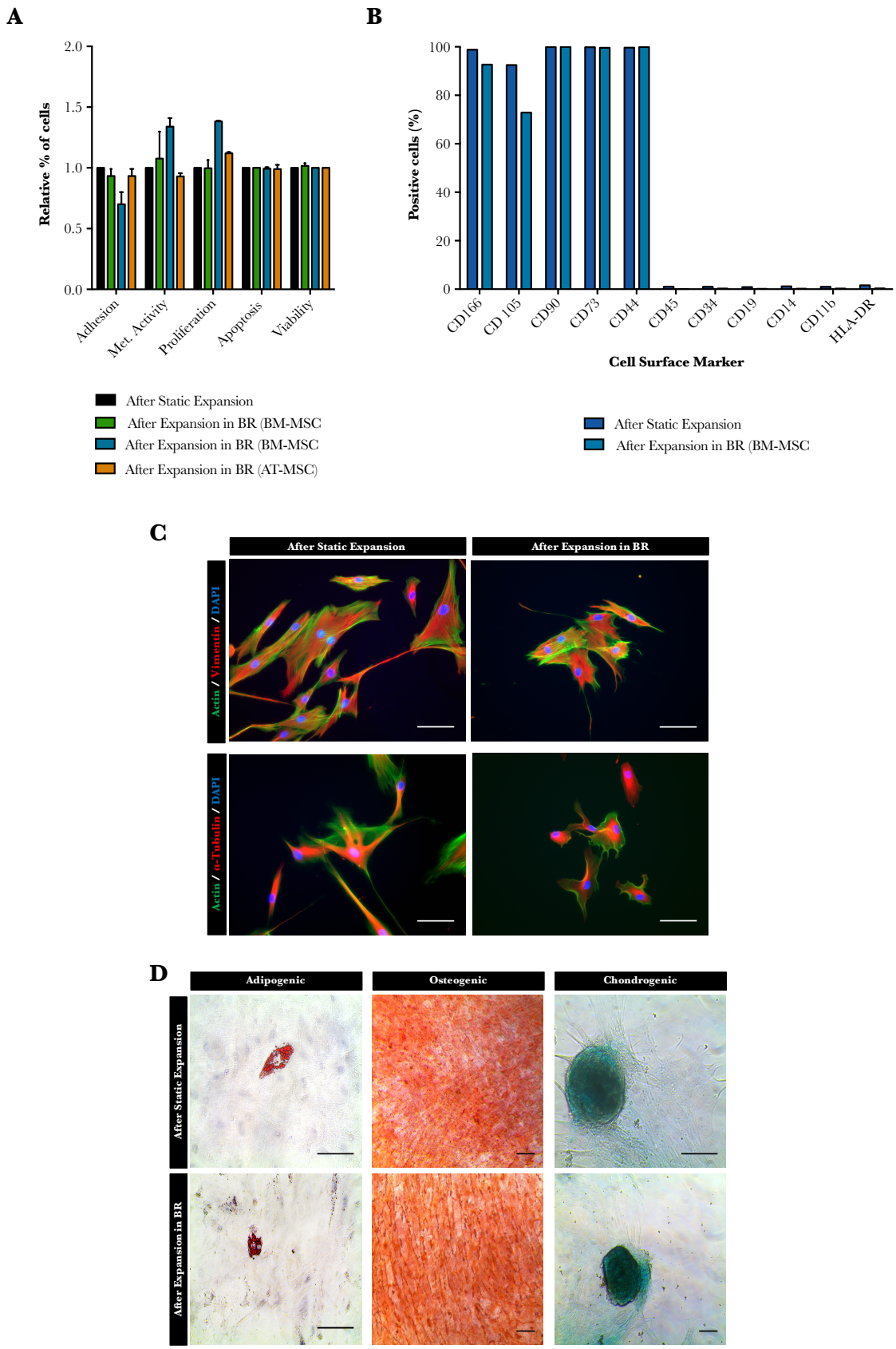

Figure 5.2 – BM-MSC and AT-MSC characterization after expansion in static conditions and in stirred-tank bioreactors (BR). (A-B) Cell adhesion, metabolic activity, cell proliferation, cell apoptosis and cell viability at the last day of BM-MSC (A) and AT-MSC (B) culture after detachment from the microcarriers. Each bar represents the fold-increase/decrease with standard deviation of 3 independent technical replicates,

relative to cells after expansion in static conditions. No significant differences were observed ($P > 0.05$). (C-D) Expression of cell-surface antigens of BM-MSC (C) and AT-MSC (D). (E) Multipotent differentiation potential of BM-MSC (top) and AT-MSC (bottom). Red-oil solution stained lipid droplets (adipocytes, left panel), alizarin red stained calcium deposits (osteoblasts, central panel), and alcian blue stained extracellular matrix proteins (chondrocytes, right panel). Scale bars: 100 µm.

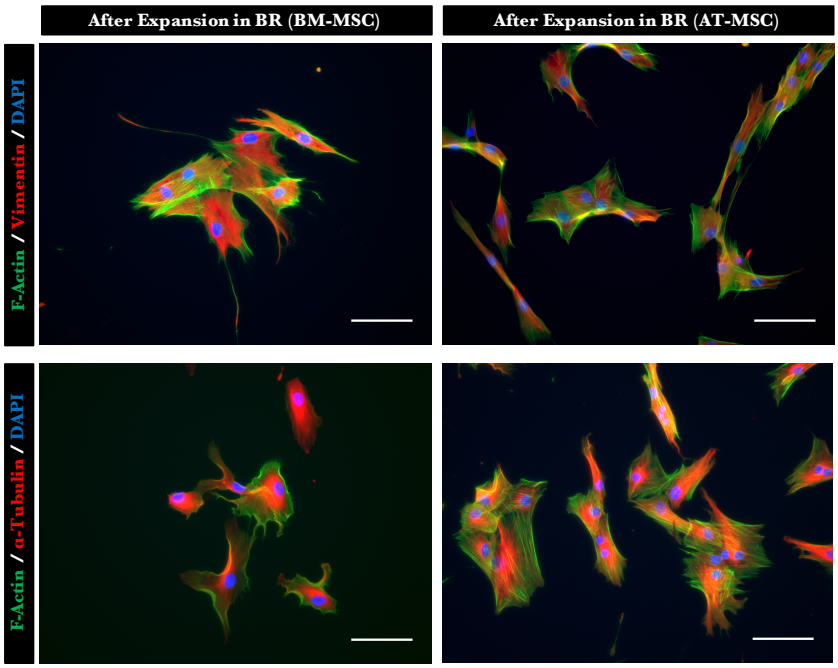

Figure 5.3 – Characterization of BM-MSC and AT-MSC expanded in single-use bioreactors. BM-MSC and AT-MSC morphology after expansion in stirred conditions - immunofluorescence staining of f-actin (green), α-tubulin (red), vimentin (red) and cell nuclei (blue). Scale bars: 100 µm.

Using HF and FSC (Figure 5.4A, 5.4B), results showed that cell recovery yield decreased throughout the concentration process, irrespectively of working scale. For the HF, upon scale-up, around 60% (*vs* 80%) of cells could be recovered after a VRF of 20 (Figure 5.4A), while an increase in the transmembrane pressure (TMP) was observed, needing an adjustment of the permeate flux from 250 to 200 LMH during the experiment. Such clogging phenomena decreased the membrane's permeability after the cleaning in place (CIP) (22%, Figure 5.4C) and may explain the observed differences. In order to maintain the load constant under all conditions, given the system's hold up volume, only a VRF of 20 was accomplished for lower scale experiments (Figure 5.4A). Conversely, when FSC were used more than 80% of viable cells were recovered after processing (Table 5.3 and Figure 5.5B) at both scales. The higher membrane permeability observed in comparison to HF (Figure 4C) may explain the increased cell recovery yield.

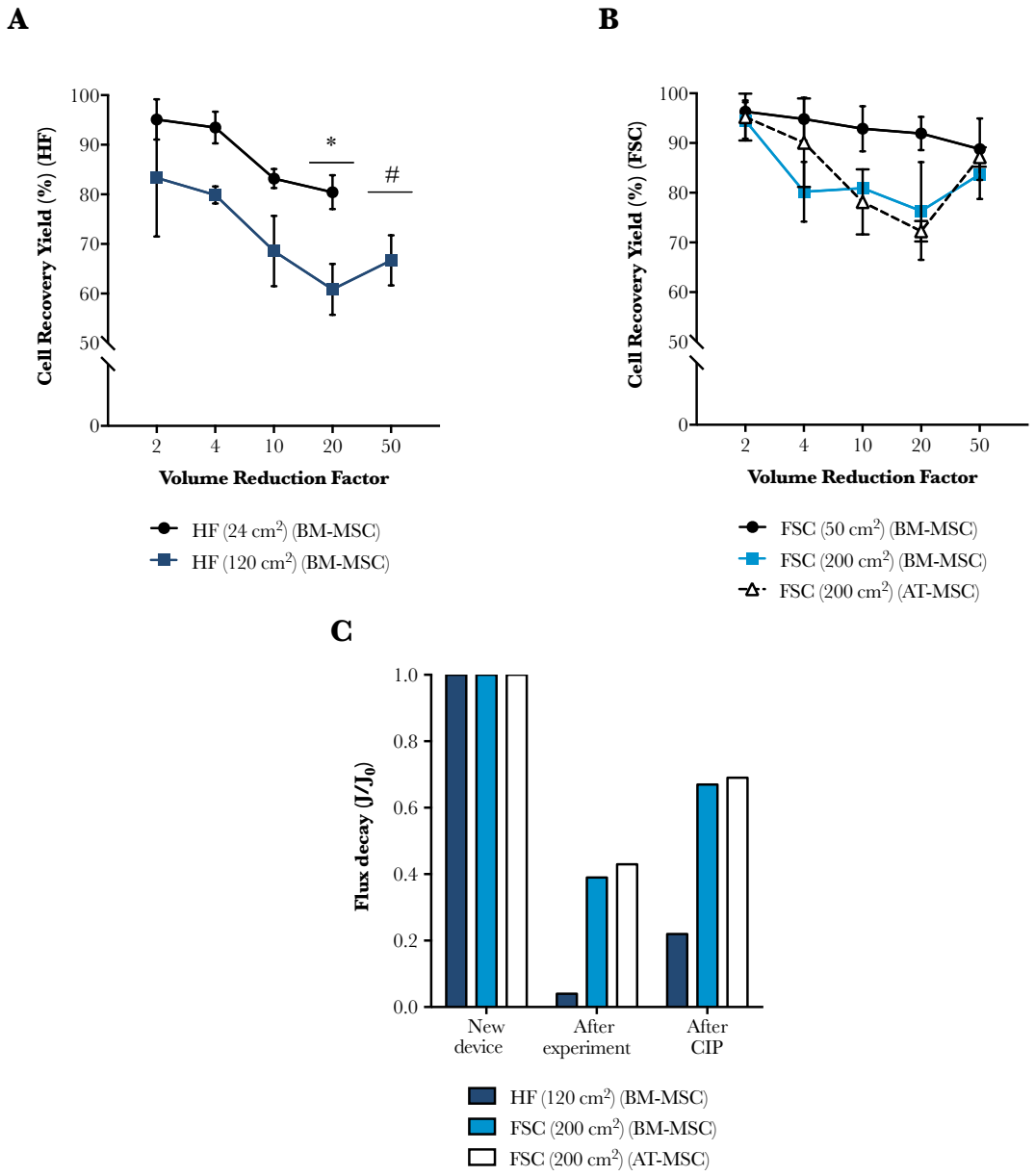

Figure 5.4 – Volume reduction step of BM-MSC and AT-MSC using hollow fibers (HF) and flat sheet cassette (FSC) devices. (A) BM-MSC recovery yield throughout the concentration process using HF in two different scales. For HF (24 cm^2) processing was conducted until the feed volume was close to the system's hold-up volume (VRF of 20). Values for VRF of 50 are not presented at this scale (#) due to this limitation. Statistically significant differences ($P < 0.05$) were observed for a VRF of 20. (B) Cell recovery yield of BM-MSC and AT-MSC throughout the concentration process using FSC in two different scales. No significant differences were observed at the end of both processes ($P > 0.05$). (C) Permeate flux decay after performing the experiments and after the cleaning in place (CIP). Flux decay was estimated regarding the initial value of permeability for each membrane (new device).
Error bars represent the standard deviation of 3 independent technical replicates.

Table 5.3 – Cell recovery yield, cell viability, cell lysis results and operational parameters for the scale-up experiments using flat sheet cassettes with BM-MSC and AT-MSC.

Process	Cell recovery yield (%)	Cell viability (%)	Cell lysis (%)	TMP (bar)	Permeate flux (LMH)	Time (min)
BM-MSC	84	98	13	0.22	110	50
AT-MSC	87	99	7	0.23	84	56

Upon scale-up of both devices (Figure 5.5A and 5.5B), FSC recovered on average 18% more cells (84 *vs* 66%) after a VRF of 50, corresponding to $8.4x10^6$ cell/mL, than HF. For both types of devices, cell loss was due to cell lysis, as validated by LDH assay (Table 5.3), since less than 5% of cells remain inside the devices after the concentration step (data not shown).

Since FSC allowed to recover more cells, only this device was used to concentrate AT-MSC. Comparing to BM-MSC, no significant differences in cell recovery yield ($P>0.05$) were observed (Figure 5.5B): more than 85% of cells were recovered after a VRF of 50 with high viability (> 98%, Table 5.3). To further increase the cell recovery yield, the permeate flux was adjusted from 110 to 84 LMH and a decrease in cell lysis (13 *vs* 7%, Table 5.3) was observed (*vs* FSC and BM-MSC). No differences were observed regarding membrane permeability (Figure 5.4C).

BM and AT-MSC's viability (> 98%, Figure 5.5A), identity and multilineage differentiation potential was not impacted by scale-up for either FSC (Figure 5.5A-5.5E) or HF (Figure 5.6). hMSC's ability in adhering to plastic surfaces was unaltered, as 84% of cells were adherent 60 min after plating (Figure 5.5A). hMSC also remained metabolically active (Figure 5.5A) and proliferative (Figure 5.5A), reaching a similar population doubling (PD = 3) after plating (data not shown). Similar to BM-MSC expanded in bioreactor, the expression of the surface receptors remained unaltered after processing (Figure 5.5B, 5.5C), morphology was unaffected (Figure 5.5D) and cells maintained their multipotent differentiation capacity (Figure 5.5E).

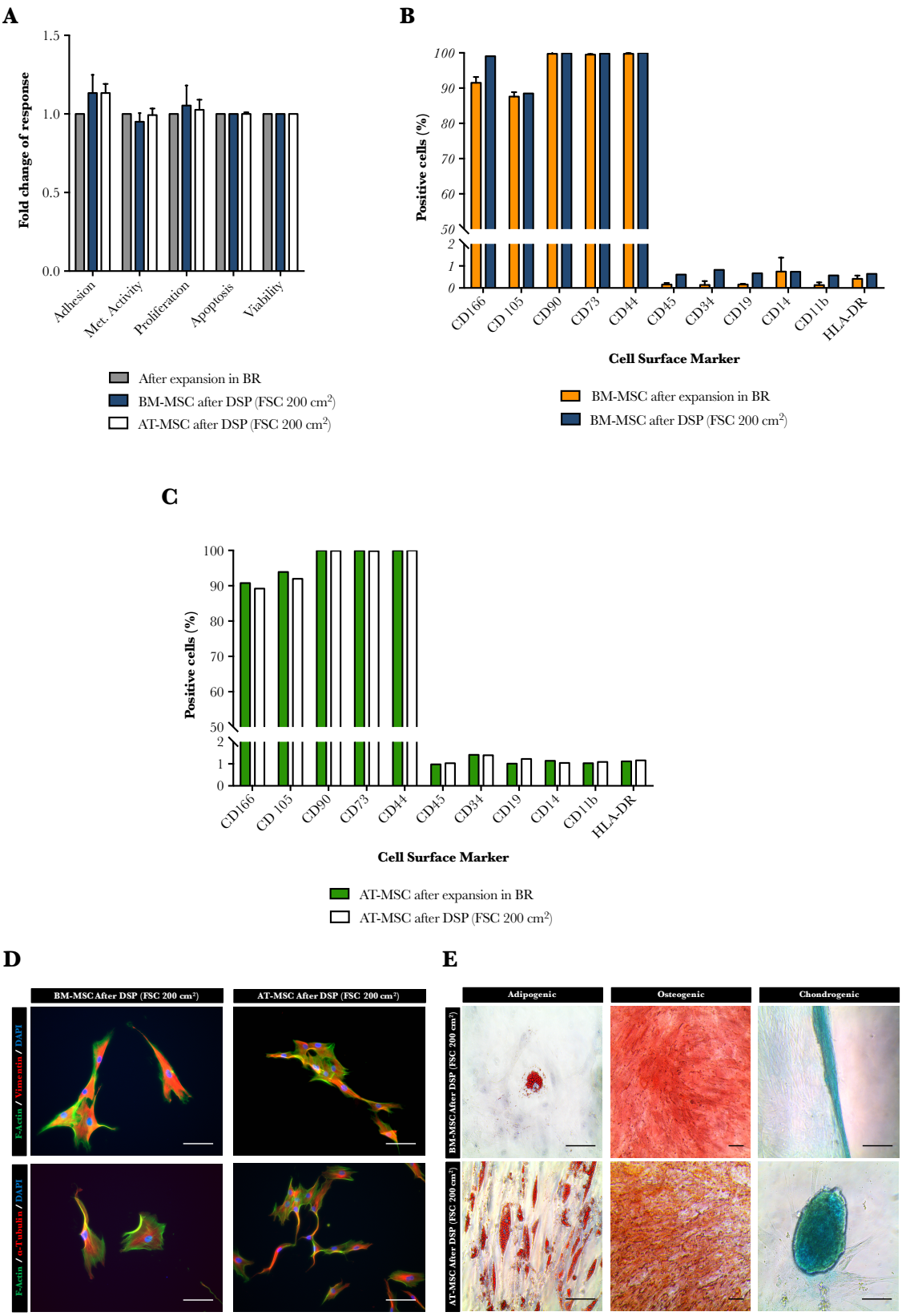

Figure 5.5 – BM-MSC and AT-MSC characterization after DSP scale-up using flat sheet cassette (FSC) devices. (A) Cell adhesion, metabolic activity, cell proliferation, cell apoptosis and cell viability of BM-MSC and AT-MSC. Each bar represents the fold-increase/decrease, relative to cells after expansion (before DSP). No significant differences were observed ($P > 0.05$). (B-C) Expression of cell-surface antigens after BM-MSC (B) and AT-MSC (C) expansion in BR and after DSP using FSC. (D) BM-MSC and AT-MSC morphology after DSP - immunofluorescence staining of f-actin (green), α-tubulin (red), vimentin (red) and cell nuclei (blue). Scale

bars: 100 µm. (E) Multipotent differentiation potential of BM-MSC and AT-MSC. Red-oil solution stained lipid droplets (adipocytes, left panel), alizarin red stained calcium deposits (osteoblasts, central panel), and alcian blue stained extracellular matrix proteins (chondrocytes, right panel). Scale bars: 100 µm.
Error bars represent the standard deviation of 3 independent technical replicates.

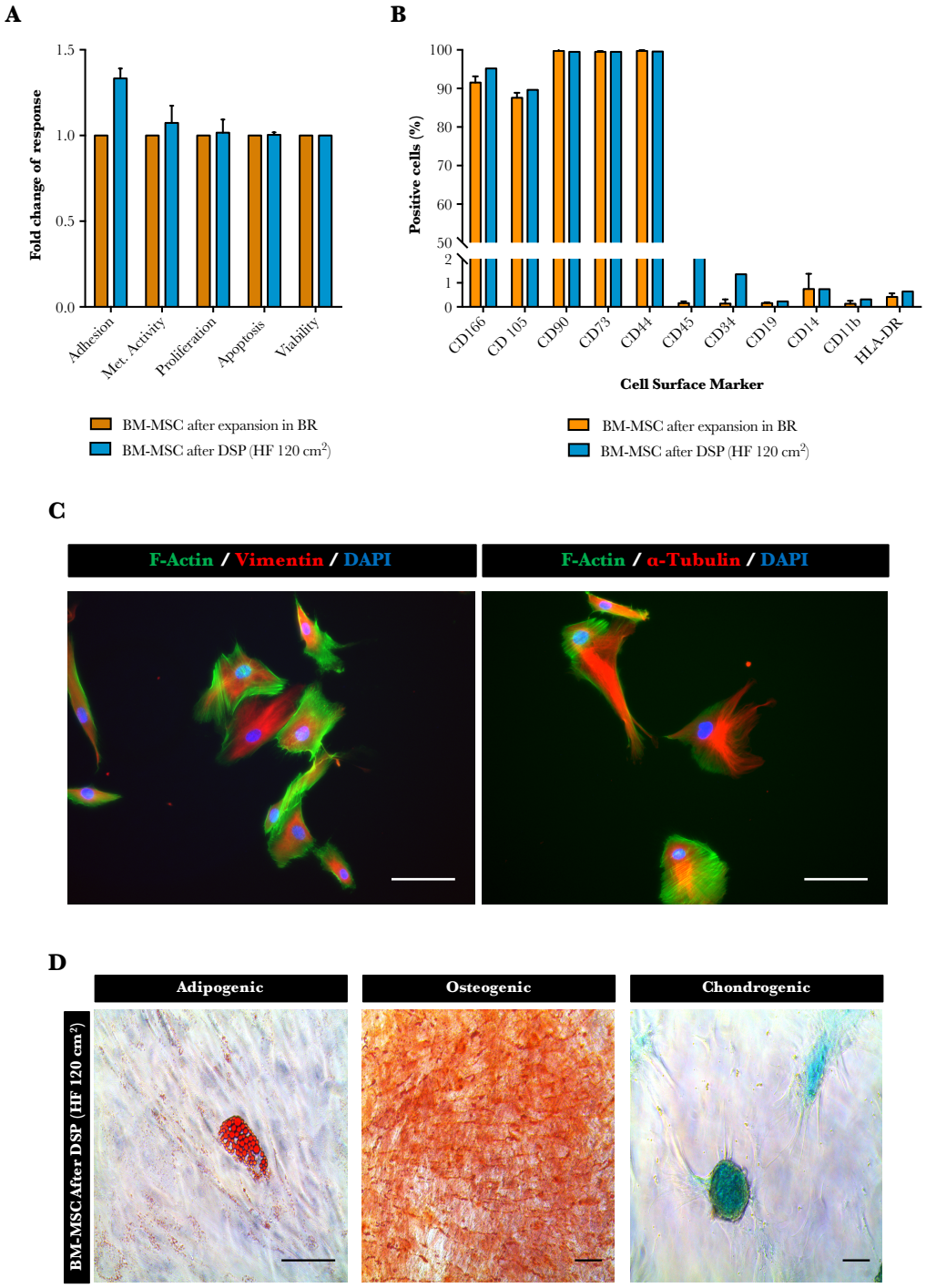

Figure 5.6 – BM-MSC characterization after DSP scale-up using hollow fiber (HF) devices. (A) Cell adhesion, metabolic activity, cell proliferation, cell apoptosis and cell viability of BM-MSC. Each bar represents the fold-increase/decrease, relative to cells after expansion (before DSP). No significant differences were observed ($P > 0.05$). (B) Expression of cell-surface antigens after BM-MSC expansion in BR and after DSP using HF. (C) BM-MSC morphology after DSP - immunofluorescence staining of f-actin (green), α-tubulin (red), vimentin (red) and cell nuclei (blue). Scale bars: 100 µm. (D) Multipotent differentiation potential of BM-MSC and AT-MSC. Red-oil solution stained lipid droplets (adipocytes, left panel), alizarin red stained calcium deposits

(osteoblasts, central panel), and alcian blue stained extracellular matrix proteins (chondrocytes, right panel). Scale bars: 100 μm.
Error bars represent the standard deviation of 3 independent technical replicates.

3.2.2 Impact of DSP in hMSC proteome dynamics

Alongside the standard quality assays presented in Figures 5.2 and 5.4, a SWATH-MS analysis was also performed assessing the impact of processing on hMSC's proteome dynamics (Figure 5.7). As stated in materials and methods section, an unsupervised analysis was conducted for data's structure (Figure 5.7A), followed by a supervised analysis to evaluate important variables (Figure 5.7B-5.7D).

First principal component analysis (PC1), accounting for the greatest amount of variance of the data (39.7%) was produced (Figure 5.5A), showing a division into two groups along PC1 — one corresponding to BM-MSC after expansion in bioreactor (positive PC1 score) and another group composed by BM-MSC after DSP and AT-MSC (after expansion and after DSP) (negative PC1 score). Some variance is also present as explained by PC2, apparently correlated with biological variance: BM-MSC after expansion #2 and its corresponding DSP (HF) have positive PC2 scores, whereas BM-MSC after expansion #1 and its DSP (FSC) have negative PC2 scores. No major differences were observed between AT-MSC after expansion and after DSP. Furthermore, noteworthy that AT-MSC data structure resembles more BM-MSC after DSP rather than after expansion (despite the different cell origin). Data was then analyzed according their PC1 scores – BM-MSC after expansion and BM-MSC after DSP.

All cell surface markers and structural proteins used in standard quality assays in Figures 2-6 were confirmed by the MS analysis (data not shown) for both hMSC in all conditions. Other cell surface markers described for hMSC but not analyzed by flow cytometry as CD276, CD99, CD59, CD82 (Al-Nbaheen et al., 2012), CD151 and CD81 (Lee et al., 2009), CD59 (Lin et al., 2003), could be identified (data not shown); several chemokines, growth factors (e.g. TIMP1, MIF, GAS6, GRN and FGF), and other molecules related with key cytokines of hMSC (e.g. prostaglandin-2, TGFβ and IGF) were also present (data not shown).

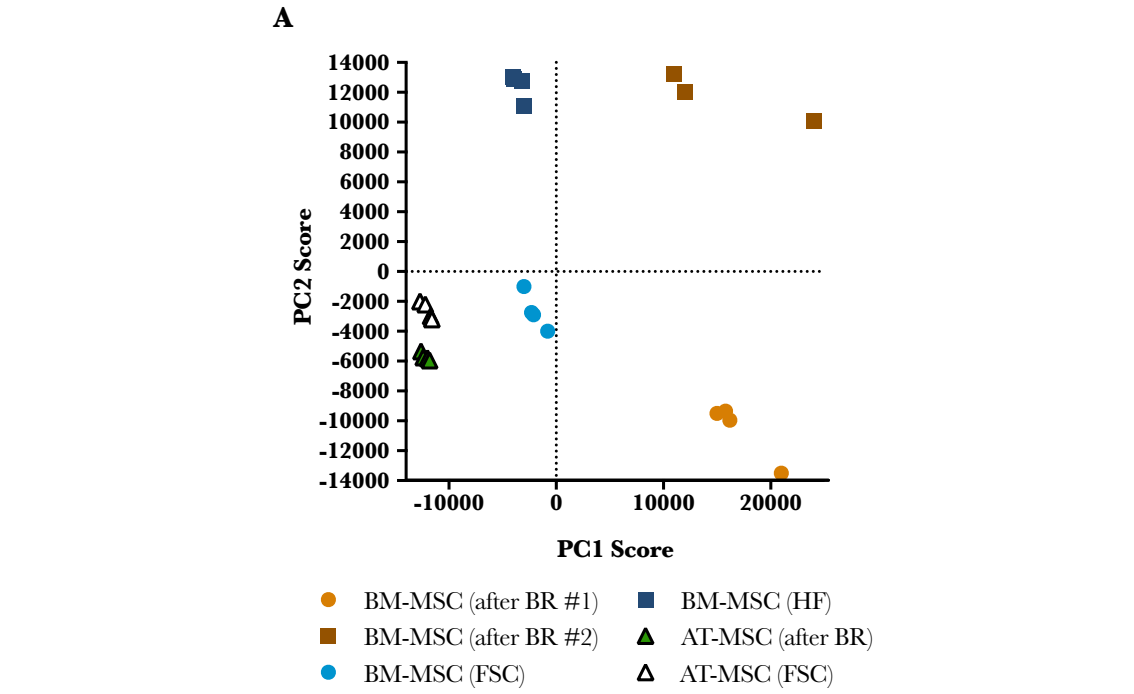

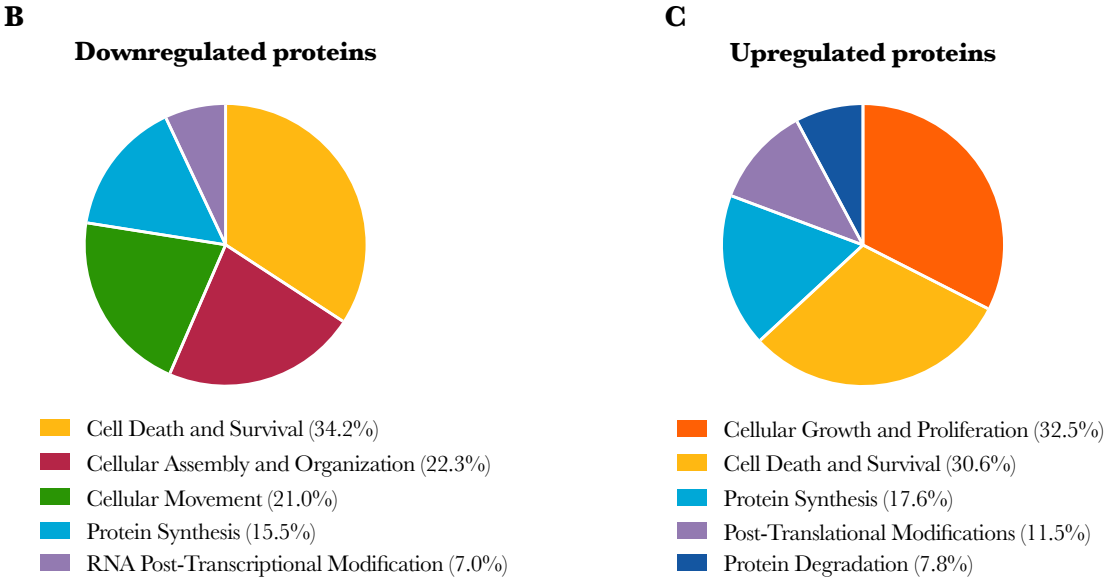

D

ID	Name	P-value	Fold Change (DSP/USP)
FGF2_HUMAN	Fibroblast Growth Factor 2	3.2×10^{-2}	1.9
TIMP1_HUMAN	TIMP metallopeptidase inhibitor 1	3.5×10^{-3}	5.8
GRN_HUMAN	Granulin	5.3×10^{-6}	2.2
GAS6_HUMAN	Growth Arrest Specific 6	2.3×10^{-4}	1.6
MIF_HUMAN	Macrophage migration inhibitory factor	4.7×10^{-1}	1.2

Figure 5.7 – Total proteome analysis of BM-MSC and AT-MSC after scaling-up the expansion and DSP operations. (A) Principal component analysis (PCA) representing the score for the higher components (39.7% and 20%) contributing to the data variance. (B-C) Distribution of the biological functions (in percentage) present on the 730 upregulated (B) and on the 629 downregulated proteins (C) of BM-MSC after DSP

comparing to BM-MSC after USP. Proteins with $P < 0.05$ and fold change > 1.5 were considered to be differently expressed. (D) Expression data of specific cytokines and growth factors identified on BM-MSC after expansion (USP) and after DSP. Fold change (towards DSP) and P-values are represented. Significantly different expressed proteins are considered to have $P < 0.05$ and Fold Change > 1.5.

To understand how DSP was affecting hMSC's, BM-MSC's proteome after expansion and DSP was compared (Figure 5.7B, 5.7C). Overall, 1359 proteins (730 upregulated and 629 downregulated) were significantly differently expressed between conditions ($P < 0.05$ and fold change >1.5) (data not shown). Biological functions associated with cellular assembly and organization (22.3%) and cellular movement (21%) were mainly associated with upregulated proteins after expansion (Figure 5.7B). Conversely, proteins related to cellular growth and proliferation (32.5%), and protein degradation (7.8%) were upregulated in BM-MSC after DSP (Figure 5.7C). Furthermore, it was possible to observe a statistically significant increased expression of several chemokines and growth factors (FGF, TIMP, GAS6 and GRN) in BM-MSC after DSP (Figure 5.7D). Biological functions highly regulated in both conditions (after expansion and after DSP) were related with cell death and survival, protein synthesis, and with post-translational/transcriptional modifications (Figure 5.7B, 5.7C).

4. Discussion

To achieve necessary cell quantities with the required quality for cell therapy, effectively scaling up production and purification processes while maintaining cells' CQA is essential.

In this work we aimed to prove scalability of an integrated and streamlined bioprocess comprising expansion, harvesting and volume reduction operations for hMSC isolated from BM and AT tissues. A proteomics workflow based on state of the art MS tools was used alongside standard quality control assays to gain better insights into the impact of processing upon cells' characteristics.

BM-MSC and AT-MSC were expanded at a 2 L scale during 7 days, in cGMP compatible conditions using xeno-free media, synthetic microcarriers and single-use bioreactors (2 L UniVessel® SU BR). Cell titers above $6.1x10^8$ and $7.4x10^8$ of BM-MSC and AT-MSC, respectively were achieved. Comparatively to other studies, this represents a 3 to 9-fold higher expansion of BM-MSC and AT-MSC at a 2 L scale in similar conditions; dos Santos and co-workers (Santos et al., 2014) have produced after 7 days of $1.1x10^8$ and $4.5x10^7$ BM-MSC and AT-MSC, respectively under xeno-free microcarrier-based culture system in 1 L scale controlled stirred-tank bioreactors. Similarly, hMSC's expansion was also reported, achieving $6.7x10^4$ at 3 L scale (Niss et al., 2013) and $2.7x10^5$ cell/mL at 35 L scale (Schirmaier et al., 2014)

after 7 days using media containing bovine serum. AT-MSC presented higher cell proliferation, with a metabolism based on oxidative phosphorylation, as in agreement with other studies (Li et al., 2015). Controlling the dissolved oxygen at low levels yielded higher cellular productivities compared to static or spinner cultures (Serra et al., 2010), bringing therapies one step closer. As an example, for the treatment of Crohn's disease $1x10^8$ cells are required *per* dose (Lipsitz et al., 2016); for the reported volumetric productivities in this work, two doses can be produced *per* liter of culture after 7 days of culture.

After cell expansion, a key step in adherent stem cell manufacturing corresponds to cell detachment (Nienow et al., 2016). Cell's characteristics are known to be affected by long exposure times to trypsin (Freshney, 2011) and by detaching methods (Santos et al., 2014). Hereby, we successfully scaled-up to the liter-scale a detachment protocol based on the application of a short period of intense agitation in the presence of a detaching agent (Nienow et al., 2016; 2014): by adjusting the stirring rates, comparable cell numbers could be recovered at different scales (0.12 and 2 L) for BM-MSC. Nonetheless, a 25% cell loss was observed when scaling this protocol for AT-MSC (in bioreactor); the protocol was repeated to ensure efficient cell detachment, and thus may explain the observed differences. Cell detachment also led to a 7% decreased expression of CD105 in BM and AT-MSC, in both static and stirred cultures, as in other studies in the literature (Potapova et al., 2008; Santos et al., 2014). To increase AT-MSC detachment and preventing the impact on cells' immunophenotype, protocol optimization is still required.

To scale-up the TFF operation, lower and larger-scale HF and FSC elements were similar (van Reis et al., 1997). The chosen scale-up criteria yielded relatively linear scale-up profiles; after conducting the trial experiments at the liter-scale, the permeate fluxes needed to be decreased by 30 and 50 LMH (for FSC and HF, respectively) to minimize fouling and maximizing cell recovery yield.

The hydrophilic nature of FSC membrane, combined with turbulence promoters in the feed channel was advantageous for the volume reduction step, allowing to recover more than 85% of cells after a VRF of 50, 18% more than when HF are used. Nevertheless, the benefit of cell recovery yield needs to be balanced with pre-sterilization issues that are still a challenge that manufacturing companies need to overcome (Schnitzler et al., 2016).

These results promise an integrated streamlined expansion, cell harvesting, volume reduction and washing operations at least for autologous cell therapy, but for scaling-up to process hundreds of liters, cost and time need to be properly evaluated. Currently, HF are commercially available as single, ready-to-use units, whereas FSC need a holder and a system

assembly. The development of models mimicking the shear rate conditions that cells face in flat sheet cassettes is needed, since its calculation is not straightforward due to the presence of a screen (Cheryan, 1998).

While carrying out cell therapy process development, it is essential to apply more sensitive (e.g. "omics") methodologies which allow a better cell characterization, increasing product and process understanding (Campbell et al., 2015; Martin et al., 2016). We applied a proteomics workflow based on MS tools to complement the standard quality controls and evaluate the impact of processing in hMSC's CQA, addressing cells characteristics in totality (not target direct), surpassing the detection and sensitivity limitations of current standard quality control assays. Fine differences observed between hMSC's after expansion and after DSP seem to correspond to biological functions essentially correlated with 3D arrangements (as cell assembly, organization and movement), as already observed in our earlier microcarrier studies (Gomes-Alves et al., 2016). It was also possible to observe that after DSP, BM-MSC present a statistically significant increased expression of chemokines and growth factors (e.g. FGF, TIMP, GAS6 and GRN) known to be involved in hMSC function (Kristensen et al., 2012; Motomura et al., 2007; Ostanin et al., 2011). Furthermore, after DSP, hMSC's proteins involved in cellular growth and proliferation are upregulated, as if "activated", explaining the increased proliferation observed also in Chapter VI. Overall, through sensitivity, robustness and throughput, this type of workflow provides the identification of specific signatures of the final product. Thus, it proves to be essential to understand the cells' final quality as well as to evaluate the impact of manufacturing at different stages of processing.

5. Conclusion

This work established scalability of a xeno-free cGMP compatible integrated bioprocess of BM-MSC and AT-MSC, comprising streamlined cell expansion, harvesting and volume reduction steps to support cell therapy. With this bioprocess, hMSC could be expanded more than 14-fold and concentrated by a volume reduction factor of 50, with an overall recovery above 65% of hMSC. Beside the standard quality assays normally used for evaluating hMSC CQA, a proteomics workflow based on MS tools characterized the impact of processing on hMSC' CQA, enhancing product and process understanding. This methodology will allow better optimization, design and ultimately will potentiate the success of cellular therapies.

6. Acknowledgments

I would like to acknowledge Eng. Marcos Sousa (iBET), Dr. Ricardo Silva (iBET), Sartorius Stedim Biotech (Javier Lobo) and the UniMS – Mass Spectrometry Unit team (ITQB-NOVA/iBET, Oeiras, Portugal), for technical and scientific discussions and advise.

This work was funded by Fundação para a Ciência e Tecnologia (FCT) through funded projects CARDIOSTEM (MITP-TB/ECE/0013/2013), and grants SFRH/BD/51940/2012 (MIT-Portugal), SFRH/BD/52302/2013, SFRH/BD/52481/2014, SFRH/BPD/86513/2012, and by iNOVA4Health Research Unit (LISBOA-01-0145-FEDER-007344), a program supported by FCT/Ministério da Ciência e do Ensino Superior (Portugal) through national funds, and cofunded by FEDER under the PT2020 Partnership Agreement.

7. Supplementary Data

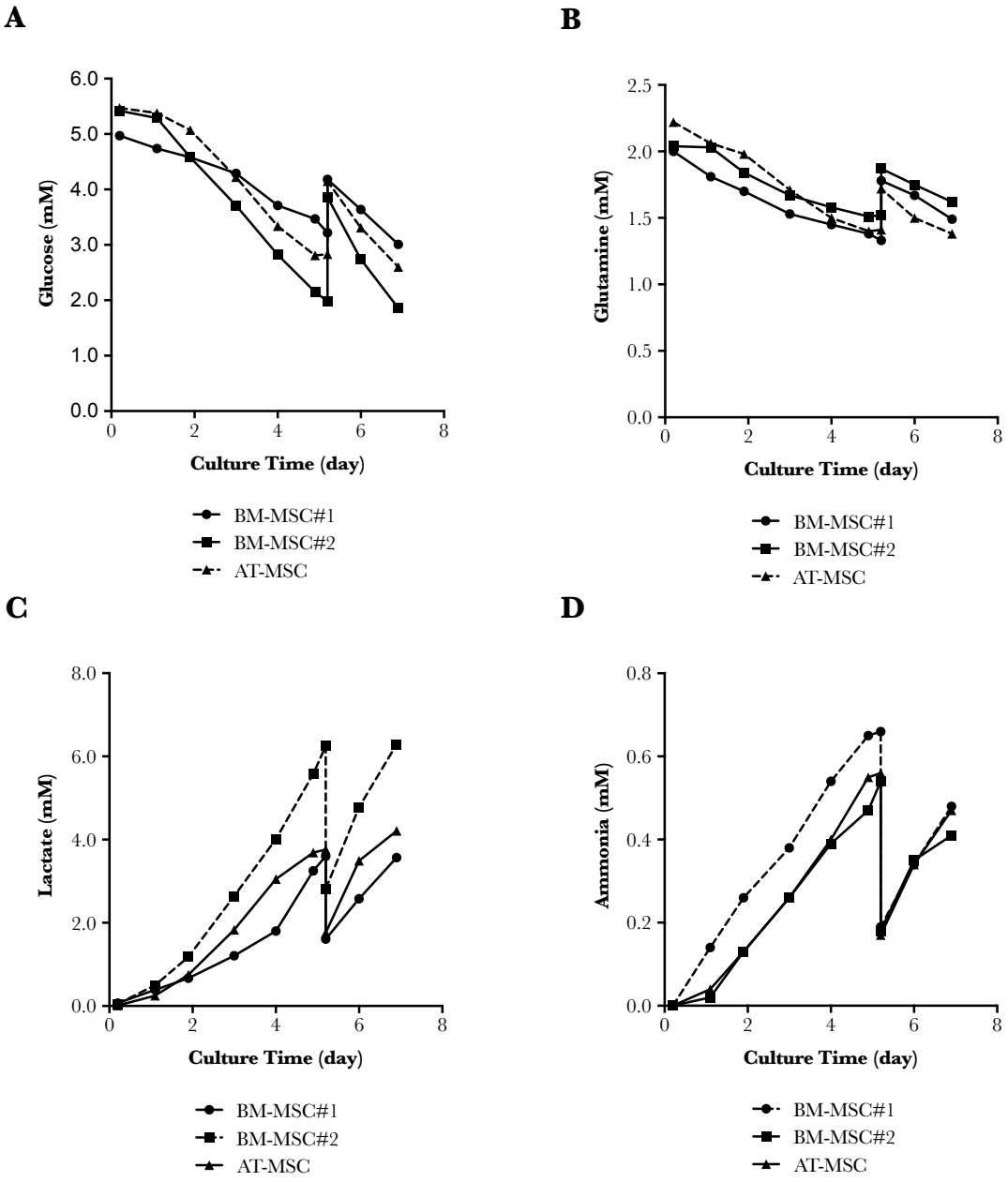

Supplementary data 5.1 – Metabolite profiles and process parameters during BM-MSC and AT-MSC cultures on 2 L UniVessel SU bioreactors. (A) Glucose, (B) glutamine, (C) lactate, and (D) ammonia concentration (expressed in mM) throughout all cultures' time.

References

Al-Nbaheen, M., vishnubalaji, R., Ali, D., Bouslimi, A., Al-Jassir, F., Megges, M., Prigione, A., Adjaye, J., Kassem, M., Aldahmash, A., 2012. Human Stromal (Mesenchymal) Stem Cells from Bone Marrow, Adipose Tissue and Skin Exhibit Differences in Molecular Phenotype and Differentiation Potential. Stem Cell Reviews and Reports 9, 32–43.

Campbell, A., Brieva, T., Raviv, L., Rowley, J., Niss, K., Brandwein, H., Oh, S., Karnieli, O., 2015. Concise Review: Process Development Considerations for Cell Therapy. Stem Cells Translational Medicine 4, 1155–1163.

Chen, A.K.-L., Reuveny, S., Oh, S.K.W., 2013. Application of human mesenchymal and pluripotent stem cell microcarrier cultures in cellular therapy: Achievements and future direction. Biotechnology Advances 31, 1032–1046.

Cheryan, M., 1998. Ultrafiltration and Microfiltration Handbook, 1st ed. Technomic Publishing AG, Basel.

Dominici, M., Le Blanc, K., Mueller, I., Slaper-Cortenbach, I., Marini, F., Krause, D., Deans, R., Keating, A., Prockop, D., Horwitz, E., 2006. Minimal criteria for defining multipotent mesenchymal stromal cells. The International Society for Cellular Therapy position statement. Cytotherapy 8, 315–317.

Fotakis, G., Timbrell, J.A., 2006. In vitro cytotoxicity assays: Comparison of LDH, neutral red, MTT and protein assay in hepatoma cell lines following exposure to cadmium chloride. Toxicol. Lett. 160, 171–177.

Freshney, R.I., 2011. Culture of Animal Cells: A Manual of Basic Technique and Specialized Applications, 6 ed. John Wiley & Sons, Inc, New York, USA.

Gomes-Alves, P., Serra, M., Brito, C., Ricardo, C.P., Cunha, R., Sousa, M.F., Sanchez, B., Bernad, A., Carrondo, M.J.T., Rodriguez-Borlado, L., Alves, P.M., 2016. In vitro expansion of human cardiac progenitor cells: exploring 'omics tools for characterization of cell-based allogeneic products. Transl Res.

Hassan, S., Simaria, A.S., Varadaraju, H., Gupta, S., Warren, K., Farid, S.S., 2015. Allogeneic cell therapy bioprocess economics and optimization: downstream processing decisions. Regen Med 10, 591–609.

Jones, K.H., Senft, J.A., 1985. An improved method to determine cell viability by simultaneous staining with fluorescein diacetate-propidium iodide. J. Histochem. Cytochem. 33, 77–79.

Kadic, E., Heindel, T.J., 2014. Stirred-Tank Bioreactors, in: An Introduction to Bioreactor Hydrodynamics and Gas-Liquid Mass Transfer, An Introduction to Bioreactor Hydrodynamics and Gas-Liquid Mass Transfer. John Wiley & Sons, Inc., Hoboken, NJ, USA, pp. 69–123.

Kristensen, L.P., Chen, L., Nielsen, M.O., Qanie, D.W., Kratchmarova, I., Kassem, M., Andersen, J.S., 2012. Temporal profiling and pulsed SILAC labeling identify novel secreted proteins during ex vivo osteoblast differentiation of human stromal stem cells. Mol Cell Proteomics 11, 989–1007.

Lee, H.J., Choi, B.H., Min, B.-H., Park, S.R., 2009. Changes in surface markers of human mesenchymal stem cells during the chondrogenic differentiation and dedifferentiation processes in vitro. Arthritis Rheum. 60, 2325–2332.

Li, C.-Y., Wu, X.-Y., Tong, J.-B., Yang, X.-X., Zhao, J.-L., Zheng, Q.-F., Zhao, G.-B., Ma, Z.-J., 2015. Comparative analysis of human mesenchymal stem cells from bone marrow and adipose tissue under xeno-free conditions for cell therapy. Stem Cell Res Ther 6.

Lin, J.-R., Guo, K.-Y., Li, J.-Q., Yan, D.-A., 2003. In vitro culture of human bone marrow mesenchymal stem cell clonies and induced differentiation into neuron-like cells. Di Yi Jun Yi Da Xue Xue Bao 23, 251–3– 264.

Lipsitz, Y.Y., Timmins, N.E., Zandstra, P.W., 2016. Quality cell therapy manufacturing by design. Nature Biotechnology 34, 393–400.

Lutz, H., 2015. Modules, in: Ultrafiltration for Bioprocessing. Elsevier, pp. 31–43.

Martin, C., Olmos, É., Collignon, M.-L., De Isla, N., Blanchard, F., Chevalot, I., Marc, A., Guedon, E., 2016. Revisiting MSC expansion from critical quality attributes to critical culture process parameters. Process Biochemistry.

Mason, C., Dunnill, P., 2009. Quantities of cells used for regenerative medicine and some implications for clinicians and bioprocessors. Regen Med 4, 153–157.

Motomura, H., Niimi, H., Sugimori, K., Ohtsuka, T., Kimura, T., Kitajima, I., 2007. Gas6, a new regulator of chondrogenic differentiation from mesenchymal cells. Biochem. Biophys. Res. Commun. 357, 997–1003.

Murphy, M.B., Moncivais, K., Caplan, A.I., 2013. Mesenchymal stem cells: environmentally responsive therapeutics for regenerative medicine. Experimental & molecular medicine 45, 54–70.

Nienow, A.W., Hewitt, C.J., Heathman, T.R.J., Glyn, V.A.M., Fonte, G.N., Hanga, M.P., Coopman, K., Rafiq, Q.A., 2016. Agitation conditions for the culture and detachment of

hMSCs from microcarriers in multiple bioreactor platforms. Biochemical Engineering Journal 108, 24–29.

Nienow, A.W., Rafiq, Q.A., Coopman, K., Hewitt, C.J., 2014. A potentially scalable method for the harvesting of hMSCs from microcarriers. Biochemical Engineering Journal 85, 79–88.

Niss, K., Sunil, N., Murrel, J., Punreddy, S., Kehoe, D., Rook, M., Jing, D., Aysola, M., 2013. Growth Kinetics of Human Mesenchymal Stem Cells in a 3L Single-Use, Stirred Tank Bioreactor, BioPharm International. BioPharm International.

Ostanin, A.A., Petrovskii, Y.L., Shevela, E.Y., Chernykh, E.R., 2011. Multiplex Analysis of Cytokines, Chemokines, Growth Factors, MMP-9 and TIMP-1 Produced by Human Bone Marrow, Adipose Tissue, and Placental Mesenchymal Stromal Cells. Bull. Exp. Biol. Med. 151, 133–141.

Pattasseril, J., Varadaraju, H., Lock, L., Rowley, J.A., Rowley, J.A., 2013. Downstream Technology Landscape for Large-Scale Therapeutic Cell Processing. BioProcess International 11, 38–47.

Potapova, I.A., Brink, P.R., Cohen, I.S., Doronin, S.V., 2008. Culturing of Human Mesenchymal Stem Cells as Three-dimensional Aggregates Induces Functional Expression of CXCR4 That Regulates Adhesion to Endothelial Cells. Journal of Biological Chemistry 283, 13100–13107.

Rowley, J., Abraham, E., Campbell, A., Brandwein, H., Oh, S., 2012. Meeting Lot-Size Challenges of Manufacturing Adherent Cells for Therapy. BioProcess International 3, 16–22.

Santos, dos, F., Campbell, A., Fernandes-Platzgummer, A., Andrade, P.Z., Gimble, J.M., Wen, Y., Boucher, S., Vemuri, M.C., da Silva, C.L., Cabral, J.M.S., 2014. A xenogeneic-free bioreactor system for the clinical-scale expansion of human mesenchymal stem/stromal cells. Biotechnology and Bioengineering 111, 1116–1127.

Schirmaier, C., Jossen, V., Kaiser, S.C., Jüngerkes, F., Brill, S., Safavi Nab, A., Siehoff, A., Bos, C., Eibl, D., Eibl, R., 2014. Scale-up of adipose tissue-derived mesenchymal stem cell production in stirred single-use bioreactors under low-serum conditions. Engineering in Life Sciences 14, 292–303.

Schnitzler, A.C., Verma, A., Kehoe, D.E., Jing, D., Murrell, J.R., Der, K.A., Aysola, M., Rapiejko, P.J., Punreddy, S., Rook, M.S., 2016. Bioprocessing of human mesenchymal stem/stromal cells for therapeutic use: Current technologies and challenges. Biochemical Engineering Journal 108, 3–13.

Schop, D., van Dijkhuizen-Radersma, R., Borgart, E., Janssen, F.W., Rozemuller, H., Prins, H.-J., de Bruijn, J.D., 2010. Expansion of human mesenchymal stromal cells on microcarriers: growth and metabolism. J Tissue Eng Regen Med 4, 131–140.

Serra, M., Brito, C., Sousa, M.F.Q., Jensen, J., Tostões, R., Clemente, J., Strehl, R., Hyllner, J., Carrondo, M.J.T., Alves, P.M., 2010. Improving expansion of pluripotent human embryonic stem cells in perfused bioreactors through oxygen control. Journal of Biotechnology 148, 208–215.

Simaria, A.S., Hassan, S., Varadaraju, H., Rowley, J., Warren, K., Vanek, P., Farid, S.S., 2014. Allogeneic cell therapy bioprocess economics and optimization: single-use cell expansion technologies. Biotechnology and Bioengineering 111, 69–83.

Strober, W., 2015. Trypan Blue Exclusion Test of Cell Viability. Curr Protoc Immunol 111, A3.B.1–3.

Tostões, R.M., Leite, S.B., Miranda, J.P., Sousa, M., Wang, D.I.C., Carrondo, M.J.T., Alves, P.M., 2011. Perfusion of 3D encapsulated hepatocytes--a synergistic effect enhancing long-term functionality in bioreactors. Biotechnology and Bioengineering 108, 41–49. doi:10.1002/bit.22920

van Reis, R., Goodrich, E.M., Yson, C.L., Frautschy, L.N., Dzengeleski, S., Lutz, H., 1997. Linear scale ultrafiltration. Biotechnology and Bioengineering 55, 737–746.

Vassault, A., 1983. Lactate dehydrogenase: UV-method with pyruvate and NADH, in: Bergmeyer, H.U., Grassl, M. (Eds.), Methods of Enzymatic Analysis. John Wiley & Sons, New York, pp. 118–126.

VI

Improving washing strategies of human mesenchymal stem cells using negative mode expanded bed chromatography

´This chapter was adapted from:

Cunha B, Silva RJS, Aguiar T, Serra M, Daicic J, Maloisel JL, Clachan J, Åkerblom A, Carrondo MJT, Peixoto C, Alves PM (2016). Improving washing strategies of human mesenchymal stem cells using negative mode expanded bed chromatography, Journal of Chromatography A, 1429:292-303.

Table of Contents

ABSTRACT **200**

1. INTRODUCTION **201**

2. MATERIALS AND METHODS **202**

2.1 Cell culture 202
2.2 Downstream processing (DSP) 203
2.3 Cell characterization assays 206
2.4 Statistical Analysis 209

3. RESULTS AND DISCUSSION **209**

3.1 Characterization of the core-shell bead prototype matrix 209
3.2 Packed bed and expanded bed chromatography 212
3.3 Integration of EBA chromatography on hMSC's DSP 217

5. CONCLUSIONS **220**

6. ACKNOWLEDGMENTS **221**

7. SUPPLEMENTARY DATA **222**

REFERENCES **223**

Abstract

The use of human mesenchymal stem cells (hMSC) in clinical applications has been increasing over the last decade. However, to be applied in a clinical setting hMSC need to comply with specific requirements in terms of identity, potency and purity.

This study reports the improvement of established tangential flow filtration (TFF)-based washing strategies, further increasing hMSC purity, using negative mode expanded bed adsorption (EBA) chromatography with a new multimodal prototype matrix based on core-shell bead technology.

The matrix was characterized and a stable, expanded bed could be obtained using standard equipment adapted from what is used for conventional packed bed chromatography processes. The effect of different expansion rates on cell recovery yield and protein removal capacity was assessed. The best trade-off between cell recovery (89%) and protein clearance (67%) was achieved using an intermediate expansion bed rate (1.4).

Furthermore, we also showed that EBA chromatography can be efficiently integrated on the already established process for the downstream processing (DSP) of hMSC, where it improved the washing efficiency more than 10-fold, recovering approximately 70% of cells after total processing. This strategy showed not to impact cell viability (> 95%), neither hMSC's characteristics in terms of morphology, immunophenotype, proliferation and adhesion capacity and multipotent differentiation potential.

Keywords: expanded bed chromatography; human mesenchymal stem cells; cell purification; cell washing; downstream processing

1. Introduction

Human mesenchymal stem cells (hMSC) have been emerging over the last decade as attractive candidates for cell therapy applications (Wei et al., 2013; Zaher et al., 2014), mainly due to their immunomodulatory capacity and trophic characteristics, as extensively described in the literature and recently reviewed by Caplan and Sorell (Caplan and Sorrell, 2015).

However, to be applied in a clinical setting, hMSC need to comply with specific requirements in terms of quantity, identity, potency and purity (Food and Drug Administration; European Medicines Agency, 2008; Pattasseril et al., 2013). These requirements include delivering high number of cells at low volumes (compatible with point of care delivery) (Hassan et al., 2015), while maintaining cell's high viability (higher than 85%) and characteristics (Pattasseril et al., 2013). Given its effect on cells' characteristics (Chapter II), the processing time should be minimized and sterility should be ensured throughout processing due to the inability of terminally sterilize cellular products. Furthermore, cells should be pure enough to be safe to administer in a clinical setting. Therefore, strategies that can successfully integrate a washing step to reduce impurity levels up to <1 ppm (Food and Drug Administration) are compulsory. Several downstream processing (DSP) technologies have been explored so far for the washing of stem cell products. In Chapter IV the use of tangential flow filtration (TFF) to integrate concentration and washing steps in the same hollow fiber device was explored, achieving 98% of protein removal, without compromising cells' characteristics. Similarly, Lonza (MD, USA) has also reported a TFF process using hollow fiber devices, where hMSC were washed efficiently while maintaining functionality (Pattasseril et al., 2013; Rowley et al., n.d.). Another study also reported the use and validation of a novel dead-end filtration to remove the DMSO from a cell suspension without fouling the filter membrane (Tostões et al., 2015).

Given the demand for highly pure biopharmaceuticals, the application of chromatography as a separation technique has been widely demonstrated. Its high selectivity and flexibility have been enabling its use for the purification of several biopharmaceuticals with different complexities (Carta and Jungbauer, 2010; Kumar and Srivastava, 2010; Nestola et al., 2015). It can be operated using radial (Cabanne et al., 2007) or axial flow (Carta and Jungbauer, 2010), the latter being the most widely used. Furthermore, benchmark purification techniques for bioproduct's recovery and purification are currently performed using packed bed columns. Nonetheless, the use of particulate-containing feedstocks hampers the use of packed bed chromatography (Chang and Chase, 1996); alternatively, expanded bed adsorption (EBA) chromatography can be used (Chase and Draeger, 1992). Due to its high interparticular voidage

and high adsorbent surface area, amongst other advantages (Chang and Chase, 1996), EBA chromatography has been applied for the separation of many biopharmaceuticals, from viral vectors (Peixoto et al., 2006) to cells (Ujam et al., 2003). In the expanded bed, the adsorbent inside the column is fluidized from its settled state by applying an upward flow, which allows that particulate products pass through the bed without becoming entrapped (Chase and Draeger, 1992), making it an attractive design for the downstream processing (DSP) of hMSC.

The main goal of this study was to improve already established TFF-based washing strategies (Chapter IV), further increasing hMSC's purity up to levels compatible with their use in cellular therapies, while maintaining cells' functionality. Within this context, we have assessed the applicability of using a chromatographic step that enables a single-pass operation making its integration in the already established DSP workflow for hMSC easier. We have implemented and characterized a new multimodal prototype resin based on core-shell bead technology. Furthermore, the impact of EBA chromatography on cells' recovery, viability and characteristics in terms of morphology, identity and potency was evaluated.

2. Materials and Methods

2.1 Cell culture

In this work, human bone marrow-derived mesenchymal stem cells were used (hMSC; STEMCELL™ Technologies, Grenoble, France). All reagents used to perform the cell culture were purchased from Life Technologies™ (Carlsbad, USA), unless otherwise stated.

hMSC were routinely expanded using xeno-free MesenCult®-XF Medium (STEMCELL™ Technologies) supplemented with 2 mM L-Glutamine and propagated in tissue culture flasks (Thermo Scientific™ Nunc™, Massachusetts, USA), previously coated with MesenCult™-SF Attachment Substrate (STEMCELL™ Technologies). Cells were expanded at 37 ºC in a humidified atmosphere of 5% CO_2 in air. 50% of the culture medium was exchanged at day 5. At 70 – 80% cell confluency, the medium was removed and cells were washed with Dulbecco's phosphate-buffered saline (DPBS) and incubated with TrypLE™ Select (1X) dissociation reagent for 10 min at 37 ºC. After detachment, cells were resuspended in MesenCult®-XF medium, and centrifuged at 300 *g* for 5 min at 20 ºC. The cell pellet was resuspended in MesenCult®-XF medium and transferred to new pre-coated culture flasks, at an inoculum cell concentration of 5 x 10^3 cell/cm^2.

For downstream processing experiments, after detachment cells were ressuspended in DMEM supplemented with 10% (v/v) Fetal Bovine Serum (FBS).

2.2 Downstream processing (DSP)

2.2.1 Chromatography

A multimodal resin prototype based on a similar concept to Capto™ Core 700, was used to perform the DSP experiments. The resin beads consist on agarose-based porous particles with a deactivated outer layer and an inner core that has been modified with octylamine ligand.

2.2.1.1 Resin prototype size distribution

Bead size was estimated using a phase contrast inverted microscope (DMI 600 B, Leica Microsystems GmbH, Wetzlar, Germany) using the software Leica Application Suite LAS AF. One perpendicular diameter of each bead was measured from 20 beads, of three different samples, from beads before and after sieving.

2.2.1.2 Batch protein adsorption characterization

To characterize the protein removal kinetics throughout time, 5 g of resin were weighed and incubated with 5 mL of DMEM (Life Technologies) supplemented with 5%, 10% or 20% (v/v) of FBS (Life Technologies). These different medium formulations were equilibrated for 60 min with the beads with a constant rotational stirring (33 rpm) in a roller mixer (SRT9, Bibby Scientific Ltd., Staffordshire, United Kingdom). Sampling was performed at 2, 5, 10, 15, 30, 45 and 60 min. These samples were centrifuged at 300x*g* for 5 min at 20 ºC and the supernatant was kept for further analysis.

To determine the binding capacity of the resin (amount of adsorbed protein *per* mass of resin), DMEM supplemented with 2%, 5%, 10%, 20% or 30% (v/v) of FBS was incubated in a 1:5 (w/v) ratio of beads:medium for 120 min (saturating conditions) with a constant rotational stirring (33 rpm) in a roller mixer (SRT9, Bibby Scientific Ltd.). Sampling was performed after the incubation period, where the suspension was centrifuged at 300x*g* for 5 min at 20 ºC and the supernatant kept for further analysis. The matrix was regenerated following the manufacturer's instructions.

The adsorption isotherm for proteins onto the adsorbent was fitted to a Langmuir isotherm equation (1):

$$q = \frac{q_{max}\, C}{K_D + C} \quad (1)$$

where q is defined as the amount of total protein (mg) adsorbed *per* mass of resin (g), q_{max} the maximum adsorption capacity, C is the equilibrium total concentration of un-adsorbed protein in the liquid phase and K_D is the dissociation constant.

2.2.1.3 Packed bed and expanded bed chromatography

The chromatographic resin was used either in a packed bed radial column or in an expanded bed column. All chromatographic experiments were performed at 20 ºC using ÄKTA explorer 10S (GE Healthcare) controlled by UNICORN™ (GE Healthcare). Special attention was given to the flowpath to avoid points of high shear; in order to do so, the flow restrictor and internal filters were removed. The cell suspension was injected via a 50 mL superloop (GE Healthcare) and monitored using a UV 280 nm detector.

To perform radial chromatography, the beads were packed into a Micro FC column (Proxcys BV, Nieuw-Amsterdam, The Netherlands), with 60 mm bed height and 5 mL of bed volume, using a 100 µm frit. According to the bed height, cells were injected inside the column at 46 $cm.h^{-1}$, in order to ensure a comparable residence time with expanded bed chromatography.

Expanded bed chromatography was performed in a regular Tricorn 10/50 column (GE Healthcare). Initially, the system was sanitized by recirculating NaOH 1 M in 30% (v/v) in 2-Propanol (VWR International, Pennsylvania, USA) for 60 min. The resin was equilibrated for at least 1 h before the experiments at the desired expansion flow rate with DPBS, until the pH was stabilized at 7 and the bed stability was attained. A control experiment was performed by incubating a similar cell suspension and resin's amount for the same period of time in batch mode under orbital shaking at 20 ºC.

Experiments using different bed expansion ratios were performed using 12 g of resin. As depicted in Figure 6.1, q was determined and given cells' expansion media quantification, the amount of injected cells in the column was adjusted accordingly.

Cells' residence time σ (min) inside the chromatographic columns was estimated using equation 2:

$$\sigma = \frac{h}{u} \quad (2)$$

where h is the bed height (cm) and u the linear velocity ($cm.h^{-1}$), which is given by trivial equation 3:

$$u = \frac{Q}{A} \quad (3)$$

where Q corresponds to the volumetric flow rate (L.h^{-1}) and A is the column's crossectional area (cm^2).

The bed expansion ratio was also characterized, using the Richardson-Zacki correlation (equation 4) (Richardson and Zaki, 1997):

$$u = u_t \, \varepsilon^n \quad (4)$$

where ε corresponds to the bed's porosity and n to the Richardson-Zacki coefficient, which for Re < 0.2 (present situation), is constant and approximately 4.7 (Anspach et al., 1999). u_t is the terminal fluidization velocity, which is described by the Stokes law (equation 5):

$$u_t = \frac{(\rho_p - \rho_l)\, d_p^2\, g}{18\mu} \quad (5)$$

where ρ_p and ρ_l are the particle's and liquid's density, respectively, d the particle's average diameter, g the acceleration of gravity and μ represents the fluid's dynamic viscosity.

The bed porosity (ε) was calculated by equation (6), as described previously in the literature (Thommes et al., 1996):

$$\frac{H}{H_0} = \frac{(1-\varepsilon_0)}{(1-\varepsilon)} \quad (6)$$

The settled bed porosity was assumed to be 0.4 (Anspach et al., 1999). H corresponds to the expanded bed height (cm) and H_0 to the settled bed height (cm).

The temperature was kept constant at 20 ºC in all performed experiments.

2.2.2 Cell concentration (volume reduction)

The cell suspension was concentrated using tangential flow filtration (TFF). Discontinuous TFF was performed as described in Chapter IV. Hollow fiber devices with 24 cm^2 from GE Healthcare Life Sciences were used.

Pressure was monitored using SciPres luer pressure sensors (SciLog, Wisconsin, USA) on the inlet, outlet and permeate stream. Inlet and permeate fluxes were fixed to 750 and 250 LMH, respectively (Chapter II). Watson Marlow Model 120 S/DV 200 rpm pump (Watson-Marlow Pumps Group, Massachusetts, USA) and Tandem Model 1081 peristaltic pumps from Sartoflow® Slice 200 benchtop crossflow system (Sartorius Stedim Biotech) were used to perform the experiments. Weight and pressure data were monitored and acquired every 15 sec.

A water flux test was performed before and after each experiment to determine the membrane's permeability. To ensure sterility, hollow fiber devices were sanitized with 0.5 M NaOH (Sigma-Aldrich, Steinheim, Germany) at 50 ºC for 45 min. The membranes were preconditioned with five membrane volumes of sterile DPBS before the concentration step.

2.2.3 Cell washing (diafiltration)

The continuous diafiltration (DF) step was performed using the same TFF cartridge and operating conditions previously used to conduct the concentration process (Chapter IV). To observe the protein removal profile, DPBS was used to perform the DF process.

2.3 Cell characterization assays

All reagents used to perform cell characterization assays were purchased from Sigma Aldrich, unless stated otherwise.

2.3.1 Cell number and viability

Cell viability and cell membrane integrity were assessed using two different methods:

2.3.1.1 Trypan Blue exclusion method

Cell concentration was estimated through counting cells using a Fuchs–Rosenthal haemocytometer (Brand, Wertheim, Germany). Viable cells were determined by using the trypan blue dye exclusion method. The cell recovery yield is always referred as a percentage, and was estimated taking into account the number of viable cells before (100%) and after processing.

2.3.1.2 Lactate Dehydrogenase (LDH) Assay

The release of intracellular lactate dehydrogenase (LDH) enzyme into the supernatant can be correlated with the extent of cell lysis (Fotakis and Timbrell, 2006). Hence, LDH activity from the supernatant of centrifuged samples was determined by monitoring the rate of oxidation of NADH to NAD^+ coupled with the reduction of pyruvate to lactate at 340 nm, as previously described in the literature (Vassault, 1983).

2.3.2 Apoptosis and metabolic activity assay

The percentage of apoptotic and metabolically active cells was evaluated using Apoptosis Assay Kit NucView™ 488 and MitoView™ 633 (Biotium, Inc., California, USA), following the manufacturer's instructions. This kit contains the green fluorescent NucView 488 caspase-3 substrate (detects intracellular caspase-3) and the far-red fluorescent MitoView 633 mitochondrial dye (detects changes in mitochondrial membrane potential). After incubation with both reagents, cells were analyzed by flow cytometry (CyFlow® space, Partec GmbH, Münster, Germany). At least ten thousand events were registered *per* sample.

2.3.3 hMSC's adhesion and growth profile

hMSC were inoculated in static culture conditions, in 24-well plates, previously coated with MesenCult™-SF Attachment Substrate. A cell inoculum of 5 x 10^3 cell/cm^2 was used and cells were cultured as described in section 2.1 (Section Cell Culture). For evaluation of the cell adhesion capacity, the number of adherent cells was monitored 60 min after inoculation, as previously performed in Chapter II.

Cells' growth profile was monitored for 8 days. Cell concentration and viability were determined as previously described in section 2.3.1.1 (Section Cell number and viability, Trypan Blue exclusion method).

2.3.4 Flow cytometry

hMSC were washed once with DPBS and a total of 2 x 10^5 cells were incubated with each of the antibodies (CD166-PE, CD105-PE, CD90-PE, CD73-PE, CD44-PE, CD45-PE, CD34-PE, CD19-PE, CD14-PE, CD11b-PE, HLA-DR-PE and isotype controls IgG_1,κ-PE, IgG_{2a},κ-PE and IgG_{2b},κ-PE, all from BD Biosciences, California, USA) for 1 h at 4 °C. Cells were washed twice in DPBS, and analyzed in a CyFlow® instrument. At least ten thousand events were registered *per* sample.

2.3.5 Immunocytochemistry

hMSC were inoculated in static culture conditions, in 24-well-plates previously coated with MesenCult™-SF Attachment Substrate, as described in section 2.1 (Cell Culture). After 24 h, cells' morphology was analyzed as previously performed in Chapter II. Cells were fixed and incubated with each one of the primary antibodies for 2 h at 20 ºC. After two washing steps with DPBS, cells were incubated with the secondary antibodies for 1 h at 20 ºC. hMSC were then washed two times with DPBS and the cell nuclei were counterstained with 4,6-diamidino-2-phenylindole (DAPI, Life Technologies). Cells were visualized using inverted (Leica Microsystems GmbH) fluorescence microscopy. Representative images were taken using a digital camera (Leica DFC 360 FX).

The primary antibodies used were Alexa Fluor® 488 Phalloidin (Life Technologies) and Anti-α-Tubulin. Anti-α-Tubulin was conjugated with secondary antibody Alexa Fluor® 594 Goat Anti-Mouse Antibody (Life Technologies).

2.3.6 *In vitro* multipotency assays

hMSC multilineage differentiation assays were performed using the StemMACS™ AdipoDiff (Miltenyi Biotec, Germany), StemMACS™ OsteoDiff (Miltenyi Biotec, Germany) and StemPro® Chondrogenesis (Life Technologies, USA) differentiation kits, as previously performed in Chapter II.

2.3.7 Total protein quantification

For total protein concentration, representative of the protein impurities content, samples were centrifuged at 300 *g* for 5 minutes at 20 ºC and the supernatant was kept at 4 ºC for further analysis. Different methods were performed according to their detection limit and following the manufacturer's instructions. When protein concentration was lower than 0.2 mg/mL, bicinchoninic acid (BCA) protein assay (Pierce Biotechnology, Rockford IL, USA) assay was performed using Infinite® 200 PRO plate reader (Tecan Group Ltd, Männedorf, Switzerland). When protein concentration was higher than 0.2 mg/mL, an infrared (IR)-based assay was performed using Direct Detect® Spectrometer (Merck Millipore).

2.3.8 Protein analysis (electrophoresis and western blot analysis)

Protein samples were analyzed by SDS-PAGE (200 V, 45 min, MES running buffer) electrophoresis (XCell SureLock mini-cell system; Life Technologies), by loading the same protein amount (5 micrograms of total protein) onto NuPAGE™ Novex™ 4–12% (w/v) bis-tris precast polyacrylamide gels (Life Technologies), unless otherwise stated. Samples that had more than 25 µL to be applied were precipitated overnight using cold absolute ethanol at -20 ºC (Bollag et al., 1996). Samples were reduced and denaturated before SDS-PAGE analysis at 90 ºC for 10 min. After separation, proteins were visualized by Instant Blue staining (Expedeon, Harston, UK).

For Western-Blot (WB) analysis, the protein samples were first separated by SDS-PAGE, as described before. A total amount of 1 µL was loaded in each lane of the gel. Samples from after cell expansion, after EBA chromatography, and after cell concentration were previously diluted in DPBS (1:10, 1:4, 1:4 (v/v), respectively). Proteins were transferred onto nitrocellulose membrane using iBlot® Dry Blotting System (Life Technologies). The membrane was blocked for 1 h using 5% (w/v) Skim Milk (Merck Millipore) and incubated with anti-BSA polyclonal rabbit antibody (Life Technologies) (diluted 1:200 in DPBS) and with anti-rabbit HRP conjugated secondary antibody (Sigma Aldrich) (diluted 1:5000 in DPBS). Revelation was performed using ECL Prime (Life Technologies) reagent in Chemidoc™ XRS device (Bio-Rad,

California, USA). A semi-quantification of albumin was performed using a standard curve of Albumin fraction V (Merck Millipore) in the same gel, using imageJ software (Schneider et al., 2012) (http://imagej.nih.gov/ij/).

2.3.9 Endotoxin quantification

Endotoxin content was quantified using Endosafe®-PTS™ (Charles River, Massachusetts, USA), following the manufacturer's instructions.

2.4 Statistical Analysis

Bead size scattering followed a gaussian distribution, as validated by D'Agostino & Pearson omnibus normality test. Differences in bead size between the resin before and after sieving were analyzed by t-test. Differences between packed bed radial chromatography and expanded bed chromatography, as well as in fold increase/decrease towards cells before DSP (n = 3 measurements) were analyzed by Mann Whitney test.

P values of less than 0.05 were considered as statistically significant.

All statistical analyses were performed using GraphPad Prism version 5 (GraphPad Software Inc., California, USA).

3. Results and Discussion

The new core prototype resin was first characterized in terms of the scattering on bead's size and for its protein removal capacity. Kinetics throughout time and determination of the resin's binding capacity in saturating conditions were determined. After having these, the impact that operating the chromatography step either in packed or in expanded bed mode have on the protein removal profile as well as on cells' recovery yield was assessed. To perform EBA, and given the high scattering of the core prototype resin, a sieving step was performed to homogenize the bead's size to be applied in expanded bed mode chromatography. Different expansion bed ratios were evaluated to perform the chromatography step. The chromatography step was successfully integrated on the DSP workflow previously established to process hMSC (Chapter IV) to further increase hMSC's purity at the end of processing.

3.1 Characterization of the core-shell bead prototype matrix

Capto™ Core 700 is a multimodal resin that has been successfully applied in flowthrough mode for the purification of viruses (Blom et al., 2014) and other biopharmaceuticals (Ji et al.,

2014). This resin is based on a bead core-shell technology, with an inactive shell surface and with an active functionalized multimodal core (both hydrophobic and positively charged) with octylamine ligands (Blom et al., 2014). Given the bead's molecular weight cut off (approximately of 700 kDa) (Blom et al., 2014), smaller particles, as proteins, can access the porous structure and are efficiently adsorbed at the core of the beads, whereas larger particles, as cells, are excluded and are collected in the flowthrough.

Commercially available Capto™ Core 700, with a mean bead size of approximately 85 µm requires the use of low mesh pore size filters (30 µm) to separate beads from cells (size range of 15 to 25 µm). Previous results showed that such low mesh pore size leads to a decreased cell recovery yield upon filtration (Chapter II). Therefore, a new prototype based on the Capto™ Core 700 concept with larger bead size (at least 300 µm, Table 6.1 and Figure 6.2) was developed for this study.

Table 6.1 – Capto™ Core 700 prototype resin's bead size characterization before and after the sieving process.

	Minimum size (µm)	**Maximum size (µm)**	**Median (µm)**	**Mean (µm)**
Before Sieving	301	827	545	553
After Sieving	416	1000	627	637

Several research groups and companies still expand hMSC using expansion media supplemented with FBS (Capelli et al., 2015; Rafiq et al., 2013). Moreover, regulatory agencies stipulate that if serum is used at any stage of the bioprocess workflow, its concentration in the final formulation shall not exceed 1:1,000,000 (1 ppm) (Food and Drug Administration). Therefore, a typical expansion media supplemented with FBS was used as proof-of-concept to conduct the protein clearance studies aiming to reach protein clearance compliant with regulatory requirements.

Protein adsorption kinetics in batch mode was characterized using the core prototype resin (Figure 6.1).

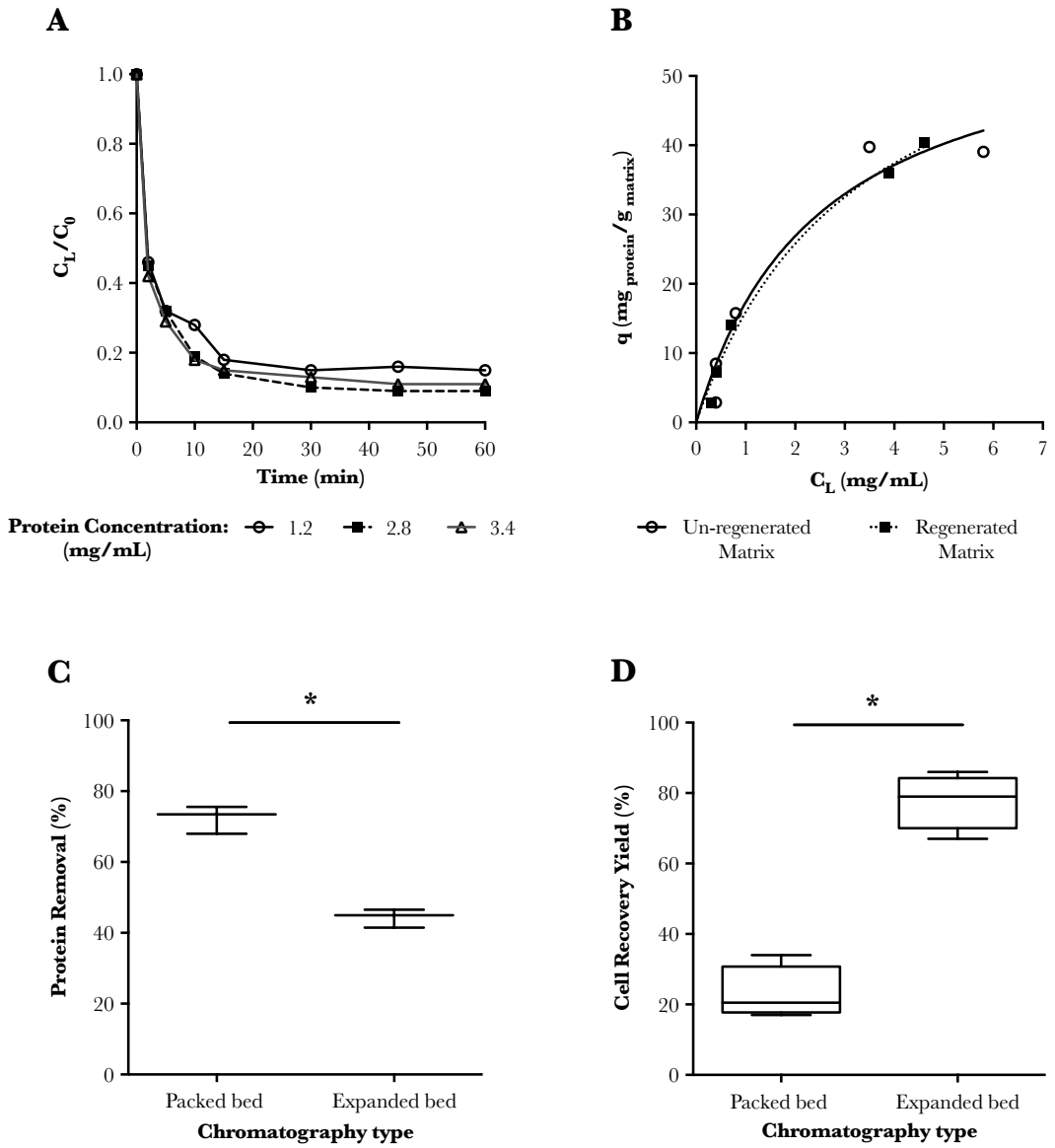

Figure 6.1 – Capto™ Core 700 prototype resin's characterization for the DSP of hMSC. Batch characterization of the chromatographic medium, (A) expressing the protein removal kinetics throughout time, and (B) the protein adsorption equilibria isotherm behavior using new and regenerated (once) resin. Langmuir adsorption isotherms (lines) are represented for both cases. Comparison of packed bed radial and expanded bed chromatography, in terms of (C) protein removal, and (D) cell recovery yield. Statistically significant differences ($P < 0.05$) are marked as *.

As observed in Figure 6.1A, the amount of protein adsorbed onto the resin increased with increasing incubation time for all medium formulations, physically reaching a plateau of 30 min after incubation.

Moreover, the protein adsorption isotherm on the core prototype resin was determined by plotting the amount of total protein adsorbed *per* mass of adsorbent (q) as a function of the protein concentration (C_L) in the liquid phase (Figure 6.1B). From what can be observed, the experimental data of the resin was well correlated with the Langmuir isotherm ($R^2 = 0.9637$,

Figure 6.1B). The maximum adsorption capacity (q_{max}) of the expansion media proteins onto the core-shell prototype resin was 68.0 ± 11.4 mg of protein *per* g of adsorbent, and the dissociation constant (K_D) 3.3 ± 1.1 mg/mL. Similarly to what has been reported for this resin (Blom et al., 2014), a binding capacity of 13 mg of protein *per* g of resin used was determined, when using standard expansion medium supplemented with 10% (v/v) FBS. We also confirmed that the regeneration process does not impact the adsorption capacity of the resin, since similar values of q_{max} (60.0 ± 13.2 mg of protein *per* g of adsorbent) and K_D (2.5 ± 1.3 mg/mL) were obtained for the regenerated resin (Figure 6.1B).

3.2 Packed bed and expanded bed chromatography

To avoid cell loss in an additional filtration step to clarify the beads from the cells (Chapter II), the resin was confined in columns, taking advantage of the cells' ability to pass in flowthrough mode. Two different chromatography modes were evaluated – radial chromatography and expanded bed chromatography (Figure 6.1C and 6.1D).

Radial chromatography has been applied successfully for the DSP of biopharmaceuticals (Cabanne et al., 2007), and its properties have already been extensively reviewed in the literature (Besselink et al., 2013; Cabanne et al., 2007); a radial flow operation has a lower flow rate at a predefined pressure drop than the equivalent axial flow column at equal bed thickness and volume (Besselink et al., 2013), offering options for large-scale applications as well (Cabanne et al., 2007). Packed bed radial flow and expanded bed chromatography were compared. Similar bed volumes and residence times were used to compare both operation modes. Results show that packed bed radial chromatography is more efficient for protein clearance (Figure 6.1C), since more than 70% of contaminants could be successfully removed, when comparing to the expanded bed chromatography operation (44%). These results were in accordance with previous studies using both types of chromatography (Cabanne et al., 2007). Nonetheless, the geometry of packed bed radial chromatography lead to substantially lower cell recovery yields (Figure 6.1D, 23% *vs* 78%). Results from other studies (Hidayat et al., 2004), point to the accumulation of cells and cell debris in packed bed, acting as a secondary filter, leading to consequent clogging of the column. In line with this finding, in the present case the lack of space between particles may have compromised the cell recovery yield, whereas in expanded bed chromatography, since particles are fluidized, cells encounter lower shear stress conditions, allowing to achieve higher cell recovery yields.

Since fluidization of the resin proved to be crucial for cell recovery yield, the core-shell bead prototype matrix was operated in expanded bed mode (Figure 6.3A). The resin was put inside a Tricorn 10/50 column, which had an adjustable piston on top (Figure 6.3B). The buffer and cell suspension were pumped at the bottom, and the cells were collected on the top of the column.

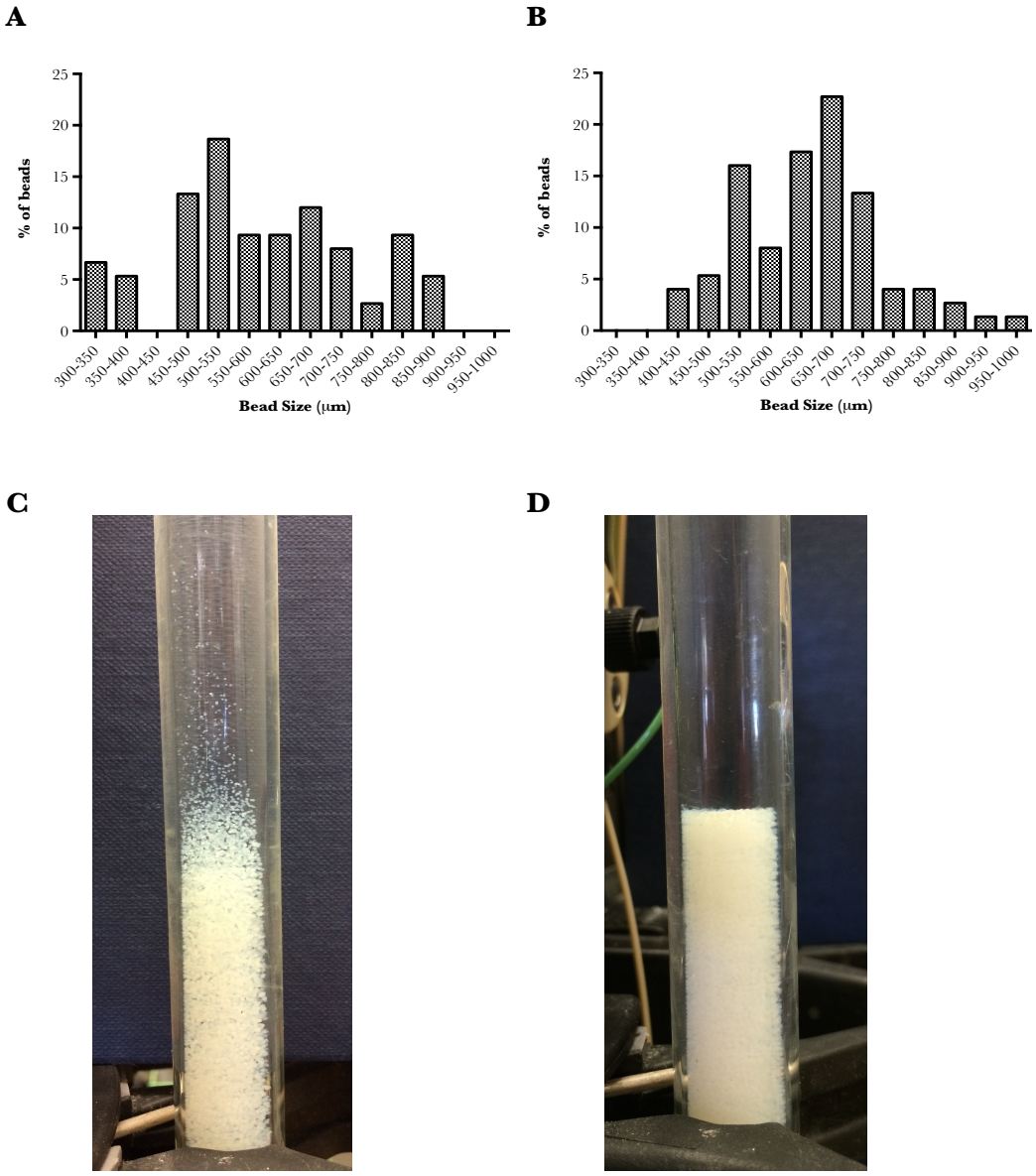

Figure 6.2 – Bead size distribution of the Capto™ Core 700 prototype resin. Bead size scattering (A) before and (B) after the sieving process. Pictures of the prototype resin's scattering (C) before and (D) after sieving. Statistically significant differences were found in bead size before and after sieving ($P < 0.05$).

Given the high scattering of the resin upon fluidization (Figure 6.2C), the resin was sieved before performing the chromatography. A higher fluidization velocity (460 $cm.h^{-1}$) was applied, removing beads with lower density/smaller size (Figure 6.2A and 6.2B), achieving a stable bed upon fluidization (Figure 6.2D). The sieving process enriched significantly the resin in beads with higher size, since the smaller bead size detected shifted from 301 µm to 416 µm (Table 6.1,

Figure 6.2A and 6.2B). The dynamic binding capacity of the resin remained unaltered after the sieving process (data not shown).

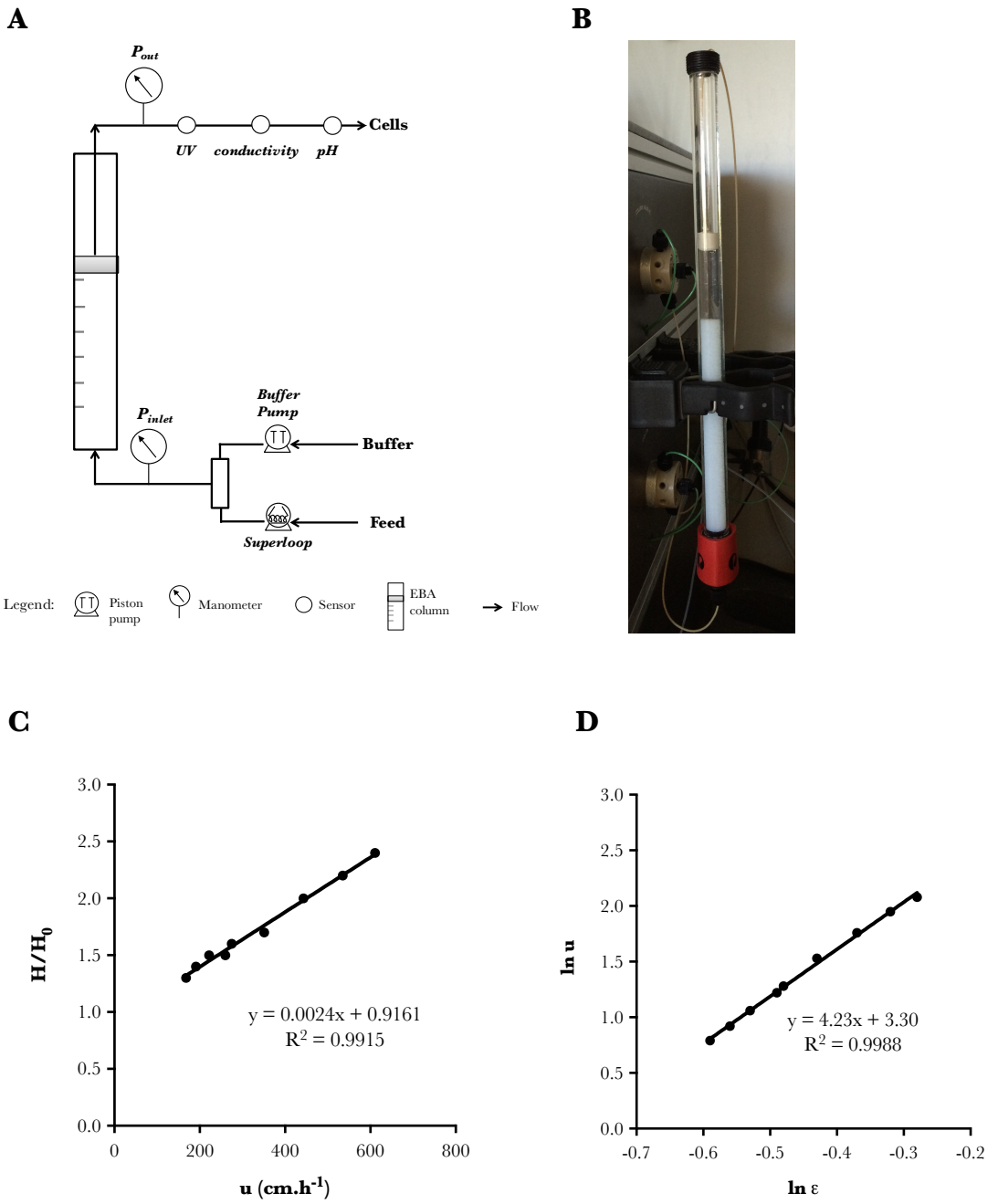

Figure 6.3 – Expanded bed chromatography characterization. (A) Schematic representation of the EBA chromatography operation. Briefly, the chromatographic medium is expanded by pumping using DPBS at a fixed flow rate until a stable bed is achieved. The cell suspension is injected into a superloop and loaded at the bottom of the EBA chromatography column. hMSC elution (flowthrough) is monitored by UV, pH and conductivity sensors. (B) EBA chromatography column. (C) Relative bed expansion ratios at different flow rates. (D) Richardson-Zacki correlation of the expanded bed chromatography.

In order to characterize the expanded bed (Figure 6.3C), different velocities ranging from 168 to 611 $cm.h^{-1}$ were applied. Results showed that the bed expansion increased linearly (R^2 = 0.9915) with the increase in the inlet velocity. Furthermore, the variation in the degree of

expansion of the bed, as a function of the fluidization velocity was found to follow the Richardson-Zacki correlation (Richardson and Zaki, 1997). A linear regression of the Richarson-Zacki equation (equation 4) was performed (Figure 6.3D), where it is possible to achieve n = 4.23 ± 0.09, which is similar with the reported value (4.65) in the literature, normally used in the laminar flow conditions (Anspach et al., 1999; Chang and Chase, 1996). Thus, the bed was assumed to be stable upon expansion.

hMSC in DMEM supplemented with 10% (v/v) were used to compare three different bed expansion ratios. Their effect on cells' recovery yield and protein removal capacity was assessed (Table 6.2, Figure 6.4).

Table 6.2 – Comparison of the results in terms of cell recovery yield, cell viability and protein removal for the three performed expansion bed ratios (1.6, 1.4 and 1.2).

H/H_0	Velocity ($cm.h^{-1}$)	Residence time (min)	Protein removal (%)	Viable cell recovery yield (%)	Cell viability (%)
1.6	290	5.1	51	95	95
1.4	168	7.0	67	89	96
1.2	99	12.7	77	78	90

Representative chromatograms for the negative mode expanded bed chromatography for the three bed expansion ratios are presented in Figure 6.4A.

Upon injection of the cell suspension in the chromatography column, it is possible to recover cells in the flowthrough. Moreover, it was possible to confirm that higher residence times, correlated with lower fluidization velocities, allowed to remove more protein contaminants (Table II, up to 77%). However, a lower bed fluidization also led to lower cell recovery yields (78%), lower cell viabilities (90%) and increased cell death (2-fold, assessed by LDH assay, data not shown).

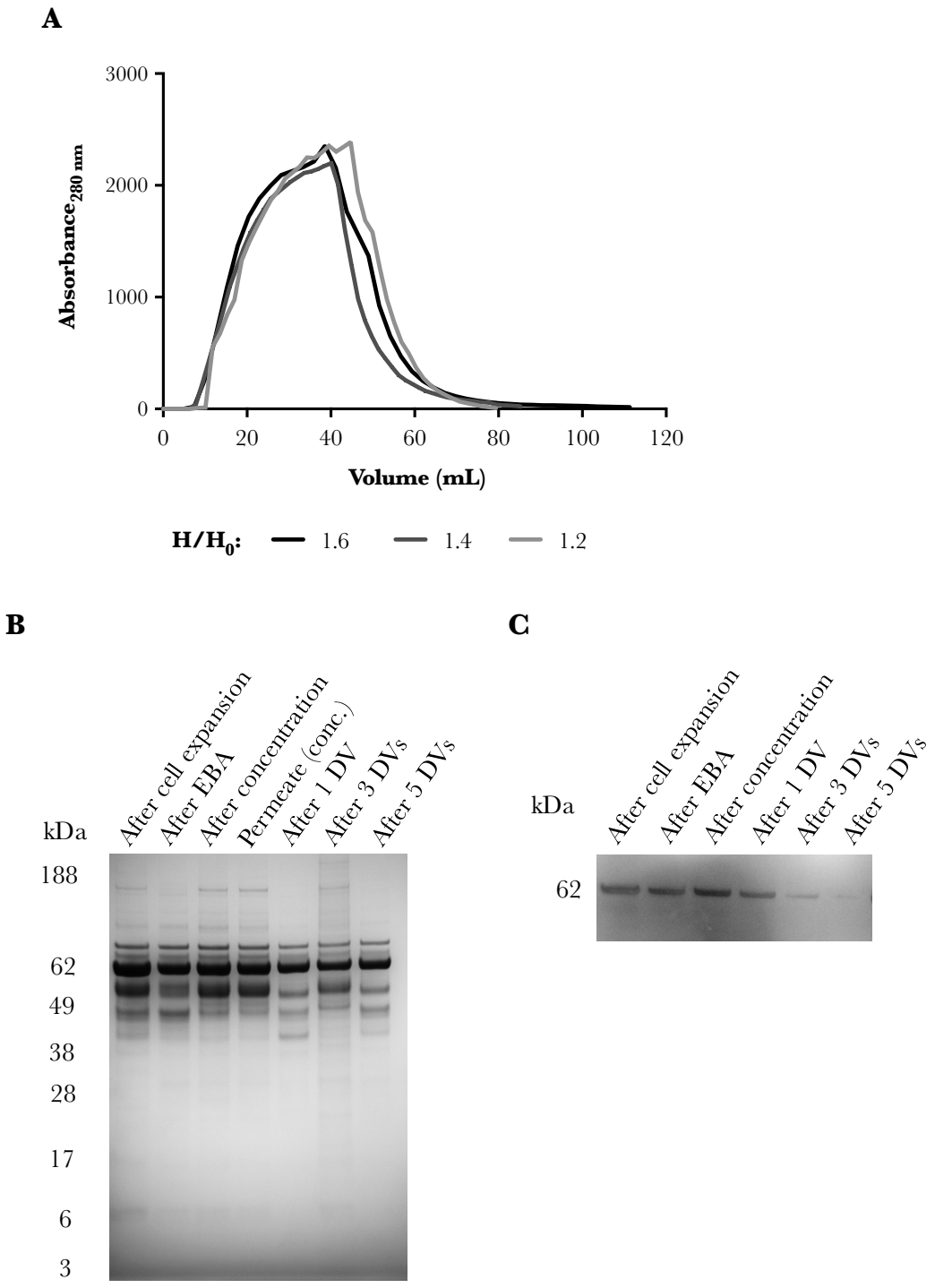

Figure 6.4 – Expanded bed chromatography. (A) Typical chromatogram profile using the Capto™ Core 700 prototype resin in flowthrough mode. The UV absorbance at 280 nm is shown for the three performed expansion bed ratios (1.6 in black, 1.4 in dark grey and 1.2 in light grey). Analysis of the protein samples throughout processing by (B) Coomassie blue staining and (C) Western Blot (anti-BSA). SDS-PAGE: after cell expansion (lane 1), after EBA chromatography (lane 2), after concentration (lane 3), the concentration's permeate (lane 4), after one (lane 5), three (lane 6) and five (lane 7) diafiltrations; Western blot: after cell expansion (lane 1), after EBA chromatography (lane 2), after concentration (lane 3), after one (lane 4), three (lane 5) and five (lane 6) diafiltrations.

Similarly to the packed bed radial chromatography, the smaller spaces in between the beads may obstruct the cell path until elution, increasing the probability of collision with the particles,

increasing the shear stress, and therefore correlating with lower cell recovery yields. The core-shell bead prototype matrix showed not to have a particular selectivity for any protein in particular, since a similar protein profile was present in all samples throughout processing (Figure 6.4B). Additionally, we confirmed that bovine serum albumin is the major protein contaminant in the expansion media (Figure 6.4C), composing 50-60% of the initial bulk, as estimated by WB. It is worth noting that the presence of cells does not have an effect on the adsorption of proteins on the matrix, since a similar binding capacity (12 mg of protein *per* g of resin used) was observed, when comparing to the batch characterization results (Figure 6.1).

3.3 Integration of EBA chromatography on hMSC's DSP

Given the best trade-off between cell recovery yield (89%) and protein clearance (67%), a bed expansion ratio of 1.4 was selected to integrate EBA chromatography with the cell concentration and diafiltration steps (Figure 6.5A).

EBA chromatography could be successfully integrated on the already established DSP process in an endotoxin-free process (< 1 EU/mL). Its incorporation allowed to improve protein clearance by more than 10-fold (80 *vs* 7 µg/mL) applying the same number of diafiltration volumes (Figure 6.5B), approaching the residual level (1 ppm) recommended by regulatory agencies (dotted line, Figure 6.5B) (Food and Drug Administration) after 3 diafiltration volumes onwards. Furthermore, to achieve the same level of residuals without applying a chromatography step, 10 diafiltration volumes should be used (Chapter IV). More specifically, it is estimated that 99.6% (*vs* 97.9% (Chapter IV)) of BSA could be removed when incorporating EBA chromatography in the process (Figure 6.4C). Also, results show that the increased protein clearance is coupled with a decrease in the cell recovery yield for both processes (Figure 6.5C) - with and without EBA chromatography - where a similar cell recovery yield profile was achieved for both processes (global yield towards initial sample of 67% and 74%, respectively). Given that DPBS was used as diafiltration solution to study the protein clearance profile throughout processing, stabilizing proteins are also removed, explaining the decrease in cell recovery.

Nonetheless, after both processes hMSC were recovered with high cell viability (> 95%) (Figure 6.6A). After DSP, hMSC maintained their ability in adhering to plastic surfaces (no significant differences observed towards hMSC before DSP, Figure 6.6A), having more than 89% of adherent cells after 1 h for both conditions.

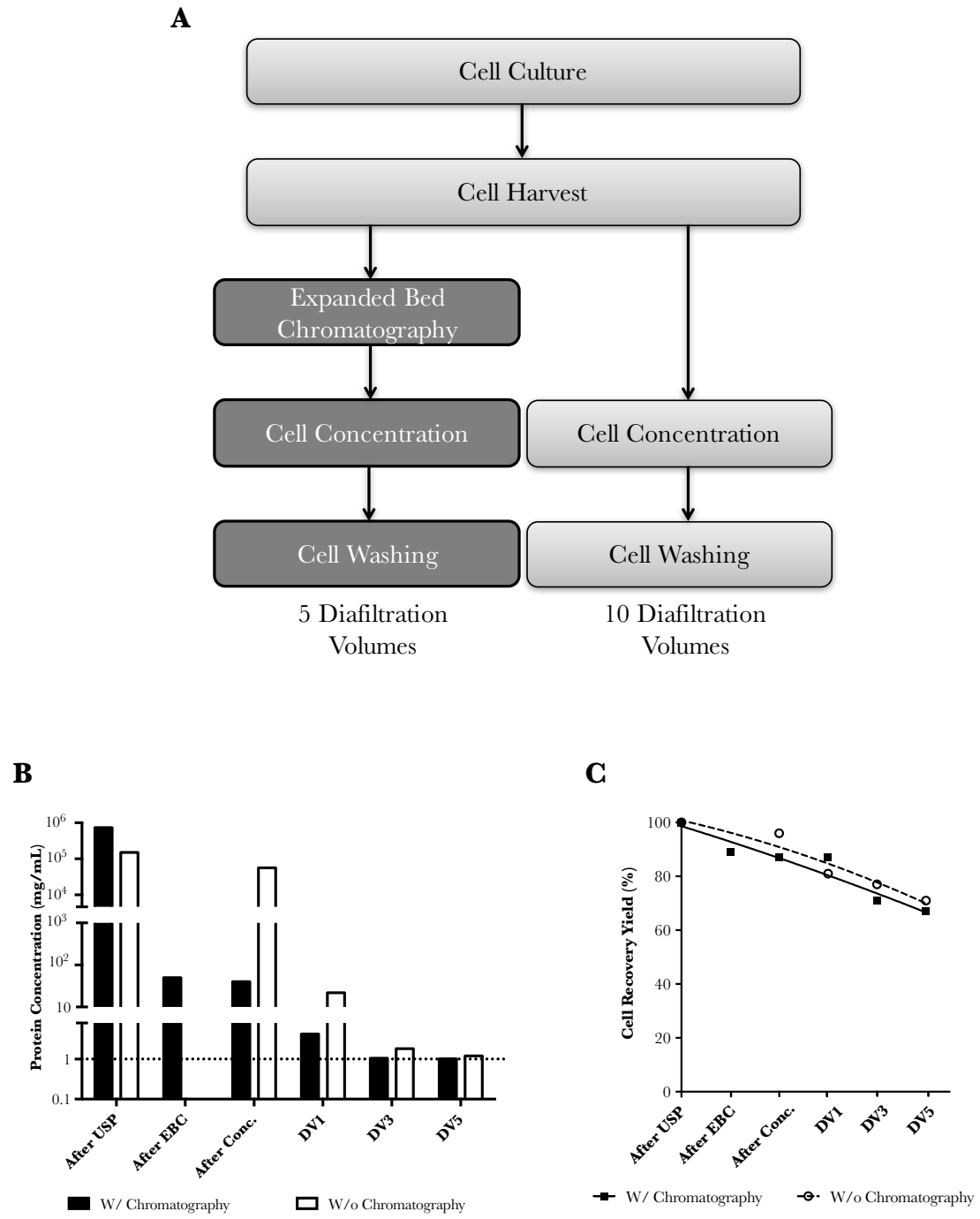

Figure 6.5 – Integration of EBA chromatography into the DSP of hMSC. (A) Comparison of the two performed workflows. After cell expansion, the cell bulk suspension was harvested. Two different strategies were evaluated – using negative mode expanded bed chromatography before the cell concentration step (dark grey) and without performing the chromatography step. hMSC were afterwards concentrated and washed. (B) Protein removal profiles and (C) cell recovery yields of the processes with and without performing EBA chromatography. The dotted line represents the minimum recommended amount of FBS by the regulatory agencies.

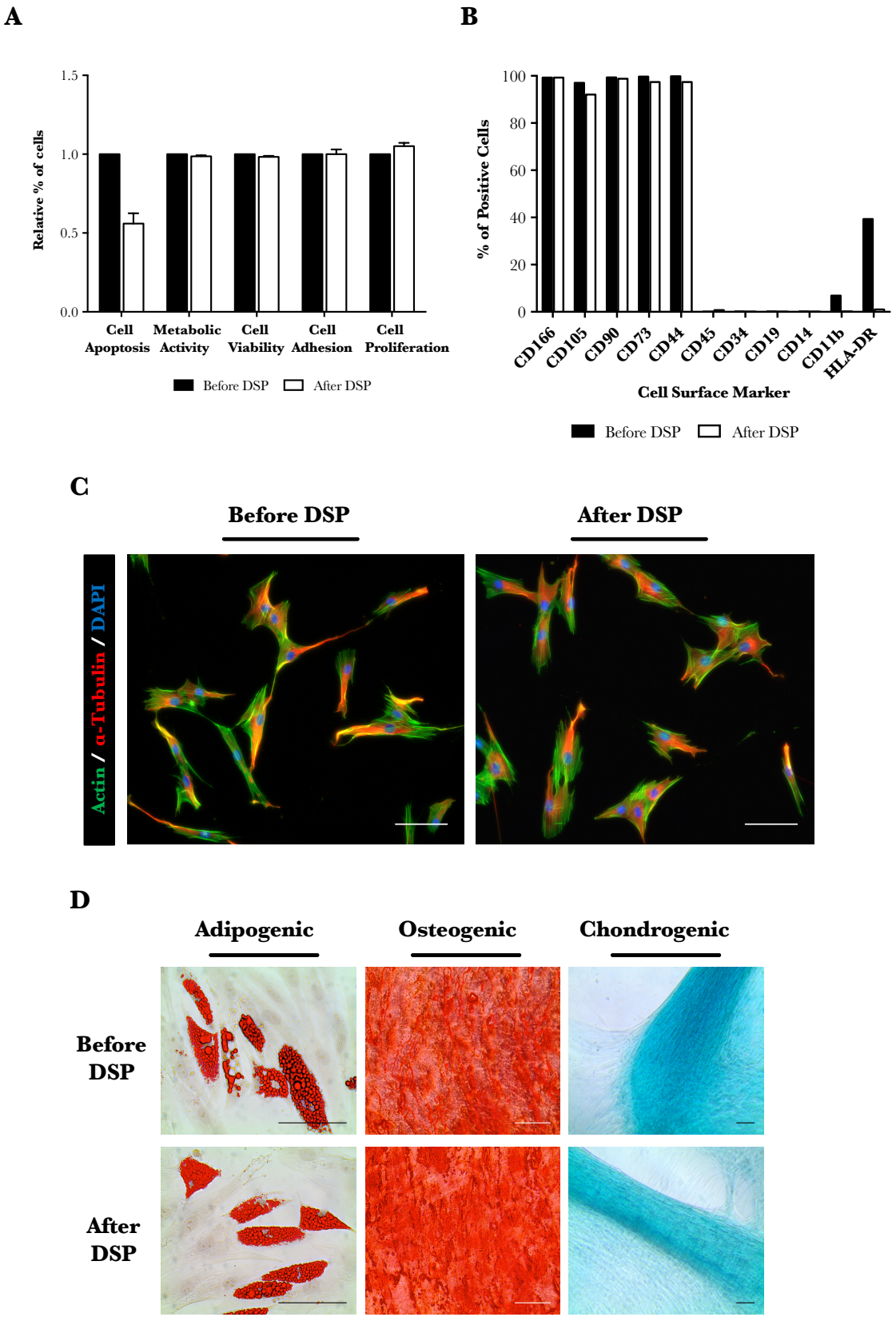

Figure 6.6 – hMSC characterization after the integrated bioprocess. (A) Cell characterization in terms of cell apoptosis, metabolic activity, cell viability, cell adhesion and cell proliferation after expansion and after downstream processing. Each bar represents the fold-increase/decrease, relative to cells before DSP. (B) Expression of specific cell-surface antigens (CD166, CD105, CD90, CD73, CD44, CD45, CD34, CD19, CD14, CD11b, HLA-DR) typical for hMSC, after up- and downstream processing. (C) hMSC morphology after up- and downstream processing - immunofluorescence staining of f-actin (green), α-tubulin (red), and cell nuclei (blue).

Scale bars: 100 µm. (D) Multipotent differentiation potential of hMSC. Red-oil solution stained lipid droplets (adipocytes, left panel), alizarin red stained calcium deposits (osteoblasts, central panel), and alcian blue stained extracellular matrix proteins (chondrocytes, right panel). Scale bars: 100 µm.

hMSC also remained metabolically active (no significant differences observed towards hMSC before DSP, Figure 6.6A), having reached a similar population doubling level (PDL = 3) after plating (Figure 6A). Additionally, a decrease in cell apoptosis (Figure 6.6A) was observed after DSP; this decrease can be due to the death of part of these apoptotic cells during DSP.

The expression of the main characteristic hMSC's surface receptors, as described in the literature (Dominici et al., 2006), remained unaltered after processing (Figure 6.6B). More specifically, hMSC lacked the expression of CD45, CD34, CD14, CD19 and CD11b, while more than 95% of hMSC population expressed CD44, CD73, CD 90, CD105 and CD166 mesenchymal stem cell surface markers. To be noted that before DSP, more than 5% of hMSC presented HLA-DR expression (39%, Supplementary data 6.1); previous studies in the literature (Sotiropoulou et al., 2006) have reported that several culture parameters can affect the expression of HLA. The high percentage of HLA-DR$^+$ cells may be justified by the expansion/harvest conditions. Given that after DSP only 1% of hMSC were HLA-DR$^+$, it appears that the DSP contributed to the elimination of HLA-DR$^+$ cells. Since no specific selection method was applied, we hypothesize that these cells died throughout processing when exposed to higher shear stress environments, and therefore are comprised in the overall 30% cell loss during DSP.

Furthermore, the integration of EBA chromatography on the process showed not to impact cell morphology, since, after plating, hMSC could successfully re-acquire their typical spindle-like morphology, presenting organized intracellular f-actin and expressing α-tubulin (no differences were observed when comparing to cells before DSP, Figure 6.6C).

Moreover, hMSC after DSP processing have maintained their multipotent differentiation capacity, as cells were able to differentiate into adipocytes, osteocytes and chondroblasts (Figure 6.6D). No spontaneous differentiation was ever observed (data not shown).

5. Conclusions

Results in this study demonstrate that a new multimodal prototype matrix based on core-shell bead technology can be successfully used in negative mode for cell therapy manufacturing, given cell's ability to elute in flowthrough. EBA chromatography could be integrated on the endotoxin-free DSP of hMSC, where it improved the efficiency of already established TFF-based washing by more than 10-fold, recovering at the end of the process approximately 70%

of hMSC, without compromising cell's characteristics in terms of identity, potency and viability. It is shown that EBA chromatography can be incorporated on the cell therapy manufacturing to wash the cell suspension before the concentration step, where a diafiltration step can be applied afterwards using a proper cryopreservation solution (Chapter IV) to stabilize cells and to formulate them to be subsequently filled and finished. By implementing this single-pass operation on the process workflow, the number of overall diafiltration volumes could be decreased, achieving overall purity levels compliant with the use of functional hMSC in therapies, and also decreasing the time hMSC are subjected to pumping shear when processed in the TFF.

Negative mode chromatography represents the beginning of a promising platform for cell therapy applications, where new adsorbents can be designed to have affinity with target impurities (e.g. BSA) and not to the final product itself, the cells. Given the scalable and universal nature of the developed methodology in this study, this strategy can be adopted to process other type of cell products relevant for both for autologous and allogeneic cell therapy applications (e.g. pluripotent stem cells). This is achieved by a negative chromatographic operation mode promoting the adsorption of impurities, as cells will flow through the expanded chromatographic bed with minimal interaction.

6. Acknowledgments

I would like to acknowledge Prof Paulo Mota for fruitful discussions of the presented work.

This work was funded by Fundação para a Ciência e Tecnologia (FCT, Portugal) (project EXPL/BBB-EBI/1003/2012 and PhD grant SFRH/BD/51940/2012, MIT-Portugal Program) and by NanoGene project (EuroNanoMed ERA-Net initiative - ENMED/0001/2010).

7. Supplementary Data

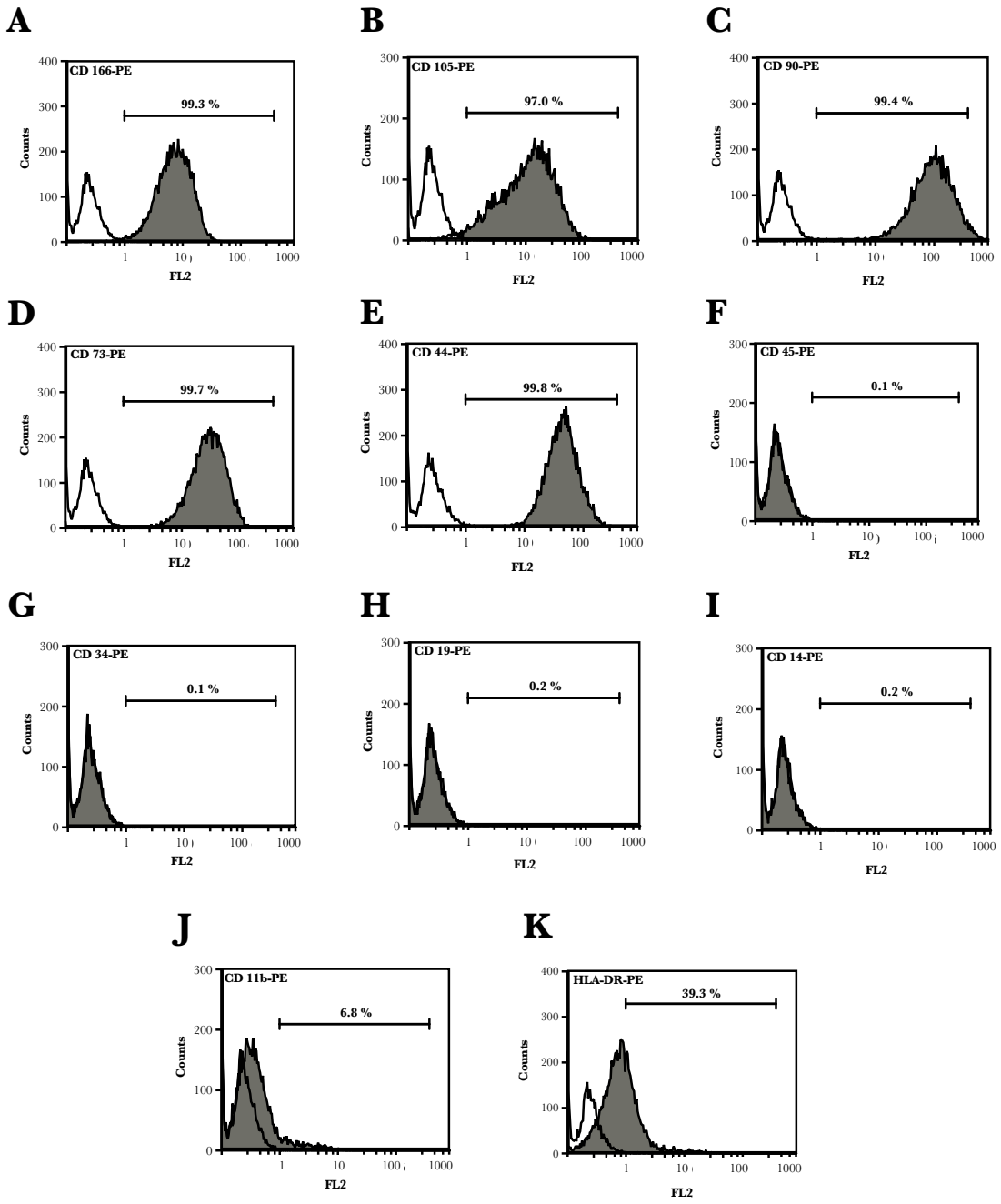

Supplementary data 6.1 – Expression of specific cell-surface antigens after the integrated bioprocess. Histograms of each one of the analyzed cell surface markers. (A) CD166, (B) CD105, (C) CD90, (D) CD73, (E) CD44, (F) CD45, (G) CD34, (H) CD19, (I) CD14, (J) CD11b, and (K) HLA-DR.

References

Anspach, F.B., Curbelo, D., Hartmann, R., Garke, G., Deckwer, W.D., 1999. Expanded-bed chromatography in primary protein purification. J. Chrom. A 865, 129–144.

Besselink, T., van der Padt, A., Janssen, A.E.M., Boom, R.M., 2013. Are axial and radial flow chromatography different? J. Chrom. A 1271, 105–114.

Blom, H., Åkerblom, A., Kon, T., Shaker, S., van der Pol, L., Lundgren, M., 2014. Efficient chromatographic reduction of ovalbumin for egg-based influenza virus purification. Vaccine 32, 3721–3724.

Bollag, D.M., Rozycki, M.D., Edelstein, S.J., 1996. Protein Methods, 2nd ed. Wiley-Liss, New York.

Cabanne, C., Raedts, M., Zavadzky, E., Santarelli, X., 2007. Evaluation of radial chromatography versus axial chromatography, practical approach. J. Chrom. B 845, 191–199.

Capelli, C., Pedrini, O., Valgardsdottir, R., Da Roit, F., Golay, J., Introna, M., 2015. Clinical grade expansion of MSCs. Immunol. Lett.168, 222–227.

Caplan, A.I., Sorrell, J.M., 2015. The MSC curtain that stops the immune system. Immunol. Lett. 168, 136–139.

Carta, G., Jungbauer, A., 2010. Protein chromatography: process development and scale-up. Wiley-VCH Verlag GmbH & Co. KGaA, Weinheim.

Chang, Y.K., Chase, H.A., 1996. Development of operating conditions for protein purification using expanded bed techniques: The effect of the degree of bed expansion on adsorption performance. Biotechnol. Bioeng. 49, 512–526.

Chase, H.A., Draeger, N.M., 1992. Affinity Purification of Proteins Using Expanded Beds. J.Chrom. A 597, 129–145.

Dominici, M., Le Blanc, K., Mueller, I., Slaper-Cortenbach, I., Marini, F., Krause, D., Deans, R., Keating, A., Prockop, D., Horwitz, E., 2006. Minimal criteria for defining multipotent mesenchymal stromal cells. The International Society for Cellular Therapy position statement. Cytother. 8, 315–317.

European Medicines Agency, 2008. EMEA/CHMP Guideline on human cell-based medicinal products (EMEA/CHMP/410869/2006).

Food and Drug Administration, Code of Federal Regulations Title 21. Subchapter F -- Biologics; Part 610 -- General Biological Products Standards; Subpart B -- General Provisions; Sec. 610.15 Constituent Materials. doi:10.1007/978-1-4615-6838-4_2

Fotakis, G., Timbrell, J.A., 2006. In vitro cytotoxicity assays: Comparison of LDH, neutral red, MTT and protein assay in hepatoma cell lines following exposure to cadmium chloride. Toxicol. Lett. 160, 171–177.

Hassan, S., Simaria, A.S., Varadaraju, H., Gupta, S., Warren, K., Farid, S.S., 2015. Allogeneic cell therapy bioprocess economics and optimization: downstream processing decisions. Regen. Med. 10, 591–609.

Hidayat, C., Takagi, M., Yoshida, T., 2004. Expanded bed adsorption for purification of alcohol dehydrogenase using a dye-iminodiacetic acid matrix. J. Biosci. Bioeng. 97, 284–287.

Ji, Y., Tian, Y., Ahnfelt, M., Sui, L., 2014. Design and optimization of a chromatographic purification process for Streptococcus pneumoniae serotype 23F capsular polysaccharide by a Design of Experiments approach. J. Chrom. A 1348, 137–149.

Kumar, A., Srivastava, A., 2010. Cell separation using cryogel-based affinity chromatography. Nat. Protoc. 5, 1737–1747.

Nestola, P., Silva, R.J.S., Peixoto, C., Alves, P.M., Carrondo, M.J.T., Mota, J.P.B., 2015. Robust design of adenovirus purification by two-column, simulated moving-bed, size-exclusion chromatography. J. Biotechnol. 213, 109–119.

Pattasseril, J., Varadaraju, H., Lock, L., Rowley, J.A., Rowley, J.A., 2013. Downstream Technology Landscape for Large-Scale Therapeutic Cell Processing. BioProcess Int. 11, 38–47.

Peixoto, C., Ferreira, T.B., Carrondo, M.J.T., Cruz, P.E., Alves, P.M., 2006. Purification of adenoviral vectors using expanded bed chromatography. J. Virol. Methods 132, 121–126.

Rafiq, Q.A., Brosnan, K.M., Coopman, K., Nienow, A.W., Hewitt, C.J., 2013. Culture of human mesenchymal stem cells on microcarriers in a 5 l stirred-tank bioreactor. Biotechnol. Lett. 35, 1233–1245.

Richardson, J.F., Zaki, W.N., 1997. Sedimentation and fluidisation: part 1. Chem. Eng. Res. Des. 75, S82–S99.

Rowley, J., Pattasseril, J., Mohamed, A., n.d. High yield method and apparatus for volume reduction and washing of therapeutic cells using tangential flow filtration. WO 2011091248 A1.

Schneider, C.A., Rasband, W.S., Eliceiri, K.W., 2012. NIH Image to ImageJ: 25 years of image analysis. Nat. Methods 9, 671–675.

Sotiropoulou, P.A., Perez, S.A., Salagianni, M., Baxevanis, C.N., Papamichail, M., 2006. Characterization of the optimal culture conditions for clinical scale production of human

mesenchymal stem cells. Stem Cells 24, 462–471.

Thommes, J., Bader, A., Halfar, M., Karau, A., Kula, M.R., 1996. Isolation of monoclonal antibodies from cell containing hybridoma broth using a protein A coated adsorbent in expanded beds. J. Chrom. A 752, 111–122.

Tostoes, R., Dodgson, J., Mason, C., Veraitch, F., 2015. A Novel Filtration Device for Point of Care Preparation of Cellular Therapies. Cytother. 17, S26–S26.

Ujam, L.B., Clemmitt, R.H., Clarke, S.A., Brooks, R.A., Rushton, N., Chase, H.A., 2003. Isolation of monocytes from human peripheral blood using immuno-affinity expanded-bed adsorption. Biotechnol. Bioeng. 83, 554–566.

Vassault, A., 1983. Lactate dehydrogenase: UV-method with pyruvate and NADH, in: Bergmeyer, H.U., Grassl, M. (Eds.), Methods of Enzymatic Analysis. John Wiley & Sons, New York, pp. 118–126.

Wei, X., Yang, X., Han, Z.-P., Qu, F.-F., Shao, L., Shi, Y.-F., 2013. Mesenchymal stem cells: a new trend for cell therapy. Acta Pharmacol. Sin. 34, 747–754.

Zaher, W., Harkness, L., Jafari, A., Kassem, M., 2014. An update of human mesenchymal stem cell biology and their clinical uses. Arch. Toxicol. 88, 1069–1082.

VII

Discussion and perspectives

Table of Contents

1. DISCUSSION 230

1.1. Establishing a DSP workflow for hMSC 230
1.2. Biomanufacturing workflow of hMSC 235

2. CONCLUSION AND PERSPECTIVES 236

REFERENCES 238

1. Discussion

Advances in the last decades in biotechnology, bioengineering and stem cell biology have been bridging fundamental research with practical clinical applications. But, as pointed out throughout this thesis, the clinical transfer of human stem cells (hSC) for cell therapy applications still faces major challenges. The production of high cell amounts required for therapeutic doses, the delivery of those high cell numbers at low volumes with minimal presence of impurities, while assuring the desired phenotype and function/potency are compulsory.

The work developed in this thesis aimed at establishing a streamlined downstream processing (DSP) workflow based on scalable and integrated DSP unit operations for clarification, volume reduction and purification (washing) for cell-based therapeutic products. Filtration methodologies and chromatographic tools were chosen for study and the critical process parameters (CPP) were optimized to maximize cell recovery yield and viability while ensuring hSC critical quality attributes (CQA) during these steps. Furthermore, analytical tools were established to understand the impact that manufacturing has in cells' characteristics during bioprocessing. Each unit operation presented particular challenges, and overall the developed methodologies showed to be scalable, compatible with current good manufacturing practices (cGMP), robust and flexible to cope with different types of hSC.

1.1. Establishing a DSP workflow for hMSC

Although human mesenchymal stem cells (hMSC) are intrinsically heterogeneous (Phinney, 2012), they are usually the only cellular entity present after expansion in bioreactors; thus, unlike other stem cells, hMSC don't require a cell separation step during the DSP workflow. This workflow is mainly characterized by the removal of process impurities (as microcarriers and components from the cell expansion unit operation), by a volume reduction step, and finally by a reformulation into a cryopreservation solution. These unit operations become more complex with processing scale-up and with the shift from planar cultures to microcarrier-based bioreactor cultures (Schnitzler et al., 2016). This thesis focused on the development of a DSP workflow for hSC, by identifying the CPP of each step of processing and understanding how they impact cells' CQA, hence maximizing cell recovery yield.

1.1.1 Cell detachment and microcarrier clarification

After cell expansion, a key step in adherent stem cell manufacturing corresponds to cell detachment from the microcarriers (Nienow et al., 2016). Typical detachment strategies include the use of proteases (e.g. trypsin), chelating agents (e.g. EDTA) (Weber et al., 2007), or the use of non-enzymatic procedures (e.g. thermo responsive polymers) (Yang et al., 2010). Since cell's characteristics are known to be affected by long exposure times to detaching agents (Freshney, 2011) and by detaching protocols (dos Santos et al., 2014), these methods should be carefully considered and optimized. Additionally, microcarrier selection should be based not only on optimal cell adhesion and expansion, but also on the feasibility to detach cells from the microcarriers. Enzymatic protocols were performed throughout this thesis by incubating hMSC with a dissociation reagent (Chapter II and IV). Although the aim of this thesis was not to optimize the cell detachment protocol, a validation up to 2 L scale in disposable bioreactors of a method developed by Nienow and co-workers (enzymatic protocol coupled to mild hydrodynamic forces) was applied to further improve the cell recovery yields (Nienow et al., 2014). The application of a short period of intense agitation in the presence of a detaching agent, enhanced cell detachment from the microcarriers, thus permitting the recovery of higher cell numbers, as explained by Nienow *et al.* (Nienow et al., 2014). Furthermore, this protocol showed to be compatible with the biomanufacturing workflow of cellular therapies, since it could be easily scaled up - by adjusting the stirring rates, comparable hMSC numbers could be recovered at different scales (0.12 and 2 L) (Chapter V).

Whereas enzymatic detachment is sufficient to separate hMSC from the planar expansion system, due to the non-biodegradable nature of the majority of microcarriers, their removal becomes compulsory when cells are expanded in stirred systems. This step is fundamental within the DSP workflow since microcarriers can be a source of particulates, which have potential risks associated with the overall product quality, and thus with patient safety (Clarke et al., 2016). In fact, therapy products need to comply with regulatory and safety standards for particulates for injectable and parenterally infused drugs (e.g. USP 788) (Schnitzler et al., 2016). Within this context, companies as Solo-Hill (recently acquired by Pall) have been developing low particulate microcarriers (Solo-Hill's Hillex® CT) that can be used as substrates for expansion of stem cells for research and cellular therapy applications.

Due to the size differences between microcarriers (100 - 200 µm) and cells (10 - 20 µm), strategies based on size exclusion are being developed for microcarrier removal. Results on Chapter II pointed to the importance that high pore size filters (> 75 µm) have on dead end filtration process using sterile microfiltration capsules (e.g. Opticap®); higher cell recovery

yields were observed comparing to lower pore size filters (30 µm), which are subjected to an easier microcarrier cake formation, entrapping part of the cell suspension on top of the filter. Following this trend, several closed technologies based on the same concept are now being commercialized, as Pall Solo-Hill's cell separation bag containing a 70 µm screen, and Thermo Scientific's HyQ Harvestainer (25 or 50 L volume) (Szczypka et al., 2014). Moreover, technologies using cell retention devices (e.g. ATF™) as described in Chapter IV, allow to perform process integration and intensification by accomplishing the cell expansion and clarification within the same unit, and are thus highly attractive for cell therapy biomanufacturing. Given the advantages of tangential flow filtration (TFF) compared to dead end filtration, some authors have proposed the possibility to use TFF for microcarrier removal (de Soure et al., 2016; Hassan et al., 2015). Nonetheless, for this goal such devices would require to have pore sizes higher than 70 µm, allowing to permeate cells, whereas the microcarriers would be physically separated, remaining inside the TFF system. However, up to this moment there are no commercially available TFF devices with pore sizes higher than 0.65 µm that would permit this operation.

Moving towards the development of dissolvable microcarriers would be a major achievement for this area. It could significantly simplify the biomanufacturing workflow by avoiding this filtration step, which ultimately would increase the overall bioprocessing yield. In this case, all process impurities would be removed in the cell washing step. As reviewed by de Soure *et al.* (de Soure et al., 2016), the development of polygalacturonic acid (PGA)-microcarriers (Henry et al., 2014) that can be dissolved using pectinase, is an example of efforts currently made towards this goal.

1.1.2 Cell concentration

Results from Chapter II to V confirmed the suitability of TFF to effectively concentrate hSC. The volume reduction unit operation by TFF showed to be flexible (allowing for different operation modes) and robust in concentrating different types of stem cells (Chapter II and III), from different sources (Chapter V), from different donors (Chapter II and V) at different scales (Chapter V), ensuring suitability for application in the biomanufacturing of both autologous and allogeneic cell-based therapies.

The design space for this unit operation was established for adult (Chapter II) and pluripotent stem cells (Chapter III) also relying on risk-based frameworks, as quality-by-design (QbD). After defining viability, identity and differentiation capacity as CQA, CPP of shear rate, permeate flux, and load, showed to impact the TFF process performance (Chapter II and III).

The use of QbD-based approaches, as design of experiments (DoE), prove that the optimization of the TFF process for cell concentration is complex and should not be performed in a stepwise manner, since all considered CPP have interacting effects that impacted differently cell recovery yield and cell viability responses.

Although it is desirable to design low shear processes to perform the volume reduction and washing steps of cell-based products in order to maintain cells' characteristics (Pattasseril et al., 2013), higher shear rates (3000 s^{-1} *vs* 700 s^{-1}) and higher permeate fluxes (250 LMH *vs* 50 LMH) maximized the cell recovery yield throughout processing without impacting cells' CQA, by decreasing both fouling during the microfiltration and the overall processing time by four-fold. In fact, results presented in Chapter II also corroborate the importance of having minimal processing times (Hassan et al., 2015; Pattasseril et al., 2013) during DSP, as a decrease in hMSC's proliferative capacity and increase in apoptosis were observed for longer TFF processes. Although TFF aims towards the prevention of cake formation, membrane fouling is an unavoidable outcome of filtration (van Reis and Zydney, 2007), where the adsorption of cells to the membrane's surface is always observed (Chapter II – V). Nonetheless, if a minimum cell load is not ensured, that adsorption can reach up to 50% of the overall cell quantity. Therefore, depending on the therapeutic use, upstream processing should aim not only to achieve high cell numbers, but also sufficient volumetric cell concentrations (after cell expansion and/or harvesting) to undergo DSP. Moreover, the membrane's material and pore size can contribute significantly to the adsorption phenomenon. Comparing the results achieved in Chapter II and V using hollow fiber cartridges (HF) and flat sheet cassettes (FSC), it is possible to observe that the materials' hydrophilicity coupled to the use of turbulence promoters is beneficial to perform the volume reduction step, where more cells can be recovered after a volume reduction factor of 50, translating in cell recovery yields of 85%. Currently, commercially available devices to operate TFF were originally designed for virus and protein processing; the results obtained in Chapter II and V on this thesis point towards the need to redesign and develop improved materials tailored to cope with the specifications of cell-based products, were cells are intended as the final product and not as by-products. The design of such materials will ultimately allow to fully explore the benefits and effects of different devices' geometries and hydrodynamics on cells' characteristics and recovery yields.

Overall, TFF showed to be a robust and universal methodology for processing different stem cell types with different characteristics and behaviors (Chapter II and III), as similar CPP levels were observed to maximize both pluripotent and adult stem cells' viability and recovery yield, achieving 70-100% cell recovery yield depending on the value of the shear rate used.

1.1.3 Cell washing

To deliver cell therapy products to the clinic, it is important to ensure that these are pure enough to be safe to administer/infuse into patients. Since cell sterilization is not possible, there is an ultimate need to minimize external contaminants. Thus, the development of integrated, closed, single-use bioprocessing strategies has been sought. Moreover, for cell-based therapies it is required to efficiently wash cells, purifying them from undesired process residuals and impurities as described in Tables 1.1 and 1.4 (European Medicines Agency, 2008). Trace amounts of host-cell DNA and proteins if injected into patients may cause allergic reactions or even cause transfection of cells, resulting in tumor formation (Wolter and Richter, 2005). Thus, efficient washing strategies should decrease impurities' below 1 ppm (Food and Drug Administration, 2014).

A manufacturing process should be designed such that the volume of cell suspension washed should be manageable to minimize processing time and volume of wash buffer used, while cells are in suspension, ideally as single cells (Pattasseril et al., 2013). Efforts towards cell washing have been focused on using filtration methodologies to accomplish the purification of cellular products. Lonza (MD, USA) has reported a TFF process using hollow fiber devices, where hMSC were washed efficiently while maintaining functionality (Pattasseril et al., 2013; Rowley et al., 2012a). Another study also reported the use and validation of a novel dead-end filtration to remove dimethyl sulfoxide (DMSO) (up to 85%) from a hMSC suspension ensuring over 70% cell recovery yield (Tostões et al., 2016). To integrate different DSP steps within the same device, thus accomplishing process intensification, the same TFF device used to previously concentrate cells was also used for cell washing. Results on Chapter IV reflected the effectiveness of first concentrating the cellular product, thus minimizing the processing time, as well as the volume of wash buffer used during diafiltration (DF). Moreover, continuous DF showed to be more efficient and gentle than discontinuous DF (Schwartz, 2003), achieving higher cell recovery yields, lower cell death and improved protein clearance. Nonetheless, to approach the residual's level in accordance with regulatory requirements, an expanded bed adsorption (EBA) chromatography step using a multimodal prototype bead resin in negative mode was used (Chapter VI). The integration of EBA on the DSP workflow using TFF allowed to improve protein clearance by more than 10-fold applying the same number of diafiltration volumes, while ensuring cells' CQA and sterility throughout processing (endotoxin-free process, <1 EU/mL). This type of combined strategy may be used in the cell therapy manufacturing workflow, where EBA is used as a first purification step to wash the cell suspension before the

concentration step; a TFF module can then be used to concentrate cells and to diafiltrate them into a proper cryopreservation solution to conclude with fill and finish steps.

1.2. Biomanufacturing workflow of hMSC

Throughout Chapters II-V it was possible to highlight the benefits of designing integrated, closed and scalable processes for the DSP of cell therapy products. The use of methods compliant with cGMP not only facilitates the transfer of these methodologies to an industrial setting, but ultimately will also facilitate regulatory approval while providing batch consistency (Campbell et al., 2015). The major achievements of this thesis are represented in Figure 7.1.

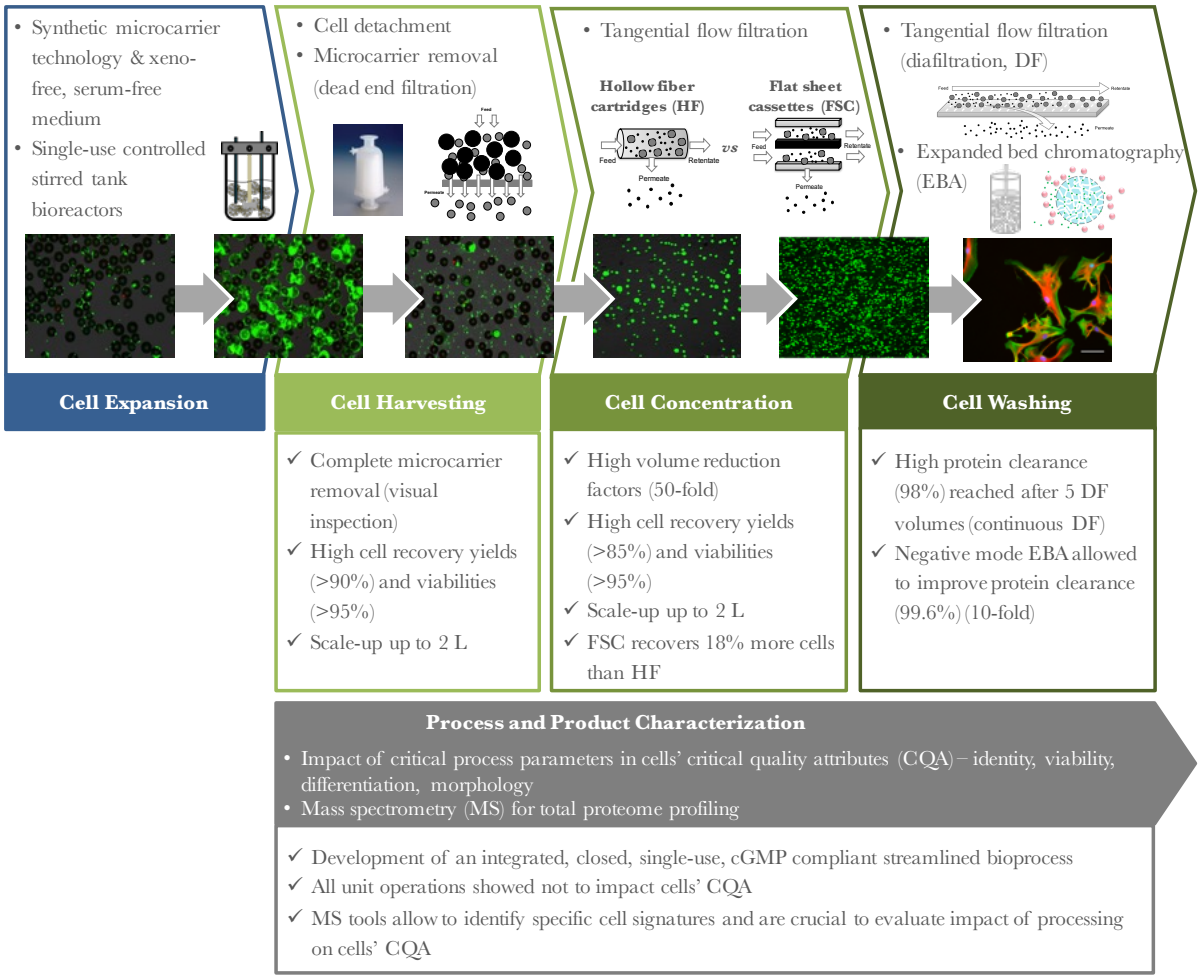

Figure 7.1 – Schematic representation of the major aims and of this thesis correspondent achievements. The biomanufacturing workflow for cell-based therapies comprising up and downstream unit operations is presented (Figure 1.9, Introduction section). The major goals and conditions tested are represented as well as the main results from each section of this work.

Results from Chapter II-VI focused on designing a DSP workflow based on: understanding the cellular product, the CPP affecting the CQA, and on applying scalable technologies that could be easily adapted for either scale-out or scale-up purposes. Adopting this strategy, it was possible to establish filtration methods that processed both adult and

pluripotent SC, achieving cell concentrations relevant for therapy (Table 1.2, Introduction) (volume reduction factor of 50), guaranteeing high cell recovery yields (more than 80%) with high purity levels (no microcarriers, endotoxin-free, and more than 99% of protein clearance), and without compromising cells' CQA of viability, identity and potency (Figure 7.1).

Additionally, for therapies it is recommended to demonstrate that manufacturing does not affect safety, identity, purity, or potency (Campbell et al., 2015; Food and Drug Administration, 1996). Given the complexity of cellular products, demonstrating such CQA can be challenging. To assess cells' quality at the end of processing it is essential to apply a diverse panel of analytical methods that allow to evaluate cell viability, membrane structure, senescence, proliferation, adhesion, potency, metabolism, apoptosis, amongst others. The combination of such diverse assays will ultimately provide a global assessment of cell quality. Moreover, it is also important to identify beforehand cells' potency for a given therapeutic use and apply assays that monitor this parameter. For instance, nowadays hMSC are mostly applied for their ability in secreting bioactive molecules and not solely by their differentiation capacity (except for regenerative medicine applications). Thus, assays that can monitor cells' secretome are fundamental if they are used in a clinical setting with this goal. Within this context, the application of more sensitive methodologies (e.g. "omics") that allow a better cell characterization, increasing product and process understanding is thus essential while carrying out cell therapy process development. In fact, the use of this type of analysis allowed for the identification of specific signatures of the final product and proved to be essential to understand the cells' final quality as well as to evaluate the impact of manufacturing at different stages of processing, as described in Chapter V.

2. Conclusion and perspectives

The cell therapy field is currently facing similar challenges as those observed for protein processing, in particular for monoclonal antibodies, over 20 years ago. To meet the high-growth demand for cell therapy products, manufacturers are developing and integrating new upstream platforms, essentially based on microcarrier-based bioreactors, to significantly increase therapeutic cell culture productivity (Rowley et al., 2012b). As these technologies mature, the bottlenecks are now shifting towards DSP, where high recoveries with minimal loss of product, while maintaining cells' characteristics, is the main driver for process development.

The cell therapy industry has then an opportunity to learn from protein and virus processing and anticipate these bottlenecks, by proactively developing strategies that address

future scales for autologous and allogeneic therapies, and by optimizing technologies that can be robust, integrated, scalable and flexible for different types of therapeutic products. Furthermore, as this field mature, it is expected that the design of materials and devices specifically tailored to cope with cells' features will bring therapies one step closer, allowing to maximize cell recovery yields, keeping manufacturing costs to a minimum.

Overall, the results presented on this thesis contributed to generate knowledge regarding the impact that critical process parameters of filtration-based methods and chromatography have on hSC's recovery, viability and characteristics. By combining membrane technology and chromatographic tools, an effective DSP workflow comprised by clarification, cell concentration and washing unit operations was established, ensuring high cell concentration factors, high recovery yields with minimal presence of impurities. This knowledge can now be used as a base to study the interaction of cells and materials (e.g. membranes), potentially developing more suitable materials and conditions for cell concentration and washing. Moreover, the chromatography principles herein described hold the potential to be used in an industrial setting, as they can be exploited for affinity selection of specific impurities or even other cellular entities or impurities, maximizing cells' recovery.

References

Campbell, A., Brieva, T., Raviv, L., Rowley, J., Niss, K., Brandwein, H., Oh, S., Karnieli, O., 2015. Concise Review: Process Development Considerations for Cell Therapy. Stem Cells Transl. Med. 4, 1155–1163.

Clarke, D., Stanton, J., Powers, D., Karnieli, O., Nahum, S., Abraham, E., Parisse, J.-S., Oh, S., 2016. Managing particulates in cell therapy: Guidance for best practice. Cytother. 18, 1063–1076.

European Medicines Agency, 2008. EMEA/CHMP Guideline on human cell-based medicinal products (EMEA/CHMP/410869/2006).

Food and Drug Administration, 2014. Code of Federal Regulations Title 21. Subchapter F -- Biologics; Part 610 -- General Biological Products Standards; Subpart B -- General Provisions; Sec. 610.15 Constituent Materials.

Food and Drug Administration, 1996. Demonstration of comparability of human biological products, including therapeutic biotechnology-derived products. http://www.fda.gov/Drugs/GuidanceComplianceRegulatoryInformation/Guidances/ucm122879.htm (accessed 9.1.16).

Freshney, R.I., 2011. Culture of Animal Cells: A Manual of Basic Technique and Specialized Applications, 6 ed. John Wiley & Sons, Inc, New York, USA.

Hassan, S., Simaria, A.S., Varadaraju, H., Gupta, S., Warren, K., Farid, S.S., 2015. Allogeneic cell therapy bioprocess economics and optimization: downstream processing decisions. Regen. Med. 10, 591–609.

Henry, D., Hervy, M., Walerack, C., 2014. Cell culture article and methods thereof. WO2014209865 A1.

Nienow, A.W., Hewitt, C.J., Heathman, T.R.J., Glyn, V.A.M., Fonte, G.N., Hanga, M.P., Coopman, K., Rafiq, Q.A., 2016. Agitation conditions for the culture and detachment of hMSCs from microcarriers in multiple bioreactor platforms. Biochem. Eng. J. 108, 24–29.

Nienow, A.W., Rafiq, Q.A., Coopman, K., Hewitt, C.J., 2014. A potentially scalable method for the harvesting of hMSCs from microcarriers. Biochem. Eng. J. 85, 79–88.

Pattasseril, J., Varadaraju, H., Lock, L., Rowley, J.A., 2013. Downstream Technology Landscape for Large-Scale Therapeutic Cell Processing. BioProcess Int. 11, 38–47.

Phinney, D.G., 2012. Functional heterogeneity of mesenchymal stem cells: Implications for cell therapy. J. Cellular Biochem. 113, 2806–2812.

Rowley, J., Pattasseril, J., Mohamed, A., Lonza Walkersville, Inc., 2012a. High yield method and apparatus for volume reduction and washing of therapeutic cells using tangential flow filtration. US20120294836 A1.

Rowley, J., Abraham, E., Campbell, A., Brandwein, H., Oh, S., 2012b. Meeting Lot-Size Challenges of Manufacturing Adherent Cells for Therapy. BioProcess Int. 3, 16–22.

dos Santos, F., Campbell, A., Fernandes-Platzgummer, A., Andrade, P.Z., Gimble, J.M., Wen, Y., Boucher, S., Vemuri, M.C., da Silva, C.L., Cabral, J.M.S., 2014. A xenogeneic-free bioreactor system for the clinical-scale expansion of human mesenchymal stem/stromal cells. Biotechnol. Bioeng. 111, 1116–1127.

Schnitzler, A.C., Verma, A., Kehoe, D.E., Jing, D., Murrell, J.R., Der, K.A., Aysola, M., Rapiejko, P.J., Punreddy, S., Rook, M.S., 2016. Bioprocessing of human mesenchymal stem/stromal cells for therapeutic use: Current technologies and challenges. Biochem. Eng. J. 108, 3–13.

Schwartz, L.M., 2003. Diafiltration for desalting or Buffer exchange. BioProcess Int. 43–49.

de Soure, A.M., Fernandes-Platzgummer, A., da Silva, C.L., Cabral, J.M.S., 2016. Scalable microcarrier-based manufacturing of mesenchymal stem/stromal cells. J. Biotechnol. *in press*.

Szczypka, M., Splan, D., Woolls, H., Brandwein, H., 2014. Single-use bioreactors and microcarriers scalable technology for cell-based therapies. BioPharm Int. 12, 54–64.

Tostões, R., Dodgson, J., Mason, C., Veraitch, F., 2015. A Novel Filtration Device for Point of Care Preparation of Cellular Therapies. Cytother. 17, S26–S26.

van Reis, R., Zydney, A., 2007. Bioprocess membrane technology. J. Membr. Sci. 297, 16–50.

Weber, C., Pohl, S., Pörtner, R., Wallrapp, C., Kassem, M., Geigle, P., Czermak, P., 2007. Expansion and Harvesting of hMSC-TERT. Open Biomed Eng. J. 1, 38–46.

Wolter, T., Richter, A., 2005. Assays for controlling host-cell impurities in biopharmaceuticals. BioProcess Int. 40–46.

Yang, H.S., Jeon, O., Bhang, S.H., Lee, S.-H., Kim, B.-S., 2010. Suspension Culture of Mammalian Cells Using Thermosensitive Microcarrier That Allows Cell Detachment Without Proteolytic Enzyme Treatment. cell transplant 19, 1123–1132.